Two and three-dimensional flows of second grade and micropolar fluids

By

Muhammad Nawaz

Supervised By

Dr. Tasawar Hayat

Department of Mathematics
Quaid-i-Azam University
Islamabad, Pakistan
2012

Two and three-dimensional flows of second grade and micropolar fluids

By

Muhammad Nawaz

A THESIS SUBMITTED IN THE PARTIAL FULFILLMENT OF THE
REQUIREMENTS FOR THE DEGREE OF
DOCTOR OF PHILOSOPHY
IN

MATHEMATICS

Supervised By

Dr. Tasawar Hayat

Department of Mathematics
Quaid-i-Azam University
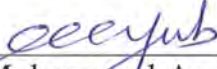# Islamabad, Pakistan
2012

CERTIFICATE

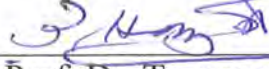## Two and three-dimensional flows of second grade and micropolar fluids

By
Muhammad Nawaz

A THESIS SUBMITTED IN THE PARTIAL FULFILLMENT OF THE
REQUIREMENTS FOR THE DEGREE OF DOCTOR OF
PHILOSOPHY IN MATHEMATICS

We accept this dissertation as conforming to the required standard

1. _____
Prof. Dr. Muhammad Ayub
(Chairman)

2. _____
Prof. Dr. Tasawar Hayat
(Supervisor)

1. _____
Dr. Muhammad Salahuddin
(External examiner)

2. _____
Dr. Qamar ul Haq
(External examiner)

Department of Mathematics
Quaid-i-Azam University
Islamabad, Pakistan
2012

Acknowledgements

First I bow my head in deep gratitude to Almighty Allah who endowed me with potential and ability to make a contribution to the already existing ocean of knowledge. Special praises to Hazrat Muhammad (peace be upon Him) the last prophet who is forever a torch of guidance, devotion and knowledge for humanity as whole.

It is difficult to overstate my gratitude to my Ph.D. supervisor, Professor Dr. Tasawar Hayat. With his enthusiasm, his inspiration, and his great efforts to explain things clearly and simply, he helped to make mathematics fun for me. Throughout my thesis-writing period, he provided encouragement, sound advice, good teaching, good company, and lots of good ideas.

I am grateful to chairman, Department of Mathematics, Prof. Dr. Muhammad Ayub for his efforts in maintaining the research atmosphere in the department. I would like to thank many people who have taught me mathematics: my high school math teacher Nadeem Ahmad, my undergraduate teachers at Bahauddin Zakaryia University Multan. My M. Phil and Ph. D teachers especially Dr. Sohail Nadeem, Dr. Malik Muhammad Yousaf, Dr. Masood Khan and others at Quiad-I-Azam University Islamabad.

I am also thankful to Brig. Imran Rahman, Vice Chancellor Institute of Space Technology Islamabad, for permitting me Friday off from IST during last semester of my Ph. D studies.

I am indebted to my many student colleagues for providing a stimulating and fun environment in which to learn and grow. I would like to share my sincere thanks to my lab mates especially Dr. Ahmad zeshan, Dr. Meraj Mustafa, Zahid Iqbal, Muhammd Awis, Muhammad Ayub, Maryiam Javed, Ansa Rafique, Rahila, Dr. Saima and Dr. Sadia for their fruitful comments and discussions. I am also grateful to my seniors Dr. Tariq Javed, Dr. Nasir Ali, Dr. Zaheer Abbas and Dr. Sher Baz for their guidance.

Lastly, and most importantly, I wish to thank my parents, wife, brothers, sisters and children, Hamza, Saim, Danial and Seemab for their prayers and love.

4 May, 2012   *Muhammad Nawaz*

Dedicated to

My loving daughter Seemab and sons Muhammad Hamza, Muhammad Saim and Muhammad Danial

Preface

There is a wide use of non-Newtonian fluids in the industrial and technological processes. The heat transfer has a central role in these processes. No doubt, the behavior of non-Newtonian fluids cannot be analyzed through implementation of the classical Navier-Stokes equations. It has been recognized that the complex behavior of non-Newtonian fluids in nature cannot be predicted by one constitutive relationship between shear stress and rate of strain. Hence many constitutive relationships have been obtained for such fluids. The second grade is one of these fluids which have essence to predict the normal stress effects. There are fluids like polymeric liquid, crystals, animal blood etc which can be well analyzed using Eringen's theory of micropolar fluids. In such case, the local effects due to the microstructure and microrotations of the fluid have substantial impact on the flow. Bearing all such issues in mind, the present thesis is structured as follows.

Chapter one briefly reviews the existing literature survey related to stretched flows. The equations of motion for axisymmetric flow of micropolar fluid are also included here.

The two-dimensional flow of non-Newtonian fluid in convergent/divergent channel is explored in chapter two. Rheological expressions of second grade fluid are employed in the development of nonlinear differential equation. Resulting nonlinear mathematical problem containing continuity and momentum equations is solved by homotopy analysis method (HAM). Convergence interval of the derived solution is explicitly identified. Numerical values of skin friction coefficient are tabulated. Results showed that the flow quantities of interest are influenced greatly by embedded parameters. **Main observations of this chapter are published in "Canadian Journal of Physics 88 (2010) 911".**

Chapter three examines the salient features of heat transfer in flow configuration studied in chapter two. For this purpose, the energy equation is solved in dimensionless form. Related convergence analysis is performed. Temperature distribution is analyzed for various pertinent parameters. Especially, the effects of angle of inclination between channel walls and Prandtl and Eckert numbers are given due attention. **The obtained results are published in "International Journal for Numerical Methods in fluids 64 (2010) 761".**

Chapter four addresses the thermal-diffusion and diffusion-thermo effects in the axisymmetric flow of second grade fluid. The fluid is electrically conducting in the presence of a constant applied magnetic field. Further, the effects of Joule heating and first order chemical reaction are taken into account. The mathematical statement of the problem is derived employing four fundamental laws namely the conversations of mass, linear momentum, energy and concentration. Transformation procedure reduces the partial differential equations into the ordinary differential equations. Homotopic solutions for physical quantities are constructed. Skin friction, Nusselt and Sherwood numbers are computed and analyzed in details. It is observed that the shear stresses on the surface of stretching sheet increases with an increase in magnetic field strength and non-Newtonian parameter of the fluid. Heat and diffusion fluxes are increased

by increasing Reynolds, Hartman, Schamidt, Soret and Prandtl numbers. **The contents of this chapter have been published in "International Journal of Heat and Mass Transfer 54 (2011) 3031".**

Hall and ion-slip effects on three-dimensional flow of second grade fluid over a stretching surface have been shown in chapter five. Mathematical formulation is carried out for small magnetic Reynolds number and constant material properties of fluid. Effects of various physical parameters on the dimensionless velocity components are examined by graphs. Variation of skin friction coefficients for different involved parameters is seen through tabulated values. Skin friction coefficients are found to increase when Hartman number and second grade parameter are increased. On the other hand there is a decrease in skin friction coefficient when ion slip parameter is increased. **These conclusions are published in "International Journal for Numerical Methods in fluids 66 (2011) 183".**

Chapter six extends the work of chapter five in the regime of heat transfer process. Viscous dissipation and Joule heating in the energy equation are considered. Effects of Prandtl number, local Eckert number, Hall parameter, ion-slip parameter and Hartman number on the dimensionless temperature are analyzed in particular. A comparative study between the present and existing limiting results is carefully made. Convergence regarding the obtained solution of temperature is shown. Nusselt number is analyzed for various values of sundry parameters. **The results have been published in "Zeitschrift Naturforchung 56a (2010) 683".**

Soret and Dufour effects on the mixed convection three-dimensional flow of a second grade fluid over a vertical stretching have been considered in chapter seven. Mathematical analysis is presented in the presence of Hall and ion-slip currents. In order to get clear insight of the considered problem, the dimensionless velocities, temperature and concentration fields are displayed and numerical computations are carried out for various values of embedded flow parameters. It is observed that boundary layer thickness can be controlled through Hartman number, convection parameters, ion-slip and Hall slip parameters. A comparative study between the present and previous limiting results is carefully seen. **The contents of this chapter are published in "International Journal for Numerical Methods in fluids 67(9) (2011) 1073".**

Chapter eight discusses magnetohydrodynamic flow of a micropolar fluid between the radially stretching sheets in the presence of constant magnetic field. A uniform magnetic field is applied in the transverse direction to flow. The governing partial differential equations are transformed into the ordinary differential equations using similarity transformations. The nonlinear problem is computed. Convergence of obtained solutions is checked. The velocity profiles are discussed for the pertinent parameters. The values of skin friction and wall couple stress coefficients are obtained for various values of Reynolds number, Hartman number and micropolar fluid parameter. **These findings have been published in "Zeitschrift Naturforchung 66a (2011) 53".**

The work of chapter eight in the presence of heat transfer is extended in chapter nine. In other words, axisymmetric flow of magnetohydrodynamic micropolar fluid between two radially stretching sheets with heat transfer is explored. Viscous dissipation, micropolar heat conduction and Joule heating are present.

Energy equation is transformed into the ordinary differential equation by appropriate variables. The resulting nonlinear problem is solved for the series solution. It is observed that the rate of heat transfer in micropolar fluid is higher than that in a Newtonian fluid. From practical point of view, micropolar fluid can be used instead of Newtonian fluid if some one is interested to increase the rate of heat transfer from surface into the fluid. This is significant when certain temperature is required to improve the quality of product in manufacturing process. **The contents of this chapter have been published in "Journal of Mechanics, 27 (2011) 607".**

Dufour and Soret effects on axisymmetric two-dimensional flow of an incompressible micropolar fluid between radially stretching sheets are studied in chapter ten. The fluid is taken electrically conducting. Joule heating and chemical reaction are considered. The energy and concentration laws develop the mathematical formulation. The related problems are solved and validity of series solutions is verified through residual errors. Dimensionless temperature and concentration are discussed through graphs. Behaviors of sundry parameters on skin friction coefficient, wall couple stress coefficient, Nusselt and Sherwood numbers are analyzed. **The contents of chapter ten have been submitted in "Computers & Fluids".**

Chapter eleven explores the MHD time-dependent flow problem of a micropolar fluid between two radially stretching sheets. Both cases of strong and weak interactions of microelements are considered. The equations along with the boundary conditions are solved. The variation of micropolar parameter on axial and radial velocity component is opposite to that of Hartmann number. The effect of unsteadiness parameter on axial, radial and angular velocity is discussed. The variations of Hartman number and micropolar parameter on angular velocity in weak and strong concentrations are opposite. **Such results are published in "Applied Mathematics and Mechanics; English Edition 32(3) (2011) 361".**

Contents

Chapter 1

Review and governing equations

1.1 Introduction

This chapter includes the review of previous information available on the selected topic. The constitutive relationships for second grade and micropolar fluids are presented. Equations of motion for axisymmetric flow of micropolar fluid are included.

1.2 Background of the considered problems

The flows of an incompressible fluid in divergent/convergent channel are of great interest to the recent researchers. This is because of their applications in aerospace, chemical, civil, environmental and biomechanical engineering [1]. The pioneering works related to such flows have been presented by Hamel [2] and Jeffery [3]. Jeffery-Hamel flow of viscous fluid is available in the text book [4]. Sobey and Drazin [5] reported on the bifurcation of two-dimensional Jeffery-Hamel flow. The perturbation solution for Jeffery-Hamel flow of viscous fluid is developed by Banks et al. [6]. Very recently Domairy et al. [7] derived an analytic solution for Jeffery-Hamrel flow of a viscous fluid by homotopy analysis method. Joneidi et al. [8] used three analytical techniques namely the homotopy analysis method (HAM), the homotopy perturbation method (HPM) and the differential transformation method (DTM) for the development of series solution for the Jeffery-Hamel flow in a viscous fluid. Studies mentioned through refs. [1 − 8] discussed the flows in a channel with fixed boundaries. However in practice, there are number of situations where

fixed walls do not represent realistic situation. Thus, Sakiadis [9 − 11] presented earliest work on boundary layer flow induced over a moving surface. After Sakiadis' work [9 − 11], several investigators considered the boundary layer flow over a surface moving with constant velocity. For instance Ericksen et al. [12] examined heat and mass transfer characteristics in boundary layer flow over a continuously moving surface subjected to suction/injection. Tsou et al. [13] conducted an analysis for heat transfer in boundary layer flow engendered by a surface moving with constant velocity. Soundalgekar and Murthy [14] studied variable surface temperature in the boundary layer flow over a continuously moving plate. Ali and Al-Yousef [15] discussed the effects of buoyancy force and suction/injection on the mixed convection boundary layer flow of viscous fluid over a vertical surface moving with constant velocity. In continuation to Sakiadis' work, the stretching flows have been discussed. Such flows are prominent in aerodynamic extrusion of plastic sheets, cooling of an infinite plate in a cooling bath, liquid film in condensation process, continuous filament extrusion from a dye, the fluid dynamic of a long thread traveling between a feed roll and wind-up roll. Crane [16] was the first when discussed the boundary layer flow over a stretching surface and derived exact similarity solution of the arising nonlinear problem. Afterwards many researchers focused on stretching flows taking various features in to account, for example, Andersson et al. [17] studied thin film flow of a power-law fluid over unsteady stretching sheet. Andersson [18] discussed slip effects on the flow of viscous fluid past a stretching surface. Wang [19] examined the combined effects of slip and suction on the flow of viscous fluid over a stretching surface. Rajagopal et al. [20] looked for the solution of viscoelastic fluid flow caused by a stretching surface. Mahapatra and Gupta [21] considered the problem regarding stagnation-point flow of a viscoelastic fluid near a stretching surface. They presented perturbative solution for momentum equation and Numerical solution of energy equation is obtained by finite difference method. Sajid and Hayat [22] established non similar solution for the stretching flow of a third-grade fluid. Abass et al. [23] computed both numerical and analytic solutions for magnetohydrodynamic flow of a second grade fluid over an oscillating stretched surface. Nazar et al. [24] looked at the numerical solution of three-dimensional boundary layer flow of viscoelastic fluid over a stretching surface. Few contributions due to radially stretching sheet have been also available. Ariel [25] studied the axisymmeytric flow of a second grade fluid over radially stretching surface. He found perturbative solution for small values of vis-

6

coelastic parameter and asymptotic solution valid for large values of viscoelastic parameter. Mirgolbabaei [26] discussed MHD axisymmetric flow of viscous fluid over a stretching sheet using adaptive variational iterative method (AVIM) and compared the obtained results with the exact solution. Ariel [27] considered slip effects on the axisymmetric flow of viscous fluid over a radially stretching surface. He computed homotopy perturbation solution (HPM) for small value of slip parameter and asymptotic solution for large values of slip parameter. It was concluded that HPM has good agreement with the exact solution. Hayat et al. [28] considered the same problem as considered by Ariel in [27] through implementation of homotopy analysis method (HAM). They compared the results with those given in [27]. They concluded that HAM solution has more agreement with the exact solution than HPM solution. The nonlinear problem describing the partial slip effects on axisymmetric flow of second grade fluid over a radially stretching surface has been solved numerically by Sahoo [29]. He used fourth order Ruge-Kutta method. Sajid et al. [30] studied analytically the axisymmetric flow of viscous fluid over a surface stretching with linear velocity in a radial direction.

Heat transfer process occurs extensively in practice. For instance, cooling of the cutting tools during machining operations, cooling of the electronic components in computers, the generation and condensation of steam in a thermal power plant, heating and cooling of buildings, cooking and the thermal control of re-entering of space craft [31]. Besides this one can find the applications of such mechanism in power generators, MHD accelerators, refrigerations coils, transmission lines, electric transformers, heating elements, levitation and pumping of liquids in mechanical engineering, boundary layer control and transpiration processes in aerodynamics. As far as the polymer industry is concerned, the heat transfer is very important mechanism. The quality of product, being manufactured, is controlled through many mechanisms like heat transfer, using electrically conducting fluid and viscoelsatic properties. In view of above mentioned applications, the heat transfer characteristics in Newtonian and non-Newtonian fluids have been studied extensively by many several researchers. For example, Hayat and Sajid [32] extended the work of ref. [25] to heat transfer analysis through (i) prescribed surface temperature (PST-case) and (ii) prescribed heat flux (PHF-case). The related energy equation is solved by homotopy analysis method (HAM). Sajid et al. [33] discussed the heat transfer in unsteady flow of viscous fluid over a radially stretching surface. Ahmed et al. [34] extended the work in

7

ref. [32] to heat transfer in an unsteady flow of second grade fluid. They developed the solution of resulting nonlinear boundary value problem by employing HAM. Cortell [35] examined the heat transfer characteristics through two modes namely (i) constant surface temperature (CST-case) (ii) prescribed surface temperature (PST-case) in the flow of thermodynamically compatible second grade fluid over a stretching surface. Mixed convection flow of second grade fluid along a vertical stretching surface with variable surface temperature has been discussed by Mushtaq et al. [36]. Cortell [37] examined the effects of suction and external magnetic field on the flow and heat transfer of thermodynamically compatible second grade fluid over a stretching sheet. Simultaneous effects of viscous dissipation, internal heat generation/absorption, work done due to deformation and Joule heating on the flow of a second grade fluid have been considered by Liu [38]. Asymptotic solution of the temperature for large Prandtl number have been given. Bataller [39] employed fourth order Runge-Kutta method for the effects of viscous dissipation and thermal radiation in the flow of heat generating/absorbing second grade fluid over a non-isothermal stretching surface. Hayat et al. [40] performed an analysis for heat transfer in the flow of a second grade fluid over a stretching surface with slip and porous medium. Abel et al. [41] analyzed the effect of non-uniform source/sink on the heat transfer in a second grade fluid flow induced by permeable stretching surface in the presence of porous medium. Gupta [42] extended the work of Crane [16] to examine the effect of suction/injection on the flow and heat transfer caused by a stretching surface. The effect of variable surface temperature on the flow of viscous fluid was examined by Grubka and Bobba [43]. Ali [44] looked at the solution of problem describing the effect of suction/injection on heat transfer in the flow of viscous fluid over a surface having power law stretching velocity.

According to Eringen [45] many fluids like polymeric liquids, liquid crystals, animal blood and fluids containing small amount of polymeric additives are those for which micro-rotational, spin inertia, couple stresses and body torque etc. are significant. The well known classical Navier-Stokes equations cannot explain such effects. Eringen [45] was first to present the theory of micropolar fluids and proposed the constitutive equations which are capable of describing the effects like micro-rotational, spin inertia, couple stresses etc. Afterwards the flows of micropolar fluid have been discussed in various geometrical configurations. For instance, finite element solution of micropolar fluid flow and heat transfer between two porous disks has been

8

found by Takhar et al. [46]. Eldabe et al. [47] successfully employed Chebyshev finite difference method (ChFD) to nonlinear problem dealing with transfer of heat in an electrically conducting micropolar fluid over a permeable stretching surface immersed in porous medium. They analyzed the effects of mass transfer, Prandtl number, magnetic field and porosity parameter on the velocity and temperature fields and compared the results in limiting sense with already existing study [48]. Pal and Chatterjee [49] performed an analysis for heat and mass transfer in MHD non-Darcian two-dimensional boundary layer flow of micropolar fluid over a stretching sheet embedded in a porous media with non-uniform heat source and thermal radiation. Mixed convection flow of micropolar fluid over a non-linearly stretching sheet has been studied by Hayat et al. [50]. Hassanien et al. [51] solved nonlinear problem for heat transfer in the stretching flow of micropolar fluid. Finite element analysis of combined heat and mass transfer in the flow of a micropolar fluid was performed by Kumar [52]. Ishak [53] analyzed the effect of thermal radiation on thermal boundary layer flow of micropolar fluid over a stretching surface.

Hall current is significant when external magnetic field is strong whereas ion-slip current can not be neglected when electron-atom collision frequency is high. Hence in view of such importance, Hall and ion-slip effects have been analyzed by few researchers. For instance Pop [54] investigated the influence of Hall current on hydromagnetic flow induced by an accelerated plate. Katagiri [55] examined the effect of Hall current on boundary layer flow of viscous fluid past an infinite flat plate. Gupta [56] extended the work of Katagiri [55] to the flow of viscous fluid past a porous flat plate in the presence of Hall current. Hossain [57] studied the effect of Hall current on unsteady free convective flow over an infinite vertical porous plate. Hossain and Mohammad [58] reported the effect of Hall current on free convection flow caused by accelerating porous plate. Watanabe and Pop [59] investigated the effects of Hall current on steady boundary layer flow of an electrically conducting fluid past a semi-infinite plate. They solved the governing problem by employing numerical technique namely the difference differential method together with Simpson's rule. Abo-Eldahab and El-Aziz [60] addressed the Hall and ion -slip effects for MHD free convection flow of heat generating fluid past a semi-infinite vertical flat plate. Similarity solutions for heat and mass transfer in MHD flow of a gas with Hall and ion-slip currents have been computed by Megahed et al. [61]. They employed the shooting method. Osalusi et al. [62] considered simultaneous effects of Ohmic heating, viscous dissipation, Hall

9

and ion-slip currents and variable properties on the flow caused by rotating porous disk with slip. In another work, Osalusi et al. [63] looked for the combined effects of viscous dissipation, Joule heating, Hall and ion-slip currents on heat transfer in the flow of Bingham fluid over a porous rotating disk . They employed shooting method to solve the governing nonlinear problems. By employing network simulation method (NSM), Beg et al. [64] solved nonlinear problem dealing with magnetohydrodynamic unsteady flow and heat transfer in a Darcian channel with Hall, ion-slip, viscous dissipation and Joule heating effects. The effects of Ohmic heating and viscous dissipation on unsteady MHD slip flow on a rotating cone with Hall and ion-slip currents have been studied by Osalusi [65]. Rana et al. [66] derived the exact solution for the transfer of heat in the Hartman flow of Burgers' fluid between two parallel electrically non-conducting planes. Salem and El-Aziz [67] considered heat and mass transfer characteristics in steady flow of heat generating/absorbing viscous fluid over a linearly stretching surface in the presence of Hall current and chemical reaction. They solved the involved problems by shooting method together with fourth order Runge-Kutta algorithm. Elgazery [68] dealt with combined effects of Hall and ion-slip currents, heat and mass transfer in the stretching flow of micropolar fluid with temperature dependent viscosity and thermal conductivity. Sutton and Sherman [69] derived expression for generalized Ohm's law in the presence of Hall and ion-slip currents.

It has been experimentally verified that the diffusion of energy can be caused by a composition gradient. This fact is known as Dufour effect or diffusion-thermo effect. The diffusion of species by temperature gradient is termed as Soret effect or thermal diffusion effect. In most of the studies dealing with the transfer of heat and mass, these effects are neglected under the assumption that these effects are smaller order of magnitude as described by Fourier's and Fick's laws [70 − 75]. However recent developments show that Dufour and Soret effects are significant when transfer of heat and mass occurs in the flow of mixture of gases with very light molecular weight (H_2, He) and of medium molecular weight (N_2, air) [70 − 75]. In view of the applications of thermal diffusion and diffusion thermo in separation of isotopes and separation of gases from their mixture, Chapman and Cowling explained these effects and derived the formulae for thermal diffusion coefficient and thermal diffusion factor for monoatomic or polyatomic gas mixtures. Such effects cannot be ignored when density difference exists. Kafoussias et al [70] computed numerical solution for mixed convection flow of viscous fluid over an isothermal

10

semi-infinite flat plate with thermal diffusion and diffusion-thermo effects. Alam and Rahman [71] and Rehman et al. [72 − 74] considered thermal diffusion and diffusion-thermo effects on the convective (mixed or free) flows over a flat plate. Heat and mass transfer characteristics in natural convection flow of an electrically conducting fluid over a vertical surface embedded in a saturated porous medium with Dufour and Soret effects have been studied numerically by Postelnicu [75]. Lakshami et al. [76] analyzed stability of Soret-driven flow by a linear stability analysis. Kairi and Murthy [77] examined the effects of melting heat transfer and diffusion-thermo on the flow of non-Newtonian fluid (Oswald-de-Waele power law model). Osalusi et al. [78] considered simultaneous effects of thermal diffusion and diffusion-thermo, viscous dissipation and Ohmic heating on mixed convection flow caused by rotating disk. It is worth mentioning that Dufour and Soret effects have been investigated by many researchers over a solid surface. However fewer studies regrading these effects on the flow induced by stretching surface are available. Few amongst these may be mentioned through refs. El-Aziz [79], Beg et al. [80], Tsai and Huang [81], Afify [82], Shatey et al. [83] and Hayat et al. [84]. Further, the works presented in the studies Menez and Sandall [85], Hayat et al. [86, 87], El-Aziz and Salem [88], Cortell [89, 90], Andersson et al. [91] and Takhar et al. [92] examined the effects of chemical reaction on the boundary layer flows.

1.3 Constitutive equations of second grade fluid

Expression of Cauchy stress tensor (τ) in a second grade fluid is

$$\tau = -p\mathbf{I} + \mu\mathbf{A}_1 + \alpha_1\mathbf{A}_2 + \alpha_2\mathbf{A}_1^2, \tag{1.1}$$

in which p is the pressure, $\mathbf{I}$ is the identity tensor, α_i $(i = 1 − 2)$ are the material constants and $\mathbf{A}_1$ and $\mathbf{A}_2$ are the Rivilin Ericksen tensors defined by

$$\mathbf{A}_1 = \nabla\mathbf{V} + (\nabla\mathbf{V})^*, \tag{1.2}$$

$$\mathbf{A}_2 = \frac{d\mathbf{A}_1}{dt} + \mathbf{A}_1(\nabla\mathbf{V}) + (\nabla\mathbf{V})^*\mathbf{A}_1, \tag{1.3}$$

11

where d/dt is the material derivative and $*$.denotes the transpose. For thermodynamic analysis of the second grade fluid requires that [20]

$$\mu \geq 0, \ \alpha_1 \geq 0, \ \alpha_1 + \alpha_2 = 0. \tag{1.4}$$

1.4 Constitutive equations of micropolar fluid

According to Eringen [45] there is a subclass of micro fluids which is known as micropolar fluids. These fluids exhibit the micro-rotational effects and micro-inertia. Eringen [45] was first to develop the theory of micropolar fluids. A complete set of basic equations for micropolar fluids is

$$\nabla \cdot \mathbf{V} \ = \ 0. \tag{1.5}$$

$$\rho\frac{d\mathbf{V}}{dt} \ = \ \nabla \cdot \tau_1 + \rho\mathbf{b}, \tag{1.6}$$

$$\rho j\frac{d\Omega}{dt} \ = \ \nabla \cdot \mathbf{M} + \epsilon : \tau_1 + \rho\mathbf{l}, \tag{1.7}$$

$$\rho c_p\frac{dT}{dt} = K_c\nabla^2 T + \Phi + \frac{DK_T}{C_s}\nabla^2 C + \frac{1}{\sigma}\mathbf{J} \cdot \mathbf{J}, \tag{1.8}$$

$$\frac{dC}{dt} = D\nabla^2 C + \frac{DK_T}{T_m}\nabla^2 T - K_n(C - C_\infty)^n. \tag{1.9}$$

in which $\mathbf{V}$, T and C are the velocity, temperature and concentration fields respectively, Ω is the angular velocity field for micro-motion of fluid particles, j is the micro-inertia per unit mass, ϵ is the third rank tensor corresponding to the Levi-Civita symbol, n is the order of chemical reaction, $\mathbf{l}$ is the volume couple force per unit mass, τ_1 and $\mathbf{M}$ respectively are the stress and couple stress tensors which are defined as follows:

$$\tau_1 \ = \ \lambda\left(tr\mathbf{d}\right)\mathbf{I} + 2\mu\mathbf{d} + 2k\epsilon \cdot \left(\omega - \Omega\right), \tag{1.10}$$

$$\mathbf{M} \ = \ \alpha_\nu\left(\nabla \cdot \Omega\right)\mathbf{I} + \beta_\nu\left(\nabla\Omega\right)^t + \gamma_\nu\nabla\Omega, \tag{1.11}$$

$$\mathbf{d} \ = \ \frac{1}{2}\left[\nabla\mathbf{V} + (\nabla\mathbf{V})^t\right], \tag{1.12}$$

$$\omega \ = \ \frac{1}{2}\left(\nabla \times \mathbf{V}\right). \tag{1.13}$$

12

where tr denotes trace of tensor, ω is the vorticity vector, λ is the bulk viscosity, μ is the shear viscosity, k is the vortex viscosity and α_ν, β_ν, γ_ν are the spin viscosities. Furthermore, λ, μ, k, α_ν, β_ν and γ_ν satisfy the following constraints [45]

$$3\lambda + 2\mu + k = 0, \ 2\mu + k \geq 0, \ k \geq 0, \ 3\alpha_\nu + \beta_\nu + \gamma_\nu \geq 0, \ \gamma_\nu \geq |\beta_\nu|. \tag{1.14}$$

The viscous dissipation term Φ for micropolar fluid is given by

$$\Phi = \tau_1 \colon (\nabla \mathbf{V} - \boldsymbol{\epsilon} \cdot \boldsymbol{\Omega}) + \mathbf{M} \colon \nabla\boldsymbol{\Omega}. \tag{1.15}$$

1.5 Equations of motion for axisymmetric flow in micropolar fluid

Considering

$$\mathbf{V} = [u(r,z), 0, w(r,z)], \ \boldsymbol{\Omega} = [0, N_2(r,z), 0], \ T = T(r,z), \ C = C(r,z) \tag{1.16}$$

Eqs. $(1.5) - (1.7)$ along with the constitutive Eqs. $(1.10) - (1.15)$ yield [46] :

$$\frac{\partial u}{\partial r} + \frac{u}{r} + \frac{\partial w}{\partial z} = 0, \tag{1.17}$$

$$
\begin{aligned}
\frac{\partial u}{\partial t} + u\frac{\partial u}{\partial r} + w\frac{\partial u}{\partial z} &= -\frac{1}{\rho}\frac{\partial p}{\partial r} + \frac{1}{\rho}(\mu+k)\left[\frac{\partial^2 u}{\partial r^2} + \frac{1}{r}\frac{\partial u}{\partial r} + \frac{\partial^2 u}{\partial z^2} - \frac{u}{r^2}\right] \\
&\quad -\frac{k}{\rho}\frac{\partial N_2}{\partial z} - \frac{\sigma B_0^2}{\rho}u,
\end{aligned}
\tag{1.18}
$$

$$
\begin{aligned}
\frac{\partial w}{\partial t} + u\frac{\partial w}{\partial r} + w\frac{\partial w}{\partial z} &= -\frac{1}{\rho}\frac{\partial p}{\partial z} + \frac{1}{\rho}(\mu+k)\left[\frac{\partial^2 w}{\partial r^2} + \frac{1}{r}\frac{\partial w}{\partial r} + \frac{\partial^2 w}{\partial z^2}\right] - \frac{k}{\rho}\left[\frac{\partial N_2}{\partial r}\right. \\
&\quad \left. + \frac{N_2}{r}\right],
\end{aligned}
\tag{1.19}
$$

$$
\begin{aligned}
\frac{\partial N_2}{\partial t} + u\frac{\partial N_2}{\partial r} + w\frac{\partial N_2}{\partial z} &= \frac{\gamma_\nu}{\rho j}\left[\frac{\partial^2 N_2}{\partial r^2} + \frac{1}{r}\frac{\partial N_2}{\partial r} + \frac{\partial^2 N_2}{\partial z^2} - \frac{N_2}{r^2}\right] - \frac{k}{\rho j}\left[2N_2 + \frac{\partial w}{\partial r}\right. \\
&\quad \left. - \frac{\partial u}{\partial z}\right].
\end{aligned}
\tag{1.20}
$$

13

Using considered forms in Eq. (1.16) we have from Eqs. (1.8) and (1.9) the following expressions

$$\frac{\partial T}{\partial t} + u\frac{\partial T}{\partial r} + w\frac{\partial T}{\partial z} = \frac{K_c}{\rho c_p}\left[\frac{\partial^2 T}{\partial r^2} + \frac{1}{r}\frac{\partial T}{\partial r} + \frac{\partial^2 T}{\partial z^2}\right] + \frac{DK_T}{c_p C_s}\left[\frac{\partial^2 C}{\partial r^2} + \frac{1}{r}\frac{\partial C}{\partial r} + \frac{\partial^2 C}{\partial z^2}\right]$$

$$+\frac{(2\mu+k)}{\rho c_p}\left[\left(\frac{\partial u}{\partial r}\right)^2 + \frac{u^2}{r^2} + \left(\frac{\partial w}{\partial z}\right)^2 + \frac{1}{2}\left(\frac{\partial u}{\partial z} + \frac{\partial w}{\partial r}\right)^2\right] + \frac{1}{\sigma}J^2$$

$$+\frac{k}{2\rho c_p}\left(\frac{\partial u}{\partial z} - \frac{\partial w}{\partial r} - 2N_2\right)^2 - 2\beta_\nu\frac{N_2}{r}\frac{\partial N_2}{\partial r} + \frac{\gamma_\nu}{\rho c_p}\left[\left(\frac{\partial N_2}{\partial r}\right)^2 + \frac{N_2^2}{r^2} + \left(\frac{\partial N_2}{\partial z}\right)^2\right], \quad (1.21)$$

$$\frac{\partial C}{\partial t} + u\frac{\partial C}{\partial r} + w\frac{\partial C}{\partial z} = D\left[\frac{\partial^2 C}{\partial r^2} + \frac{1}{r}\frac{\partial C}{\partial r} + \frac{\partial^2 C}{\partial z^2}\right] + \frac{DK_T}{T_m}\left[\frac{\partial^2 T}{\partial r^2} + \frac{1}{r}\frac{\partial T}{\partial r} + \frac{\partial^2 T}{\partial z^2}\right] - K_1 C,$$

$$(1.22)$$

where u and w are the velocity components along the radial (r) and axial (z) directions respectively, N_2 is the azimuthal component of microrotation vector, J is the magnitude of current density, T is the temperature field, C is the concentration field, c_p is the specific heat, σ is the electrical conductivity of the fluid, K_c is the thermal conductivity, D is the diffusion coefficient, C_s is the concentration susceptibility, K_1 is the reaction rate, K_T is the thermal-diffusion ratio and T_m is the mean fluid temperature.

Chapter 2

Steady flow of second grade fluid in convergent/divergent channel

The aim of this chapter is to describe the flow of a differential type fluid in convergent/divergent channel. Constitutive relationships for second grade fluid are invoked in the mathematical modelling. Resulting non-linear problem is solved by homotopy analysis method (HAM). Convergence of developed series solution is checked. The effects of different physical parameters on velocity profile are shown and discussed. Numerical values of skin friction coefficient for different values of parameters are first tabulated and then analyzed.

2.1   Mathematical analysis

We consider the steady two-dimensional incompressible flow of second grade fluid in a converging/diverging channel. Flow is driven by a source/sink at the intersection of channel walls. The channel walls are inclined at an angle $2\alpha^*$. Symmetric nature of flow is taken about the central line $\vartheta = 0$. The radial and the axial directions are chosen parallel and perpendicular to the free stream flow respectively. Physical model is shown in Fig. 2.1. On defining the velocity field

$$\mathbf{V} = [u(r, \vartheta), 0] \tag{2.1}$$

and invoking continuity and momentum equations in the absence of body force one can write

$$\frac{\partial}{\partial r}\left(ru\right) = 0. \tag{2.2}$$

Integration of above equation with respect to r gives

$$u = \frac{1}{r}F\left(\vartheta\right), \tag{2.3}$$

where $F\left(\vartheta\right)$ is a constant of integration.

$$
\begin{aligned}
u\frac{\partial u}{\partial r} &= -\frac{1}{\rho}\frac{\partial p}{\partial r} + \nu\left[\frac{\partial^2 u}{\partial r^2} + \frac{1}{r}\frac{\partial u}{\partial r} + \frac{1}{r^2}\frac{\partial^2 u}{\partial \vartheta^2} - \frac{u}{r^2}\right] \\
&\quad - \frac{\alpha_1}{\rho}\left[2\frac{\partial u}{\partial r}\frac{\partial^3 u}{\partial r^3} + 2u\frac{\partial^2 u}{\partial r^2} - \frac{2}{r^3}\left(\frac{\partial u}{\partial \vartheta}\right)^2 - 2u\frac{\partial^2 u}{\partial \vartheta^2}\right. \\
&\quad \left. - \frac{4}{r^2}u\frac{\partial u}{\partial r} + \frac{4}{r}\left(\frac{\partial u}{\partial r}\right)^2 + \frac{2}{r^2}\frac{\partial u}{\partial r}\frac{\partial^2 u}{\partial r\partial\vartheta}\right],
\end{aligned} \tag{2.4}
$$

$$
\begin{aligned}
0 &= -\frac{1}{\rho r}\frac{\partial p}{\partial \vartheta} + \frac{2\nu}{r^2}\frac{\partial u}{\partial r} - \frac{\alpha_1}{\rho}\left[\frac{2}{r^2}u\frac{\partial^2 u}{\partial r\partial\vartheta} + \frac{2}{r^2}\frac{\partial u}{\partial r}\frac{\partial u}{\partial \vartheta}\right. \\
&\quad \left. \frac{2}{r}\frac{\partial^2 u}{\partial r^2}\frac{\partial u}{\partial \vartheta} + \frac{2}{r^2}\frac{\partial u}{\partial r}\frac{\partial^2 u}{\partial r\partial\vartheta} + \frac{2}{r^2}\frac{\partial u}{\partial \vartheta}\frac{\partial^2 u}{\partial \vartheta^2}\right],
\end{aligned} \tag{2.5}
$$

where $\alpha_1 \geq 0$ is the material constant of a second grade fluid.
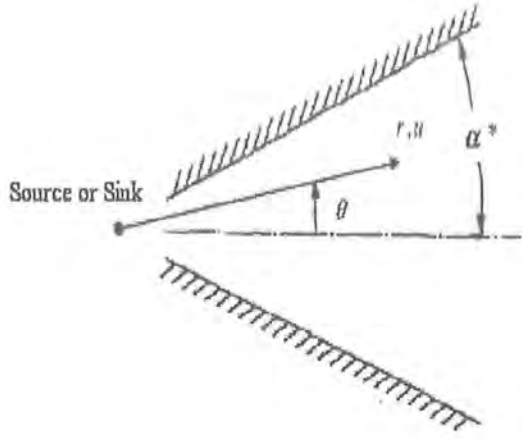
Fig. 2.1. Flow configuration $[1-8]$.

The corresponding boundary conditions are

$$
\begin{aligned}
u &= U, \ \frac{\partial u}{\partial \vartheta} = 0, \ \text{at} \ \vartheta = 0, \\
u &= 0, \qquad \text{at} \ \vartheta = \alpha^*,
\end{aligned}
\tag{2.6}
$$

where U is free stream velocity at the central line of the channel.

Introducing

$$
u = \frac{1}{r} F(\vartheta), \ \frac{u}{U} = f(\eta), \ \theta(\eta) = \frac{T}{T_w}, \ \eta = \frac{\vartheta}{\alpha^*},
\tag{2.7}
$$

in Eqs. $(2.2) - (2.6)$ and eliminating pressure terms one obtains

$$
f''' + 4\alpha^{*2} f' + 2\alpha^* \operatorname{Re} f f' + 4De \left(f f''' + 4\alpha^{*2} f f' \right) = 0,
\tag{2.8}
$$

$$
f(0) = 1, \ f(1) = 0, \ f'(0) = 0,
\tag{2.9}
$$

where $\operatorname{Re} (= r\alpha U/\nu)$, $De (= \alpha_1 U/r\mu)$ are the local Reynolds number and the local Deborah

17

number respectively. Furthermore

$$
\begin{cases}
\alpha^* > 0, \quad U > 0 \quad \text{for divergent channel,} \\
\alpha^* < 0, \quad U < 0 \quad \text{for convergent channel.}
\end{cases}
$$

It should be pointed out that the problem consisting of Eqs. (2.8) and (2.9) reduce to the case of a viscous fluid when $De = 0$ (Domairy et al. [7]).

The skin friction coefficient C_f is defined as

$$
C_f = \frac{\tau_{r\vartheta}|_{\vartheta=\alpha^*}}{\rho U^2} = \frac{\frac{\mu}{r}\frac{\partial u}{\partial \vartheta} + \alpha_1 \left(-\frac{2}{r^2} u \frac{\partial u}{\partial \vartheta} + \frac{1}{r} u \frac{\partial^2 u}{\partial r \partial \vartheta} + \frac{1}{r}\frac{\partial u}{\partial r}\frac{\partial u}{\partial \vartheta} \right)\Big|_{\vartheta=\alpha^*}}{\rho U^2}. \tag{2.10}
$$

The above expression in view of Eqs. (2.7) and (2.9) becomes

$$
\operatorname{Re} C_f = f'(1). \tag{2.11}
$$

Now the problem given in Eqs. (2.8) and (2.9) is computed by employing the homotopy analysis method [93 − 115].

2.2 Solution for $f(\eta)$

We express $f(\eta)$ by the set of base functions

$$
\left\{ \eta^{2n},\ n \geq 0 \right\}, \tag{2.12}
$$

in the form

$$
f(\eta) = \sum_{n=0}^{\infty} a_n \eta^{2n}, \tag{2.13}
$$

where a_n are the coefficients. The initial guess and linear operator are chosen as follows:

$$
f_0(\eta) = 1 - \eta^2, \tag{2.14}
$$

$$
\pounds_f(f) = \frac{d^3 f}{d\eta^3}. \tag{2.15}
$$

18

The above operator satisfies the following property

$$\pounds_f \left[C_1 + C_2\eta + C_3\eta^2 \right] = 0, \tag{2.16}$$

where C_i $(i = 1 - 3)$ are the arbitrary constants.

2.2.1 Zeroth order deformation problem

The zeroth order deformation problem can be written as

$$(1-q)\pounds_f \left[\hat{f}(\eta; q) - f_0(\eta) \right] = q\hbar_f \mathcal{N}_f \left[\hat{f}(\eta; q) \right], \tag{2.17}$$

$$\hat{f}(0; q) = 1, \quad \hat{f}(1; q) = 0, \quad \left. \frac{\partial \hat{f}(\eta; q)}{\partial \eta} \right|_{\eta=0} = 0. \tag{2.18}$$

Setting $q = 0$ and $q = 1$ in Eq. (2.17), one arrives at

$$\hat{f}(\eta; 0) = f_0(\eta),$$
$$\hat{f}(\eta; 1) = f(\eta),$$

It means when q varies from 0 to 1, then $\hat{f}(\eta; q)$ varies from the initial guess $f_0(\eta)$ to $f(\eta)$. We further led to define the following nonlinear operator $\mathcal{N}_f$

$$\mathcal{N}_f \left[\hat{f}(\eta; q) \right] = \frac{\partial^3 \hat{f}(\eta; q)}{\partial \eta^3} + 4\alpha^{*2} \frac{\partial \hat{f}(\eta; q)}{\partial \eta} + 2 \operatorname{Re} \alpha^* \hat{f}(\eta; q) \frac{\partial \hat{f}(\eta; q)}{\partial \eta}$$
$$+ 4De \left[\hat{f}(\eta; q) \frac{\partial^3 \hat{f}(\eta; q)}{\partial \eta^3} + 4\alpha^{*2} \hat{f}(\eta; q) \frac{\partial \hat{f}(\eta; q)}{\partial \eta} \right]. \tag{2.19}$$

With the help of Taylor's theorem one obtains

$$\hat{f}(\eta; q) = f_0(\eta) + \sum_{m=1}^{\infty} f_m(\eta) q^m, \tag{2.20}$$

with

$$f_m(\eta) = \frac{1}{m!} \left. \frac{\partial^m \hat{f}(\eta; q)}{\partial \eta^m} \right|_{q=0}. \tag{2.21}$$

19

2.2.2 Higher-order deformation problems

Taking mth order homotopy derivative $(d^m/dq^m)/m!$ to zeroth order deformation (*i.e.* Eq. (2.17)) and setting $q = 1$ we get the following mth order deformation problems

$$\mathcal{L}_f\left[f_m(\eta) - \chi_m f_{m-1}(\eta)\right] = \hbar_f \mathcal{R}_m^f\left(f_{m-1}(\eta)\right), \tag{2.22}$$

$$f_m(0) = 0, \ f_m(1) = 0, \ f_m'(0) = 0, \tag{2.23}$$

in which

$$\chi_m = \begin{cases} 0, m \leq 1, \\ 1, m > 1, \end{cases}$$

$$\mathcal{R}_m^f\left(f_{m-1}(\eta)\right) = f_{m-1}'''(\eta) + 4\alpha^{*2}f_{m-1}'(\eta) + 2\alpha^* \operatorname{Re} \sum_{n=0}^{m-1} f_n(\eta) f_{m-1-n}'(\eta)$$

$$+ 4De \sum_{n=0}^{m-1}\left[f_n(\eta) f_{m-1-n}'''(\eta) + 4\alpha^{*2}f_n(\eta) f_{m-1-n}'(\eta)\right]. \tag{2.24}$$

The general solution of boundary value problem given in Eqs . (2.22) and (2.22) is

$$f_m(\eta) = f_m^*(\eta) + C_1^m + C_2^m\eta + C_3^m\eta^3, \tag{2.25}$$

in which $f_m^*(\eta)$ is the particular solution of problem given in Eqs. (2.22) and (2.23). The coefficients $C_i^m (i = 1 - 3)$ can be determined by the boundary conditions given in Eq. (2.23).

In order to proceed for the dual solutions, let us make the change of variable $y = 4Def$ in Eqs. (2.8) and (2.9) to get

$$y''' + 4\alpha^{*2}\frac{y}{1+y} + \left(\frac{\alpha^* \operatorname{Re}}{2De} + 4\alpha^{*2}\right)\frac{yy'}{1+y} = 0, \tag{2.26}$$

$$y(0) = 4De, \ y'(0) = 0, \ y(1) = 0. \tag{2.27}$$

Integration of Eq. (2.26) with respect to variable η yields

$$y'' + 4\alpha^{*2}\ln|1+y| + \left(\frac{\alpha^* \operatorname{Re}}{2De} + 4\alpha^{*2}\right)\left[y - \ln|1+y|\right] = C_4, \tag{2.28}$$

where C_4 is the constant of integration. Multiplying Eq. (2.28) by y' and then integrating with respect to variable η one can write

$$
\begin{aligned}
&\left(y'\right)^2 + 4\alpha^{*2}\left[(1+y)\ln|1+y| - y\right] + \left(\frac{\alpha^*\operatorname{Re}}{2De} + 4\alpha^{*2}\right)\left[\frac{y^2}{2} + y - (1+y)\ln|1+y|\right] \\
&= C_4 y + C_5,
\end{aligned}
\tag{2.29}
$$

in which C_5 is also constant of integration. Using the boundary conditions $y(0) = 4De$ and $y'(0) = 0$ in Eq. (2.29) we get

$$
4DeC_4 + C_5 = A,
$$

with

$$
A = 4\alpha^{*2}\left[(1+4De)\ln|14De| - 4De\right] + \left(\frac{\alpha^*\operatorname{Re}}{2De} + 4\alpha^{*2}\right)\left[8De + 4De - (1+4De)\ln|1+4De|\right].
$$

Separating the variables and then integrating we have

$$
\pm \int \frac{1}{\sqrt{2\left(\begin{array}{l} C_4 y + C_5 - 4\alpha^{*2}\left[(1+y)\ln|1+y| - y\right] \\ -\left(\frac{\alpha^*\operatorname{Re}}{2De} + 4\alpha^{*2}\right)\left(\frac{y^2}{2} + y - (1+y)\ln|1+y|\right) \end{array}\right)}} dy = \eta + C_6,
\tag{2.30}
$$

where C_6 is the constant of integration.

2.3 Results and discussion

The convergence of HAM solution (2.25) strongly depends upon the value of convergence control parameter (auxiliary parameter) $\hbar_f$. Therefore we plot the $\hbar_f$ - curves (Fig. 2.2) for different values of Deborah number De. Range for convergence of solution in present flow situation is $-0.45 \leq \hbar_f \leq -0.25$ when $0 \leq \eta \leq 1$. The convergence is ensured up to $12th$ order of approximation when $\hbar_f$ is equal to -0.3. (see Table 2.1). Tables 2.2 and 2.3 are constructed in order to examine the behavior of dimensionless parameters on skin friction coefficient $\operatorname{Re}_r C_f$ in convergent and divergent channels.

Figs. $2.3 - 2.6$ are sketched to examine the influence of different dimensionless quantities,

21

for instance, Reynolds number Re, Deborah number De and the angle α^* between the central line $\vartheta = 0$ and one of the channel walls. Fig. 2.3 shows that dimensionless velocity $f(\eta)$ decreases with an increase of Reynolds number Re in divergent channel whereas $f(\eta)$ increases in convergent channel as shown in Fig. 2.4. Figs. 2.5 and 2.6 depict the effect of Deborah number De on dimensionless velocity $f(\eta)$. These Figs. indicate that in divergent channel $f(\eta)$ is an increasing function of Deborah number De but in convergent channel $f(\eta)$ decreases as Deborah number De increases. The influence of variation of inclination $(2\alpha^*)$ between the channel walls on $f(\eta)$ is analyzed in the Figs. 2.7 and 2.8. It is observed from Fig. 2.7 that with an increase in inclination between the walls of divergent channel $f(\eta)$ decreases . However in case of convergent channel, $f(\eta)$ increases when α^* increases (see Fig. 2.8). Tables 2.2 and 2.3 are constructed to see the effects of Reynolds number Re, Deborah number De and angle α^* on the skin friction coefficient $\mathrm{Re}_r\, C_f$. Table 2.2 shows that, in divergent channel, the magnitude of skin friction coefficient $\mathrm{Re}_r\, C_f$ decreases when Reynolds number Re and angle α^* are increased whereas, in convergent channel, the magnitude of $\mathrm{Re}_r\, C_f$ increases when Deborah number De is increased. However, in convergent channel, the skin friction coefficient $\mathrm{Re}_r\, C_f$ is an increasing function of Re and α^* but $\mathrm{Re}_r\, C_f$ is a decreasing function of De when $\alpha^* > 0$. This shows that stresses on the walls of divergent channel are increasing function of De whereas stresses on the walls of convergent channel are decreased when De is increased. From Table 2.2 one can see that the skin friction coefficient $\mathrm{Re}_r\, C_f$ in case of non-Newtonian fluid is higher than that of viscous fluid in divergent channel. In convergent channel the skin friction coefficient $\mathrm{Re}_r\, C_f$ in viscous fluid is higher than that in second grade fluid (Table 2.3) and vice versa in divergent channel (see Table 2.2).
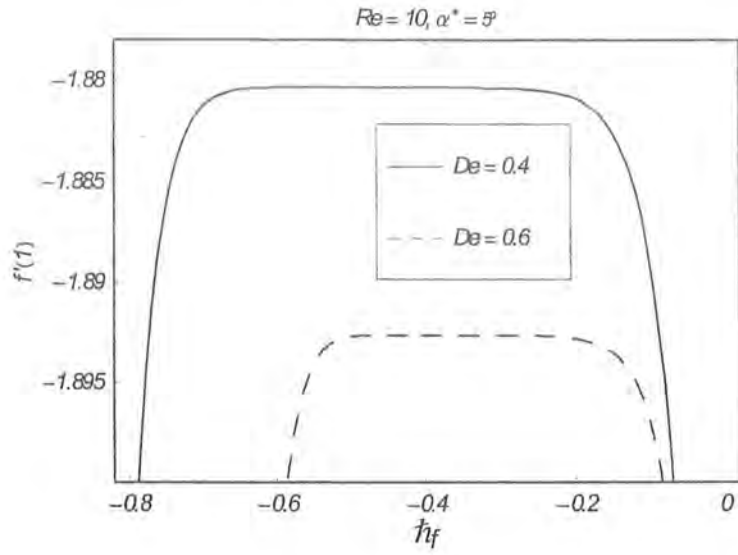
Fig. 2.2. $\hbar_f$-curves of 12th order of approximation of $f'(1)$ for different values of De.
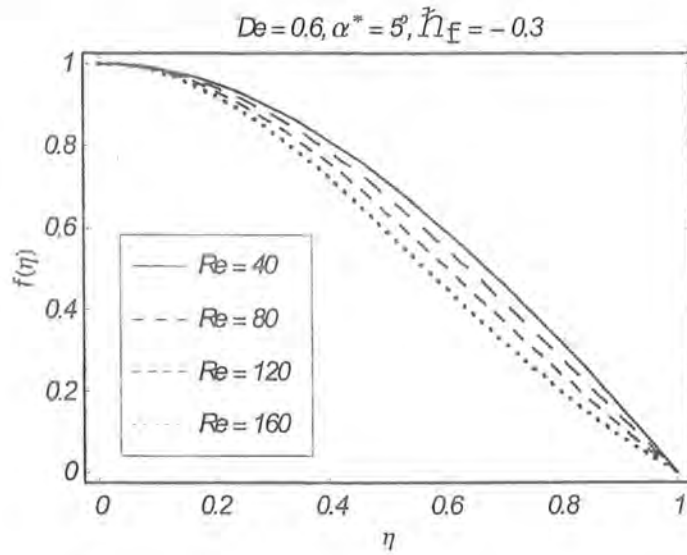
Fig. 2.3. Variation of $f(\eta)$ for different values of Reynolds number Re in divergent channel.
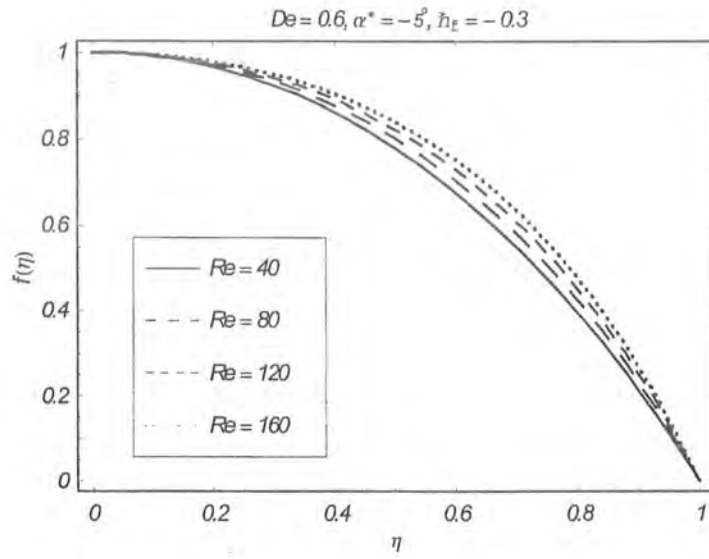
Fig. 2.4. Variation of $f(\eta)$ for different values of Reynolds number Re in convergent channel.
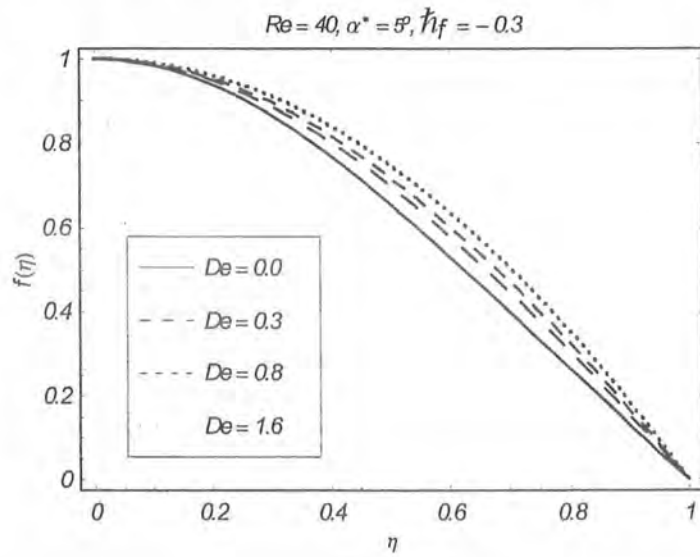
Fig. 2.5. Variation of $f(\eta)$ for different values of Deborah number De in divergent channel.

24
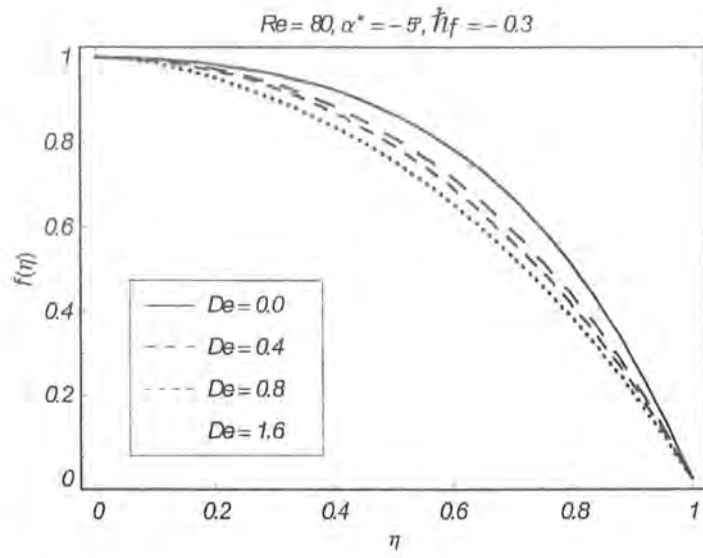
Fig. 2.6. Variation of $f(\eta)$ for different values of Deborah number De in convergent channel.
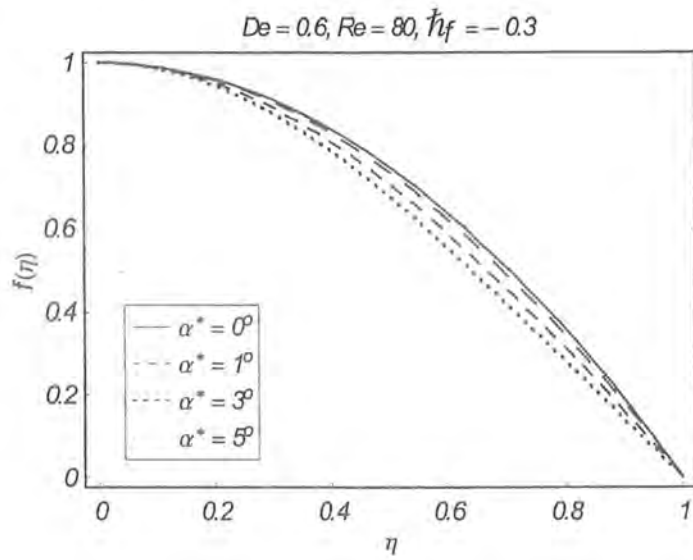
Fig. 2.7. Variation of radial velocity $f(\eta)$ for different values of $\alpha^* \geq 0$.
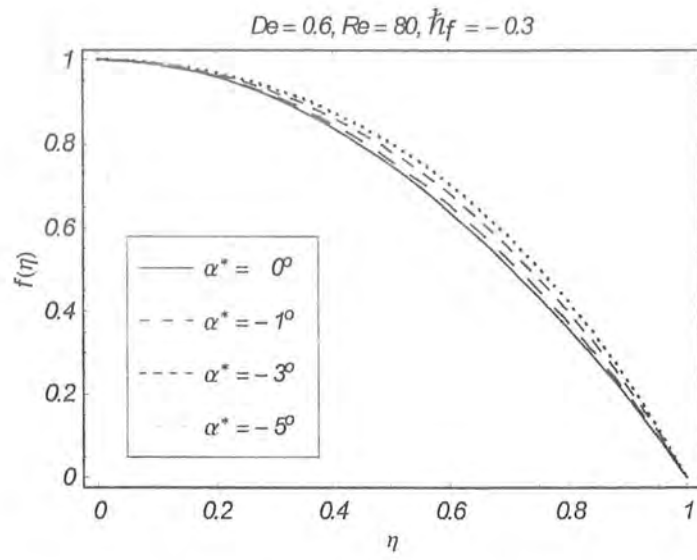
Fig. 2.8. Variation of radial velocity $f(\eta)$ for different values of $\alpha^* \leq 0$.

Table 2.1. Convergence of HAM solution when Re = 100, $De = 0.5$ and $\alpha^* = 5^o$

order of approximations	$f'(1)$
1	-1.72644
5	-1.59923
10	-1.59413
15	-1.59389
20	-1.59388
25	-1.59388
30	-1.59388

Table 2.2. Numerical values of skin friction coefficient $\mathrm{Re}_r\, C_f$ for different values of Re, De and α^* in divergent channel.

Re	De	α^*	$\mathrm{Re}_r\, C_f$
40	0.8	2°	-1.90964
80			-1.81347
120			-1.71881
160			-1.62295
100	0.0	2°	-1.28910
	0.4		-1.65067
	0.8		-1.76629
	1.2		-1.77509
100	0.8	0°	-2.00000
		2°	-1.76629
		4°	-1.52330
		6°	-1.27140

Table 2.3. Numerical values of skin friction coefficient $\text{Re}_r C_f$ for different values of Re, De and α^* in convergent channel.

Re	De	α^*	$\text{Re}_r C_f$
40	0.8	-2°	-2.09020
80			-2.17999
120			-2.26856
160			-2.35591
100	0.0	-2°	-2.67796
	0.4		-2.33315
	0.8		-2.24443
	1.2		-2.11700
100	0.8	0°	-2.00000
		-2°	-2.24443
		-4°	-2.43997
		-6°	-2.64644

2.4 Conclusions

The flow of second grade fluid in convergent/divergent channel is analyzed by homotopy analysis method (HAM). The effects of different physical quantities are presented via graphs. Following points are worth mentioning

- The effects of Re, De and α^* on $f(\eta)$ in divergent channel are quite opposite to the effects of Re, De and α^* on $f(\eta)$ in convergent channel.

- The dimensionless velocity $f(\eta)$ in divergent channel is a decreasing function of Reynold number Re. However opposite trend are noted for the case of convergent channel.

- $f(\eta)$ increases in case of divergent channel when Deborah number De increases whereas $f(\eta)$ decreases in divergent channel when α^* increases. Furthermore the dimensionless velocity $f(\eta)$ of Newtonian ($De = 0$) fluid is less than that of non-Newtonian fluid ($De \neq 0$) in divergent channel but in convergent channel the velocity of Newtonian ($De = 0$) is higher than that in non-Newtonian fluid ($De \neq 0$).

28

- The effects of Re, De and α^* on the skin friction coefficient $\mathrm{Re}_r\, C_f$ in divergent and convergent channel are opposite.

- In case of divergent channel, the magnitude of skin friction coefficient $\mathrm{Re}_r\, C_f$ decreases when Reynolds number Re is increased. It means that stresses at the surface of the channel walls decreases with an increase in Reynolds number Re whereas in case of convergent channel the magnitude of skin friction coefficient $\mathrm{Re}_r\, C_f$ increases when Reynolds number Re is increased. Increase in Reynolds number Re means to increase free stream velocity (velocity U at the central line of the channel). Hence we conclude that the behavior of free stream on the velocity in divergent channel is opposite to that of velocity in convergent channels.

- For non-Newtonian fluid ($De \neq 0$), the magnitude of stresses at walls of divergent channel is higher than Newtonian fluid ($De = 0$) whereas for convergent channel opposite trend is observed.

- An an increase in angle between channel walls results to decrease magnitude of stresses at the surface of walls of divergent channel. However opposite trend has been noted for the case of convergent channel.

Chapter 3

Heat transfer effect on the flow of a second grade fluid in convergent/divergent channel

This chapter extends the flow analysis of previous chapter in the presence of heat transfer. Attention has been focused for the analysis of temperature. The relevant expression is modeled by using law of conservation of energy. Dissipation effects are taken into account. Homotopic solution along with convergence analysis is presented. Results of dimensionless temperature are presented and discussed. Variation of Nusselt number for the physical parameters is analyzed.

3.1 Heat transfer analysis

We consider the heat transfer analysis for the steady two-dimensional incompressible flow of a second grade fluid in a converging/diverging channel. Here source/sink at the intersection of channel walls is responsible for the flow. Both of the channel walls are maintained at constant temperature T_w. The channel walls are inclined at an angle $2\alpha^*$. Both of the channel walls are maintained at constant temperature T_w. Symmetric nature of the flow is taken into account about the central line $\vartheta = 0$. The radial and axial directions are chosen parallel and perpendicular to the free stream flow. Velocity and temperature fields for the flow under consideration

are

$$\mathbf{V} = [u(r,\vartheta),0], \ T = T(r,\vartheta), \tag{3.1}$$

and invoking the energy equation in the absence of Joule heating we have

$$\rho c_p u \frac{\partial T}{\partial r} = K_c \left[\frac{\partial^2 T}{\partial r^2} + \frac{1}{r} \frac{\partial T}{\partial r} + \frac{1}{r^2} \frac{\partial^2 T}{\partial \vartheta^2} \right] + \mu \left[4 \left(\frac{\partial u}{\partial r} \right)^2 + \frac{1}{r^2} \left(\frac{\partial u}{\partial \vartheta} \right)^2 \right]$$

$$+ \alpha_1 \left[u \frac{\partial}{\partial r} \left(\frac{\partial u}{\partial r} \right)^2 + \frac{u}{r^2} \frac{\partial u}{\partial \vartheta} \frac{\partial^2 u}{\partial r \partial \vartheta} + 4 \frac{u^2}{r^2} \frac{\partial u}{\partial r} - \frac{u}{r^3} \left(\frac{\partial u}{\partial \vartheta} \right)^2 \right], \tag{3.2}$$

where $\alpha_1 \geq 0$ is the material constant of a second grade fluid. The subjected boundary conditions are

$$\frac{\partial T}{\partial \vartheta} = 0 \ \text{ at } \ \vartheta = 0, \ T = T_w \ \text{ at } \ \vartheta = \alpha^*, \tag{3.3}$$

where T_w indicates the constant wall temperature. Utilizing the following dimensionless variables

$$u = \frac{1}{r} F(\vartheta), \ \frac{u}{U} = f(\eta), \ \theta(\eta) = \frac{T}{T_w}, \ \eta = \frac{\vartheta}{\alpha^*}, \tag{3.4}$$

in Eq. (3.2) we arrive at

$$\theta'' + Ec \Pr \left(4\alpha^{*2} f^2 + f'^2 \right) + 2De \Pr Ec \left(4\alpha^{*2} f^3 + f f'^2 \right) = 0. \tag{3.5}$$

Boundary conditions (3.3) take the form

$$\theta(1) = 1, \ \ \theta'(0) = 0, \tag{3.6}$$

where Re $(= r\alpha U/\nu)$, De $(= \alpha_1 U/r\mu)$, Pr $(= \mu c_p/K_c)$ and Ec $(= U^2/c_p T_w)$ are the Reynold number, local Deborah number, Prandtl number and Eckert number respectively and

$$\begin{cases} \alpha^* > 0, \ \ U > 0 \ \ \text{for divergent channel,} \\ \alpha^* < 0, \ \ U < 0 \ \ \text{for convergent channel.} \end{cases}$$

It is important to note that dimensionless parameters Pr, Ec, De and Re have similar effects on dimensionless temperature $\theta(\eta)$ in both the convergent and the divergent channels because Eq.

31

(3.5) contains α^{*2} where $\alpha^* < 0$ characterizes convergent channel whereas $\alpha^* > 0$ corresponds to divergent channel. Nusselt number N_u is given by

$$Nu = \frac{\alpha q_w|_{\vartheta=\alpha^*}}{K_c T_w}, \tag{3.7}$$

where the heat flux q_w through Fourier law of conduction is defined as

$$q_w = -K_c \frac{\partial T}{\partial \vartheta}. \tag{3.8}$$

Equations. (3.4), (3.7) and (3.8) yield

$$Nu = -\theta'(1).$$

In the next section, series solution of the boundary value problem consisting of Eqs. (3.5) and (3.6) will be constructed.

3.2 Solution for $\theta(\eta)$

The dimensionless temperature $\theta(\eta)$ in term of base functions

$$\left\{ \eta^{2n}, \ n \geq 0 \right\}, \tag{3.9}$$

can be expressed as

$$\theta(\eta) = \sum_{n=0}^{\infty} a_n \eta^{2n}, \tag{3.10}$$

where a_n are the coefficients. Initial guess and the linear operator are selected as follows:

$$\theta_0(\eta) = \eta^2, \tag{3.11}$$

$$\mathcal{L}_\theta(\theta) = \frac{d^2\theta}{d\eta^2}. \tag{3.12}$$

32

The above linear operator satisfies

$$\pounds_\theta \left[C_1 + C_2 \eta \right] = 0, \tag{3.13}$$

where C_i $(i = 1, 2)$ are the arbitrary constants.

3.2.1 Zeroth order deformation problem

The zeroth order deformation problem is constructed in the following forms

$$(1 - q)\pounds_\theta \left[\hat{\theta}(\eta; q) - \theta_0(\eta) \right] = q \hbar_\theta \mathcal{N}_\theta \left[\hat{\theta}(\eta; q) \right], \tag{3.14}$$

$$\hat{\theta}(1; q) = 1, \quad \left. \frac{\partial \hat{\theta}(\eta; q)}{\partial \eta} \right|_{\eta=1} = 0. \tag{3.15}$$

where $q \in [0, 1]$ is an embedding parameter. For $q = 0$ and $q = 1$, we obtain

$$\hat{\theta}(\eta, 0) = \theta_0(\eta), \quad \hat{\theta}(\eta, 1) = \theta(\eta). \tag{3.16}$$

It is worth mentioning that the initial guess $\theta_0(\eta)$ approaches $\theta(\eta)$, when q varies from 0 to 1. With the help of Taylor's series we can express $\hat{\theta}(\eta, q)$ in the form of following infinite series

$$\hat{\theta}(\eta, q) = \theta_0(\eta) + \sum_{m=1}^{\infty} \theta_m(\eta) q^m, \tag{3.17}$$

with

$$\theta_m(\eta) = \frac{1}{m!} \left. \frac{\partial^m \hat{\theta}(\eta, q)}{\partial q^m} \right|_{q=0} \tag{3.18}$$

and nonlinear operator $\mathcal{N}_\theta$ is

$$\mathcal{N}_\theta \left[\hat{\theta}(\eta; q), \hat{f}(\eta; q) \right] = \frac{\partial^2 \hat{\theta}}{\partial \eta^2} + Ec \Pr \left[4\alpha^{*2} \left(\hat{f}(\eta; q) \right)^2 + \left(\frac{\partial \hat{f}(\eta; q)}{\partial \eta} \right)^2 \right]$$

$$+ 2De \Pr Ec \left[4\alpha^{*2} \left(\hat{f}(\eta; q) \right)^3 + \hat{f}(\eta; q) \left(\frac{\partial \hat{f}(\eta; q)}{\partial \eta} \right)^2 \right]. \tag{3.19}$$

33

3.2.2 Higher-order deformation problem

Differentiating the zeroth order deformation Eq. (3.14) with respect q then dividing by $m!$ and then having $q = 1$, we obtain the following mth-order formation problems

$$\mathcal{L}_\theta \left[\theta_m(\eta) - \chi_m \theta_{m-1}(\eta) \right] = \hbar_\theta \mathcal{R}_m^\theta \left(\theta_{m-1}(\eta), f_{m-1}(\eta) \right),$$
$$\theta_m(1) = 0, \ \theta_m'(0) = 0, \tag{3.20}$$

in which

$$\chi_m = \begin{cases} 0, m \le 1, \\ 1, m > 1, \end{cases}$$

$$\mathcal{R}_m^\theta \left(\theta_{m-1}(\eta) \right) = \theta_{m-1}''(\eta) + Ec\,Pr \left(\begin{array}{c} 4\alpha^{*2} \sum_{n=0}^{m-1} f_n(\eta) f_{m-1-n}(\eta) \\ + \sum_{n=0}^{m-1} f_n'(\eta) f_{m-1-n}'(\eta) \end{array} \right)$$
$$+ 2De\,Pr\,Ec \left[\begin{array}{c} 4\alpha^{*2} \sum_{n=0}^{m-1} \sum_{l=0}^{n} f_{m-1-n}(\eta) f_{n-l}(\eta) f_l(\eta) \\ + \sum_{n=0}^{m-1} \sum_{l=0}^{n} f_{m-1-n}(\eta) f_{n-l}'(\eta) f_l'(\eta) \end{array} \right]. \tag{3.21}$$

The general solution of the boundary value problem (3.20) is

$$\theta_m(\eta) = \theta_m^*(\eta) + C_1^m + C_2^m \eta, \tag{3.22}$$

in which $\theta_m^*(\eta)$ is the particular solution of problem (3.20). The coefficients $C_i^m (i = 1, 2)$ can be determined using the boundary conditions given in Eq. (3.20).

3.3 Convergence analysis for $\theta(\eta)$

Obviously the series solution (3.22) has auxiliary parameter $\hbar_\theta$. As pointed out by Liao [93], the convergence of series solution depends upon the suitable choice of $\hbar_\theta$. Having this in mind, $\hbar_\theta$−curves are plotted for different values of De. These $\hbar_\theta$−curves depict that the range for convergence of solution $\theta(\eta)$ is $-1.4 \le \hbar_\theta \le -0.6$ in the whole domain $0 \le \eta \le 1$ (see Fig. 3.1). The convergence is ensured when $\hbar_\theta = -0.7$.

Table 3.1. Convergence of series solution (3.22) when $\Pr = 5$, $\mathrm{Re} = 100$, $De = Ec = 0.5$ and $\alpha^* = 5^o$.

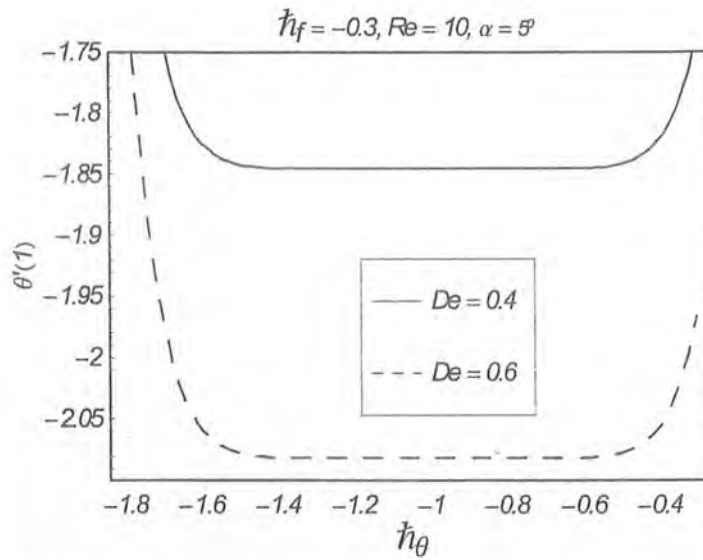| order of approximations	$\theta'(1)$
1	-3.3933086
5	-4.2357855
10	-4.2674518
15	-4.2692967
20	-4.2694280
25	-4.2694391
30	-4.2694402
35	-4.2694403
40	-4.2694403
45	-4.2694403

Fig. 3.1. $\hbar_\theta$-curves of $\theta'(1)$ for different values of Deborah number De.

35

3.4 Discussion

In this section we have examined the behavior of dimensionless parameters on the dimensionless temperature $\theta(\eta)$. Variation of Nusselt number Nu against various values of the dimensionless parameters is presented in Table 3.2. Since dimensionless parameters have similar effects on dimensionless temperature $\theta(\eta)$ for both the cases (i) $\alpha^* > 0$ (ii) $\alpha^* < 0$ (see Eq. (3.5)). Therefore temperature profiles are sketched for positive values of α^*. Fig. 3.2 reveals that dimensionless temperature $\theta(\eta)$ increases when Prandtl number Pr is increased. It is clear from Fig. 3.3 that $\theta(\eta)$ is an increasing function of the local Deborah number De. This Fig. also shows that temperature in second grade fluid $(De \neq 0)$ is higher than that of Newtonian fluid $(De = 0)$. The dimensionless temperature is an increasing function of Reynolds number Re (as shown in Fig. 3.4). It is observed from Fig. 3.5 that dimensionless temperature $\theta(\eta)$ increases by increasing inclination between the channel walls. Since Ec is the ratio of kinetic energy to enthalpy. Thus an increase in Eckert number Ec increases kinetic energy and consequently temperature increases. This fact is obvious from Fig. 3.6. Note that $Ec = 0$ when viscous dissipation is negligible and $Ec \neq 0$ is the case when viscous dissipation is significant. In other words an increase in Eckert number Ec results to dissipates more heat and so temperature increases. Table 3.2 shows the variation of Nusselt number Nu for different values of parameters. From Table 3.2 one can conclude that Nu is an increasing function of De, Pr, Ec. It decreases with an increase in Re and α^*. This Table also depicts that the Nusselt number Nu for second grade fluid $(De \neq 0)$ is higher than Newtonian fluid $(De = 0)$.

Table 3.2. Numerical values of Nusselt number Nu for different values of Re, De, α^*, Pr and Ec.

Re	De	Pr	Ec	α^*	$-Nu$
40	0.8	5	0.5	5°	5.34102
80					5.19476
120					5.09998
160					5.06849
100	0.00	5	0.5	5°	2.96815
	0.25				3.54436
	0.50				4.26952
	0.75				5.03598
100	0.8	1	0.5	5°	1.02804
		3			3.08413
		5			5.14021
		7			7.19630
100	0.8	100	0.3	5°	3.08413
			0.5		5.14021
			0.7		7.19630
			0.9		9.25239
100	0.8	5	0.5	0°	5.46667
				2^0	5.28043
				4°	5.16667
				6°	5.13443

Fig. 3.2. Variation of dimensionless temperature $\theta\left(\eta\right)$ for different values of Prandtl number Pr.

Fig. 3.3. Variation of dimensionless temperature $\theta\left(\eta\right)$ for different values of Deborah number De.
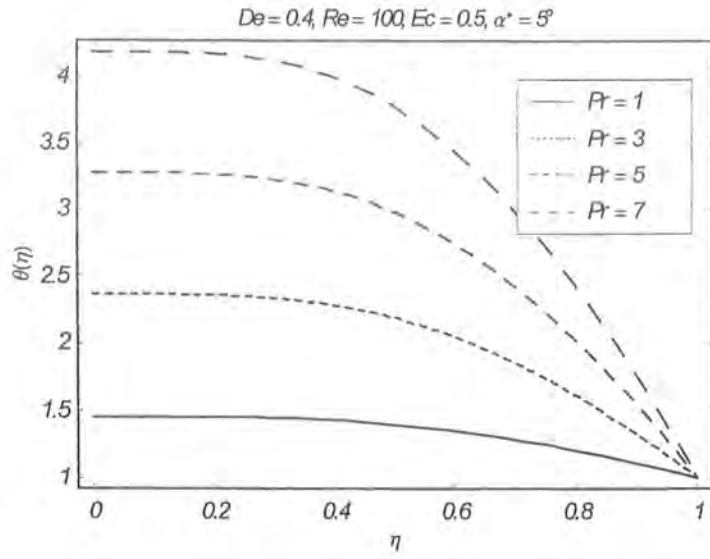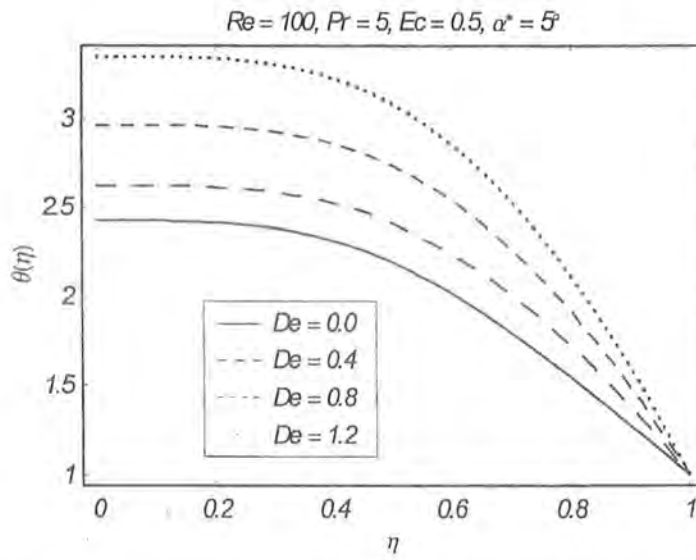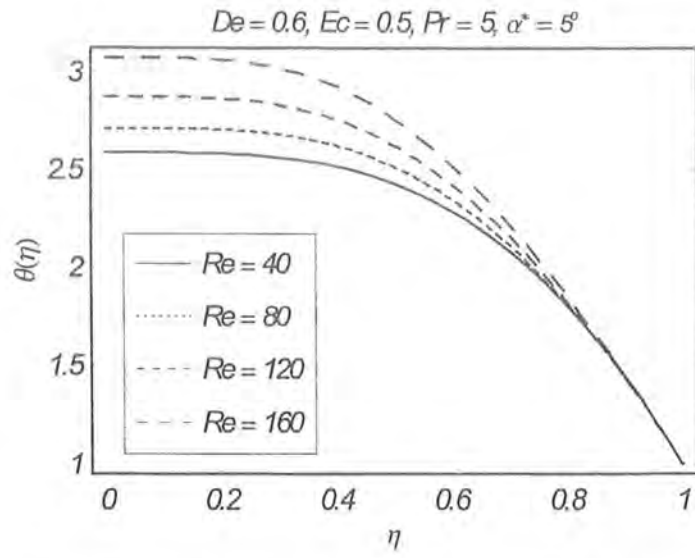
Fig. 3.4. Variation of dimensionless temperature $\theta(\eta)$ for different values of Reynolds number Re.
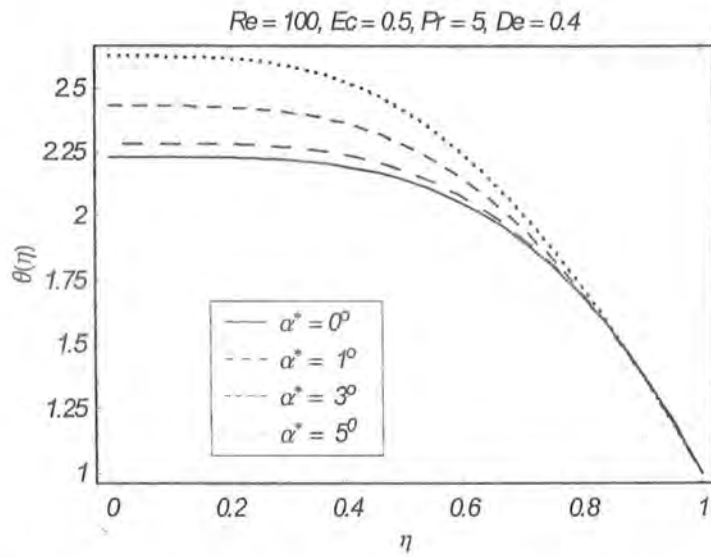
Fig. 3.5. Variation of dimensionless temperature $\theta(\eta)$ for different values of α^*.
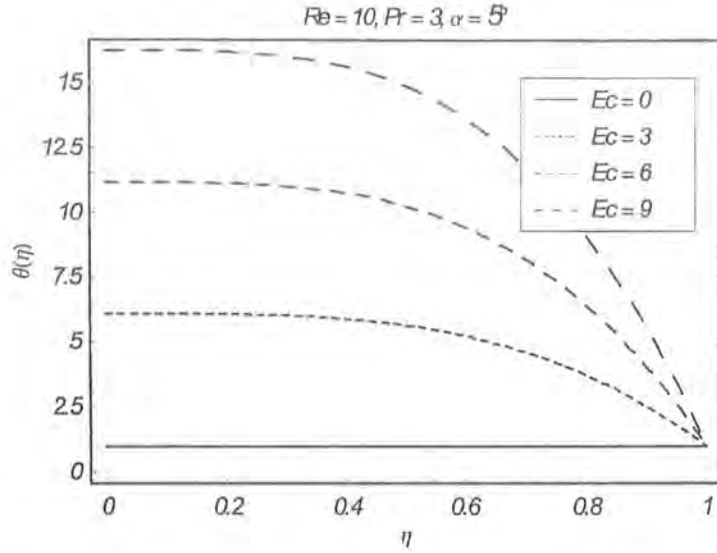
Fig. 3.6. Variation of dimensionless temperature $\theta(\eta)$ for different values of Ec.

3.5 Concluding remarks

The work here is concerned with the influence of heat transfer on the flow of a second grade fluid in divergent/convergent channel. The presented analysis has following interesting observations.

- Dimensionless temperature $\theta(\eta)$ in second grade fluid $(De \neq 0)$ is higher than that in Newtonian fluid $(De = 0)$.

- $\theta(\eta)$ is an increasing function of Re, De, Pr and Ec.

- Nusselt number Nu increases by increasing De, Pr and Ec. However it decreases with an increase in Re and α^*.

- Nusselt number Nu for second grade fluid $(De \neq 0)$ is higher than Newtonian fluid $(De = 0)$.

- Rate of heat transfer from channel walls into the fluid increases when De and Ec are increased whereas it decreases by increasing Re.

- Temperature $\theta(\eta)$ is an increasing function of angle α^* between the walls of channel whereas Nusselt number Nu decreases when α^* (angle between channel walls) increases.

Chapter 4

Thermal-diffusion and diffusion-thermo effects on axisymmetric flow of a second grade fluid between radially stretching sheets

This chapter investigates the thermal-diffusion and diffusion-thermo effects on two-dimensional magnetohydrodynamic (MHD) axisymmertric flow of a second grade fluid. Mathematical analysis has been carried out in the presence of Joule heating, viscous dissipation and first order chemical reaction. Using momentum and energy equations and Fick's second law, the governing partial differential equations have been reduced to the ordinary differential equations by suitable transformations. Series solutions are constructed by homotopy analysis method (HAM). Plots are displayed in order to examine the influence of emerging parameters on the dimensionless components of velocity, temperature and concentration fields. Numerical computations for skin friction coefficient, Nusselt number and Sherwood number are tabulated.

4.1 Problem statement

We consider heat and mass transfer characteristics on axisymmetric flow of an electrically conducting second grade fluid between two infinite parallel radially stretching sheets at $z = \pm L$. The flow is induced by the stretching of sheets. The flow is considered symmetric about $z = 0$. A uniform magnetic field $\mathbf{B}_o$ perpendicular to the planes of sheets is applied. It is assumed that the magnetic Reynolds number is very small and induced magnetic field is neglected. There is no external electric field. Joule heating and viscous dissipation are taken into account. Both the sheets have constant temperature T_w and constant concentration at the sheets is denoted by C_w. Physical model and coordinate system are shown in Fig. 4.1. Flow quantities for the problem under consideration are defined by

$$\mathbf{V} = [u(r,z), 0, w(r,z)], \ T = T(r,z), \ C = C(r,z). \tag{4.1}$$

By virtue of above definitions, continuity equation, momentum equation (in the absence of buoyancy force), energy equation and advection diffusion equation (with first order chemical reaction *i.e.* $n = 1$) along with constitutive equations $(1.1) - (1.4)$ give

$$\frac{\partial u}{\partial r} + \frac{u}{r} + \frac{\partial w}{\partial z} = 0, \tag{4.2}$$

$$
\begin{aligned}
u\frac{\partial u}{\partial r} + w\frac{\partial u}{\partial z} =\ & -\frac{1}{\rho}\frac{\partial p}{\partial r} + \nu\left[\frac{\partial^2 u}{\partial r^2} + \frac{1}{r}\frac{\partial u}{\partial r} + \frac{\partial^2 u}{\partial z^2} - \frac{u}{r^2}\right] \\
& + \frac{\alpha_1}{\rho}\left[\frac{2u^2}{r^3} - \frac{2w}{r^2}\frac{\partial u}{\partial z} - \frac{1}{r}\left(\frac{\partial u}{\partial z}\right)^2 - \frac{\partial u}{\partial z}\frac{\partial^2 w}{\partial z^2} + w\frac{\partial^3 u}{\partial z^3}\right. \\
& - \frac{2u}{r^2}\frac{\partial u}{\partial r} + \frac{\partial u}{\partial r}\frac{\partial^2 u}{\partial z^2} + \frac{\partial w}{\partial r}\frac{\partial^2 w}{\partial z^2} + \frac{1}{r}\left(\frac{\partial w}{\partial z}\right)^2 + w\frac{\partial^3 w}{\partial r\partial z^2} \\
& + \frac{2w}{r}\frac{\partial^2 u}{\partial r\partial z} + 2\frac{\partial w}{\partial z}\frac{\partial^2 w}{\partial r\partial z} - \frac{\partial u}{\partial r}\frac{\partial^2 w}{\partial r\partial z} + u\frac{\partial^2 u}{\partial r\partial z^2} + \frac{2u}{r}\frac{\partial^2 u}{\partial r^2} \\
& + 2\frac{\partial u}{\partial r}\frac{\partial^2 u}{\partial r^2} + \frac{\partial u}{\partial z}\frac{\partial^2 w}{\partial r^2} + 2\frac{\partial w}{\partial r}\frac{\partial^2 w}{\partial r^2} + 2w\frac{\partial^3 u}{\partial r^2\partial z} \\
& \left. + u\frac{\partial^3 w}{\partial r^2\partial z} + 2u\frac{\partial^3 u}{\partial r^3}\right] - \frac{\sigma B_0^2}{\rho}u,
\end{aligned}
\tag{4.3}
$$

$$u\frac{\partial w}{\partial r} + w\frac{\partial w}{\partial z} = -\frac{1}{\rho}\frac{\partial p}{\partial z} + \nu\left[\frac{\partial^2 w}{\partial r^2} + \frac{1}{r}\frac{\partial w}{\partial r} + \frac{\partial^2 w}{\partial z^2}\right]$$

$$+\frac{\alpha_1}{\rho}\left[\frac{w}{r}\frac{\partial^2 u}{\partial z^2} - \frac{1}{r}\frac{\partial u}{\partial z}\frac{\partial w}{\partial z} + 2\frac{\partial u}{\partial z}\frac{\partial^2 u}{\partial z^2} + 2\frac{\partial w}{\partial z}\frac{\partial^2 w}{\partial z^2} + \frac{u}{r}\frac{\partial^2 u}{\partial r\partial z}\right.$$

$$+2w\frac{\partial^2 w}{\partial z^3} + \frac{1}{r}\frac{\partial u}{\partial r}\frac{\partial u}{\partial z} + \frac{1}{r}\frac{\partial w}{\partial r}\frac{\partial w}{\partial z} + \frac{\partial w}{\partial r}\frac{\partial^2 u}{\partial z^2} - \frac{1}{r}\frac{\partial u}{\partial r}\frac{\partial w}{\partial r}$$

$$-\frac{\partial w}{\partial z}\frac{\partial^2 u}{\partial r\partial z} + 2\frac{\partial u}{\partial r}\frac{\partial^2 u}{\partial r\partial z} + \frac{w}{r}\frac{\partial^2 w}{\partial r\partial z} + \frac{\partial u}{\partial z}\frac{\partial^2 w}{\partial r\partial z} + w\frac{\partial^3 u}{\partial r\partial z^2}$$

$$+2u\frac{\partial^3 w}{\partial r\partial z^2} + \frac{\partial u}{\partial z}\frac{\partial^2 u}{\partial r^2} - \frac{\partial w}{\partial r}\frac{\partial^2 u}{\partial r^2} + \frac{u}{r}\frac{\partial^2 w}{\partial r^2} + \frac{\partial w}{\partial z}\frac{\partial^2 w}{\partial r^2} + u\frac{\partial^3 u}{\partial r^2\partial z}$$

$$\left.+w\frac{\partial^3 w}{\partial r^2\partial z} + u\frac{\partial^3 w}{\partial r^3}\right], \tag{4.4}$$

$$u\frac{\partial T}{\partial r} + w\frac{\partial T}{\partial z} = \frac{K_c}{\rho c_p}\left[\frac{\partial^2 T}{\partial r^2} + \frac{1}{r}\frac{\partial T}{\partial r} + \frac{\partial^2 T}{\partial z^2}\right] + \left[2\frac{u^2}{r^2} + 2\left(\frac{\partial u}{\partial r}\right)^2\right]$$

$$+\frac{\nu}{c_p}\left[\left(\frac{\partial u}{\partial z}\right)^2 + 2\frac{\partial w}{\partial r}\left(\frac{\partial u}{\partial z} + \frac{\partial w}{\partial r}\right) + 2\left(\frac{\partial w}{\partial z}\right)^2 + u\frac{\partial w}{\partial r}\frac{\partial^2 w}{\partial r^2}\right.$$

$$+\frac{2u^2}{r^2}\frac{\partial u}{\partial r} - \frac{2u^3}{r^3} + 2u\frac{\partial u}{\partial r}\frac{\partial^2 u}{\partial r^2} + 2w\frac{\partial u}{\partial r}\frac{\partial^2 u}{\partial r\partial z} + 2\frac{wu}{r^2}\frac{\partial u}{\partial z}$$

$$+u\frac{\partial u}{\partial z}\frac{\partial^2 u}{\partial r\partial z} + w\frac{\partial u}{\partial z}\frac{\partial^2 u}{\partial z^2} + u\frac{\partial w}{\partial r}\frac{\partial^2 u}{\partial r\partial z} + w\frac{\partial^2 u}{\partial z^2}\frac{\partial w}{\partial r} + u\frac{\partial u}{\partial z}\frac{\partial^2 w}{\partial r^2}$$

$$\left.+w\frac{\partial u}{\partial z}\frac{\partial^2 w}{\partial r\partial z} + w\frac{\partial w}{\partial r}\frac{\partial^2 w}{\partial r\partial z} + 2u\frac{\partial w}{\partial z}\frac{\partial^2 w}{\partial r\partial z} + 2w\frac{\partial w}{\partial z}\frac{\partial^2 w}{\partial z^2}\right]$$

$$+\frac{\sigma B_o^2}{\rho c_p}u^2 + \frac{DK_T}{c_p C_s}\left[\frac{\partial^2 C}{\partial r^2} + \frac{1}{r}\frac{\partial C}{\partial r} + \frac{\partial^2 C}{\partial z^2}\right], \tag{4.5}$$

$$u\frac{\partial C}{\partial r} + w\frac{\partial C}{\partial z} = D\left[\frac{\partial^2 C}{\partial r^2} + \frac{1}{r}\frac{\partial C}{\partial r} + \frac{\partial^2 C}{\partial z^2}\right] + \frac{DK_T}{T_m}\left[\frac{\partial^2 T}{\partial r^2} + \frac{1}{r}\frac{\partial T}{\partial r} + \frac{\partial^2 T}{\partial z^2}\right]$$

$$-K_1 C, \tag{4.6}$$

where $\alpha_1\,(\geq 0)$ designates the material constant, ρ the density, $\nu = (\mu/\rho)$ the kinematic viscosity, μ the dynamic viscosity, c_p the specific heat, σ the electrical conductivity of the fluid, p the pressure, K_c the thermal conductivity, D the diffusion coefficient, C_s the concentration susceptibility, T_m the mean fluid temperature, K_T the thermal-diffusion ratio and K_1

the chemical reaction constant.
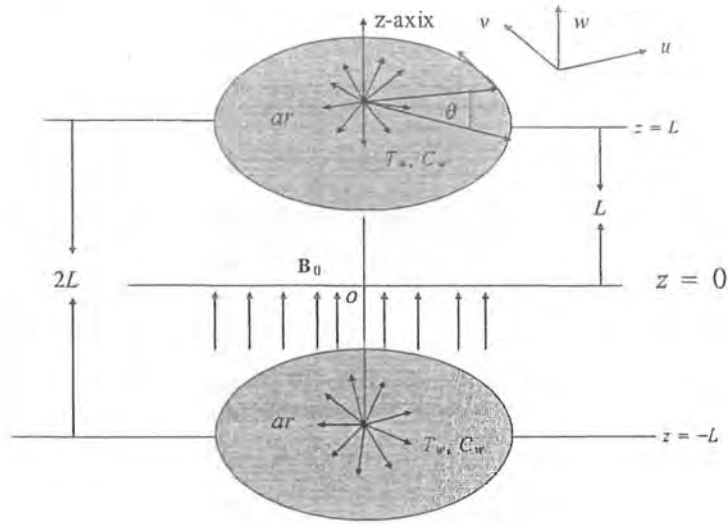
Fig. 4.1. Sketch of the physical model and coordinate system.

The associated boundary conditions are

$$\frac{\partial u}{\partial z} = 0, \ w = 0, \ \frac{\partial T}{\partial z} = 0, \ \frac{\partial C}{\partial z} = 0, \ \text{at} \ z = 0,$$

$$u = ar, \ w = 0, \ T = T_w, \ C = C_w \ \text{at} \ z = L, \qquad (4.7)$$

Employing the following dimensionless variables

$$u = arf'(\eta), \ w = -2aLf(\eta), \ \theta = \frac{T}{T_w}, \ \phi = \frac{C}{C_w}, \ \eta = \frac{z}{L}. \qquad (4.8)$$

in Eqs. $(4.2) - (4.7)$, one obtains

$$f'''' - \operatorname{Re} M f'' + 2 \operatorname{Re} f f''' - 2\alpha f f''''' = 0,$$

$$f(0) = 0, \ f(1) = 0, \ f'(1) = 1, \ f''(0) = 0, \qquad (4.9)$$

44

$$\left.\begin{array}{c} \theta'' + 2\operatorname{Re}\operatorname{Pr} f\theta'(\eta) + \operatorname{Pr}Ec\left((f'')^2 + 24\tfrac{1}{\delta}(f')^2\right) \\[4pt] +\alpha\operatorname{Pr}Ec\left(f'(f'')^2 - 2ff''f''' - 24\tfrac{1}{\delta}ff'f''\right) \\[4pt] +\operatorname{Re}M\operatorname{Pr}Ec(f')^2 + Du\operatorname{Pr}\phi'' = 0, \\[4pt] \theta'(0) = 0, \ \theta(1) = 1, \end{array}\right\} \qquad (4.10)$$

$$\begin{array}{c} \phi'' + 2Sc\operatorname{Re}f\phi'(\eta) + ScSr\theta'' - \operatorname{Re}Sc\gamma\phi = 0, \\[4pt] \phi'(0) = 0, \ \phi(1) = 1, \end{array} \qquad (4.11)$$

where

$$\alpha = \frac{\alpha_1 a}{\mu}, \ \operatorname{Re} = \frac{aL^2}{\nu}, \ M = \frac{\sigma B_0^2}{\rho a}, \ \operatorname{Pr} = \frac{\mu c_p}{K_c}, \ Du = \frac{DK_T C_w}{\nu C_s c_p T_w},$$

$$Sc = \frac{\nu}{D}, \ Sr = \frac{DK_T T_w}{\nu T_m C_w}, \ Ec = \frac{a^2 r^2}{c_p T_w}, \ \gamma = \frac{K_1}{a}, \ \delta = \frac{r^2}{L^2},$$

respectively denotes the second grade parameter, the Reynolds number (Re), the Hartman number (M), the Prandtl number (Pr), the Dufour number (Du), the Schmidt number (Sc), the Soret number (Sr), the local Eckert number (Ec), the first order chemical reaction parameter (γ) and dimensionless length (δ). The dimensionless parameters Du and Sr correspond to Dufour and Soret effects respectively. It is evident from the expressions for Dufour and Soret numbers that these are arbitrary constants provided that their product remains constant. This fact is stated in [70 − 74]. Furthermore $Du = 0$ and $Sr = 0$ correspond to the situation when thermal diffusion and diffusion-thermo effects are of a smaller order of magnitude than the effects described by Fourier's and Fick's laws [70 − 74]. There is controversy on the sign of Soret number Sr. In some studies [70, 71, 75], Sr $(= DK_T(T_w - T_\infty)/\nu T_m(C_w - C_\infty))$ is considered as positive dimensionless parameter based on the fact that surface temperature T_w and surface concentration C_w are higher than the corresponding temperature and concentration at ambient fluid $i.e.$ $T_w > T_\infty$ and $C_w > C_\infty$. However some investigators [77, 78] have taken S_r negative as well. In fact they have considered both the cases when (i) $T_w > T_\infty$ and $C_w > C_\infty$ and (ii) $T_w > T_\infty$ and $C_w < C_\infty$. However in present study Sr is taken positive because all quantities in the expression for Soret number Sr are positive $i.e.$ $Sr = DK_T T_w/\nu T_m C_w$. Hence all forthcoming computations have been carried out for positive values of Sr.

45

The skin friction coefficient C_f, Nusselt number Nu and Sherwood number Sh are

$$
\begin{aligned}
C_f &= \frac{\tau_{rz}|_{z=L}}{\rho\,(ar)^2} \\
&= \frac{\mu\left(\frac{\partial u}{\partial z}+\frac{\partial w}{\partial r}\right)\big|_{z=L}+\alpha_1\left[u\frac{\partial^2 u}{\partial r\partial z}+u\frac{\partial^2 w}{\partial r^2}+w\frac{\partial^2 u}{\partial z^2}\right]\big|_{z=L}}{\rho\,(ar)^2} \\
&\quad +\alpha_1\frac{\left[w\frac{\partial^2 w}{\partial r\partial z}+\frac{\partial u}{\partial r}\frac{\partial u}{\partial z}+\frac{\partial w}{\partial r}\frac{\partial w}{\partial z}-\frac{\partial w}{\partial z}\frac{\partial u}{\partial z}-\frac{\partial u}{\partial z}\frac{\partial w}{\partial r}\right]\big|_{z=L}}{\rho\,(ar)^2} \\
&= \frac{1}{\text{Re}_r}\,(1+4\alpha)\,f''(1), \tag{4.12}
\end{aligned}
$$

$$
Nu = -\frac{Lq_w}{KT_w}=-\frac{LK_c\,\frac{\partial T}{\partial z}\big|_{z=l}}{KT_w}=-\theta'(1), \tag{4.13}
$$

$$
Sh = -\frac{LM_w}{DC_w}=-\frac{LD\,\frac{\partial C}{\partial z}\big|_{z=L}}{DC_w}=-\phi'(1), \tag{4.14}
$$

where $\text{Re}_r\ (=arL/\nu)$ denotes the local Reynolds number.

4.2 Homotopic solutions

Here $f(\eta)$, $\theta(\eta)$ and $\phi(\eta)$ in the form of base functions

$$
\left\{\eta^{2n+1},\ n\ge 0\right\},\ \left\{\eta^{2n},\ n\ge 0\right\}, \tag{4.15}
$$

can be written as

$$
f(\eta)=\sum_{n=0}^{\infty}a_n\eta^{2n+1},\ \theta(\eta)=\sum_{n=0}^{\infty}b_n\eta^{2n},\ \phi(\eta)=\sum_{n=0}^{\infty}c_n\eta^{2n}, \tag{4.16}
$$

in which a_n, b_n and c_n are the coefficients to be determined. The initial guesses $f_0(\eta)$, $\theta_0(\eta)$, $\phi_0(\eta)$ and the linear operators $\pounds_f$, $\pounds_\theta$, $\pounds_\phi$ are chosen of the following forms

$$
f_0(\eta)=\frac{1}{2}\eta\left(\eta^2-1\right),\ \theta_0(\eta)=\eta^2,\ \phi_0(\eta)=\eta^2, \tag{4.17}
$$

$$
\pounds_f[f(\eta)]=\frac{d^4f}{d\eta^4},\ \pounds_\theta[\theta(\eta)]=\frac{d^2\theta}{d\eta^2},\ \pounds_\phi[\phi(\eta)]=\frac{d^2\phi}{d\eta^2}, \tag{4.18}
$$

46

whence

$$\mathcal{L}_f\left[C_1 + C_2\eta + C_3\eta^2 + C_4\eta^3\right] = 0, \; \mathcal{L}_\theta\left[C_5 + C_6\eta\right] = 0,$$
$$\mathcal{L}_\phi\left[C_7 + C_8\eta\right] = 0 \tag{4.19}$$

and $C_i\,(i = 1 - 8)$ are the constants.

4.2.1 Zeroth-order deformation problems

The zeroth order deformation problems are constructed as follows:

$$(1-q)\mathcal{L}_f\left[\hat{f}(\eta; q) - f_0(\eta)\right] = q\hbar_f\mathcal{N}_f\left[\hat{f}(\eta; q)\right],$$
$$\hat{f}(0; q) = 0, \; \hat{f}(1; q) = 0 \; \left.\frac{\partial\hat{f}(\eta; q)}{\partial\eta}\right|_{\eta=1} = 1, \; \left.\frac{\partial^2\hat{f}(\eta; q)}{\partial\eta^2}\right|_{\eta=0} = 0, \tag{4.20}$$
$$(1-q)\mathcal{L}_\theta\left[\hat{\theta}(\eta; q) - \theta_0(\eta)\right] = q\hbar_\theta\mathcal{N}_\theta\left[\hat{\theta}(\eta; q), \hat{f}(\eta; q), \hat{\phi}(\eta; q)\right],$$
$$\hat{\theta}(1; q) = 1, \; \left.\frac{\partial\hat{\theta}(\eta; q)}{\partial\eta}\right|_{\eta=0} = 0 \tag{4.21}$$
$$(1-q)\mathcal{L}_\phi\left[\hat{\phi}(\eta; q) - \phi_0(\eta)\right] = q\hbar_\phi\mathcal{N}_\phi\left[\hat{\theta}(\eta; q), \hat{f}(\eta; q), \hat{\phi}(\eta; q)\right],$$
$$\hat{\phi}(1; q) = 1, \; \left.\frac{\partial\hat{\phi}(\eta; q)}{\partial\eta}\right|_{\eta=0} = 0. \tag{4.22}$$

In above expressions $q \in [0, 1]$ and $\hbar_{f,\theta,\phi} \neq 0$ are respectively the embedding and auxiliary parameters and $\hat{f}(\eta; 0) = f_0(\eta)$, $\hat{\theta}(\eta; 0) = \theta_0(\eta)$, $\hat{\phi}(\eta; 0) = \phi_0(\eta)$ and $\hat{f}(\eta; 1) = f(\eta)$, $\hat{\theta}(\eta; 1) = \theta(\eta)$, $\hat{\phi}(\eta; 1) = \phi(\eta)$. When q varies from 0 to 1, then $\hat{f}(\eta; q)$ varies from the initial guess $f_0(\eta)$ to $f(\eta)$, $\hat{\theta}(\eta; q)$ varies from the initial guess $\theta_0(\eta)$ to $\theta(\eta)$ and $\hat{\phi}(\eta; q)$ varies from the initial guess $\phi_0(\eta)$ to $\phi(\eta)$. The non linear operators $\mathcal{N}_f$, $\mathcal{N}_\theta$ and $\mathcal{N}_\phi$ are given below

$$\mathcal{N}_f\left[\hat{f}(\eta; q)\right] = \frac{\partial^4\hat{f}(\eta; q)}{\partial\eta^4} - \text{Re}\,M\frac{\partial^2\hat{f}(\eta; q)}{\partial\eta^2} + 2\,\text{Re}\,\hat{f}(\eta; q)\frac{\partial^3\hat{f}(\eta; q)}{\partial\eta^3}$$
$$-2\alpha\hat{f}(\eta; q)\frac{\partial^5\hat{f}(\eta; q)}{\partial\eta^5}, \tag{4.23}$$

47

$$\mathcal{N}_\theta \left[\hat{\theta}(\eta; q), \hat{\theta}(\eta; q), \hat{f}(\eta; q) \right] = \frac{\partial^2 \hat{\theta}(\eta; q)}{\partial \eta^2} + 2 \operatorname{Re} \Pr \hat{f}(\eta; q) \frac{\partial \theta(\eta; q)(\eta; q)}{\partial \eta}$$

$$+ \Pr Ec \left[\left(\frac{\partial^2 \hat{f}(\eta; q)}{\partial \eta^2} \right)^2 + \frac{12}{\delta} \left(\frac{\partial \hat{f}(\eta; q)}{\partial \eta} \right)^2 \right]$$

$$+ \alpha \Pr Ec \left[\frac{\partial \hat{f}(\eta; q)}{\partial \eta} \left(\frac{\partial^2 \hat{f}(\eta; q)}{\partial \eta^2} \right)^2 - 2 \hat{f}(\eta; q) \frac{\partial^2 \hat{f}(\eta; q)}{\partial \eta^2} \frac{\partial^3 \hat{f}(\eta; q)}{\partial \eta^3} \right.$$

$$\left. - \frac{24}{\delta} \hat{f}(\eta; q) \frac{\partial \hat{f}(\eta; q)}{\partial \eta} \frac{\partial^2 \hat{f}(\eta; q)}{\partial \eta^2} \right] + Du \Pr \frac{\partial^2 \hat{\phi}}{\partial \eta^2} + \Pr \operatorname{Re} EcM \left(\frac{\partial \hat{f}(\eta; q)}{\partial \eta} \right)^2, \tag{4.24}$$

$$\mathcal{N}_\phi \left[\hat{\phi}(\eta; q), \hat{\theta}(\eta; q), \hat{f}(\eta; q) \right] = \frac{\partial^2 \hat{\phi}}{\partial \eta^2} + 2 \operatorname{Re} Sc \frac{\partial \hat{\phi}(\eta; q)}{\partial \eta} \hat{f}(\eta; q)$$

$$+ Sc Sr \frac{\partial^2 \hat{\theta}}{\partial \eta^2} - \operatorname{Re} Sc \gamma \hat{\phi}(\eta). \tag{4.25}$$

In view of Taylor's series, one can write

$$\hat{f}(\eta; q) = f_0(\eta) + \sum_{m=1}^\infty f_m(\eta) q^m, \tag{4.26}$$

$$\hat{\theta}(\eta; q) = \theta_0(\eta) + \sum_{m=1}^\infty \theta_m(\eta) q^m, \tag{4.27}$$

$$\hat{\phi}(\eta; q) = \phi_0(\eta) + \sum_{m=1}^\infty \phi_m(\eta) q^m, \tag{4.28}$$

$$\left. \begin{array}{c} f_m(\eta) = \frac{1}{m!} \frac{\partial^m \hat{f}(\eta; q)}{\partial \eta^m} \Big|_{q=0}, \quad \theta_m(\eta) = \frac{1}{m!} \frac{\partial^m \hat{\theta}(\eta; q)}{\partial \eta^m} \Big|_{q=0}, \\ \phi_m(\eta) = \frac{1}{m!} \frac{\partial^m \hat{\phi}(\eta; q)}{\partial \eta^m} \Big|_{q=0} \end{array} \right\}. \tag{4.29}$$

4.2.2 Higher order deformation problems

Writing

$$f_m(\eta) = \{ f_0(\eta), \ f_1(\eta), \ f_2(\eta), \ f_3(\eta) \ldots \ldots f_m(\eta) \},$$

$$\theta_m(\eta) = \{ \theta_0(\eta), \ \theta_1(\eta), \ \theta_2(\eta), \ \theta_3(\eta) \ldots \ldots \theta_m(\eta) \},$$

$$\phi_m(\eta) = \{ \phi_0(\eta), \ \phi_1(\eta), \ \phi_2(\eta), \ \phi_3(\eta) \ldots \ldots \phi_m(\eta) \}, \tag{4.30}$$

48

we have the following mth order deformation problems

$$\pounds_f \left[f_m(\eta) - \chi_m f_{m-1}(\eta) \right] = \hbar_f \mathcal{R}_f^m \left(f_{m-1}(\eta) \right),$$
$$f_m(0) = 0, \ f_m(1) = 0, \ f_m'(1) = 0, \ f_m''(0) = 0, \tag{4.31}$$

$$\pounds_\theta \left[\theta_m(\eta) - \chi_m \theta_{m-1}(\eta) \right] = \hbar_\theta \mathcal{R}_\theta^m \left(\theta_{m-1}(\eta), f_{m-1}(\eta), \phi_{m-1}(\eta) \right),$$
$$\theta_m'(0) = 0, \ \theta_m(1) = 0, \tag{4.32}$$

$$\pounds_\phi \left[\phi_m(\eta) - \chi_m \phi_{m-1}(\eta) \right] = \hbar_\phi \mathcal{R}_\phi^m \left(\phi_{m-1}(\eta), \theta_{m-1}(\eta), f_{m-1}(\eta) \right),$$
$$\phi_m'(0) = 0, \ \phi_m(1) = 0, \tag{4.33}$$

$$\chi_m = \begin{cases} 0, m \leq 1, \\ 1, m > 1, \end{cases}$$

$$\mathcal{R}_f^m \left(f_{m-1}(\eta) \right) = f_{m-1}''''(\eta) - \operatorname{Re} M f_{m-1}''(\eta) + 2\operatorname{Re} \sum_{n=0}^{m-1} f_n(\eta) f_{m-1-n}'''(\eta)$$
$$-2\alpha \sum_{n=0}^{m-1} f_n(\eta) f_{m-1-n}''''''(\eta), \tag{4.34}$$

$$\mathcal{R}_\theta^m \left(\theta_{m-1}(\eta), f_{m-1}(\eta) \right) = \theta_{m-1}''(\eta) + 2\operatorname{Re}\operatorname{Pr} \sum_{n=0}^{m-1} f_n(\eta) \theta_{m-1-n}'(\eta)$$
$$+Ec\operatorname{Pr} \sum_{n=0}^{m-1} \left[f_n''(\eta) f_{m-1-n}''(\eta) + \frac{12}{\delta} f_n'(\eta) f_{m-1-n}'(\eta) \right]$$
$$+\alpha Ec\operatorname{Pr} \sum_{l=0}^{n} \sum_{n=0}^{m-1} \left[f_{m-1-n}'(\eta) f_{n-l}''(\eta) f_l''(\eta) - 2 f_{m-1-n}(\eta) f_{n-l}''(\eta) f_l'''(\eta) \right]$$
$$-\frac{24\alpha Ec\operatorname{Pr}}{\delta} \sum_{l=0}^{n} \sum_{n=0}^{m-1} f_{m-1-n}(\eta) f_{n-l}'(\eta) f_l''(\eta) + M\operatorname{Pr}\operatorname{Re} Ec \sum_{n=0}^{m-1} f_n'(\eta) f_{m-1-n}'(\eta), \tag{4.35}$$

49

$$\mathcal{R}_\phi^m \left(\phi_{m-1}(\eta), \theta_{m-1}(\eta), f_{m-1}(\eta) \right) = \phi''_{m-1}(\eta) + ScSr\theta''_{m-1}(\eta) - \text{Re}\,Sc\gamma \times$$
$$\phi_{m-1}(\eta) + 2\,\text{Re}\,Sc \sum_{n=0}^{m-1} f_n(\eta)\,\phi'_{m-1-n}(\eta). \quad (4.36)$$

It is found that problems $(4.31) - (4.33)$ have the following general solutions

$$f(\eta) = f^*(\eta) + C_1^m + C_2^m\eta + C_3^m\eta^2 + C_4^m\eta^3, \quad (4.37)$$

$$\theta(\eta) = \theta^*(\eta) + C_5^m + C_6^m\eta, \quad (4.38)$$

$$\phi(\eta) = \phi^*(\eta) + C_7^m + C_8^m\eta, \quad (4.39)$$

where $f^*(\eta)$, $\theta^*(\eta)$ and $\phi^*(\eta)$ are the corresponding particular solutions of the problems consisting of Eqs. $(4.31) - (4.33)$.

Table 4.1. Convergence of HAM solutions when $M = 1$, $\text{Re} = 2$, $Sc = Sr = Du = Ec = \gamma = 0.5$, $\alpha = 0.1$ and $\text{Pr} = 0.72$.

Order of approximations	$f''(1)$	$\theta'(1)$	$\phi'(1)$
1	3.628571429	-1.720457143	0.06666666667
5	3.582788925	-1.848114903	0.9224303214
10	3.582255862	-1.856866160	0.9231611758
20	3.582256365	-1.856873885	0.9231650285
25	3.582256359	-1.856873885	0.9231650281
30	3.582256361	-1.856873886	0.9231650278
35	3.582256367	-1.856873886	0.9231650274
40	3.582256367	-1.856873884	0.9231650277

4.3 Convergence of solutions

The convergence and rate of approximations of series solutions $(4.37) - (4.39)$ strongly depend upon the values of auxiliary parameters. For this purpose, the $\hbar$−curves are plotted through Figs. $4.2 - 4.4$. These Figs. show that the admissible ranges for $\hbar_{f,\theta,\phi}$ are $-1.3 \leq \hbar_f \leq -0.5$, $-1.15 \leq \hbar_\theta \leq -0.8$ and $-1.2 \leq \hbar_\phi \leq -0.65$. However all the calculations are made when $\hbar_f = \hbar_\theta = \hbar_\phi = -1.0$. In order to ensure the convergence of solutions, Table 5.1 is constructed.

From this table it is evident that the convergence is achieved at 20th order of approximations up to 9th decimal places.
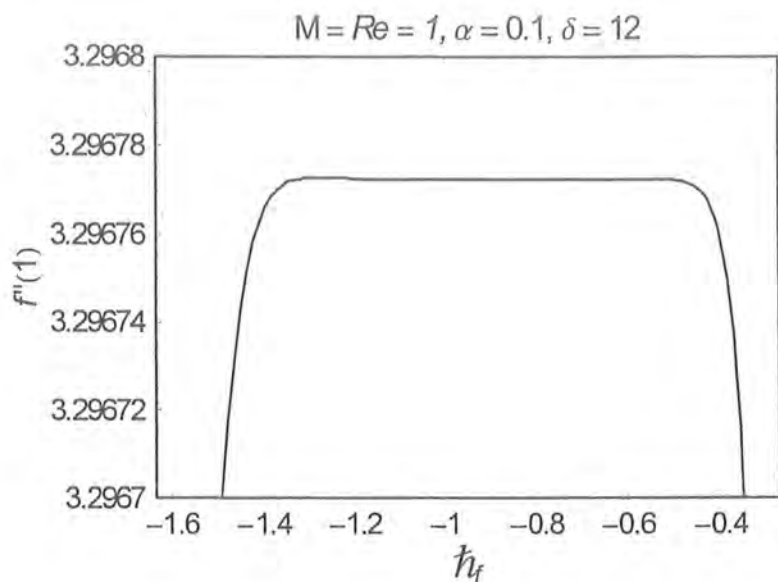

Fig. 4.2. $\hbar_f-$ curve of $f''(1)$ at 15th order of approximation.
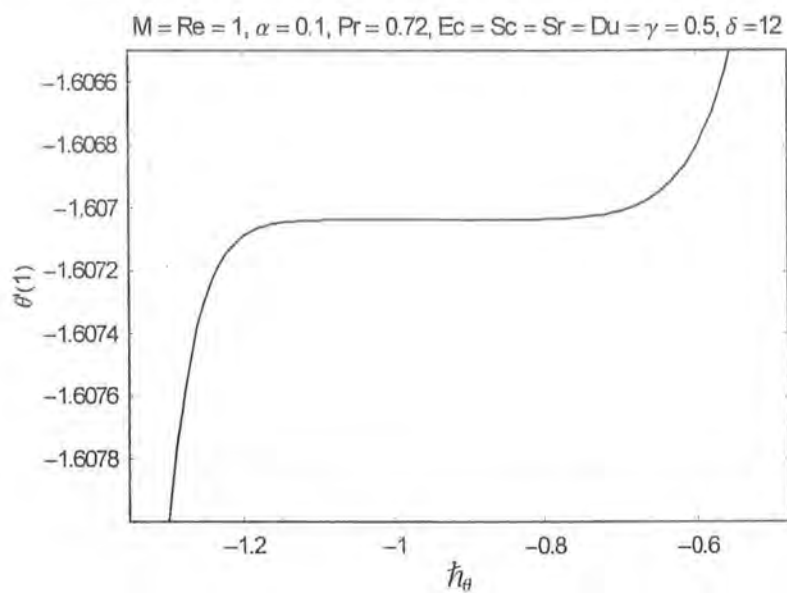

Fig. 4.3. $\hbar_\theta-$ curve for $\theta'(1)$ at 15th order of approximation.
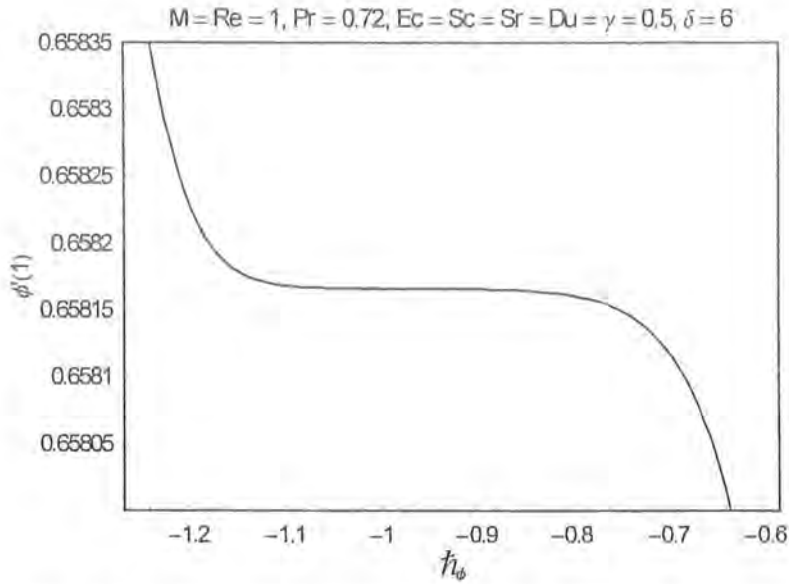
Fig. 4.4. $\hbar_\phi-$ curve for $\phi'(1)$ at $15th$ order of approximation.

4.4 Discussion

In this section, the behavior of emerging parameters on dimensionless velocities, temperature and concentration fields are presented. Numerical computations for skin friction coefficient $\mathrm{Re}_r\, C_f$, Nusselt number Nu and Sherwood number Sh are also tabulated. Figs. $4.5 - 4.10$ are displayed to see the variations of dimensionless radial velocity $f'(\eta)$ and dimensionless axial velocity $f(\eta)$ for various values of Hartman number M, Reynolds number Re and second grade parameter α. Effects of Hartman number M, Reynolds number Re, Schmidt number Sc, Soret number Sr, Prandtl number Pr, local Eckert number Ec , Dufour number Du, second grade parameter α and first order chemical reaction parameter γ on the dimensionless temperature $\theta(\eta)$ are shown in Figs. $4.11 - 4.20$. Figs. $4.21 - 4.29$ depict the variation of dimensionless concentration field $\phi(\eta)$ for different values of Reynolds number Re, Schmidt number Sc, Soret number Sr, Prandtl number Pr, local Eckert number Ec, Dufour number Du, second grade parameter α and first order chemical reaction parameter γ. It is important to mention here that we have varied Du and Sr arbitrarily provided that their product is constant keeping in mind the studies $[70 - 75]$. It is obvious from Fig. 4.5 that with an increase in Hartman number M radial velocity $f'(\eta)$ decreases in the vicinity of stretching sheet $(0.5 \leq \eta \leq 1)$ whereas it increases away from the stretching sheet $(0 \leq \eta < 0.5)$. In fact the magnetic field retards the

52

fluid particles and slows down the motion of fluid particles in the vicinity of stretching sheets but obviously to satisfy mass conservation constraint a decrease in fluid velocity in the vicinity of stretching sheets is compensated by an increase in fluid velocity in the central region. This gives rise to a cross-over behavior which is obvious from Fig. 4.5. It is noted from Fig. 4.6 that radial velocity $f'(\eta)$ is decreasing function of Reynolds number Re. Basically Reynolds number characterizes the viscous effects which are dominant in the vicinity of stretching sheets and consequently $f'(\eta)$ decreases in the region $(0.5 \leq \eta \leq 1)$ near to the stretching sheet whereas it increases away from the stretching sheet $(0 \leq \eta < 0.5)$ in order to satisfy mass conservation constraint. In the vicinity of stretching sheet the radial velocity $f'(\eta)$ increases by increasing second grade parameter α. However it decreases away from the stretching sheets as shown in Fig. 4.7. Again this cross-over behavior of $f'(\eta)$ is to satisfy the mass conservation constraint. Fig. 4.8 elucidates that the magnitude of axial velocity $f(\eta)$ is an increasing function of second grade parameter α. Figs. 4.7 and 4.8 demonstrate that dimensionless velocity components in radial and axial directions for second grade fluid $(\alpha \neq 0)$ are higher than those of viscous fluid $(\alpha = 0)$. Fig. 4.9 shows that the magnitude of axial velocity $f(\eta)$ is a decreasing function of Hartman number M. The magnitude of axial velocity $f(\eta)$ decreases by increasing Reynolds number Re (Fig. 4.10). Figs. $4.5 - 4.7$ depict that the boundary layer thickness in radial and axial directions decreases by increasing M and Re. However, it increases with an increase in α. Figs. $4.11 - 4.18$ represent that the dimensionless temperature $\theta(\eta)$ increases by increasing the Hartman number M, Reynolds number Re, Schamidt number Sc, Soret number Sr, Prandtl number Pr, local Eckert number Ec, Dufour number Du and second grade parameter α. From Figs. 4.18 and 4.19, one can see that the effects of destructive chemical reaction $(\gamma > 0)$ and constructive chemical reaction $(\gamma < 0)$ on dimensionless concentration field $\phi(\eta)$ are opposite. From Figs. $4.21 - 4.26$, we can observe that the dimensionless concentration field $\phi(\eta)$ is a decreasing function of Re, Sc, Sr, Pr, Ec and Du. Fig. 4.27 reveals that dimensionless concentration $\phi(\eta)$ increases with an increase in second grade parameter α. Fig. 4.28 shows that for destructive chemical reaction $(\gamma > 0)$, the dimensionless concentration field $\phi(\eta)$ decreases while it increases for $\gamma < 0$ (generative case) as shown in Fig. 4.28. Comparison of Figs. $4.11 - 4.20$ with Figs. $4.21 - 4.29$ indicates that the effects of Re, Sc, Sr, Du, Pr, Ec and γ on dimensionless temperature $\theta(\eta)$ and the dimensionless concentration field $\phi(\eta)$ are opposite.

Table 4.2 shows the variation of skin friction coefficient $\mathrm{Re}_r\, C_f$. From this Table, it is obvious that skin friction coefficient $\mathrm{Re}_r\, C_f$ is an increasing function of M, Re and α. Table 4.3 is prepared for the influence of physical parameters on Nusselt number Nu and Sherwood number Sh. This Table also shows that the Nusselt number Nu and Sherwood number Sh are increasing functions of Re, M, Sc, Sr, Du, Pr, Ec, γ and α. Hence we can conclude that heat and mass transfer rates increase when Re, M, Sc, Sr, Du, Pr, Ec, γ and α are increased.
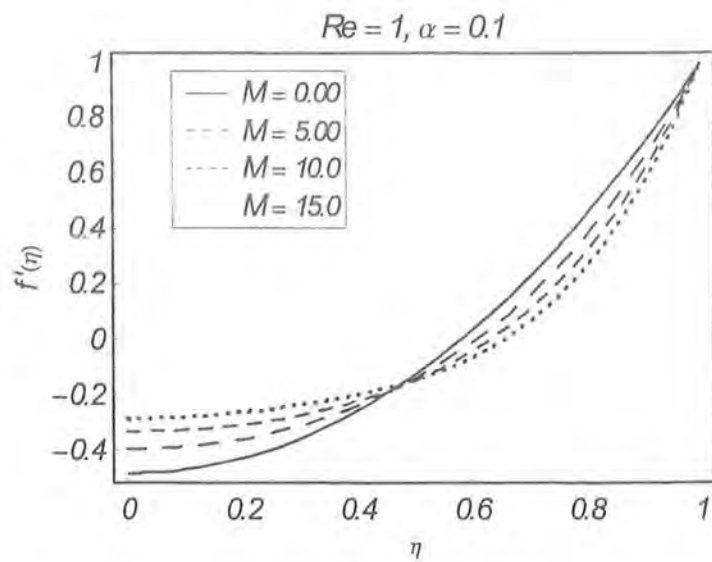
Fig. 4.5. Influence of Hartman number M on dimensionless radial velocity $f'(\eta)$.
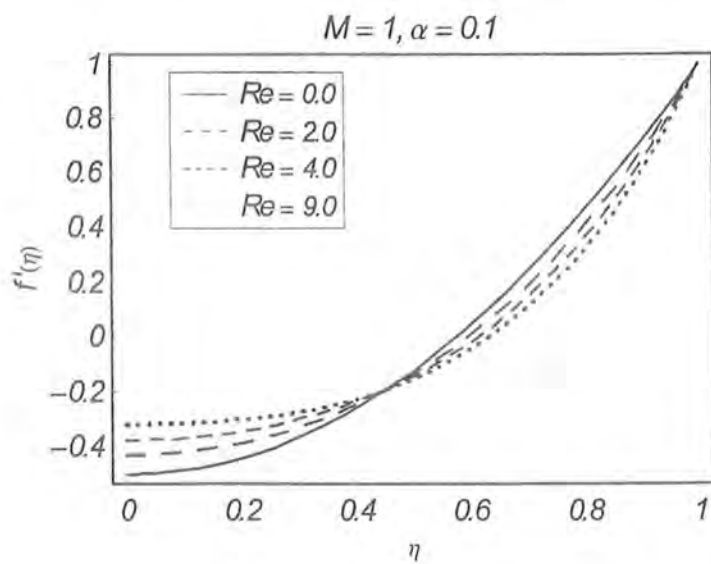
Fig. 4.6. Influence of Reynolds number Re on dimensionless radial velocity $f'(\eta)$.
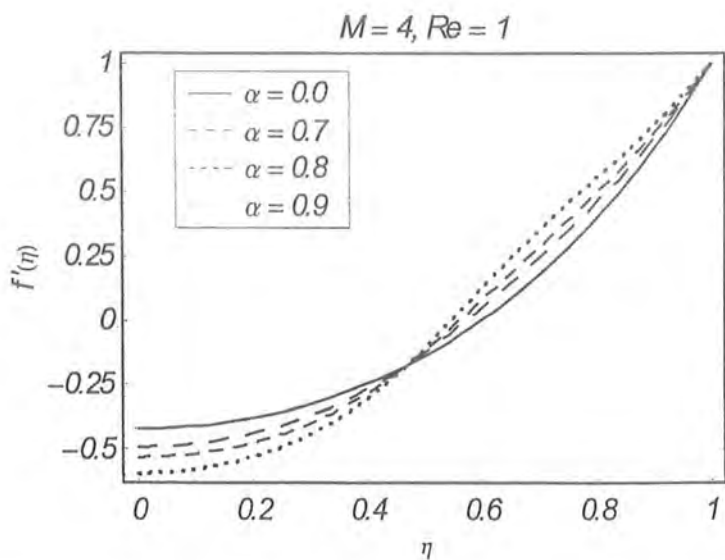
Fig. 4.7. Influence of second grade parameter α on dimensionless radial velocity $f'(\eta)$.
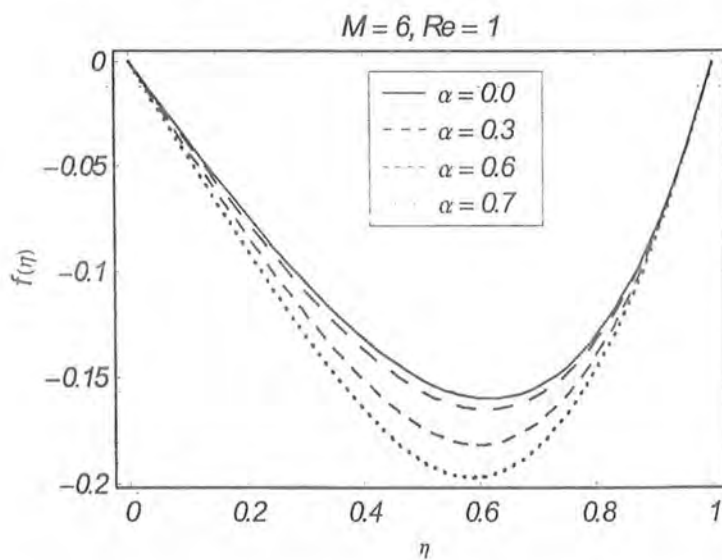
Fig. 4.8. Influence of second grade parameter α on dimensionless axial velocity $f(\eta)$.
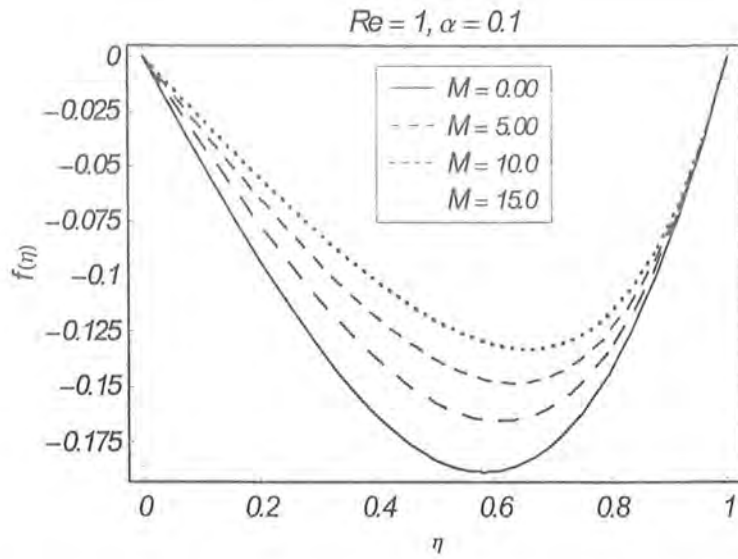
Fig. 4.9. Influence of Hartman number M on dimensionless axial velocity $f(\eta)$.
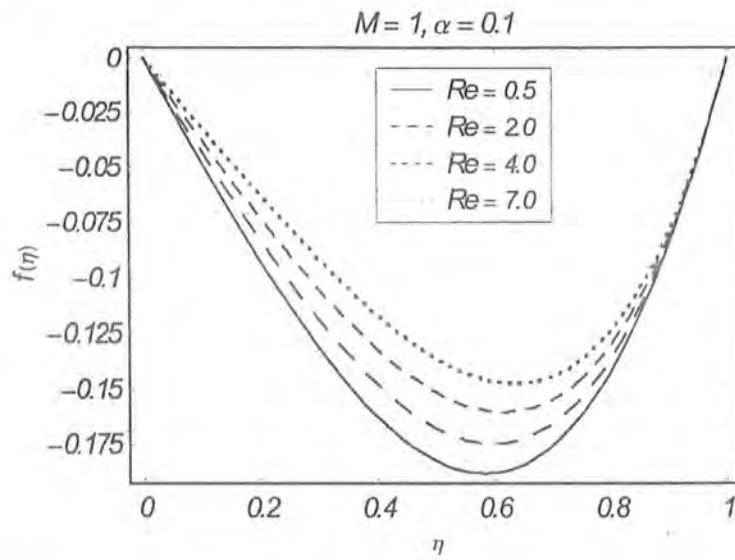
Fig. 4.10. Influence of Reynolds number Re on dimensionless axial velocity $f(\eta)$.
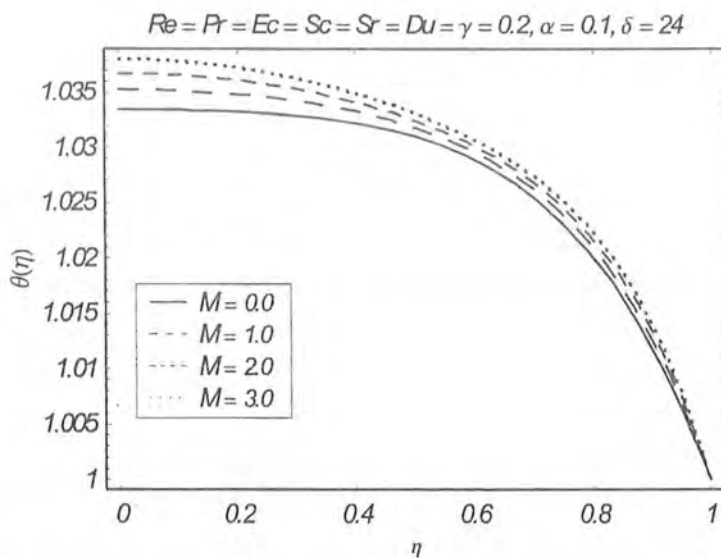
Fig. 4.11. Influence of Hartman number M on dimensionless temperature $\theta(\eta)$.
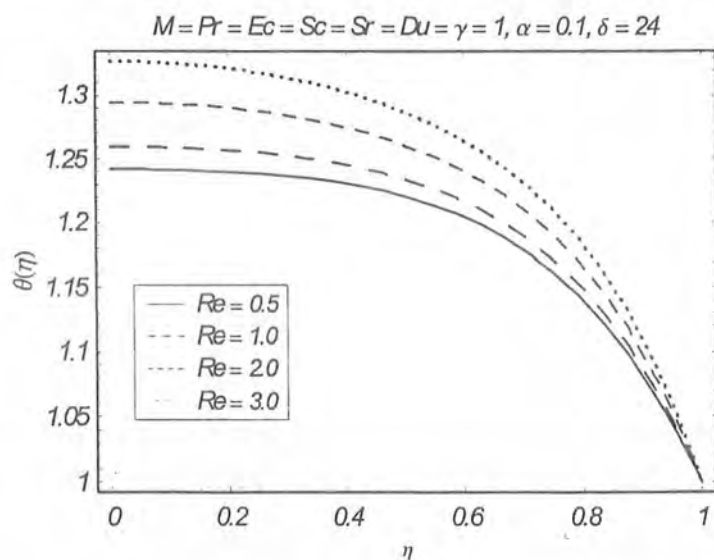
Fig. 4.12. Influence of Reynolds number Re on dimensionless temperature $\theta(\eta)$.

$M = 3, Re = 2, Pr = Ec = Sr = Du = \gamma = 0.2, \alpha = 0.5, \delta = 24$
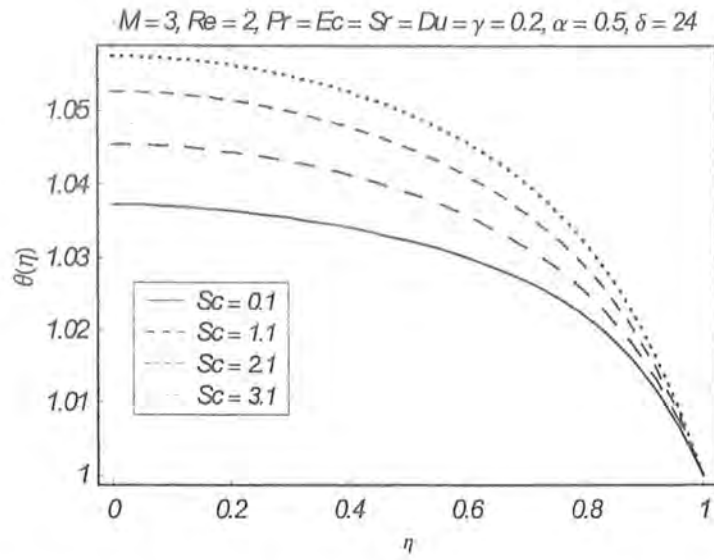
Fig. 4.13. Influence of Schmidt number Sc on dimensionless temperature $\theta(\eta)$.

$M = Re = 2, Pr = Ec = Sc = Du = \gamma = 0.2, \alpha = 0.1, \delta = 24$
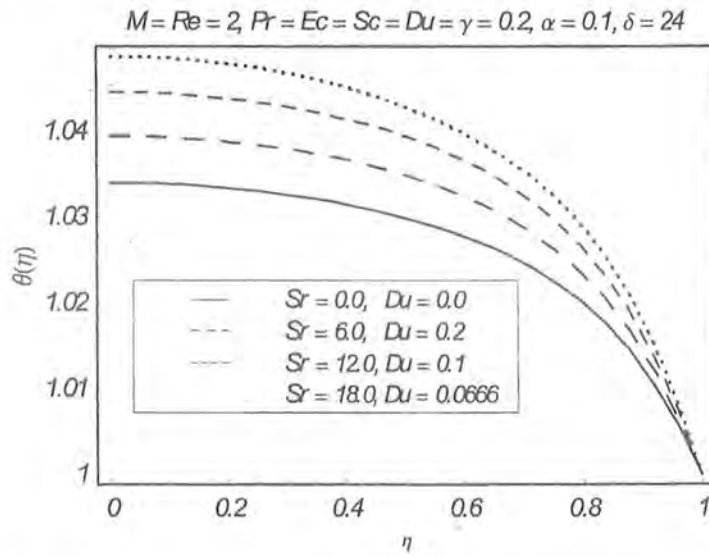
Fig. 4.14. Influence of Soret number Sr on dimensionless temperature $\theta(\eta)$.
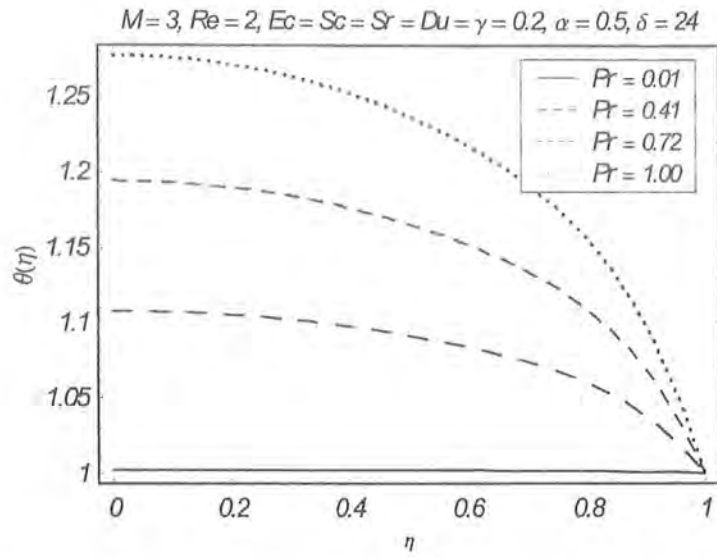
Fig. 4.15. Influence of Prandtl number Pr on dimensionless temperature $\theta\left(\eta\right)$.
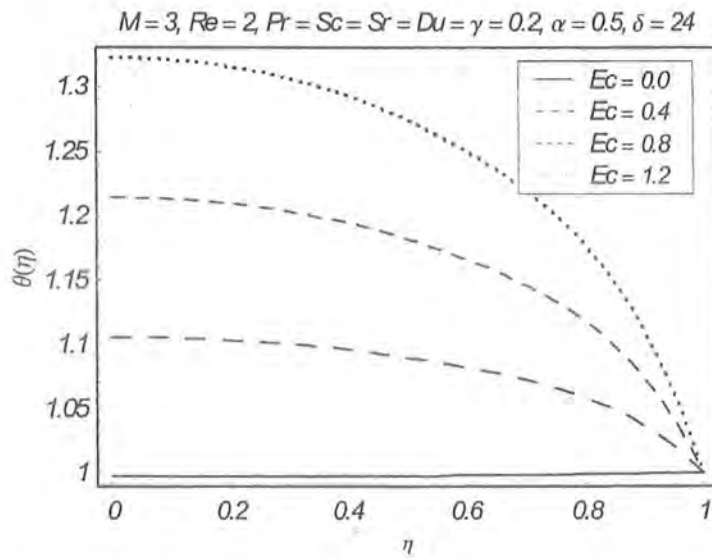
Fig. 4.16. Influence of Eckert number Ec on dimensionless temperature $\theta\left(\eta\right)$.
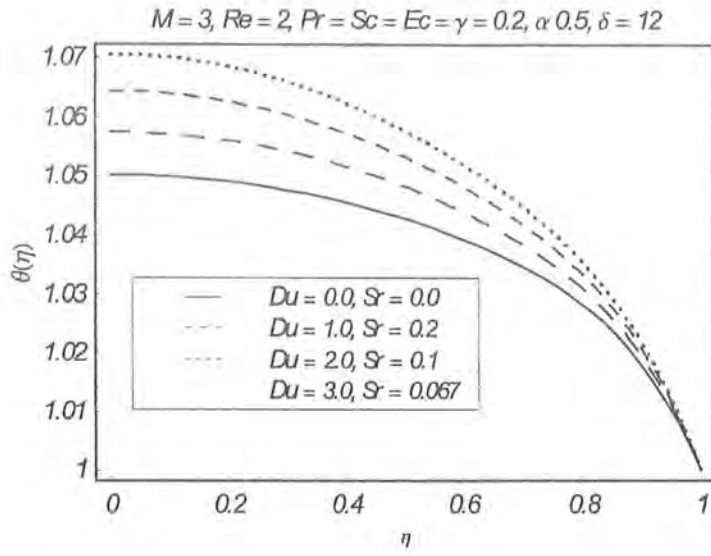
Fig. 4.17. Influence of Dufour number Du on dimensionless temperature $\theta(\eta)$.
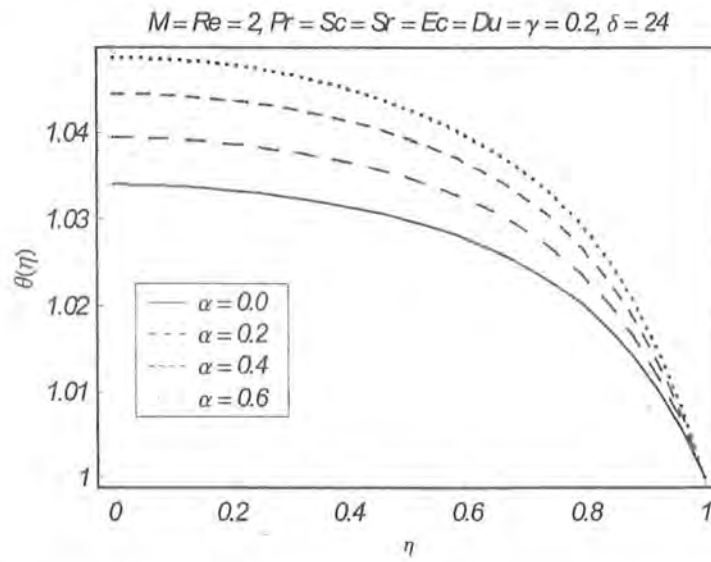
Fig. 4.18. Influence of second grade parameter α on dimensionless temperature $\theta(\eta)$.
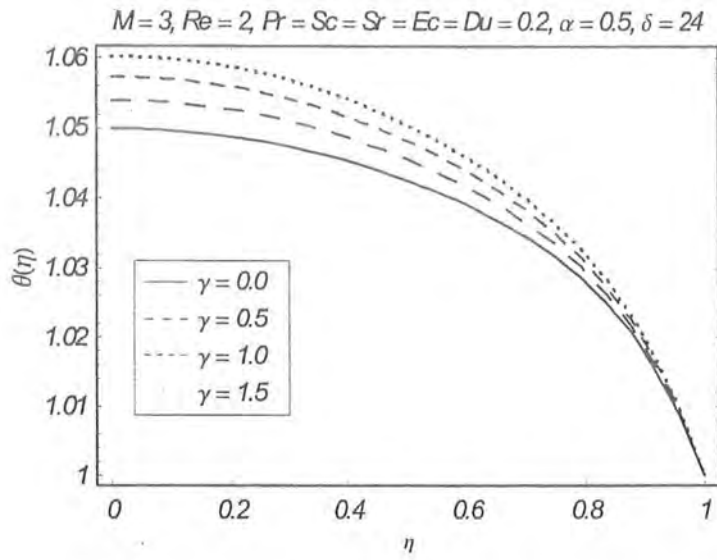
Fig. 4.19. Influence of chemical reaction parameter $\gamma \geq 0$ on dimensionless temperature $\theta(\eta)$.
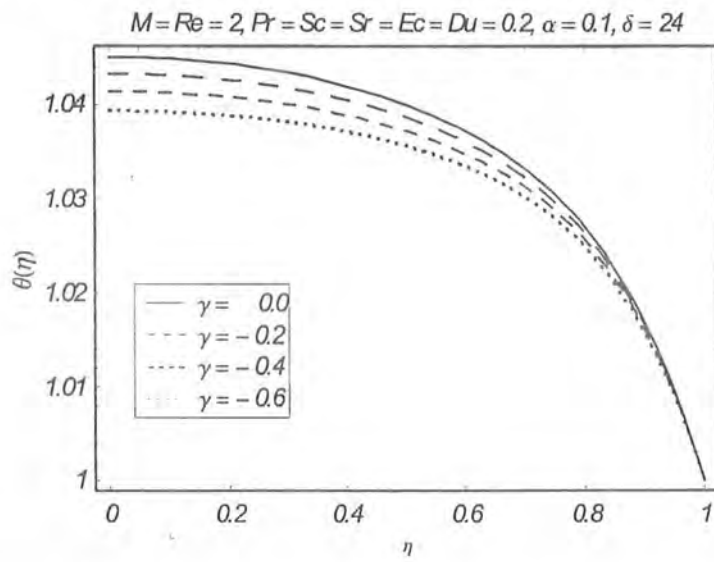
Fig. 4.20. Influence of chemical reaction parameter $\gamma \leq 0$ on dimensionless temperature $\theta(\eta)$.
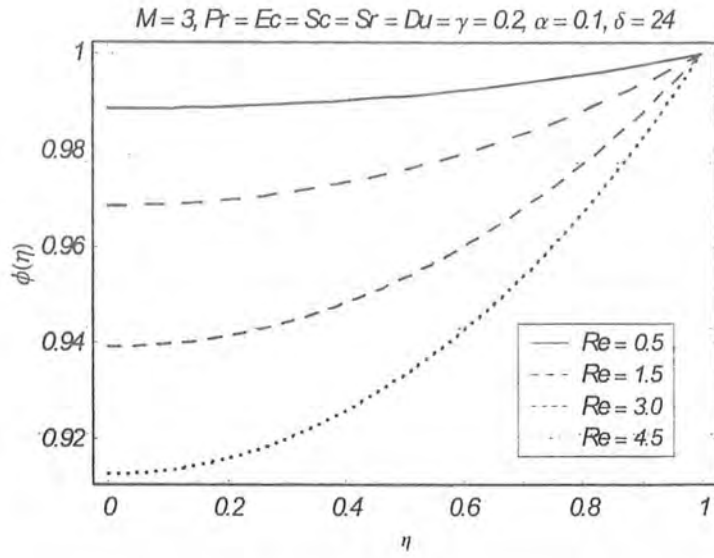
Fig. 4.21. Influence of Reynolds number Re on dimensionless concentration $\phi(\eta)$.
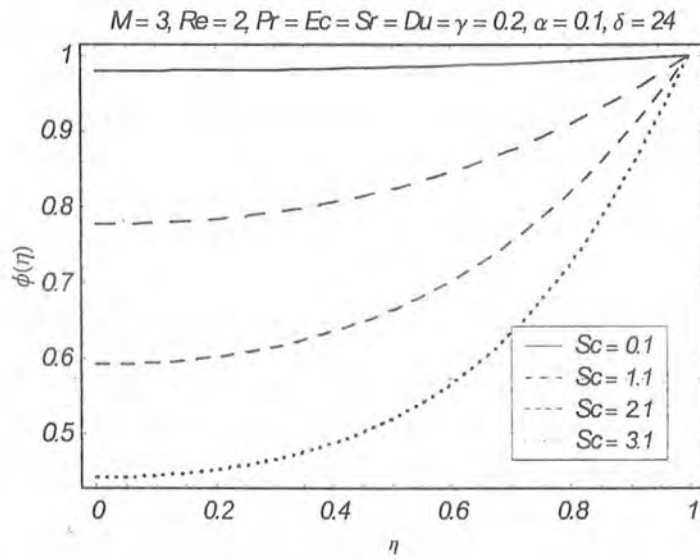
Fig. 4.22 . Influence of Schamidt number Sc on dimensionless concentration $\phi(\eta)$.
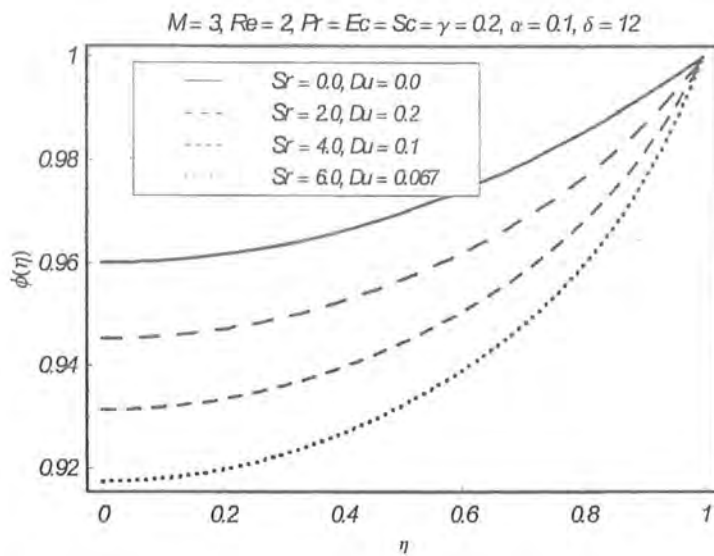
Fig. 4.23. Influence of Soret number Sr on dimensionless concentration $\phi(\eta)$.
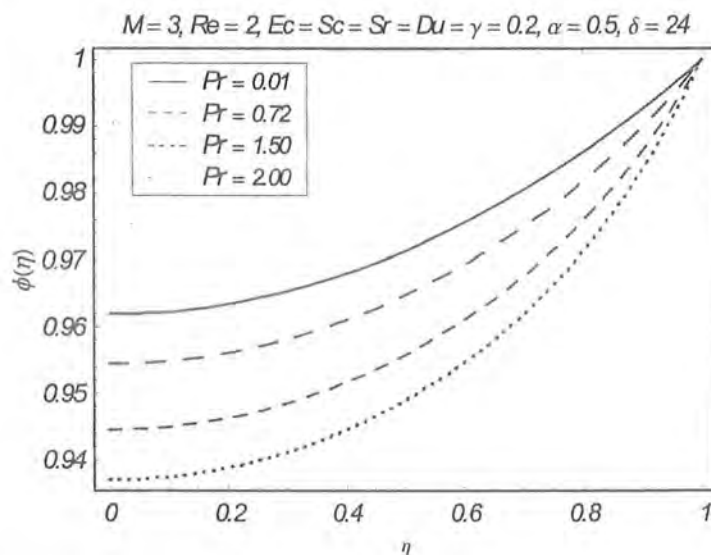
Fig. 4.24. Influence of Prandtl number Pr on dimensionless concentration $\phi(\eta)$.
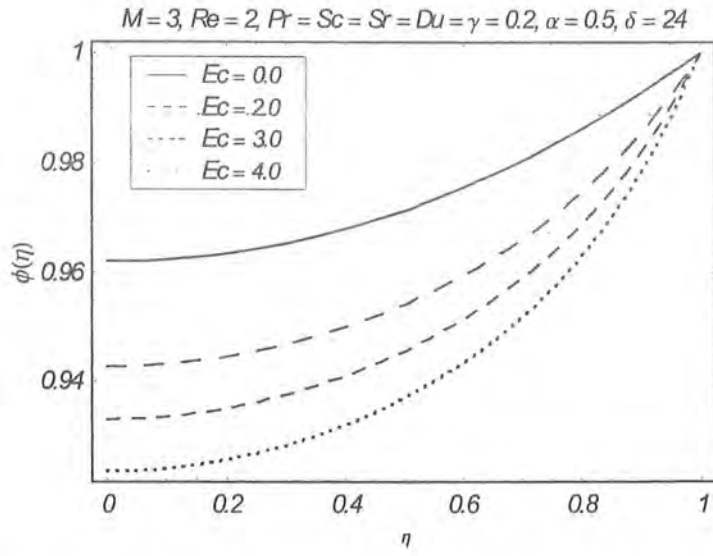
Fig. 4.25. Influence of Eckert number Ec on dimensionless concentration $\phi(\eta)$.
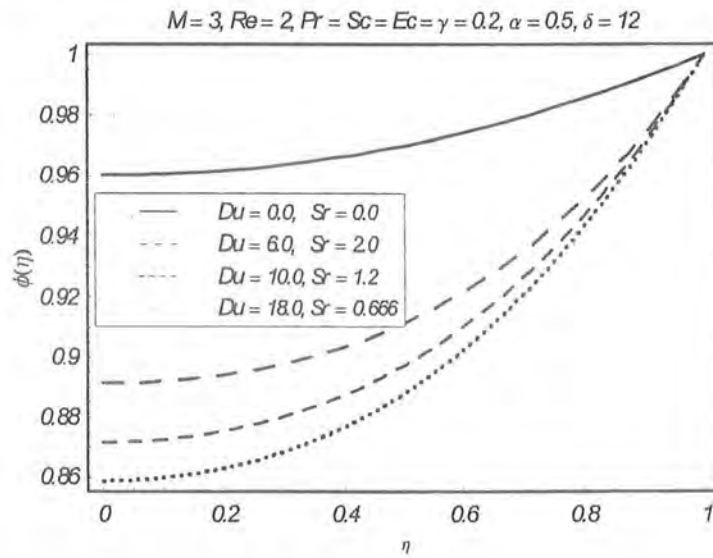
Fig. 4.26. Influence of Dufour number Du on dimensionless concentration $\phi(\eta)$.
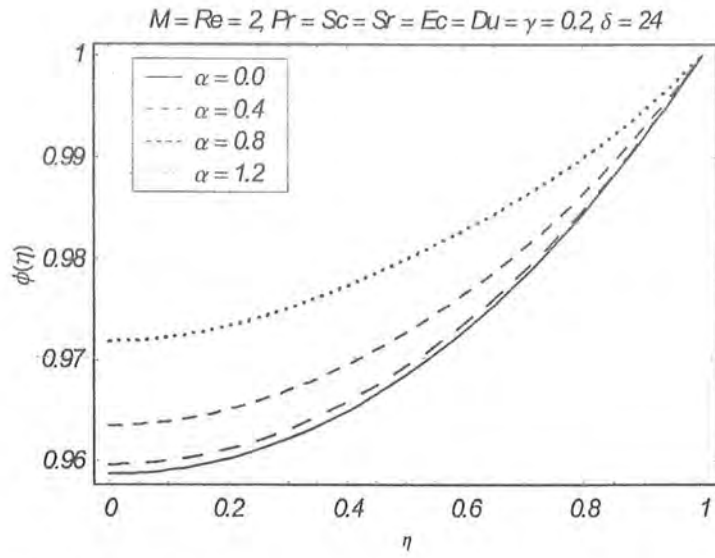
Fig. 4.27. Influence of second grade parameter α on dimensionless concentration $\phi(\eta)$.
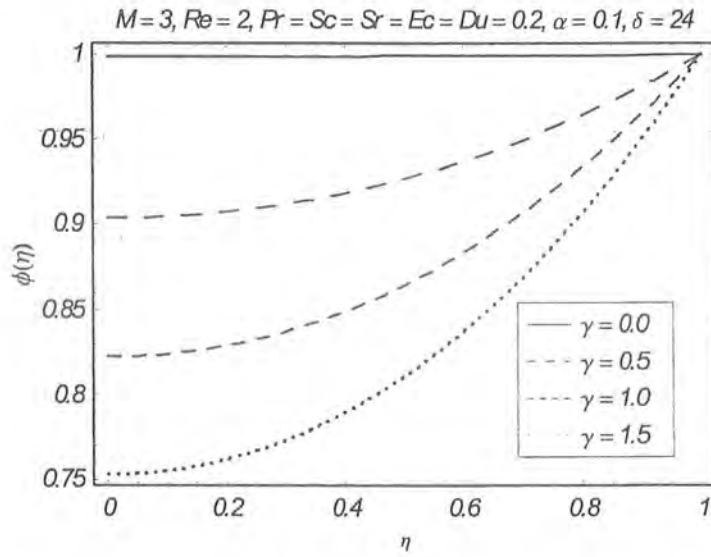
Fig. 4.28. Influence of chemical reaction parameter $\gamma \geq 0$ on dimensionless concentration $\phi(\eta)$.
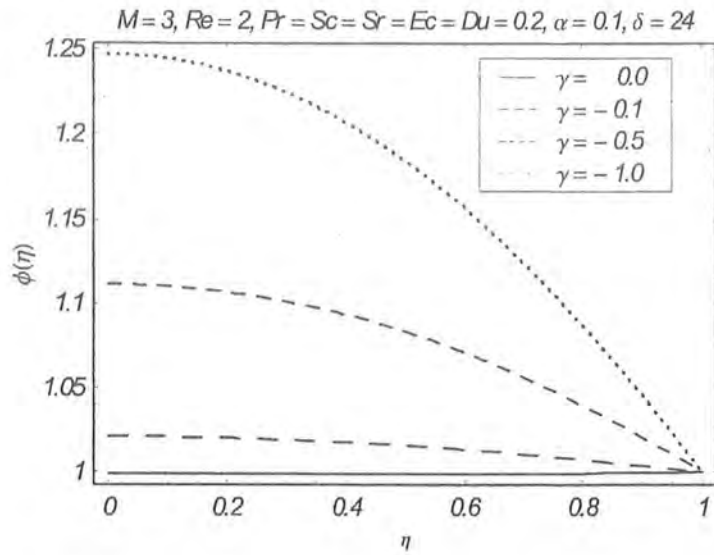
Fig. 4.29. Influence of chemical reaction parameter $\gamma \leq 0$ on dimensionless concentration $\phi(\eta)$.

Table 4.2. Variation of skin friction coefficient $\mathrm{Re}_r \, C_f$ for different values of physical parameters.

Re	M	α	$\mathrm{Re}_r \, C_f$
0.5	2.0	0.1	2.295862607
1.5			2.387369042
2.0			2.474864952
3.5			2.558678308
2.0	0.0	0.1	2.293711299
	1.0		2.432902547
	2.0		2.558678306
	3.0		2.673843959
1.0	2.0	0.0	1.000000000
		0.10	2.387369042
		0.11	2.524979840
		0.12	2.662392197

Table 4.3. Variation of Nusselt number Nu and Sherwood number Sh for different values of physical parameters.

Re	M	Du	Sc	Sr	Pr	Ec	γ	α	δ	$-Nu$	Sh
0.5	2.0	0.2	0.7	0.2	0.72	0.2	0.2	0.1	12	0.5572823525	0.1499488398
1.0										0.6078896512	0.2314349408
1.5										0.6582551099	0.3147043200
2.0										0.7083941054	0.3991814640
2.0	0.0	0.2	0.7	0.2	0.72	0.2	0.2	0.1		0.6032644724	0.3893545426
	1.0									0.6584262697	0.3944533395
	2.0									0.7083941042	0.3991814658
	3.0									0.7542785215	0.4036244986
2.0	2.0	0.0	0.7	0.0	0.72	0.2	0.2	0.1	12	0.6423726011	0.2988010699
		1.0		0.2						1.008135891	0.4429357595
		2.0		0.1						1.296355746	0.3921108526
2.0	2.0	0.2	0.5	0.2	0.72	0.2	0.2	0.1	12	0.6886926506	0.2792291568
			1.0							0.7391194961	0.5875959691
			1.5							0.7931378557	0.9226377462
2.0	2.0	0.2	0.0	0.0	0.72	0.2	0.2	0.1	12	0.6423726011	0.29880106699
			0.2	1.0						0.7775600060	0.8495350270
			0.1	2.0						0.7487380201	1.3577841090
2.0	2.0	0.2	0.7	0.2	0.12	0.2	0.2	0.1	12	0.1093003604	0.3142860256
					0.42					0.3971934827	0.3550788689
					0.72					0.7083941016	0.3991814687
					1.02					1.0463556620	0.4470813137

Re	M	Du	Sc	Sr	Pr	Ec	γ	α	δ	$-Nu$	Sh
2.0	2.0	0.2	0.7	0.2	0.72	0.0	0.2	0.1	12	0.051867388	0.3064548595
						0.5				1.693184181	0.5382713766
						1.0				3.334500972	0.7700878937
						1.5				4.975817764	1.0019044110
2.0	2.0	0.2	0.7	0.2	0.72	0.2	-1.0	0.1	12	-0.1513052154	-4.552303388
							-0.5			0.4509955418	-1.104145829
							0.0			0.6574373924	0.0979681252
							0.5			0.7680094111	0.7552777471
							1.0			0.8404624491	1.195313802
2.0	2.0	0.2	0.7	0.2	0.72	0.2	0.2	0.0	12	0.6599550320	0.3919055561
								0.10		0.7083941044	0.3991814628
								0.11		0.7131808691	0.3998987391
								0.12		0.7179577502	0.4006142258

4.5 Final remarks

The study here examine the thermal diffusion and diffusion-thermo effects on axisymmetric flow of thermodynamically compatible second grade fluid between radially stretching sheets when viscous dissipation, Joule heating and first order chemical reaction are present. The main findings are.

- Variation of Re on $f'(\eta)$ and $f(\eta)$ are similar to that of M.

- Magnitude of $f'(\eta)$ and $f(\eta)$ for second grade fluid ($\alpha \neq 0$) is higher than that of viscous fluid ($\alpha = 0$)

- There are opposite effects of Re, Sc, Du, Sr, Pr, Ec and γ on $\theta(\eta)$ and $\phi(\eta)$.

- Qualitatively, the effects of Re, M and α on the skin friction coefficient $\text{Re}_r\, C_f$, Nusselt number Nu and Sherwood number Sh are similar.

- Shear stresses increase on surface of stretching sheet with an increase in magnetic field strength and non-Newtonian nature of the fluid.

- Variation of Re, M, Sc, Sr, Pr, Ec, Du, γ and α on Nusselt number Nu and Sherwood number Sh are similar.

- Heat flux and diffusion flux can be increased by increasing Re, M, Sc, Sr, Pr, Ec, Du, γ and α. It means that heat and diffusion fluxes can enhanced by increasing strength of applied magnetic field or by using second grade fluid instead of Newtonian one.

- Boundary layer thickness in radial and axial directions decreases when M increase and Re while it increases by increasing α.

Chapter 5

Hall and ion-slip effects on three-dimensional flow of a second grade fluid

This chapter describes the effects of Hall and ion-slip currents on three-dimensional magneto-hydrodynamic flow of an incompressible second grade fluid. The partial differential equations are reduced into the ordinary differential equations by using similarity variables. The resulting problems are solved for homotopy solutions. The convergence of derived solutions is ensured. The influence of different physical parameters on the dimensionless velocities is examined by sketching plots. Variation of skin friction coefficients for different involved parameters is seen through tabulated values.

5.1 Definition of problem

We examine the steady three-dimensional flow of an incompressible second grade fluid bounded by a stretching sheet at $y = 0$. The fluid is electrically conducting whereas the stretching sheet is non-conducting. In addition, Hall and ion-slip effects are considered. Due to Hall current, there is a force in z-direction which induces a cross flow in that direction and hence flow becomes three-dimensional [60, 67, 68]. Furthermore, the magnetic Reynolds number is taken small and hence induced magnetic field is neglected.

The resulting boundary layer problems are

$$\frac{\partial u}{\partial x} + \frac{\partial v}{\partial y} = 0, \tag{5.1}$$

$$u\frac{\partial u}{\partial x} + v\frac{\partial u}{\partial y} = \nu\frac{\partial^2 u}{\partial y^2} + \frac{\alpha_1}{\rho}\left[u\frac{\partial^3 u}{\partial x \partial y^2} + v\frac{\partial^3 u}{\partial y^3} + \frac{\partial u}{\partial x}\frac{\partial^2 u}{\partial y^2} + \frac{\partial u}{\partial y}\frac{\partial^2 u}{\partial x \partial y} + \frac{\partial w}{\partial y}\frac{\partial^2 w}{\partial x \partial y} + \frac{\partial w}{\partial x}\frac{\partial^2 w}{\partial y^2}\right]$$
$$-\frac{\sigma B_0^2}{\rho\left[(1+\beta_e\beta_i)^2 + \beta_e^2\right]}\left[(1+\beta_e\beta_i)\,u + \beta_e w\right], \tag{5.2}$$

$$u\frac{\partial w}{\partial x} + v\frac{\partial w}{\partial y} = \nu\frac{\partial^2 w}{\partial y^2} + \frac{\alpha_1}{\rho}\left[u\frac{\partial^3 w}{\partial x \partial y^2} + v\frac{\partial^3 w}{\partial y^3}\right] + \frac{\sigma B_0^2}{\rho\left[(1+\beta_e\beta_i)^2 + \beta_e^2\right]}\left[\beta_e u - (1+\beta_e\beta_i)\,w\right], \tag{5.3}$$

$$\begin{aligned} u &= ax, v = 0,\, w = 0, \quad \text{at} \quad y = 0; \quad a > 0,\\ u &\rightarrow 0, \qquad\qquad\qquad\qquad \text{as} \quad y \rightarrow \infty. \end{aligned} \tag{5.4}$$

Here (u, v, w) are the velocity components in the $x-$, $y-$ and $z-$directions, $\alpha_1 \,(\geq 0)$ is the material constant, ρ is the density of the fluid, $\nu \,(= \mu/\rho)$ is the kinematic viscosity, μ is the dynamic viscosity, a is the stretching rate, $\sigma \,(= e^2 n_e \tau_e / m_e)$ is the electrical conductivity, $\beta_e \,(= \omega_e \tau_e)$ is the Hall parameter and $\beta_i \,(= e n_e B_0 / (1 + n_e/n_a) K_{ai})$ is the ion-slip parameter, τ_e is the electron collision time, me is the mass of electron, ω_e is the cyclotron frequency, n_e is the electron number density, n_a is the neutral particle density, K_{ai} is the friction coefficient between ions and neutral particles and B_0 is applied magnetic field.

In order to non-dimensionlize the problem, we introduce the following dimensionless variables

$$u = axf'(\eta), \quad v = -\sqrt{a\nu}f(\eta), \quad w = axg(\eta), \quad \eta = \sqrt{\frac{a}{\nu}}y. \tag{5.5}$$

With the help of introduced dimensionless variables in above equation, Eqs. $(5.1) - (5.4)$

become

$$f''' - \frac{M}{(1+\beta_e\beta_i)^2+\beta_e^2}\left[(1+\beta_e\beta_i)f' + \beta_e g\right] + ff'' - (f')^2 + \alpha\left[2f'f''' - ff^{(iv)} + (f'')^2\right]$$

$$+\alpha\left[(g')^2 + gg''\right] = 0, \tag{5.6}$$

$$f(0) = 0, \quad f'(0) = 1, \quad f'(\infty) = 0, \tag{5.7}$$

$$g'' + \frac{M}{(1+\beta_e\beta_i)^2+\beta_e^2}\left[\beta_e f' - (1+\beta_e\beta_i)g\right] - f'g + fg' + \alpha\left[f'g'' - fg'''\right] = 0, \tag{5.8}$$

$$g(0) = 0, \quad g(\infty) = 0, \tag{5.9}$$

where $\alpha\,(=\alpha_1 a/\mu)$ is the dimensionless second grade parameter and M is the Hartman number. It is noted that $\beta_e = 0$ corresponds to the case when Hall current is absent and $\beta_i = 0$ leads to the situation when ion-slip current is not present. It is also worth mentioning that for $\beta_e = 0$ there is no cross flow in $z-$direction and consequently flow becomes two dimensional i.e. $g = 0$. It is also found from Eqs. (5.6) and (5.8) the Lorentz force (in the presence Hall and ion currents) has two components $-\frac{M}{(1+\beta_e\beta_i)^2+\beta_e^2}\left[(1+\beta_e\beta_i)f' + \beta_e g\right]$ and $+\frac{M}{(1+\beta_e\beta_i)^2+\beta_e^2}\left[\beta_e f' - (1+\beta_e\beta_i)g\right]$. The x-component of Lorentz force is negative and it in x-direction behaves as drag force. Since $g(\eta)$ is very small as compared to $f'(\eta)$ (See Figs. 5.3 − 5.10). Therefore $\frac{M}{(1+\beta_e\beta_i)^2+\beta_e^2}\left[\beta_e f' - (1+\beta_e\beta_i)g\right]$ is positive. Hence component of Lorentz force in z-direction acts as assisting force and increases the lateral velocity $g(\eta)$.

The skin friction coefficients C_{fx} and C_{gx} are given by

$$\begin{aligned}
C_{fx} &= \frac{\tau_{xy}|_{y=0}}{\rho(ax)^2} = \frac{\mu\frac{\partial u}{\partial y}\Big|_{y=0} + \alpha_1\left[u\frac{\partial^2 u}{\partial x\partial y} + v\frac{\partial^2 u}{\partial y^2} + 2\frac{\partial u}{\partial x}\frac{\partial u}{\partial y} + \frac{\partial w}{\partial x}\frac{\partial w}{\partial y}\right]\Big|_{y=0}}{\rho(ax)^2} \\
&= (\mathrm{Re}_x)^{-1/2}(1+3\alpha)f''(0), \tag{5.10}
\end{aligned}$$

$$\begin{aligned}
C_{gx} &= \frac{\tau_{zy}|_{y=0}}{\rho(ax)^2} = \frac{\mu\frac{\partial w}{\partial y}\Big|_{y=0} + \alpha_1\left[\frac{\partial u}{\partial x}\frac{\partial w}{\partial y} + v\frac{\partial^2 w}{\partial y^2} - \frac{\partial w}{\partial x}\frac{\partial v}{\partial x} + u\frac{\partial^2 w}{\partial x\partial y}\right]\Big|_{y=0}}{\rho(ax)^2} \\
&= (\mathrm{Re}_x)^{-1/2}(1+3\alpha)g'(0), \tag{5.11}
\end{aligned}$$

where $\mathrm{Re}_x\,(=ax^2/\nu)$ is the local Reynold number.

73

5.2 Solutions by homotopy analysis method

In order to proceed for the homotopy solutions we express $f(\eta)$ and $g(\eta)$ by the set of base functions

$$\left\{\eta^k \exp(-n\eta), \; k \geq 0, \; n \geq 0\right\} \tag{5.12}$$

as follows

$$f(\eta) = a_{0,0}^0 + \sum_{n=1}^{m}\sum_{k=1}^{m} a_{m,n}^k \eta^k \exp(-n\eta), \;\; g(\eta) = \sum_{n=0}^{m}\sum_{k=0}^{m} b_{m,n}^k \eta^k \exp(-n\eta), \tag{5.13}$$

in which $a_{m,n}^k$ and $b_{m,n}^k$ are the coefficients. The initial guesses after invoking the so called rule of solution expression can be written

$$f_0(\eta) = 1 - \exp(-\eta), \;\; g_0(\eta) = 0. \tag{5.14}$$

The definitions of auxiliary linear operators $\mathcal{L}_f$ and $\mathcal{L}_g$ along with properties are

$$\mathcal{L}_f[f(\eta)] = \frac{d^3 f}{d\eta^3} - \frac{df}{d\eta}, \qquad \mathcal{L}_g[g(\eta)] = \frac{d^2 g}{d\eta^2} - g, \tag{5.15}$$

$$\mathcal{L}_f[C_1 + C_2 \exp(\eta) + C_3 \exp(-\eta)] = 0, \qquad \mathcal{L}_g[C_4 \exp(\eta) + C_5 \exp(-\eta)] = 0, \tag{5.16}$$

where $C_i \, (i = 1 - 5)$ are the arbitrary constants.

5.2.1 Zeroth-order deformation problems

The corresponding problems at this order are

$$(1-q)\mathcal{L}_f\left[\hat{f}(\eta; q) - f_0(\eta)\right] = q\hbar_f \mathcal{N}_f\left[\hat{g}(\eta; q), \hat{f}(\eta; q)\right],$$

$$\hat{f}(0; q) = 0, \; \left.\frac{\partial \hat{f}(\eta; q)}{\partial \eta}\right|_{\eta=0} = 1, \; \left.\frac{\partial^2 \hat{f}(\eta; q)}{\partial \eta^2}\right|_{\eta \to \infty} = 0, \tag{5.17}$$

$$(1-q)\mathcal{L}_g[\hat{g}(\eta; q) - g_0(\eta)] = q\hbar_g \mathcal{N}_g\left[\hat{g}(\eta; q), \hat{f}(\eta; q)\right],$$

$$\hat{g}(0; q) = 0, \; \left.\frac{\partial \hat{g}(\eta; q)}{\partial \eta}\right|_{\eta \to \infty} = 0, \tag{5.18}$$

in which $q \in [0, 1]$ is the embedding parameter and $\hbar_f$, $\hbar_g$ are non-zero auxiliary parameters. Nonlinear operators $\mathcal{N}_f$ and $\mathcal{N}_g$ are

$$
\begin{aligned}
\mathcal{N}_f \left[\hat{f}(\eta; q), \hat{g}(\eta; q) \right] &= \frac{\partial^3 \hat{f}(\eta; q)}{\partial \eta^3} - \frac{M}{(1 + \beta_e \beta_i)^2 + \beta_e^2} \left[(1 + \beta_e \beta_i) \frac{\partial \hat{f}(\eta; q)}{\partial \eta} + \beta_e \hat{g}(\eta; q) \right] \\
&+ \hat{f}(\eta; q) \frac{\partial^2 \hat{f}(\eta; q)}{\partial \eta^2} - \left(\frac{\partial \hat{f}(\eta; q)}{\partial \eta} \right)^2 + \alpha \left[2 \frac{\partial \hat{f}(\eta; q)}{\partial \eta} \frac{\partial^3 \hat{f}(\eta; q)}{\partial \eta^3} \right] \\
&+ \alpha \left[\left(\frac{\partial^2 \hat{f}(\eta; q)}{\partial \eta^2} \right)^2 - \hat{f}(\eta; q) \frac{\partial^4 \hat{f}(\eta; q)}{\partial \eta^4} + \hat{g}(\eta; q) \frac{\partial^2 \hat{g}(\eta; q)}{\partial \eta^2} \right] \\
&+ \alpha \left(\frac{\partial \hat{g}(\eta; q)}{\partial \eta} \right)^2,
\end{aligned}
\tag{5.19}
$$

$$
\begin{aligned}
\mathcal{N}_g \left[\hat{f}(\eta; q), \hat{g}(\eta; q) \right] &= \frac{\partial^2 \hat{g}}{\partial \eta^2} + \frac{M}{(1 + \beta_e \beta_i)^2 + \beta_e^2} \left[\beta_e \frac{\partial \hat{f}(\eta; q)}{\partial \eta} - (1 + \beta_e \beta_i) \hat{g}(\eta; q) \right] \\
&+ \alpha \left[\frac{\partial \hat{f}(\eta; q)}{\partial \eta} \frac{\partial^2 \hat{g}(\eta; q)}{\partial \eta^2} - \hat{f}(\eta; q) \frac{\partial^3 \hat{g}(\eta; q)}{\partial \eta^3} \right] + \hat{f}(\eta; q) \frac{\partial \hat{g}(\eta; q)}{\partial \eta} \\
&- \hat{g}(\eta; q) \frac{\partial \hat{f}(\eta; q)}{\partial \eta}.
\end{aligned}
\tag{5.20}
$$

For $q = 0$ and $q = 1$, above zeroth deformation Eqs. (5.17) and (5.18) give

$$
\hat{f}(\eta; 0) = f_0(\eta), \qquad \hat{g}(\eta; 0) = g_0(\eta)
\tag{5.21}
$$

$$
\hat{f}(\eta; 1) = f(\eta), \qquad \hat{g}(\eta; 1) = g(\eta)
\tag{5.22}
$$

Expanding $\hat{f}(\eta; q)$ and $\hat{g}(\eta; q)$ in Taylor's series with respect to q, we have

$$
\hat{f}(\eta; q) = f_0(\eta) + \sum_{m=1}^{\infty} f_m(\eta) q^m, \quad \hat{g}(\eta; q) = g_0(\eta) + \sum_{m=1}^{\infty} g_m(\eta) q^m,
\tag{5.23}
$$

where

$$
f_m(\eta) = \frac{1}{m!} \left. \frac{\partial^m \hat{f}(\eta; q)}{\partial \eta^m} \right|_{q=0}, \qquad g_m(\eta) = \frac{1}{m!} \left. \frac{\partial^m \hat{g}(\eta; q)}{\partial \eta^m} \right|_{q=0}.
\tag{5.24}
$$

75

5.2.2 Higher order deformation problems

The associated problems at this order are

$$\mathcal{L}_f \left[f_m(\eta) - \chi_m f_{m-1}(\eta) \right] = \hbar_f \mathcal{R}_m^f \left(f_{m-1}(\eta), g_{m-1}(\eta) \right),$$

$$f_m(0) = 0, \ f_m'(0) = 0, \ f_m'(\infty) = 0, \tag{5.25}$$

$$\mathcal{L}_f \left[g_m(\eta) - \chi_m g_{m-1}(\eta) \right] = \hbar_g \mathcal{R}_m^g \left(f_{m-1}(\eta), g_{m-1}(\eta) \right),$$

$$g_m(0) = 0, \quad g_m(\infty) = 0, \tag{5.26}$$

$$\chi_m = \begin{cases} 0, m \leq 1, \\ 1, m > 1, \end{cases}$$

$$\begin{aligned}
\mathcal{R}_m^f \left(f_{m-1}(\eta), g_{m-1}(\eta) \right) &= f_{m-1}'''(\eta) - \frac{M}{(1+\beta_e \beta_i)^2 + \beta_e^2} \left[\begin{array}{c} (1+\beta_e \beta_i) f_{m-1}'(\eta) \\ +\beta_e g_{m-1}(\eta) \end{array} \right] \\
&\quad + \sum_{n=0}^{m-1} \left[f_n(\eta) f_{m-1-n}''(\eta) - f_n'(\eta) f_{m-1-n}'(\eta) \right] \\
&\quad + \alpha \sum_{n=0}^{m-1} \left[2f_n'(\eta) f_{m-1-n}'''(\eta) - f_n'(\eta) f_{m-1-n}''''(\eta) \right] \\
&\quad + \alpha \sum_{n=0}^{m-1} \left[\begin{array}{c} f_n''(\eta) f_{m-1-n}''(\eta) + g_n(\eta) g_{m-1-n}''(\eta) \\ +g_n'(\eta) g_{m-1-n}'(\eta) \end{array} \right], \tag{5.27}
\end{aligned}$$

$$\begin{aligned}
\mathcal{R}_m^g \left(f_{m-1}(\eta), g_{m-1}(\eta) \right) &= g_{m-1}''(\eta) + \frac{M}{(1+\beta_e \beta_i)^2 + \beta_e^2} \left[\begin{array}{c} \beta_e f_{m-1}'(\eta) \\ -(1+\beta_e \beta_i) g_{m-1}(\eta) \end{array} \right] \\
&\quad + \alpha \sum_{n=0}^{m-1} \left[f_n'(\eta) g_{m-1-n}''(\eta) - f_n(\eta) g_{m-1-n}'''(\eta) \right] \\
&\quad + \sum_{n=0}^{m-1} \left[f_n(\eta) g_{m-1-n}'(\eta) - f_n'(\eta) g_{m-1-n}(\eta) \right]. \tag{5.28}
\end{aligned}$$

The general solutions of problems given by Eqs. (5.25) and (5.26) are given by

$$f(\eta) = f^*(\eta) + C_1^m + C_2^m \exp(\eta) + C_3^m \exp(-\eta),$$ (5.29)

$$g(\eta) = g^*(\eta) + C_4^m \exp(\eta) + C_5^m \exp(-\eta),$$ (5.30)

where $f^*(\eta)$ and $g^*(\eta)$ are the particular solutions of the problems consisting of Eqs. (5.25) and (5.26).

5.3 Convergence of HAM solutions

It is clear that the derived solutions consist of auxiliary parameters. The convergence and rate of approximation of series solutions given by Eqs. (5.29) and (5.30) strongly depend upon the values of auxiliary parameters. Hence the $\hbar_{f,g}$−curves are plotted (Figs. 5.1 and 5.2). These Figs. elucidate that the admissible values of $\hbar_f$ and $\hbar_g$ are $-1.05- \leq \hbar_f \leq -0.65$ and $-1.2- \leq \hbar_g \leq -0.6$. All computations are performed when $\hbar_f = \hbar_g = -0.9$. In order to ensure the convergence of solutions, Table 4.1 is made. This Table clearly shows that the convergence is obtained at 25th order of approximations.

Table 5.1. Convergence of HAM solutions when $M = \beta_i = \beta_e = 0.5$, $\alpha = 0.1$ and $\hbar_f = \hbar_g = -0.9$.

Order of approximations	$f''(0)$	$g'(0)$
1	-1.205344828	0.1241379310
5	-1.177879701	0.1128106267
10	-1.178433731	0.1130714946
15	-1.178434982	0.1130721427
20	-1.178434970	0.1130721353
25	-1.178434970	0.1130721354
28	-1.178434970	0.1130721354

5.4 Results and discussion

The purpose of this section is to see the influence of Hartman number M, second grade parameter α, Hall parameter β_e and ion-slip parameter β_i on the dimensionless tangential velocity $f'(\eta)$ and lateral velocity $g(\eta)$. Figs. $5.3 - 5.6$ describe the effects of M, α, β_e and β_i on the dimensionless tangential velocity $f'(\eta)$ and Figs. $5.7 - 5.10$ show the variation of dimensionless lateral velocity $g(\eta)$ for various values of M, α, β_i and β_e. Fig. 5.3 shows that dimensionless tangential velocity $f'(\eta)$ decreases with an increase of Hartman number M. This Fig. also indicates that the boundary layer thickness decreases when M is increased. Actually when M increases the drag force $-\frac{M}{(1+\beta_e\beta_i)^2+\beta_e^2}\left[(1+\beta_e\beta_i)f'+\beta_e g\right]$ increases and consequently $f'(\eta)$ decreases. From Fig. 5.4 one can see that $f'(\eta)$ increases when second grade parameter α increases and consequently the boundary layer thickness increases. Dimensionless tangential velocity $f'(\eta)$ is an increasing function of Hall and ion-slip parameters (Figs. 5.5 and 5.6). Fig. 5.7 witnesses that the lateral velocity $g(\eta)$ increases with an increase in Hartman number M. In fact assisting force $\frac{M}{(1+\beta_e\beta_i)^2+\beta_e^2}\left[\beta_e f' - (1+\beta_e\beta_i)g\right]$ increases when M is increased. Fig. 5.7 also shows that dimensionless lateral velocity $g(\eta)=0$ for $M=0$ $(\beta_e=0)$ which is expected since the flow in $z-$direction is due to Hall force. Fig. 5.8 depicts that $g(\eta)$ decreases near the stretching sheet by increasing second grade parameter α but it increases away from the stretching sheet. Fig. 5.9 represents that the dimensionless lateral velocity $g(\eta)$ increases when Hall parameter β_e is increased. Furthermore, it is also noted from Fig. 5.9 that for $\beta_e=0$ (in the absence of Hall current) $g(\eta)=0$. Lateral velocity $g(\eta)$ is a decreasing functions of ion-slip parameter β_i (see Fig. 5.10). Table 5.2 is constructed to analyze the influence of parameters on the skin friction coefficients $(\mathrm{Re}_x)^{1/2}C_{fx}$ and $(\mathrm{Re}_x)^{1/2}C_{gx}$ in the x- and z-direction respectively. From this Table one can further see that the skin friction coefficients $(\mathrm{Re}_x)^{1/2}C_{fx}$ and $(\mathrm{Re}_x)^{1/2}C_{gx}$ increase when M and α are increased but decrease with an increase of β_i. From this table one can also see that effect of β_e on $(\mathrm{Re}_x)^{1/2}C_{fx}$ and $(\mathrm{Re}_x)^{1/2}C_{gx}$ is opposite.
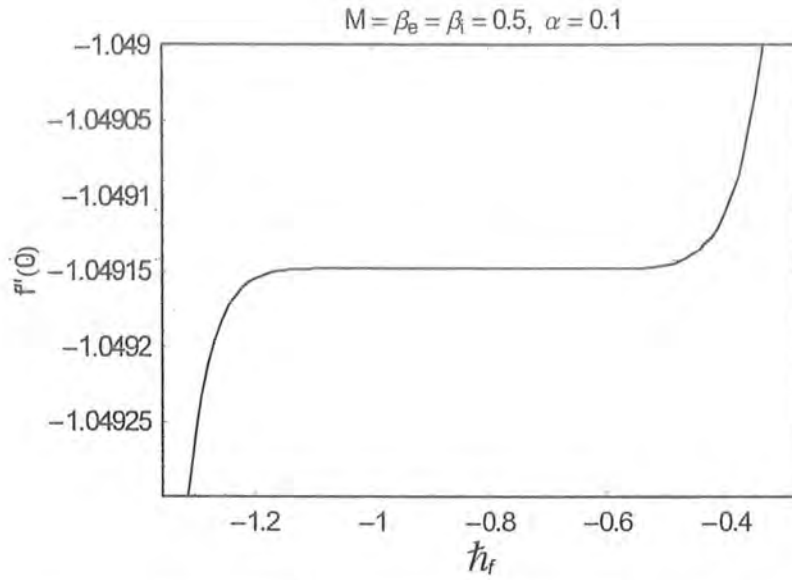
Fig. 5.1. $\hbar_f$−curve of $f''(0)$ at 13th order of approximation.
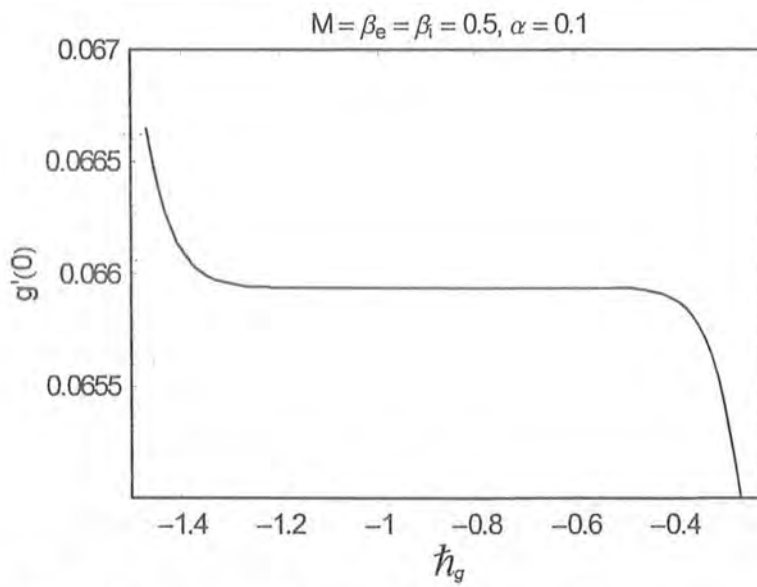
Fig. 5.2. $\hbar_g$−curve of $g'(0)$ at 13th order of approximation.
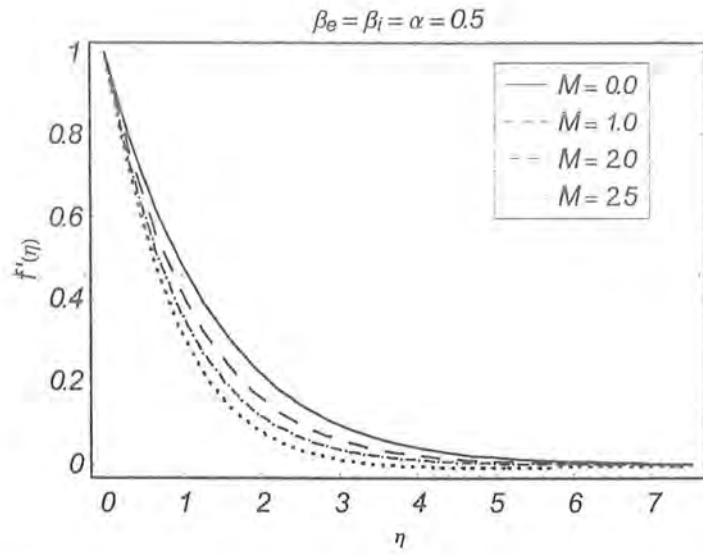
Fig. 5.3. Influence of Hartman number M on dimensionless tangential velocity $f'(\eta)$.
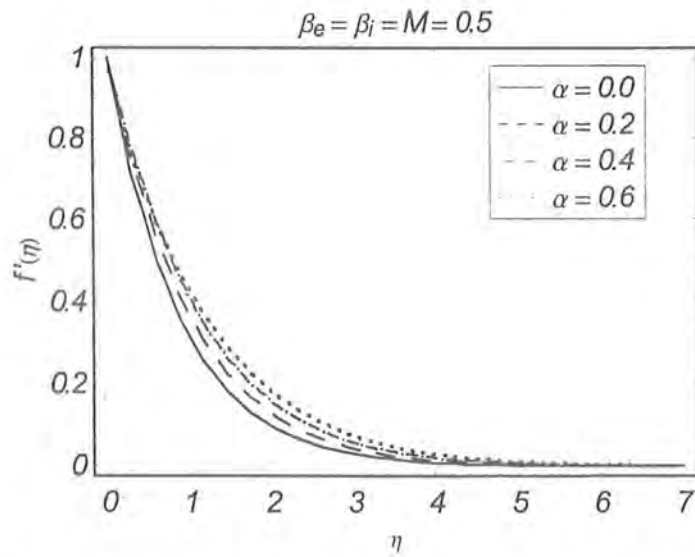
Fig. 5.4. Influence of second grade parameter α on dimensionless tangential velocity $f'(\eta)$.
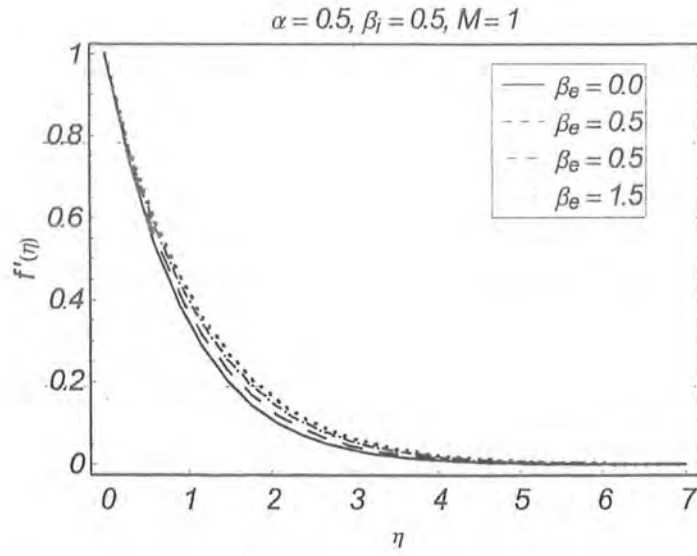
Fig. 5.5. Influence of Hall parameter β_e on dimensionless tangential velocity $f'(\eta)$.
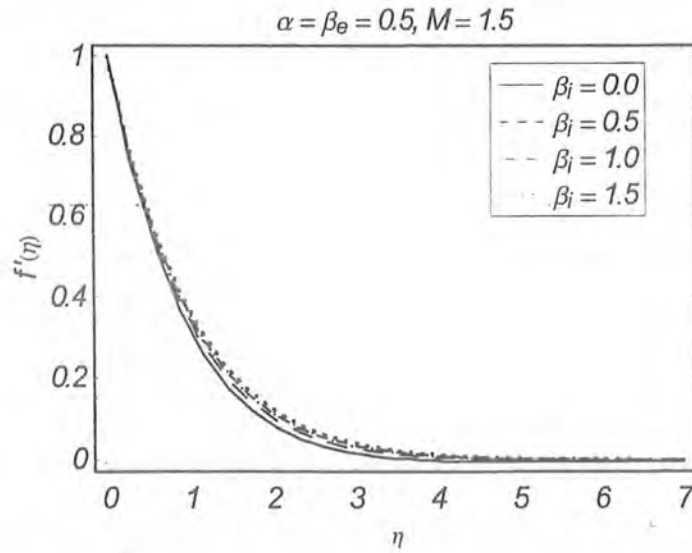
Fig. 5.6. Influence of ion slip parameter β_i on dimensionless tangential velocity $f'(\eta)$.
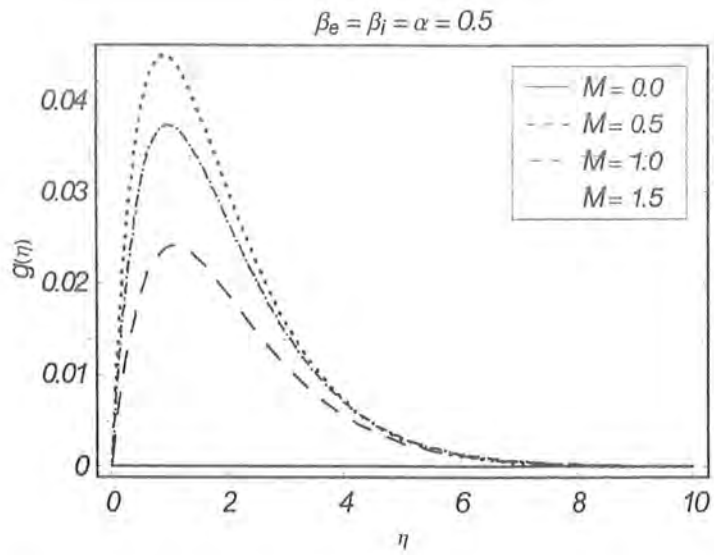
Fig. 5.7. Influence of Hartman number M on dimensionless lateral velocity $g(\eta)$.
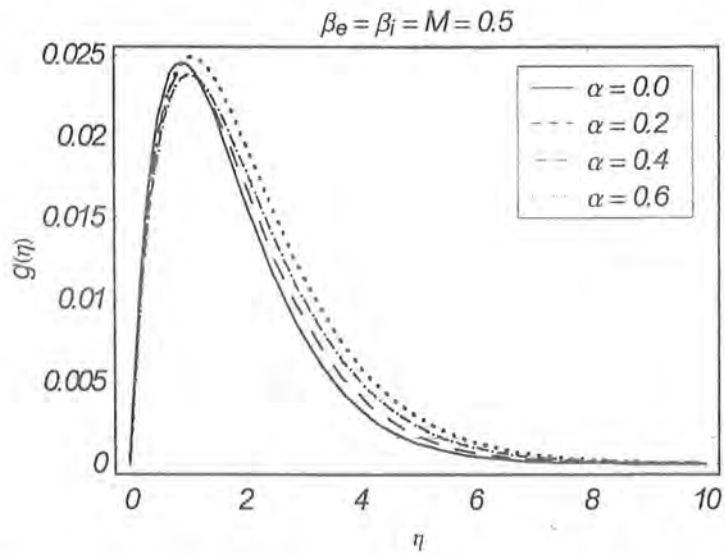
Fig. 5.8. Influence of second grade parameter α on dimensionless lateral velocity $g(\eta)$.
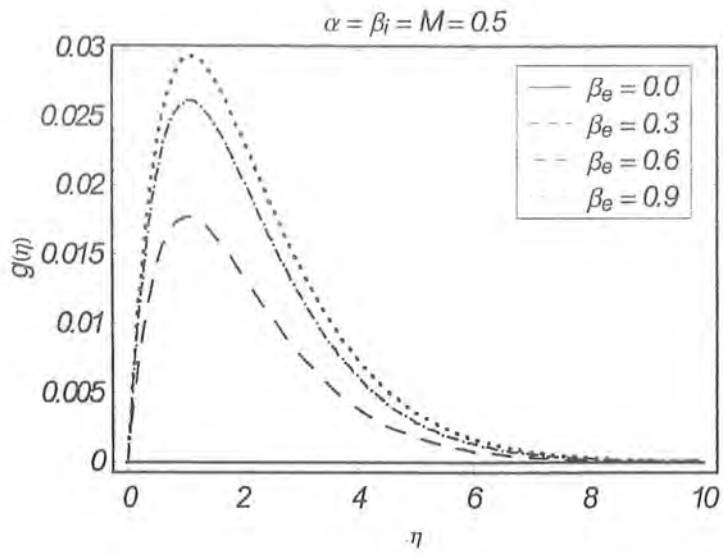
Fig. 5.9. Influence of Hall parameter β_e on dimensionless lateral velocity $g(\eta)$.
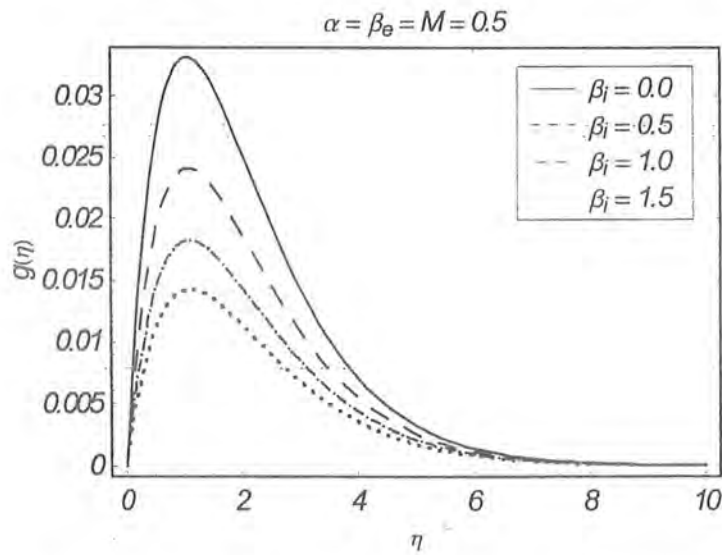
Fig. 5.10. Influence of ion slip parameter β_i on dimensionless lateral velocity $g(\eta)$.

Table 5.2. The variation of skin friction coefficients for various values of M, α, β_e and β_i when $\hbar_f = \hbar_g = -0.9$.

M	α	β_e	β_i	$-\left(\text{Re}_x\right)^{1/2} C_{fx}$	$\left(\text{Re}_x\right)^{1/2} C_{gx}$
0.0	0.1	0.5	0.1	1.17479	0.000000
0.5				1.38741	0.112205
1.0				1.57482	0.190247
1.5				1.74309	0.252128
1.0	0.0	0.5	0.5	1.30575	0.118612
	0.1			1.53197	0.146994
	0.2			1.73331	0.172694
	0.3			1.91639	0.196193
1.0	0.1	0.0	0.5	1.65837	0.000000
		0.5		1.63573	0.044114
		1.0		1.61020	0.080085
		1.5		1.58361	0.108541
1.0	0.1	0.5	0.0	1.58674	0.203916
			0.2	1.56338	0.177857
			0.4	1.54197	0.156350
			0.6	1.52240	0.138434

5.5 Closing remarks

In this chapter we have discussed the Hall and ion-slip effects on three-dimensional MHD steady flow of an incompressible second grade fluid. The salient features of the conducted analysis can be summarized in the points given below.

- Effects of M and α on dimensionless tangential velocity $f'\left(\eta\right)$ are opposite.

- Effects of β_e and β_i on $f'\left(\eta\right)$ are similar in qualitative sense.

- Dimensionless lateral velocity $g\left(\eta\right)$ is an increasing function of M.

- Behaviors of M and β_i on the dimensionless lateral velocity $g\left(\eta\right)$ are opposite.

- Behavior of α on the dimensionless tangential velocity $f'(\eta)$ and lateral velocity $g(\eta)$ is different.

- Skin friction coefficients $(\mathrm{Re}_x)^{1/2} C_{fx}$ and $(\mathrm{Re}_x)^{1/2} C_{gx}$ are increasing functions of M and α. However $(\mathrm{Re}_x)^{1/2} C_{fx}$ and $(\mathrm{Re}_x)^{1/2} C_{gx}$ decrease when β_i is increased.

- Behavior of β_e on $(\mathrm{Re}_x)^{1/2} C_{fx}$ and $(\mathrm{Re}_x)^{1/2} C_{gx}$ is opposite.

Chapter 6

Hall and ion slip effects on magnetohydrodynamic three-dimensional flow of a second grade fluid with heat transfer

The flow analysis of previous chapter with heat transfer is analyzed here. Energy equation including viscous dissipation and Joule heating results in the relevant mathematical expression. The modelled differential system is solved for convergent series solution. The effects of Prandtl number (Pr), local Eckert number (Ec), Hall parameter (β_e), ion-slip parameter (β_i) and Hartman number (M) on the dimensionless temperature are analyzed graphically. A comparative study between the present and existing limiting results is carefully made. Convergence regarding the obtained solution is discussed and shown. Nusselt number is analyzed for various values of sundry parameters.

6.1 Problem formulation

We consider heat transfer characteristics in steady, laminar and three-dimensional MHD flow of an incompressible second grade fluid over stretching surface coinciding at $y = 0$. The fluid

is electrically conducting and stretching surface is electrically non-conducting. A uniform magnetic field $\mathbf{B}_0$ is applied parallel to y-axis. The effects of Hall and ion-slip currents are taken into account. Due to Hall current, there is a force (Hall force) in $z-$direction which induces a cross flow in that direction and hence flow becomes three-dimensional (see [60, 67, 68]). Furthermore, viscous dissipation and Joule heating are considered. The steady thermal boundary layer equation after taking into account the energy equation is expressed as

$$u\frac{\partial T}{\partial x} + v\frac{\partial T}{\partial y} = K_c\frac{\partial^2 T}{\partial y^2} + \frac{\sigma B_0^2}{\rho c_p\left[(1+\beta_e\beta_i)^2 + \beta_e^2\right]}\left[u^2 + w^2\right] + \frac{\nu}{c_p}\left[\left(\frac{\partial u}{\partial y}\right)^2 + \left(\frac{\partial w}{\partial y}\right)^2\right]$$
$$+ \frac{\alpha_1}{\rho c_p}\left[u\frac{\partial u}{\partial y}\frac{\partial^2 u}{\partial x\partial y} + v\frac{\partial u}{\partial y}\frac{\partial^2 u}{\partial y^2} + v\frac{\partial w}{\partial y}\frac{\partial^2 w}{\partial y^2} + u\frac{\partial w}{\partial y}\frac{\partial^2 w}{\partial x\partial y}\right], \qquad (6.1)$$

with appropriate conditions

$$T = T_w, \text{ at } y = 0;$$
$$T \longrightarrow T_\infty \text{ as } y \longrightarrow \infty. \qquad (6.2)$$

Here for the convenience of readers we define u, v and w as the velocity components in x, y and z directions, $\alpha_1 (\geq 0)$ is the material constant, ν is the kinematic viscosity, ρ is the density of fluid, $\sigma \left(= e^2 n_e \tau_e / m_e\right)$ is the electrical conductivity, $\beta_e \left(= \omega_e \tau_e\right)$ is the Hall parameter, β_i $\left(= e n_e B_0 / (1 + n_e/n_a) K_{ai}\right)$ is the ion-slip parameter, τ_e is the electron collision time, $m e$ is the mass of electron, ω_e is the cyclotron frequency, n_e is the electron number density, n_a is the neutral particle density, K_{ai} is the friction coefficient between ions and neutral particles, K_c is the thermal conductivity and c_p is the specific heat of the fluid.

The following similarity variables

$$u = axf'(\eta), \; v = -\sqrt{a\nu}f(\eta), \; w = axg(\eta), \; \theta(\eta) = \frac{T - T_\infty}{T_w - T_\infty}, \; \eta = \sqrt{\frac{a}{\nu}}y, \qquad (6.3)$$

along with Eqs. (6.1) and (6.2) provides

$$\theta'' + \Pr f\theta' + \frac{\Pr EcM}{(1+\beta_e\beta_i)^2+\beta_e^2}\left[(f')^2+g^2\right] + \Pr Ec\left[(f'')^2+(g')^2\right]$$
$$+\alpha\Pr Ec\left[f'(g')^2-fg'g''-ff''f'''+f'(f'')^2\right]=0. \tag{6.4}$$

$$\theta(0)=1, \quad \theta(\infty)=0, \tag{6.5}$$

Here

$$\alpha=\frac{\alpha_1 a}{\mu}, \quad M=\frac{\sigma B_0^2}{\rho a}, \quad \Pr=\frac{\mu c_p}{K_c}, \quad Ec=\frac{(ax)^2}{c_p(T_w-T_\infty)},$$

respectively are called the second grade parameter (α), the Hartman number (M), the Prandtl number (Pr) and the local Eckert number. Here it is worth mentioning that the case for $\beta_e=0$ corresponds to the situation when Hall current is absent and $\beta_i=0$ corresponds to the situation when ion-slip current is not present. $Ec=0$ leads to the situation when Joule heating and viscous dissipation are not significant. It is also noted that Joule heating is proportional to M and inversely proportional to β_e and β_i (see expression $\frac{\Pr EcM}{(1+\beta_e\beta_i)^2+\beta_e^2}\left[(f')^2+g^2\right]$). Hence it is expected to increase dimensionless temperature with an increase in M whereas temperature decreases by increasing β_e and β_i.

The physical quantity of interest is Nusselt number Nu_x which is defined by the following expression

$$Nu_x=\frac{xq_w}{K_c}=-\frac{x}{K_c(T_w-T_\infty)}K_c\frac{\partial T}{\partial y}\bigg|_{y=0}=-(\text{Re}_x)^{1/2}\theta'(0), \tag{6.6}$$

where the local Reynolds number $\text{Re}_x=ax^2/\nu$.

6.2 Solutions by homotopy analysis method

6.2.1 Zeroth-order solutions

HAM solution for $\theta(\eta)$ in the form of base functions

$$\left\{\eta^k\exp(-n\eta), \; k\geq 0, \; n\geq 0\right\}, \tag{6.7}$$

88

can be expressed by the following infinite series

$$\theta(\eta) = \sum_{n=1}^{m} \sum_{k=1}^{m} c_{m,n}^{k} \eta^{k} \exp(-n\eta),$$ (6.8)

where $c_{m,n}^{k}$ is the coefficient. By rule of solution expression, the initial guess $\theta_0(\eta)$ and linear operator $\pounds_\theta$ are chosen as

$$\theta_0(\eta) = \eta \exp(-\eta) + \exp(-\eta),$$ (6.9)

$$\pounds_\theta [\theta_0(\eta)] = \frac{d^2\theta}{d\eta^2} - \theta.$$ (6.10)

Above mentioned linear operator $\pounds_\theta$ satisfies the following property

$$\pounds_\theta [C_1 \exp(\eta) + C_2 \exp(-\eta)] = 0,$$ (6.11)

where $C_i (i = 1, 2)$ are the arbitrary constants.

6.2.2 Zeroth order deformation problems

The problem statement here is

$$(1 - q)\pounds_\theta \left[\hat{\theta}(\eta; q) - \theta_0(\eta) \right] = q\hbar_\theta \mathcal{N}_\theta \left[\hat{f}(\eta; q), \hat{g}(\eta; q), \hat{\theta}(\eta; q) \right],$$ (6.12)

$$\hat{\theta}(0) = 1, \qquad \hat{\theta}(\infty) = 0,$$ (6.13)

while the definitions of nonlinear operator $\mathcal{N}_\theta$ is

$$
\begin{aligned}
\mathcal{N}_\theta \left[\hat{\theta}(\eta;q), \hat{g}(\eta;q), \hat{f}(\eta;q) \right] &= \frac{\partial^2 \hat{\theta}(\eta;q)}{\partial \eta^2} + \Pr \hat{f}(\eta;q) \frac{\partial \hat{\theta}(\eta;q)}{\partial \eta} + \frac{\Pr EcM}{(1+\beta_e\beta_i)^2 + \beta_e^2} \\
&\times \left(\begin{array}{c} \left(\frac{\partial \hat{f}(\eta;q)}{\partial \eta}\right)^2 \\ + (\hat{g}(\eta;q))^2 \end{array} \right) + \Pr Ec \left(\begin{array}{c} \left(\frac{\partial^2 \hat{f}(\eta;q)}{\partial \eta^2}\right)^2 \\ + \left(\frac{\partial \hat{g}(\eta;q)}{\partial \eta}\right)^2 \end{array} \right) \\
&+ \alpha \Pr Ec \frac{\partial \hat{f}(\eta;q)}{\partial \eta} \left(\frac{\partial \hat{g}(\eta;q)}{\partial \eta} \right)^2 + \alpha \Pr Ec \\
&\times \frac{\partial \hat{f}(\eta;q)}{\partial \eta} \left(\frac{\partial^2 \hat{f}(\eta;q)}{\partial \eta^2} \right)^2 \\
&- \alpha \Pr Ec \hat{f}(\eta;q) \frac{\partial \hat{g}(\eta;q)}{\partial \eta} \frac{\partial^2 \hat{g}(\eta;q)}{\partial \eta^2} \\
&- \alpha \Pr Ec \hat{f}(\eta;q) \frac{\partial^2 \hat{f}(\eta;q)}{\partial \eta^2} \frac{\partial^3 \hat{f}(\eta;q)}{\partial \eta^3}.
\end{aligned}
\tag{6.14}
$$

In view of Taylor's theorem, one can expand

$$
\hat{\theta}(\eta;q) = \theta_0(\eta) + \sum_{m=1}^{\infty} \theta_m(\eta) q^m,
\tag{6.15}
$$

$$
\theta_m(\eta) = \frac{1}{m!} \left. \frac{\partial^m \hat{\theta}(\eta;q)}{\partial \eta^m} \right|_{q=0}.
\tag{6.16}
$$

6.2.3 Higher order deformation problems

We write the deformation problems at the mth-order in the following expressions:

$$
\mathcal{L}_\theta [\theta_m(\eta) - \chi_m \theta_{m-1}(\eta)] = \hbar_\theta \mathcal{R}_m^\theta (\theta_{m-1}(\eta)),
$$
$$
\theta_m(0) = 1, \ \theta_m(\infty) = 0,
\tag{6.17}
$$

$$
\chi_m = \begin{cases} 0, m \le 1, \\ 1, m > 1, \end{cases}
$$

90

$$
\begin{aligned}
\mathcal{R}_m^\theta \left(\theta_{m-1}(\eta),\, f_{m-1}(\eta),\, g_{m-1}(\eta)\right) \;=\; & \theta''_{m-1}(\eta) + \Pr \sum_{n=0}^{m-1} f_n(\eta)\,\theta'_{m-1-n}(\eta) \\
& + \frac{\Pr Ec M}{(1+\beta_e \beta_i)^2 + \beta_e^2} \sum_{n=0}^{m-1}
\left[
\begin{array}{c}
f'_n(\eta)\, f'_{m-1-n}(\eta) \\
+ g_n(\eta)\, g_{m-1-n}(\eta)
\end{array}
\right] \\
& + \Pr Ec \sum_{n=0}^{m-1} \left[f''_n(\eta)\, f''_{m-1-n}(\eta) + g'_n(\eta)\, g'_{m-1-n}(\eta) \right] \\
& - \alpha \Pr Ec \sum_{l=0}^{n} \sum_{n=0}^{m-1} f_{m-1-n}(\eta)\, f''_{n-l}(\eta)\, f'''_l(\eta) \\
& + \alpha \Pr Ec \sum_{l=0}^{n} \sum_{n=0}^{m-1} f'_{m-1-n}(\eta)\, f''_{n-l}(\eta)\, f''_l(\eta) \\
& + \alpha \Pr Ec \sum_{l=0}^{n} \sum_{n=0}^{m-1} f'_{m-1-n}(\eta)\, g'_{n-l}(\eta)\, g'_l(\eta) \\
& - \alpha \Pr Ec \sum_{l=0}^{n} \sum_{n=0}^{m-1} f_{m-1-n}(\eta)\, g'_{n-l}(\eta)\, g''_l(\eta), \qquad (6.18)
\end{aligned}
$$

If $\theta^*(\eta)$ denotes the particular solution of problem (6.17) then general solution is

$$
\theta(\eta) = \theta^*(\eta) + C_1^m \exp(\eta) + C_2^m \exp(-\eta), \qquad (6.19)
$$

where C_1^m and C_2^m are the arbitrary constants which are determined by using the boundary conditions (6.17).

6.3 Convergence of HAM solutions

This section aims to discuss the convergence of series solution (6.19). As pointed out by Liao [93] the convergence of HAM solution(s) and its rate of approximation strongly depend upon the values of auxiliary parameter(s). Hence $\hbar_\theta$–curve for temperature is plotted in Fig. 6.1. This Fig. clearly indicates that the admissible range for $\hbar_\theta$ is $-1.25 \leq \hbar_\theta \leq -0.45$. Table 6.1 is constructed just to ensure the convergence of solution. The tabulated values show that

convergence is achieved at 40th order of approximation.

$M = 1, \beta_e = \beta_i = 0.5, \text{Ec} = 0.2, \text{Pr} = 0.72, \alpha = 0.2$
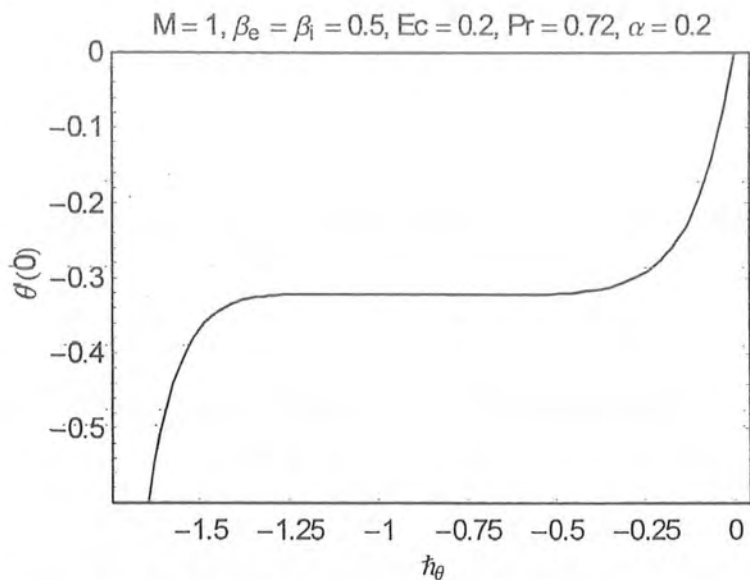
Fig. 6.1. $\hbar_\theta$-curve of $\theta'(0)$ at 12th order of approximation.

Table 6.1. Convergence of HAM solution when $M = 1$, $\beta_e = \beta_i = Ec = 0.5$, $\alpha = 0.1$, $\Pr = 0.72$, $\hbar_f = \hbar_g = \hbar_\theta = -1$.

Order of approximations	$-\theta'(0)$
1	0.121434
5	0.146520
10	0.141908
15	0.138153
20	0.13615
25	0.13450
30	0.13451
35	0.13412
40	0.13401
42	0.13401
44	0.13401

6.4 Results and discussion

Here in this section we have examined the influence of pertinent parameters on the dimensionless temperature $\theta(\eta)$. Fig. 6.2 reveals that dimensionless temperature $\theta(\eta)$ increasers by increasing Hartman number M. This Fig. also shows that thermal boundary layer thickness increases when Hartman number M is increased. The temperature $\theta(\eta)$ increases when Hartman number increases. As a result the thermal boundary layer thickness increases. It is found from Fig. 6.3 that the fluid temperature $\theta(\eta)$ decreases by increasing Hall parameter β_e. Since temperature increases with an increases in Hartman number M and an increase in Hall parameter β_e results to a decrease in Hartman number M.(see expression $\Pr EcM / \left((1 + \beta_e\beta_i)^2 + \beta_e^2 \right)$). Consequently temperature decreases. From physical point of view it can be concluded that Hall current prevents Joule heating. Similar arguments for the behavior of ion slip parameter β_i on dimensionless temperature $\theta(\eta)$ can be established (see Fig. 6.4). It is observed from Fig. 6.5 that an increase in Prandtl number $\Pr$ leads to a decrease in the dimensionless temperature $\theta(\eta)$. Note that $\Pr < 1$ corresponds to the fluids for which momentum diffusivity is less than

thermal diffusivity and vice versa for Pr > 1. It is also noted from Fig. 6.5 that an increase in Pr results in thinning the thermal boundary layer. Fig. 6.6 depicts that dimensionless temperature $\theta(\eta)$ increases when local Eckert number Ec is increased. Physically it means that an increase in external magnetic field causes to increase kinetic energy of fluid particles. This increase in kinetic energy implies an increase in Joule heating (Ohmic dissipation) and viscous dissipation and hence give rise in temperature. Thus effect of local Eckert number Ec is opposite to that of Pr on dimensionless temperature $\theta(\eta)$. Table 6.2 gives the comparison between the present and already existing results for a special case when $M = \beta_i = \beta_e = Ec = \alpha = 0$. This Table shows an excellent agreement between the present and existing limiting results. Table 6.3. is constructed to analyze the effects of different parameters on local Nusselt number $(\text{Re}_x)^{-1/2} Nu_x$. This Table shows that the local Nusselt Number $(\text{Re}_x)^{-1/2} Nu_x$ is an increasing function of α, β_i and Pr whereas it decreases when M, β_e and Ec are increased. In fact heat transfer rate increases when α, β_i and Pr are increased whereas it decreases by increasing M, β_e and Ec.
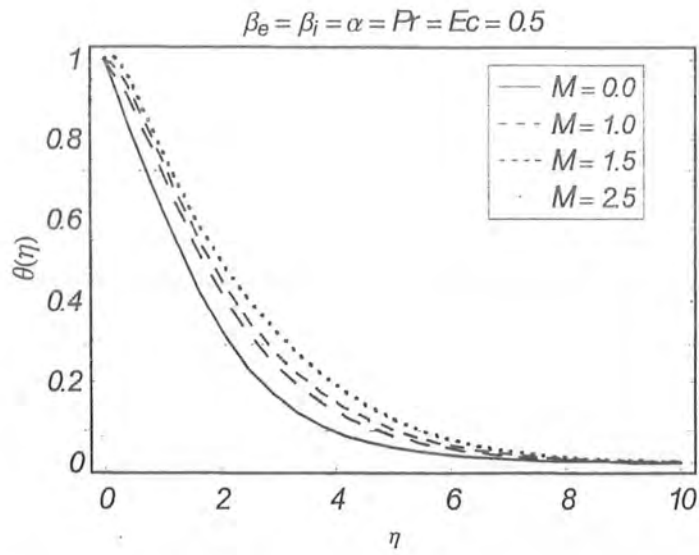
Fig. 6.2. Influence of Hartman number M on dimensionless temperature $\theta(\eta)$.
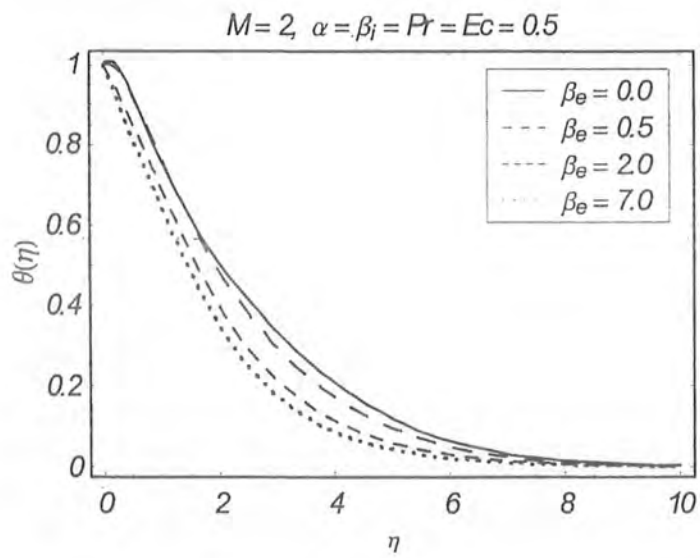
Fig. 6.3. Influence of Hall parameter β_e on dimensionless temperature $\theta(\eta)$.
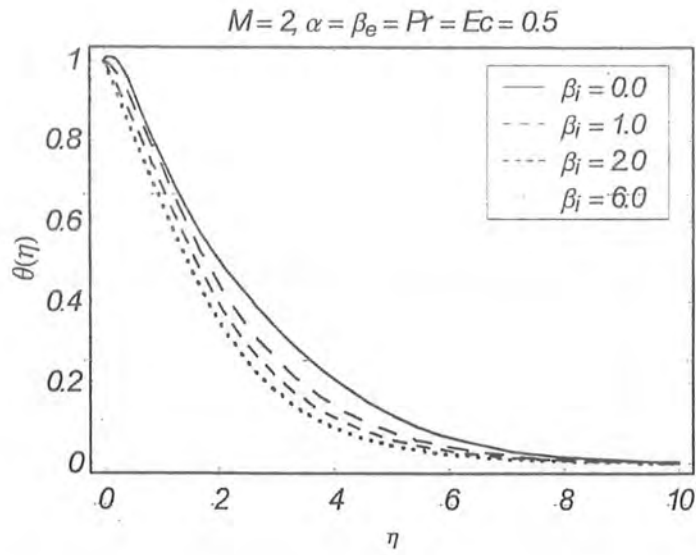
Fig. 6.4. Influence of ion slip parameter β_i on dimensionless temperature $\theta(\eta)$.
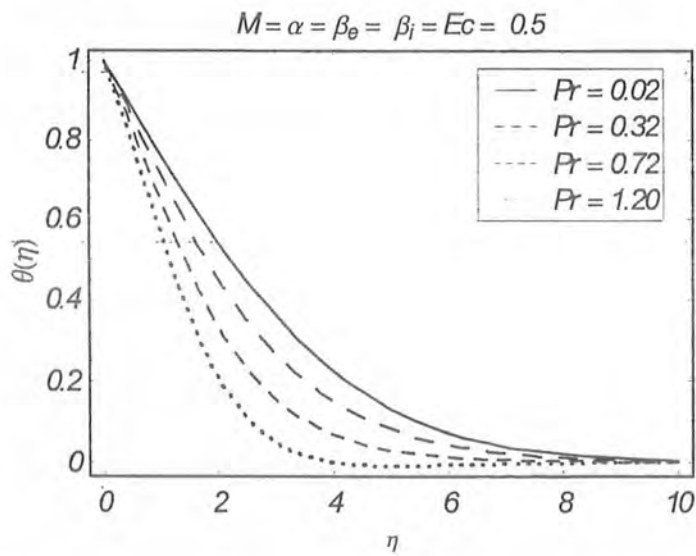
Fig. 6.5. Influence of Prandtl number Pr on dimensionless temperature $\theta(\eta)$.

96
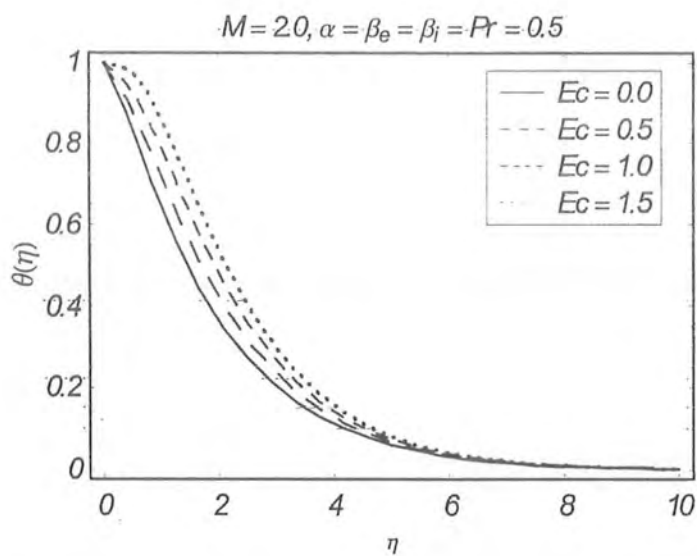
Fig. 6.6. Influence of local Eckert number Ec on dimensionless temperature $\theta(\eta)$.

Table 6.2. Comparison of the values of $\theta'(0)$ for various values of Pr when $M = \beta_i = \beta e = Ec = \alpha = 0$.

Pr	Gupta and Gupta [42]	Grubka and Bobba [43]	Ali [44]	Salem and El-Aziz [67]	present case
0.7			-0.45255	-0.45605	-0.45394
1.0	-0.5820	-0.5820	-0.59988	-0.58223	-0.58197
10.0		-2.3080	2.29589	-2.30789	-2.30806

Table 6.3. Variation of Nusselt number Nu_x for various values of M, α, β_e, β_i Pr and Ec when $\hbar_\theta = \hbar_f = \hbar_g = -1$.

M	α	p	β_i	Pr	Ec	$-(\mathrm{Re}_x)^{-1/2} Nu_x$
0.0	0.1	0.5	0.5	0.72	0.5	0.322583
0.5						0.221351
1.0						0.135440
1.5						0.061121
1.0	0.0	0.5	0.5	0.72	0.5	0.126223
	0.1					0.136803
	0.2					0.144720
	0.3					0.150787
1.0	0.1	0.0	0.5			0.322583
		0.5				0.221351
		1.0				0.135440
		1.5				0.061121
1.0	0.1	0.5	0.0	0.72	0.5	0.096266
			0.5			0.142932
			1.0			0.174617
			1.5			0.196692
1.0	0.1	0.5	0.5	0.02	0.5	0.122447
				0.37		0.115851
				0.72		0.135440
				1.07		0.151798
1.0	0.1	0.5	0.5	0.72	0.0	-0.422768
					0.5	-0.134301
					1.0	0.154166
					1.5	0.442633

99

6.5 Final remarks

This chapter investigated the effect of heat transfer on MHD steady three-dimensional flow of an incompressible thermodynamically second grade fluid in the presence of Joule heating, Hall and ion-slip currents and viscous dissipation. Main findings of the analysis can be summarized as follows:

- Behavior of M is opposite to that of β_e, β_i and Pr on $\theta(\eta)$ but similar to that of Ec.

- Effects of β_e and β_i on $f'(\eta)$ and $\theta(\eta)$ are opposite.

- Qualitatively, influence of β_i on $g(\eta)$ and $\theta(\eta)$ is opposite.

- Skin friction coefficient $(\text{Re}_x)^{1/2} C_{f_x}$ is an increasing function of M and α whereas it decreases when β_e and β_i are increased.

- $(\text{Re}_x)^{1/2} C_{g_x}$ increases by increasing M, α and β_e and decreases with an increase in β_i.

- Effects of Pr and Ec on $\theta(\eta)$ are opposite.

- $(\text{Re}_x)^{-1/2} Nu_x$ is an increasing function of α, β_i, Pr and Ec but it decreases when β_e is increased. This witnesses that heat transfer from surface into fluid increases when α, β_i and Pr are increased whereas it decreases by increasing M, β_e and Ec.

- Thermal boundary layer thickness can be controlled through β_e, β_i and Pr.

Chapter 7

Soret and Dufour effects on the mixed convection three-dimensional flow of a second grade fluid subject to Hall and ion-slip currents

This chapter investigates the Soret and Dufour effects on mixed convection boundary layer three-dimensional flow of an electrically conducting second grade fluid over a linearly stretching vertical sheet. Hall and ion-slip effects are retained in the presence mass diffusion of chemically reacting species. Joule heating is present. The governing partial differential equations are transformed into the ordinary differential equations using appropriate transformations. The resulting problems are solved by homotopy analysis method (HAM). A comparative study between the present and existing limiting results is shown. The variations embedded flow parameters on dimensionless velocities, temperature and concentration field are examined. The skin friction coefficients, Nusselt number and Sherwood number for different values of involved parameters are analyzed.

7.1 Description of the problem

Here we examine the steady and laminar three-dimensional mixed convection boundary-layer flow of a second grade fluid over a linearly stretching vertical sheet at $y = 0$. The fluid is electrically conducting and stretching surface is insulating. A sheet is maintained at constant temperature T_w and constant concentration C_w. However, T_∞ and C_∞ are the temperature and concentration regarding ambient fluid respectively. A uniform magnetic field perpendicular to sheet is applied and Hall, ion-slips and buoyancy effects are taken into account. Magnetic Reynolds number is small and therefore induced magnetic field is neglected. Due to Hall current, there is a force (Hall force) in z-direction which induces a cross flow in that direction and hence flow becomes three-dimensional (see [60, 67, 68]). Physical model is given in Fig. 7.1. Velocity, temperature and concentration fields do not depend upon variable z. This assumption is valid because stretching sheet is of infinite width in z-direction. Hence $\mathbf{V} = [u(x, y), v(x, y), w(x, y)]$, $T = T(x, y)$, $C = C(x, y)$. Moreover, viscous dissipation, Joule heating, higher order chemical reaction, thermal-diffusion and diffusion-thermo effects are considered. The steady boundary layer equations for present flow are

$$\frac{\partial u}{\partial x} + \frac{\partial v}{\partial y} = 0, \tag{7.1}$$

$$u\frac{\partial u}{\partial x} + v\frac{\partial u}{\partial y} = \nu\frac{\partial^2 u}{\partial y^2} + \frac{\alpha_1}{\rho}\left[u\frac{\partial^3 u}{\partial x \partial y^2} + v\frac{\partial^3 u}{\partial y^3} + \frac{\partial u}{\partial x}\frac{\partial^2 u}{\partial y^2} + \frac{\partial u}{\partial y}\frac{\partial^2 u}{\partial x \partial y} + \frac{\partial w}{\partial y}\frac{\partial^2 w}{\partial x \partial y} + \frac{\partial w}{\partial x}\frac{\partial^2 w}{\partial y^2}\right]$$
$$- \frac{\sigma B_0^2}{\rho\left[(1 + \beta_e\beta_i)^2 + \beta_e^2\right]}\left[(1 + \beta_e\beta_i)u + \beta_e w\right] + \beta_T\bar{g}(T - T_\infty) + \beta_C\bar{g}(C - C_\infty), \tag{7.2}$$

$$u\frac{\partial w}{\partial x} + v\frac{\partial w}{\partial y} = \nu\frac{\partial^2 w}{\partial y^2} + \frac{\alpha_1}{\rho}\left[u\frac{\partial^3 w}{\partial x \partial y^2} + v\frac{\partial^3 w}{\partial y^3}\right] + \frac{\sigma B_0^2 * [\beta_e u - (1 + \beta_e\beta_i)w]}{\rho\left[(1 + \beta_e\beta_i)^2 + \beta_e^2\right]}, \tag{7.3}$$

$$u\frac{\partial T}{\partial x} + v\frac{\partial T}{\partial y} = \frac{K_c}{\rho c_p}\frac{\partial^2 T}{\partial y^2} + \frac{\sigma B_0^2}{\rho c_p\left[(1 + \beta_e\beta_i)^2 + \beta_e^2\right]}\left[u^2 + w^2\right] + \frac{\nu}{c_p}\left[\left(\frac{\partial u}{\partial y}\right)^2 + \left(\frac{\partial w}{\partial y}\right)^2\right]$$
$$+ \frac{\alpha_1}{\rho c_p}\left[u\frac{\partial u}{\partial y}\frac{\partial^2 u}{\partial x \partial y} + v\frac{\partial u}{\partial y}\frac{\partial^2 u}{\partial y^2} + v\frac{\partial w}{\partial y}\frac{\partial^2 w}{\partial y^2} + u\frac{\partial w}{\partial y}\frac{\partial^2 w}{\partial x \partial y}\right] + \frac{DK_T}{\rho c_p C_s}\frac{\partial^2 C}{\partial y^2}, \tag{7.4}$$

$$u\frac{\partial C}{\partial x} + v\frac{\partial C}{\partial y} = D\frac{\partial^2 C}{\partial y^2} - K_1(C - C_\infty)^n + \frac{DK_T}{T_m}\frac{\partial^2 T}{\partial y^2}. \tag{7.5}$$

102
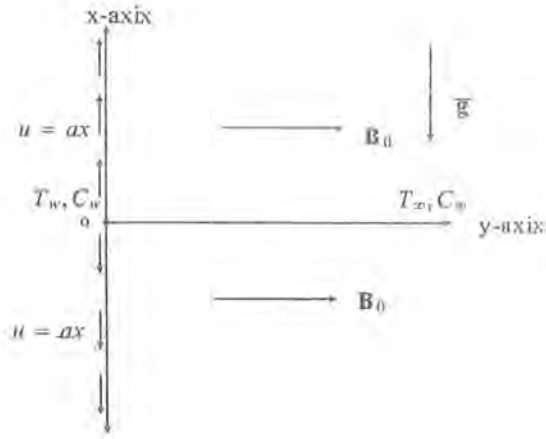
Fig. 7.1. Geometry of the problem and coordinate system.

The relevant boundary conditions are

$$u = ax, \quad v = 0, \quad w = 0, \quad T = T_w, \quad C = C_w \quad \text{at} \quad y = 0,$$

$$u \to 0, \quad T \to T_\infty, \quad C \to C_\infty \qquad \text{as} \quad y \to \infty. \tag{7.6}$$

In above equations u, v and w are the velocity components in the $x-$, $y-$ and $z-$directions, $\alpha_1 (\geq 0)$ is the material constant, ρ is the density of fluid, $\sigma \left(= e^2 n_e \tau_e / m_e\right)$ is the electrical conductivity, $\beta_e \left(= \omega_e \tau_e\right)$ is the Hall parameter, $\beta_i \left(= e n_e B_0 / \left(1 + n_e/n_a\right) K_{ai}\right)$ is the ion-slip parameter, where τ_e is the electron collision time, me is the mass of electron, ω_e is the electron frequency, n_e is the electron number density, n_a is neutral particle density, K_{ai} is the friction coefficient between ions and neutral particles, K_c is the thermal conductivity, K_T is the concentration susceptibility, T_m is the mean temperature of the fluid, K_1 is the chemical reaction constant, D is the coefficient of mass diffusivity, c_p is the specific heat of fluid, $\overline{g}$ is the gravitational acceleration, β_T is the coefficient of thermal expansion, β_C is the coefficient of expansion with concentration and n $(n = 1, 2, 3)$ is the order of chemical reaction.

103

Defining

$$u = axf'(\eta), \quad v = -\sqrt{a\nu}f(\eta), \quad w = axg(\eta),$$

$$\theta(\eta) = \frac{T - T_\infty}{T_w - T_\infty}, \quad \phi(\eta) = \frac{C - C_\infty}{C_w - C_\infty}, \quad \eta = \sqrt{\frac{a}{\nu}}y, \tag{7.7}$$

equations. $(7.1) - (7.5)$ can be presented as

$$f''' - \frac{M\left[(1 + \beta_e\beta_i)f' + \beta_e g\right]}{(1 + \beta_e\beta_i)^2 + \beta_e^2} + ff'' - (f')^2 + Gr\theta + Gc\phi$$
$$+ \alpha\left[2f'f''' - ff^{(iv)} + (f'')^2 + (g')^2 + gg''\right] = 0, \tag{7.8}$$

$$g'' + \frac{M}{(1 + \beta_e\beta_i)^2 + \beta_e^2}\left[\beta_e f' - (1 + \beta_e\beta_i)g\right] - f'g + fg'$$
$$+ \alpha\left[f'g'' - fg'''\right] = 0, \tag{7.9}$$

$$\theta'' + \Pr f\theta' + \frac{\Pr EcM}{(1 + \beta_e\beta_i)^2 + \beta_e^2}\left[(f')^2 + g^2\right] + \Pr Ec\left[(f'')^3\right.$$
$$\left. + (g')^2\right] + \Pr Du\phi''$$
$$+ \alpha\Pr Ec\left[f'(g')^2 - fg'g'' - ff''f''' + f'(f'')^2\right] = 0, \tag{7.10}$$

$$\phi'' + Scf\phi' + SrSc\theta'' - Sc\gamma\phi^n = 0, \tag{7.11}$$

and boundary conditions now are

$$f(0) = 0, \quad f'(0) = 1, \quad f'(\infty) = 0,$$

$$g(0) = 0, \quad g(\infty) = 0,$$

$$\theta(0) = 1, \quad \theta(\infty) = 0,$$

$$\phi(0) = 1, \quad \phi(\infty) = 0, \tag{7.12}$$

in which

$$M = \frac{\sigma B_0^2}{\rho a}, \quad \alpha = \alpha_1 a/\mu, \quad \Pr = \frac{\mu c_p}{K_c}, \quad Ec = \frac{(ax)^2}{c_p(T_w - T_\infty)}, Sc = \frac{\nu}{D},$$

$$Sr = \frac{DK_T(T_w - T_\infty)}{\nu(C_w - C_\infty)T_m}, \quad Du = \frac{DK_T(C_w - C_\infty)}{\nu c_p C_s(T_w - T_\infty)}, \quad \gamma = \frac{K_1(C_w - C_\infty)^{n-1}}{a},$$

$$Gr = \frac{\bar{g}\beta_T(T_w - T_\infty)}{a^2 x}, \quad Gc = \frac{\bar{g}\beta_C(C_w - C_\infty)}{a^2 x}$$

are respectively the Hartman number, the second grade parameter, the Prandtl number, the local Eckert number, the Schmidt number, the Soret number, the Dufour number, the chemical reaction parameter, the local Grashof number due to temperature differences and the local Grashof number due to concentration differences. It is worth mentioning to note that the case for $\beta_e = 0$ corresponds to the situation when Hall current is absent and $\beta_i = 0$ corresponds to the case when ion-slip current is not present. It should be mentioned that $\gamma > 0$ corresponds to destructive chemical reaction, $\gamma < 0$ indicates a constructive chemical reaction and $\gamma = 0$ holds when there is no chemical reaction occurring in the flow regime. Furthermore, for $Gr > 0$, $Gc > 0$ buoyancy forces assist the flow whereas $Gr < 0$, $Gc < 0$ corresponds to the opposing flow. The skin friction coefficients C_{f_x}, C_{g_z}, Nusselt number Nu_x and Sherwood number Sh_x are defined by the following expressions

$$
\begin{aligned}
C_{f_x} &= \frac{\tau_{wy}|_{y=0}}{\rho\,(ax)^2} = \frac{\mu \frac{\partial u}{\partial y}\big|_{y=0} + \alpha_1 \left[u\frac{\partial^2 u}{\partial x \partial y} + v\frac{\partial^2 u}{\partial y^2} + 2\frac{\partial u}{\partial x}\frac{\partial u}{\partial y} + \frac{\partial w}{\partial x}\frac{\partial w}{\partial y} \right]\big|_{y=0}}{\rho\,(ax)^2} \\
&= (1 + 3\alpha)\,(\mathrm{Re}_x)^{-1/2}\,f''(0), \qquad\qquad\qquad\qquad\qquad\qquad (7.13)
\end{aligned}
$$

$$
\begin{aligned}
C_{g_z} &= \frac{\tau_{wz}|_{y=0}}{\rho\,(ax)^2} = \frac{\mu \frac{\partial w}{\partial y}\big|_{y=0} + \alpha_1 \left[\frac{\partial u}{\partial x}\frac{\partial w}{\partial y} + v\frac{\partial^2 w}{\partial y^2} - \frac{\partial w}{\partial x}\frac{\partial v}{\partial x} + u\frac{\partial^2 w}{\partial x \partial y} \right]\big|_{y=0}}{\rho\,(ax)^2} \\
&= (1 + 3\alpha)\,(\mathrm{Re}_x)^{-1/2}\,g'(0), \qquad\qquad\qquad\qquad\qquad\qquad (7.14)
\end{aligned}
$$

$$
Nu_x = \frac{x q_w}{K_c (T_w - T_\infty)} = -\frac{x\,K_c \frac{\partial T}{\partial y}\big|_{y=0}}{K_c (T_w - T_\infty)} = -(\mathrm{Re}_x)^{1/2}\,\theta'(0), \qquad (7.15)
$$

$$
Sh_x = \frac{x h_w}{D} = -\frac{x\,D \frac{\partial C}{\partial y}\big|_{y=0}}{D (C_w - C_\infty)} = -(\mathrm{Re}_x)^{1/2}\,\phi'(0), \qquad (7.16)
$$

where Re_x is the local Reynolds number, τ_{wx}, τ_{wz} shear stresses in the x- and z-directions, q_w is the heat flux and h_w is the mass flux at the stretching surface. These physical quantities are defined by the following expressions

$$
\mathrm{Re}_x = \frac{ax^2}{\nu},\ \tau_{wx} = \tau_{xy}|_{y=0},\ \tau_{wz} = \tau_{zy}|_{y=0},\ q_w = -K\frac{\partial T}{\partial y}\Big|_{y=0},\ h_w = -D\frac{\partial C}{\partial y}\Big|_{y=0}.
$$

7.2 Solutions by homotopy analysis method

7.2.1 Zeroth-order solutions

For HAM solutions we write $f(\eta)$, $g(\eta)$, $\theta(\eta)$ and $\phi(\eta)$ in the form of base functions

$$\left\{ \eta^k \exp(-p\eta), \ k \geq 0, \ p \geq 0 \right\}, \tag{7.17}$$

by the following expressions

$$f(\eta) = a_{0,0}^0 + \sum_{p=1}^{m} \sum_{k=1}^{m} a_{m,p}^k \eta^k \exp(-p\eta), \tag{7.18}$$

$$g(\eta) = \sum_{p=1}^{m} \sum_{k=1}^{m} b_{m,l}^k \eta^k \exp(-p\eta), \tag{7.19}$$

$$\theta(\eta) = \sum_{p=1}^{m} \sum_{k=1}^{m} c_{m,p}^k \eta^k \exp(-p\eta), \tag{7.20}$$

$$\phi(\eta) = \sum_{p=1}^{m} \sum_{k=1}^{m} d_{m,p}^k \eta^k \exp(-p\eta), \tag{7.21}$$

where $a_{m,p}^k$, $b_{m,p}^k$, $c_{m,p}^k$ and $d_{m,p}^k$ are the coefficients. Employing rule of solution expressions, the initial guesses and linear operators $\mathcal{L}_f$, $\mathcal{L}_g$, $\mathcal{L}_\theta$ and $\mathcal{L}_\phi$ are chosen of the form

$$f_0(\eta) = 1 - \exp(-\eta), \tag{7.22}$$

$$g_0(\eta) = 0, \tag{7.23}$$

$$\theta_0(\eta) = \frac{1}{2}\eta \exp(-\eta) + \exp(-\eta), \tag{7.24}$$

$$\phi_0(\eta) = \frac{1}{2}\eta \exp(-\eta) + \exp(-\eta), \tag{7.25}$$

106

$$\mathscr{L}_f\left[f\left(\eta\right)\right] = \frac{d^3 f}{d\eta^3} - \frac{df}{d\eta}, \tag{7.26}$$

$$\mathscr{L}_g\left[g\left(\eta\right)\right] = \frac{d^2 g}{d\eta^2} - g, \tag{7.27}$$

$$\mathscr{L}_\theta\left[\theta\left(\eta\right)\right] = \frac{d^2\theta}{d\eta^2} - \theta, \tag{7.28}$$

$$\mathscr{L}_\phi\left[\phi\left(\eta\right)\right] = \frac{d^2\phi}{d\eta^2} - \phi. \tag{7.29}$$

The linear operators $\mathscr{L}_f$, $\mathscr{L}_g$, $\mathscr{L}_\theta$ and $\mathscr{L}_\phi$ have the following properties

$$\mathscr{L}_f\left[C_1 + C_2\exp\left(\eta\right) + C_3\exp\left(-\eta\right)\right] = 0,$$

$$\mathscr{L}_g\left[C_4\exp\left(\eta\right) + C_5\exp\left(-\eta\right)\right] = 0,$$

$$\mathscr{L}_\theta\left[C_6\exp\left(\eta\right) + C_7\exp\left(-\eta\right)\right] = 0,$$

$$\mathscr{L}_\phi\left[C_8\exp\left(\eta\right) + C_9\exp\left(-\eta\right)\right] = 0, \tag{7.30}$$

where $C_i\,(i = 1 - 9)$ are the arbitrary constants.

7.2.2 Zeroth order deformation problems

The problems at the zeroth order satisfy

$$(1-q)\mathscr{L}_f\left[\hat{f}(\eta;q) - f_0(\eta)\right] = q\hbar_f\mathcal{N}_f\left[\hat{f}(\eta;q), \hat{g}(\eta;q), \hat{\theta}(\eta;q), \hat{\phi}(\eta;q)\right],$$

$$(1-q)\mathscr{L}_g\left[\hat{g}(\eta;q) - g_0(\eta)\right] = q\hbar_g\mathcal{N}_g\left[\hat{g}(\eta;q), \hat{f}(\eta;q), \hat{\theta}(\eta;q), \hat{\phi}(\eta;q)\right],$$

$$(1-q)\mathscr{L}_\theta\left[\hat{\theta}(\eta;q) - \theta_0(\eta)\right] = q\hbar_\theta\mathcal{N}_\theta\left[\hat{\theta}(\eta;q), \hat{g}(\eta;q), \hat{f}(\eta;q), \hat{\phi}(\eta;q)\right],$$

$$(1-q)\mathscr{L}_\phi\left[\hat{\phi}(\eta;q) - \phi_0(\eta)\right] = q\hbar_\phi\mathcal{N}_\phi\left[\hat{\theta}(\eta;q), \hat{g}(\eta;q), \hat{f}(\eta;q), \hat{\phi}(\eta;q)\right], \tag{7.31}$$

$$\hat{f}(0;q) = 0, \quad \left.\frac{\partial\hat{f}(\eta;q)}{\partial\eta}\right|_{\eta=0} = 1, \quad \left.\frac{\partial\hat{f}(\eta;q)}{\partial\eta}\right|_{\eta\to\infty} = 0,$$

$$\hat{g}(0;q) = 0, \quad \left.\frac{\partial\hat{g}(\eta;q)}{\partial\eta}\right|_{\eta\to\infty} = 0,$$

$$\hat{\theta}(0;q) = 1, \quad \hat{\theta}(\infty;q) = 0,$$

$$\hat{\phi}(0;q) = 1, \quad \hat{\phi}(\infty;q) = 0. \tag{7.32}$$

The nonlinear operators $\mathcal{N}_f$, $\mathcal{N}_g$, $\mathcal{N}_\theta$, and $\mathcal{N}_f$ are expressed by the following expressions

$$\mathcal{N}_f\left[\hat{f}(\eta;q),\hat{g}(\eta;q),\hat{\theta}(\eta;q),\hat{\phi}(\eta;q)\right] = \frac{\partial^3 \hat{f}(\eta;q)}{\partial\eta^3} + \hat{f}(\eta;q)\frac{\partial^2 \hat{f}(\eta;q)}{\partial\eta^2} - \left(\frac{\partial \hat{f}(\eta;q)}{\partial\eta}\right)^2$$

$$+\alpha\left[2\frac{\partial \hat{f}(\eta;q)}{\partial\eta}\frac{\partial^3 \hat{f}(\eta;q)}{\partial\eta^3} + \left(\frac{\partial^2 \hat{f}(\eta;q)}{\partial\eta^2}\right)^2 - \hat{f}(\eta;q)\frac{\partial^4 \hat{f}(\eta;q)}{\partial\eta^4} + \hat{g}(\eta;q)\frac{\partial^2 \hat{g}(\eta;q)}{\partial\eta^2}\right]$$

$$+\alpha\left(\frac{\partial \hat{g}(\eta;q)}{\partial\eta}\right)^2 + Gr\hat{\theta}(\eta;q) + Gc\hat{\phi}(\eta;q) - \frac{M}{(1+\beta_e\beta_i)^2+\beta_e^2}\left[\begin{array}{c}(1+\beta_e\beta_i)\frac{\partial \hat{f}(\eta;q)}{\partial\eta}\\+\beta_e\hat{g}(\eta;q)\end{array}\right] \quad (7.33)$$

$$\mathcal{N}_g\left[\hat{g}(\eta;q),\hat{f}(\eta;q),\hat{\theta}(\eta;q),\hat{\phi}(\eta;q)\right] = \frac{\partial^2 \hat{g}}{\partial\eta^2} + \alpha\left[\frac{\partial \hat{f}(\eta;q)}{\partial\eta}\frac{\partial^2 \hat{g}(\eta;q)}{\partial\eta^2} - \hat{f}(\eta;q)\frac{\partial^3 \hat{g}(\eta;q)}{\partial\eta^3}\right]$$

$$+\hat{f}(\eta;q)\frac{\partial \hat{g}(\eta;q)}{\partial\eta} - \hat{g}(\eta;q)\frac{\partial \hat{f}(\eta;q)}{\partial\eta} + \frac{M}{(1+\beta_e\beta_i)^2+\beta_e^2}\left[\begin{array}{c}\beta_e\frac{\partial \hat{f}(\eta;q)}{\partial\eta}\\-(1+\beta_e\beta_i)\hat{g}(\eta;q)\end{array}\right], (7.34)$$

$$\mathcal{N}_\theta\left[\hat{\theta}(\eta;q),\hat{g}(\eta;q),\hat{f}(\eta;q),\hat{\phi}(\eta;q)\right] = \frac{\partial^2 \hat{\theta}(\eta;q)}{\partial\eta^2} + \Pr\hat{f}(\eta;q)\frac{\partial \hat{\theta}(\eta;q)}{\partial\eta}$$

$$+\frac{\Pr EcM}{(1+\beta_e\beta_i)^2+\beta_e^2}\left[\left(\frac{\partial \hat{f}(\eta;q)}{\partial\eta}\right)^2 + (\hat{g}(\eta;q))^2\right]$$

$$+\Pr Ec\left[\left(\frac{\partial^2 \hat{f}(\eta;q)}{\partial\eta^2}\right)^2 + \left(\frac{\partial \hat{g}(\eta;q)}{\partial\eta}\right)^2\right] + \alpha\Pr Ec\frac{\partial \hat{f}(\eta;q)}{\partial\eta}\left(\frac{\partial^2 \hat{f}(\eta;q)}{\partial\eta^2}\right)^2$$

$$+\alpha\left[\Pr Ec\frac{\partial \hat{f}(\eta;q)}{\partial\eta}\left(\frac{\partial \hat{g}(\eta;q)}{\partial\eta}\right)^2 - \Pr Ec\hat{f}(\eta;q)\frac{\partial \hat{g}(\eta;q)}{\partial\eta}\frac{\partial^2 \hat{g}(\eta;q)}{\partial\eta^2}\right]$$

$$-\alpha\Pr Ec\hat{f}(\eta;q)\frac{\partial^2 \hat{f}(\eta;q)}{\partial\eta^2}\frac{\partial^3 \hat{f}(\eta;q)}{\partial\eta^3} + \Pr Du\frac{\partial^2 \hat{\theta}(\eta;q)}{\partial\eta^2}, \quad (7.35)$$

$$\mathcal{N}_\phi\left[\hat{\theta}(\eta;q),\hat{g}(\eta;q),\hat{f}(\eta;q),\hat{\phi}(\eta;q)\right] = \frac{\partial^2 \hat{\phi}(\eta;q)}{\partial\eta^2} + Sc\hat{f}(\eta;q)\frac{\partial \hat{\phi}(\eta;q)}{\partial\eta}$$

$$+ScSr\frac{\partial^2 \hat{\theta}(\eta;q)}{\partial\eta^2} - \gamma\left(\hat{\phi}(\eta;q)\right)^n. \quad (7.36)$$

In above expressions embedding parameter $q \in [0,1]$. $\hbar_f$, $\hbar_g$, $\hbar_\theta$, and $\hbar_\phi$ are non zero auxiliary

parameters. For $q = 0$ and $q = 1$ the above zeroth order deformation equations reduce to

$$
\begin{aligned}
\hat{f}(\eta; 0) &= f_0(\eta), & \hat{f}(\eta; 1) &= f(\eta) \\
\hat{g}(\eta; 0) &= g_0(\eta), & \hat{g}(\eta; 1) &= g(\eta) \\
\hat{\theta}(\eta; 0) &= \theta_0(\eta), & \hat{\theta}(\eta; 1) &= \theta(\eta) \\
\hat{\phi}(\eta; 0) &= \phi_0(\eta), & \hat{\phi}(\eta; 1) &= \phi(\eta)
\end{aligned}
$$

Upon making use of Taylor's series we obtain

$$
\hat{f}(\eta; q) = f_0(\eta) + \sum_{m=1}^{\infty} f_m(\eta,) q^m, \quad \hat{g}(\eta; q) = g_0(\eta) + \sum_{m=1}^{\infty} g_m(\eta) q^m,
$$

$$
\hat{\theta}(\eta; q) = \theta_0(\eta) + \sum_{m=1}^{\infty} \theta_m(\eta) q^m, \quad \hat{\phi}(\eta; q) = \phi_0(\eta) + \sum_{m=1}^{\infty} \phi_m(\eta) q^m, \tag{7.37}
$$

in which

$$
f_m(\eta) = \frac{1}{m!} \left. \frac{\partial^m \hat{f}(\eta; q)}{\partial \eta^m} \right|_{q=0}, \quad g_m(\eta) = \frac{1}{m!} \left. \frac{\partial^m \hat{g}(\eta; q)}{\partial \eta^m} \right|_{q=0},
$$

$$
\theta_m(\eta) = \frac{1}{m!} \left. \frac{\partial^m \hat{\theta}(\eta; q)}{\partial \eta^m} \right|_{q=0}, \quad \phi_m(\eta) = \frac{1}{m!} \left. \frac{\partial^m \hat{\phi}(\eta; q)}{\partial \eta^m} \right|_{q=0}. \tag{7.38}
$$

7.2.3 Higher order deformation problems

The deformation problems at the mth-order satisfy

$$
\mathcal{L}_f \left[f_m(\eta) - \chi_m f_{m-1}(\eta) \right] = \hbar_f \mathcal{R}_m^f \left(f_{m-1}(\eta), g_{m-1}(\eta), \theta_{m-1}(\eta), \phi_{m-1}(\eta) \right),
$$

$$
f_m(0) = 0, \; f_m'(0) = 0, \; f_m'(\infty) = 0, \tag{7.39}
$$

$$
\mathcal{L}_g \left[g_m(\eta) - \chi_m g_{m-1}(\eta) \right] = \hbar_f \mathcal{R}_m^g \left(f_{m-1}(\eta), g_{m-1}(\eta), \theta_{m-1}(\eta), \phi_{m-1}(\eta) \right),
$$

$$
g_m(0) = 0, \; g_m(\infty) = 0, \tag{7.40}
$$

109

$$\mathcal{L}_\theta \left[\theta_m(\eta) - \chi_m \theta_{m-1}(\eta) \right] = \hbar_\theta \mathcal{R}_m^\theta \left(f_{m-1}(\eta), g_{m-1}(\eta), \theta_{m-1}(\eta), \phi_{m-1}(\eta) \right), \qquad (7.41)$$

$$\theta_m(0) = 1, \ \theta_m(\infty) = 0,$$

$$\mathcal{L}_\phi \left[\phi_m(\eta) - \chi_m \phi_{m-1}(\eta) \right] = \hbar_\phi \mathcal{R}_m^\phi \left(f_{m-1}(\eta), g_{m-1}(\eta), \theta_{m-1}(\eta), \phi_{m-1}(\eta) \right),$$

$$\phi_m(0) = 1, \ \phi_m(\infty) = 0, \qquad (7.42)$$

$$\chi_m = \begin{cases} 0, m \leq 1, \\ 1, m > 1, \end{cases}$$

$$\mathcal{R}_m^f \left(f_{m-1}(\eta), g_{m-1}(\eta), \theta_{m-1}(\eta), \phi_{m-1}(\eta) \right) = f_{m-1}'''(\eta) - \frac{M}{(1 + \beta_e \beta_i)^2 + \beta_e^2} \times$$

$$\left[(1 + \beta_e \beta_i) f_{m-1}'(\eta) + \beta_e g_{m-1}(\eta) \right] + \sum_{r=0}^{m-1} \left[f_r(\eta) f_{m-1-r}''(\eta) - f_r'(\eta) f_{m-1-r}'(\eta) \right]$$

$$+ \alpha \sum_{r=0}^{m-1} \left[f_r''(\eta) f_{m-1-r}''(\eta) + 2 f_r'(\eta) f_{m-1-r}'''(\eta) - f_r(\eta) f_{m-1-r}''''(\eta) \right]$$

$$+ \alpha \sum_{r=0}^{m-1} \left[g_r(\eta) g_{m-1-r}''(\eta) + g_r'(\eta) g_{m-1-r}'(\eta) \right] + Gr \theta_{m-1}(\eta) + Gc \phi_{m-1}(\eta), \qquad (7.43)$$

$$\mathcal{R}_m^g \left(f_{m-1}(\eta), g_{m-1}(\eta), \theta_{m-1}(\eta), \phi_{m-1}(\eta) \right) = g_{m-1}''(\eta) + \frac{M}{(1 + \beta_e \beta_i)^2 + \beta_e^2} \times$$

$$\left[\beta_e f_{m-1}'(\eta) - (1 + \beta_e \beta_i) g_{m-1}(\eta) \right]$$

$$+ \sum_{r=0}^{m-1} \left[f_r(\eta) g_{m-1-r}'(\eta) - f_r'(\eta) g_{m-1-r}(\eta) \right]$$

$$+ \alpha \sum_{r=0}^{m-1} \left[f_r'(\eta) g_{m-1-r}''(\eta) - f_r(\eta) g_{m-1-r}'''(\eta) \right], \qquad (7.44)$$

$$\mathcal{R}_m^\theta \left(f_{m-1}(\eta), g_{m-1}(\eta), \theta_{m-1}(\eta), \phi_{m-1}(\eta) \right) = \theta''_{m-1}(\eta)$$

$$+ \Pr \sum_{r=0}^{m-1} f_r(\eta)\, \theta'_{m-1-r}(\eta) + \Pr Du\phi''_{m-1}(\eta) \qquad (7.45)$$

$$+ \frac{M}{(1 + \beta_e \beta_i)^2 + \beta_e^2} \sum_{r=0}^{m-1} \left[\begin{array}{c} f'_r(\eta)\, f'_{m-1-r}(\eta) \\ + g_r(\eta)\, g_{m-1-r}(\eta) \end{array} \right]$$

$$+ \Pr Ec \sum_{r=0}^{m-1} \left[f''_r(\eta)\, f''_{m-1-r}(\eta) + g'_r(\eta)\, g'_{m-1-r}(\eta) \right]$$

$$- \alpha \Pr Ec \sum_{l=0}^{r} \sum_{r=0}^{m-1} f_{m-1-r}(\eta)\, f''_{r-l}(\eta)\, f'''_l(\eta)$$

$$+ \alpha \Pr Ec \sum_{l=0}^{r} \sum_{r=0}^{m-1} f'_{m-1-r}(\eta)\, f''_{r-l}(\eta)\, f''_l(\eta)$$

$$+ \alpha \Pr Ec \sum_{l=0}^{r} \sum_{r=0}^{m-1} f'_{m-1-r}(\eta)\, g'_{r-l}(\eta)\, g'_l(\eta)$$

$$- \alpha \Pr Ec \sum_{l=0}^{r} \sum_{r=0}^{m-1} f_{m-1-r}(\eta)\, g'_{r-l}(\eta)\, g''_l(\eta), \qquad (7.46)$$

$$\mathcal{R}_m^\phi \left(\phi_{m-1}(\eta), \theta_{m-1}(\eta), f_{m-1}(\eta), g_{m-1}(\eta) \right) = \phi''_{m-1}(\eta)$$

$$+ Sc \sum_{r=0}^{m-1} f_r(\eta)\, \phi'_{m-1-n}(\eta) - Sc\gamma \sum_{l=0}^{n} \sum_{r=0}^{m-1} \left(\begin{array}{c} \phi_{m-1-r}(\eta)\, \phi_{r-l}(\eta)\, \phi_l(\eta) \\ + Sr Sc\theta''_{m-1}(\eta) \end{array} \right). \qquad (7.47)$$

The general solutions of problems $(7.39) - (7.42)$ can be expressed as

$$
\begin{aligned}
f(\eta) &= f^*(\eta) + C_1^m + C_2^m \exp(\eta) + C_3^m \exp(-\eta), \\
g(\eta) &= g^*(\eta) + C_4^m \exp(\eta) + C_5^m \exp(-\eta), \\
\theta(\eta) &= \theta^*(\eta) + C_6^m \exp(\eta) + C_7^m \exp(-\eta), \\
\phi(\eta) &= \phi^*(\eta) + C_8^m \exp(\eta) + C_9^m \exp(-\eta), \qquad (7.48)
\end{aligned}
$$

where $f^*(\eta)$, $g^*(\eta)$, $\theta^*(\eta)$ and $\phi^*(\eta)$ are the particular solutions of problems given in Eqs. $(7.39) - (7.42)$.

111

7.3 Convergence of homotopy solutions

The convergence of series solutions and their rate of approximations strongly depend upon the values of auxiliary parameters. In order to examine the admissible values of $\hbar$−curves, Figs. $7.2 - 7.4$ are displayed. These Figs. clearly indicate that the admissible ranges for $\hbar_f$ $\hbar_g$, $\hbar_\theta$ and $\hbar_\phi$ are $-1.12 \leq \hbar_f \leq -0.75$, $-1.12 \leq \hbar_g \leq -0.6$ and $-1.2 \leq \hbar_\theta, \hbar_\phi \leq -0.8$. The convergence of derived solutions is achieved at 40th order of approximations (see Table 6.1).
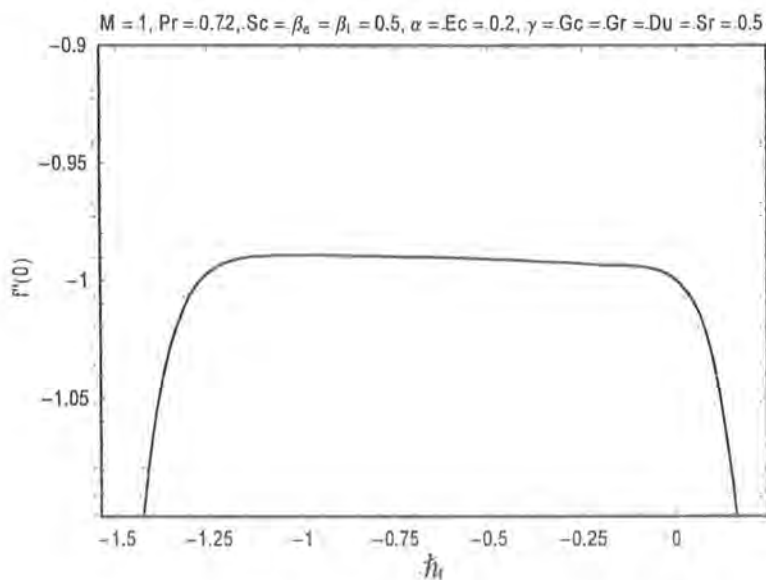

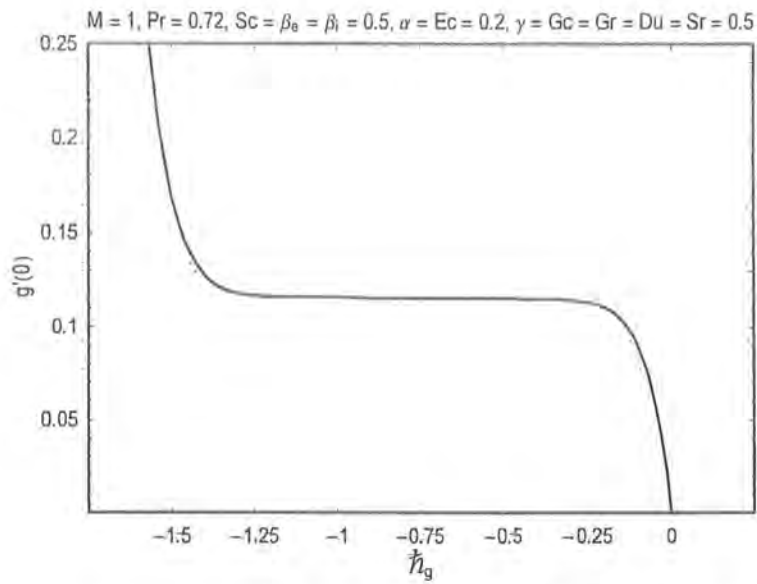Fig. 7.2. $\hbar_f$-curve of $f''(0)$ at 20th order of approximation.

Fig. 7.3. $\hbar_g$-curve of $g'(0)$ at 20th order of approximation.
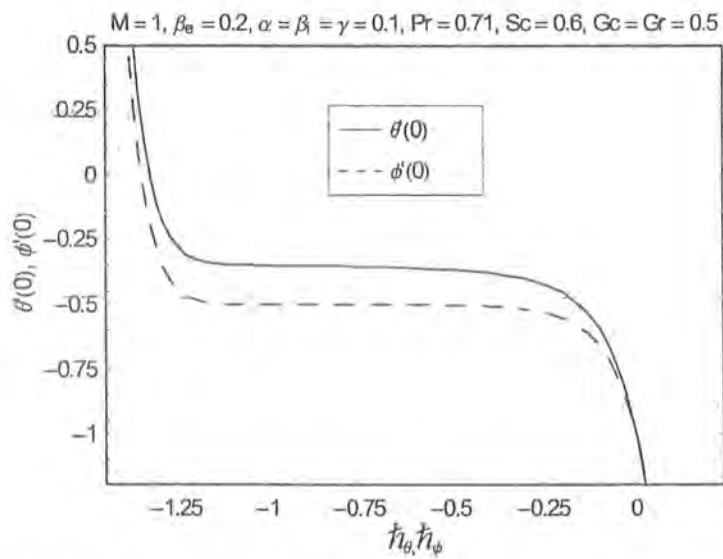

Fig. 7.4. $\hbar_\theta, \hbar_\phi$-curves of $\theta'(0)$ and $\phi'(0)$ at 20th order of approximation.

113

Table 7.1. Convergence of HAM solutions when $M = 1$, $\beta_e = \beta_i = Sc = 0.5$, $Ec = \alpha = 0.2$, $\Pr = 0.72$, $Du = Sr = Gr = Gc = \gamma = 0.1$ and $\hbar_f = \hbar_g = \hbar_\theta = \hbar_\phi = -1.0$.

Order of approximations	$-f''(0)$	$g'(0)$	$-\theta'(0)$	$-\phi'(0)$
1	0.98649425	0.13793103	0.39191724	0.47638889
5	0.98966383	0.11527065	0.34229330	0.43791050
10	0.98928526	0.11578203	0.33571741	0.42694004
15	0.98897231	0.11588232	0.33468969	0.42420425
20	0.98889839	0.11591094	0.33453559	0.42338530
25	0.98887654	0.11591943	0.33452482	0.42311680
30	0.98886972	0.11592212	0.33453139	0.42302427
34	0.98886775	0.11592290	0.33453553	0.42299563
35	0.98886747	0.11592301	0.33453626	0.42299144
36	0.98886724	0.11592310	0.33453690	0.42299903

7.4 Results and discussion

In order to get clear insight of the considered physical problem, dimensionless velocities, temperature and concentration fields are displayed and numerical computations are carried out for various values of pertinent parameters. It is obvious from Fig. 7.5 that velocity component $f'(\eta)$ in x-direction decreases by increasing Schmidt number. This makes sense because Schmidt number Sc is the ratio of momentum diffusivity to the concentration diffusivity and increase in Sc results to increase in viscosity and consequently $f'(\eta)$ decreases. Fig. 7.6 reveals that tangential velocity $f'(\eta)$ increases when Soret number Sr is increased. This is due to the fact that increase in Sr increases the difference between surface temperature and temperature of ambient fluid which reduces the viscosity and consequently tangential velocity $f'(\eta)$ increases. From Fig. 7.7 one can see that tangential velocity $f'(\eta)$ in an increasing function of Dufour number Du. Figs. 7.8 and 7.9 represent the variation of tangential velocity $f'(\eta)$ for various values of convection parameters Gr and Gc. These Figs. show that the tangential velocity $f'(\eta)$ increases for $Gr > 0$ and $Gc > 0$ while it decreases for $Gr < 0$ and $Gc < 0$. It means that for positive values of convection parameters, buoyancy forces act as favorable pressure gradient

whereas for negative values of convection parameters buoyancy forces behave like an adverse pressure gradient. Fig. 7.10 illustrates that the generative chemical reaction ($\gamma < 0$) enhances the motion of fluid in x-direction but for $\gamma > 0$ (a destructive chemical reaction) the motion in x-direction slows down. Figs. $7.5 - 7.10$ reflect that boundary layer thickness corresponding to the tangential velocity $f'(\eta)$ increases when Sr, Du, $Gr(> 0)$, $Gc(> 0)$ and $\gamma(< 0)$ are increased whereas it decreases for an increase in Sc, α, $Gr(< 0)$, $Gc(< 0)$ and $\gamma(> 0)$. It is clear from Fig. 7.11 and 7.12 that for positive values of convection parameters Gr and Gc, the buoyancy forces assist the flow while buoyancy forces oppose the flow when $Gr < 0$ and $Gc < 0$. Hence the buoyancy forces play a vital role in controlling the momentum boundary layer. Effect of Dufour number Du on the dimensionless temperature $\theta(\eta)$ is displayed in Fig. 7.13. Here, one can conclude that dimensionless temperature $\theta(\eta)$ and thermal boundary layer are increased by increasing Du. Figs. 7.14 and 7.15 represent the influence of convection parameters Gr and Gc on dimensionless temperature $\theta(\eta)$. These Figs. illustrate that dimensionless temperature $\theta(\eta)$ increases when $Gr < 0$ and $Gc < 0$ while it decreases for $Gr > 0$ and $Gc > 0$ which shows that the buoyancy forces are important in controlling the temperature and thus thermal boundary layer. Fig. 7.16 shows that concentration field $\phi(\eta)$ decreases when Sc is increased but it increases by increasing Sr (Fig. 7.17). From Figs. 7.18 and 7.19 we can observed that concentration field $\phi(\eta)$ increases for $Gr < 0$ and $Gc < 0$. However, it decreases for $Gr > 0$ and $Gc > 0$. Hence through buoyancy forces the concentration boundary layer can be controlled. Fig. 7.20 indicates that the dimensionless concentration field $\phi(\eta)$ decreases when second grade parameter α is increased and it increases with an increase in Hartmann number M (Fig. 7.21). Three-dimensional view of velocity components are given by Figs. $7.22(a) - (c)$. x-component of velocity $\mathbf{V}$ i.e. $u(x, \eta)$ is maximum near the stretching sheet and vanishes away from the sheet (as shown in Fig 7.22a) whereas y-component of velocity $\mathbf{V}$ i.e. $v(x, \eta)$ is zero near the stretching sheet but it increases away from the stretching sheet (Fig. 7.22b). Fig. 7.22c represents the behavior of z-component of velocity $\mathbf{V}$ i.e. $w(x, \eta)$. From this Fig. one can see that $w(x, \eta)$ increases from zero to maximum value near $\eta = 1$ and then decreases away from the stretching sheet. Tables 7.2 and 7.3 give the comparative study between the present and existing limiting results. These Tables show an excellent agreement between the present and already published results. Table 7.4 gives the variation of skin friction coefficients

115

$-\left(\text{Re}_x\right)^{1/2} C_{fx}$ and $\left(\text{Re}_x\right)^{1/2} C_{g_x}$ in x- and z-directions for various values of physical parameters. From this Table one can see that $-\left(\text{Re}_x\right)^{1/2} C_{fx}$ increases by increasing M, Sc, $\Pr$, γ, $Gr < 0$, $Gc < 0$ and α. However $-\left(\text{Re}_x\right)^{1/2} C_{fx}$ decreases for β_e, β_i, Du, Sr, Ec, α, $Gr > 0$ and $Gc > 0$. Skin friction coefficient $\left(\text{Re}_x\right)^{1/2} C_{g_x}$ in z-direction is an increasing function of M, β_e, Du, Sr, Ec, α, $Gr < 0$, and $Gc < 0$ whereas it decreases when β_i, Sc, $\Pr$, γ $Gr > 0$ and $Gc > 0$ are increased. It is noted from Table 6.4 that $\left(\text{Re}_x\right)^{1/2} C_{g_x} = 0$. This is due to the fact that $M = 0$ corresponds to the situation when there is no magnetic field. Consequently Hall force is zero and flow becomes two-dimensional (later velocity $g\left(\eta\right) = 0$). Therefore skin friction coefficient $\left(\text{Re}_x\right)^{1/2} C_{g_x}$ in z-direction is zero. Variation of local Nusselt number $-\left(\text{Re}_x\right)^{-1/2} Nu_x$ and Sherwood number $-\left(\text{Re}_x\right)^{-1/2} Sh_x$ is presented in Table 7.5. This table shows that local Nusselt number $-\left(\text{Re}_x\right)^{-1/2} Nu_x$ increases with the increase of β_e, Sr, $\Pr$, Gr, Gc, α and n while it decreases for M, β_i, Sc, Du, γ and Ec. Local Sherwood number $-\left(\text{Re}_x\right)^{-1/2} Sh_x$ is an increasing function of β_e, β_i, Sc, Ec and α but it decreases by increasing M, Sr, Du, $\Pr$, Gr, Gc, γ and n.
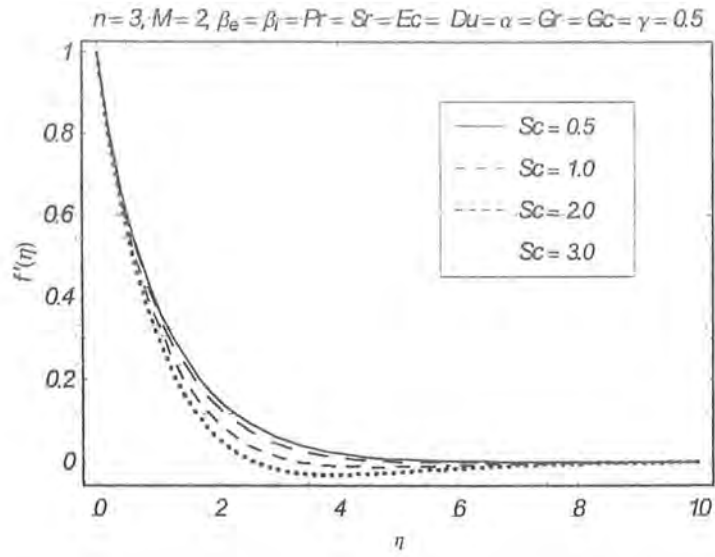
Fig. 7.5. Influence of Schamidt number Sc on dimensionless tangential velocity $f'(\eta)$.
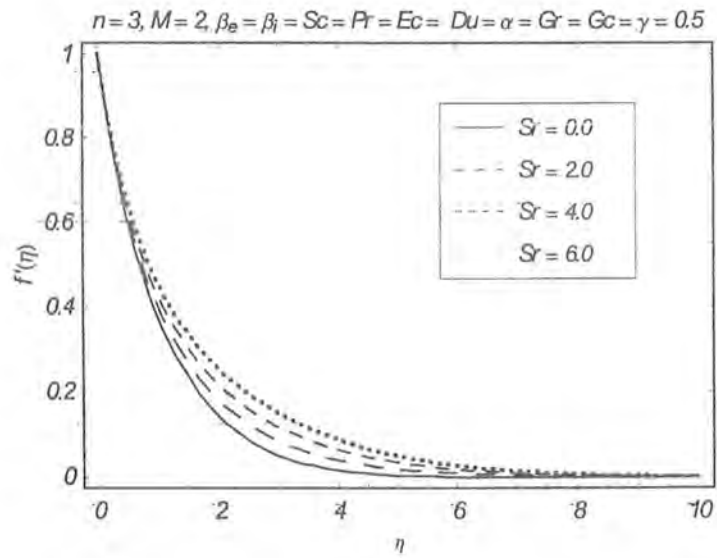
Fig. 7.6. Influence of Soret number Sr on dimensionless tangential velocity $f'(\eta)$.

117

$$n = 3, M = 2, \beta_e = \beta_i = Sc = Sr = Pr = Ec = \alpha = Gr = Gc = \gamma = 0.5$$

Fig. 7.7. Influence of Dufour number Du on dimensionless tangential velocity $f'(\eta)$.

$$n = 3, M = 2, \beta_e = \beta_i = Sc = Sr = Pr = Ec = Du = \alpha = Gc = \gamma = 0.5$$

Fig. 7.8. Influence of Grashof number Gr on dimensionless velocity $f'(\eta)$.

118
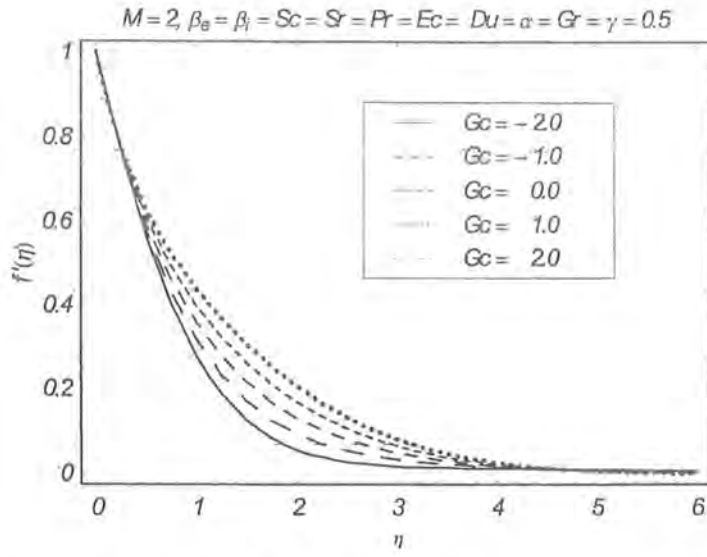
Fig. 7.9. Influence of mass Grashof number Gc on dimensionless tangential velocity $f'(\eta)$.
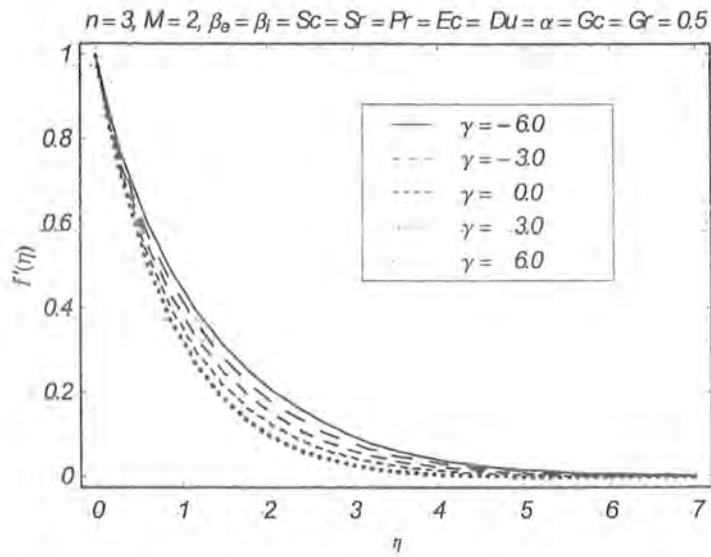
Fig. 7.10. Influence of chemical reaction parameter γ on dimensionless tangential velocity $f'(\eta)$.

Fig. 7.11. Influence of Grashof number Gr on dimensionless lateral velocity $g(\eta)$.
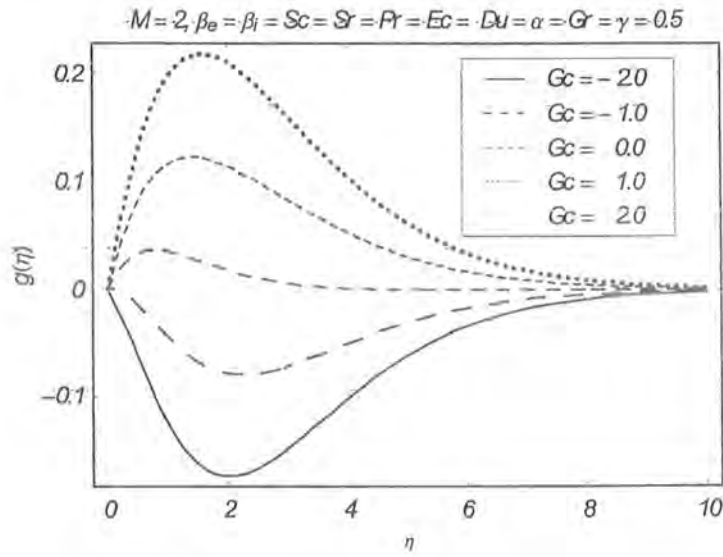
Fig. 7.12. Influence of mass Grashof number Gc on dimensionless lateral velocity $g(\eta)$.
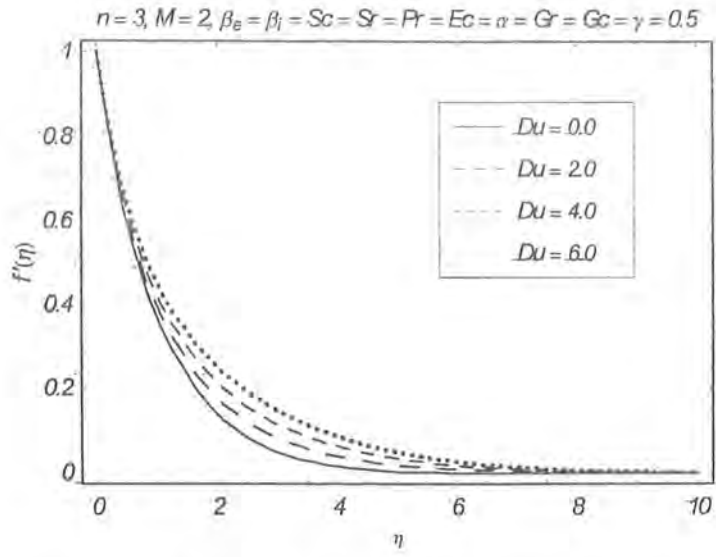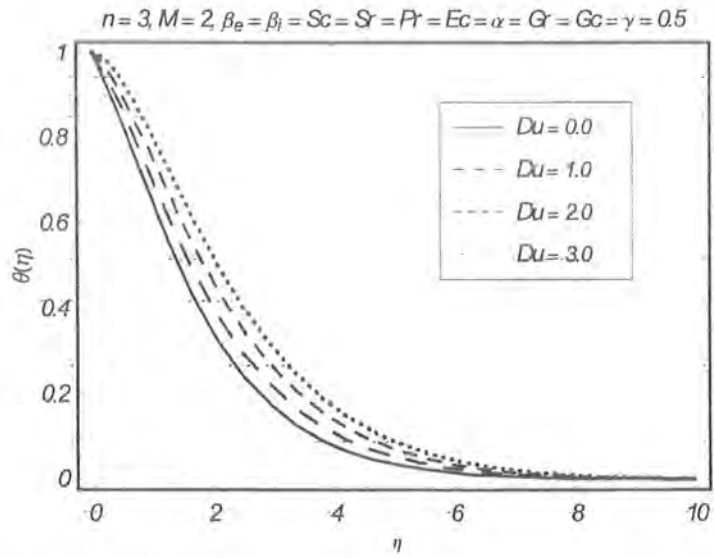
Fig. 7.13. Influence of Dufour number Du on dimensionlesss temperature $\theta(\eta)$.
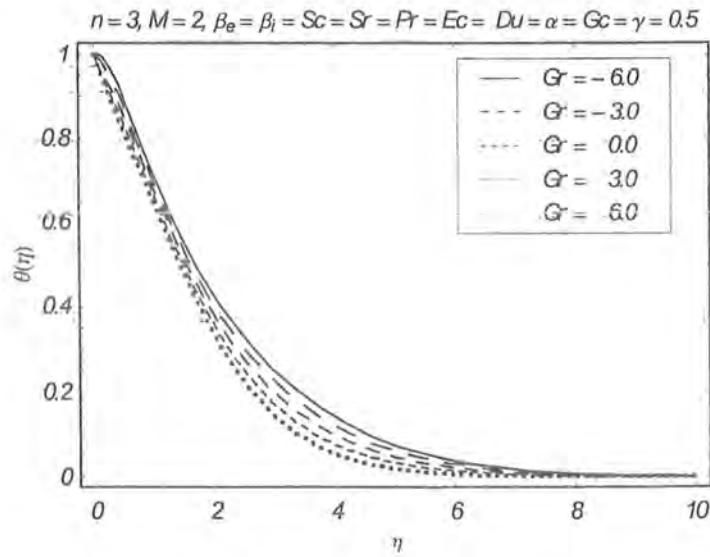
Fig. 7.14. Influence of Grashof number Gr on dimensionless temperature $\theta(\eta)$.

$n = 3, M = 2, \beta_e = \beta_i = Sc = Sr = Pr = Ec = Du = \alpha = Gr = \gamma = 0.5$
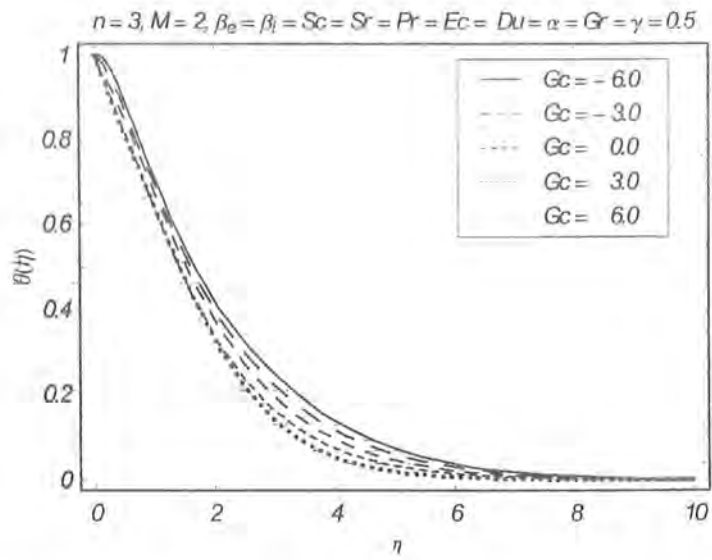
Fig. 7.15. Influence of mass Grashof number Gc on dimensionless temperature $\theta(\eta)$.

$n = 3, M = 2, \beta_e = \beta_i = Pr = Sr = Ec = Du = \alpha = Gr = Gc = \gamma = 0.5$

Fig. 7.16. Influence of Schamidt number Sc on dimensionless concentration $\phi(\eta)$.

122

$n = 3, M = 2, \beta_e = \beta_i = Sc = Pr = Ec = Du = \alpha = Gr = Gc = \gamma = 0.5$
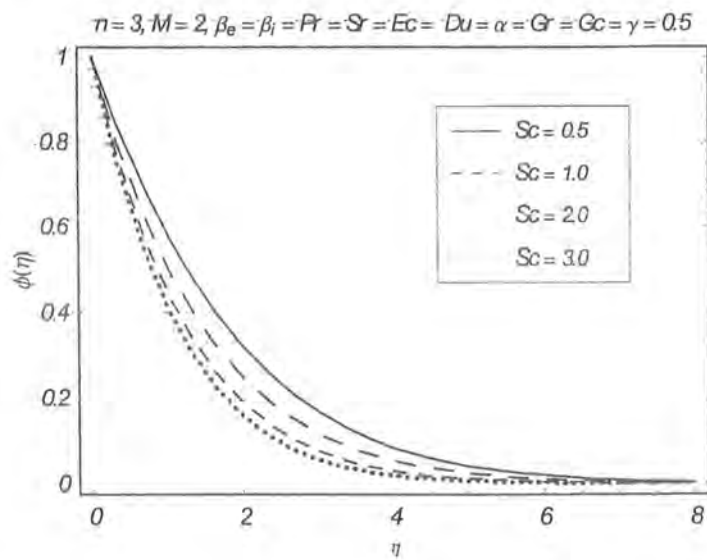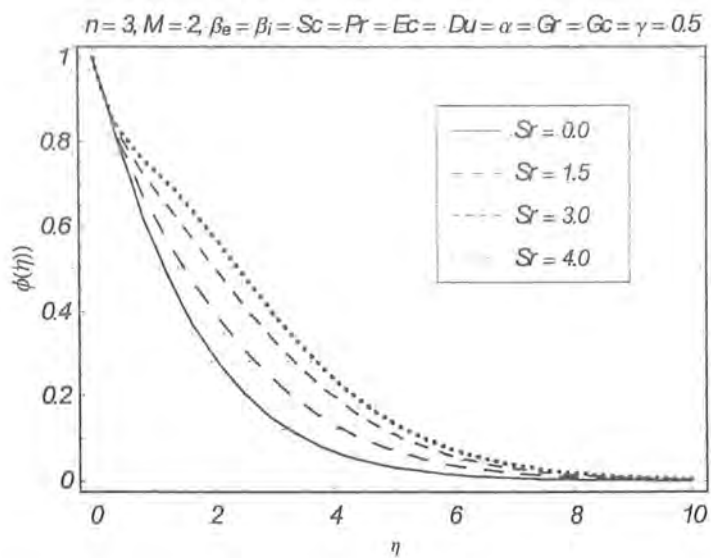
Fig. 7.17. Influence of Soret number Sr on dimensionless concentration $\phi(\eta)$.

$n = 3, M = 2, \beta_e = \beta_i = Sc = Sr = Pr = Ec = Du = \alpha = Gc = \gamma = 0.5$
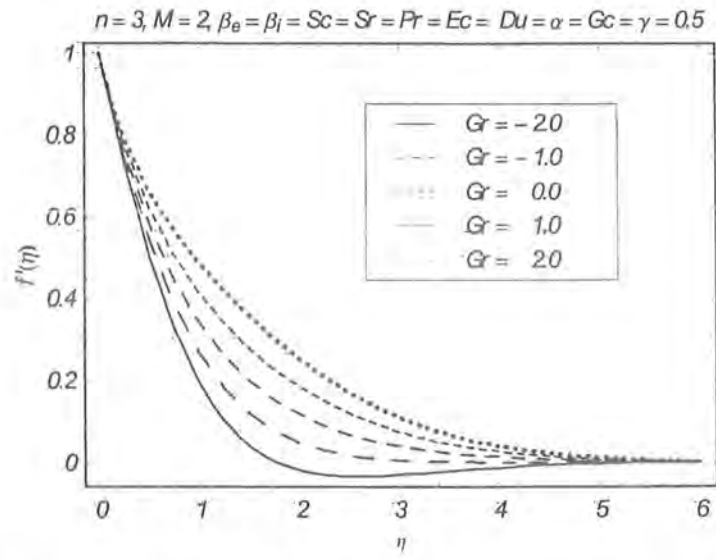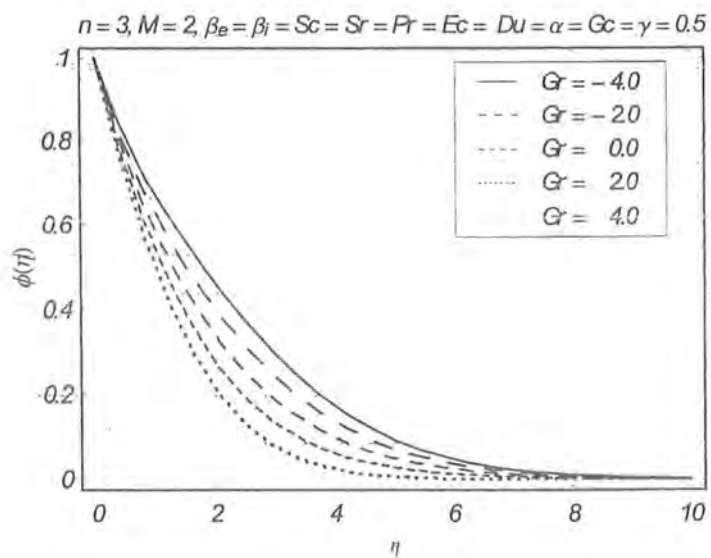

Fig. 7.18. Influence of Grashof number Gr on dimensionless concentration $\phi(\eta)$.

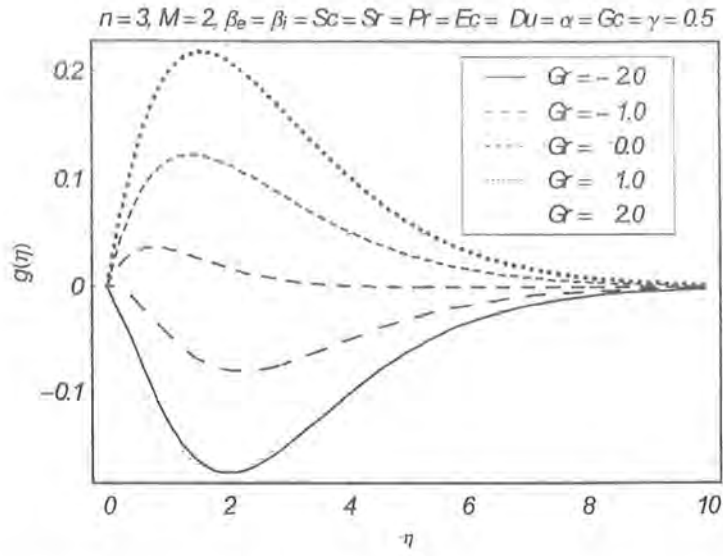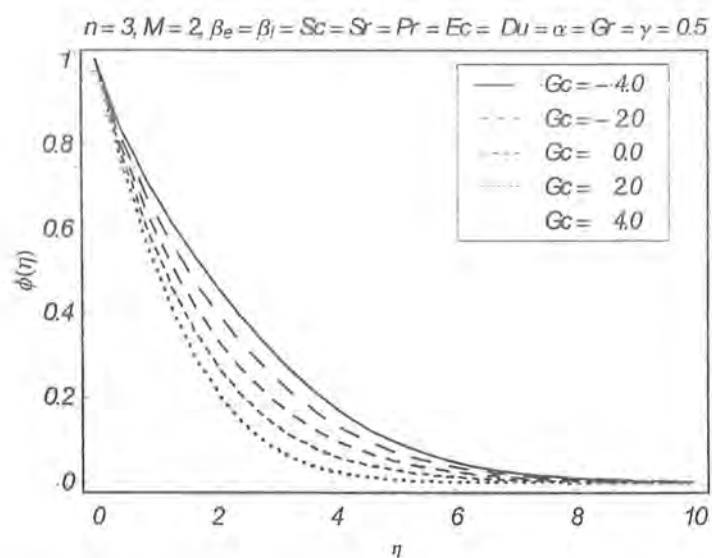Fig. 7.19. Influence of mass Grashof number Gc on dimensionless concentration $\phi(\eta)$.
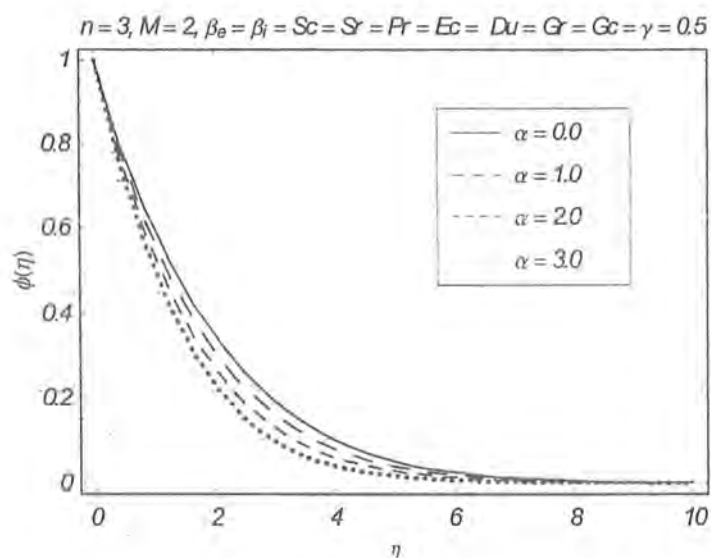
Fig. 7.20. Influence of second grade parameter α on dimensionless concentration $\phi(\eta)$.
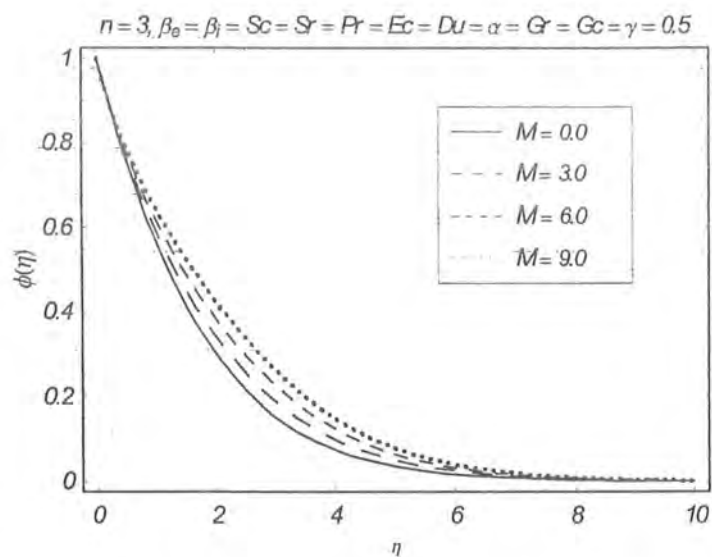
Fig. 7.21. Influence of Hartman number M on dimensionless concentration $\phi(\eta)$.

(a)

125
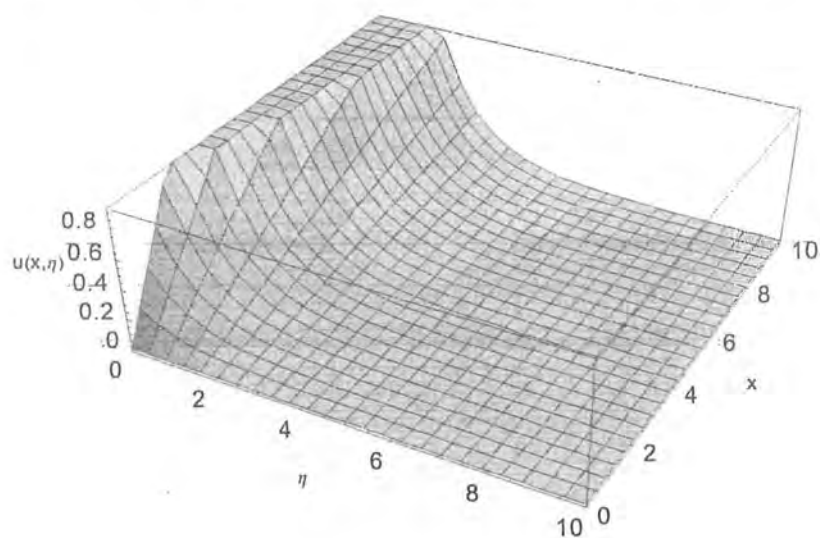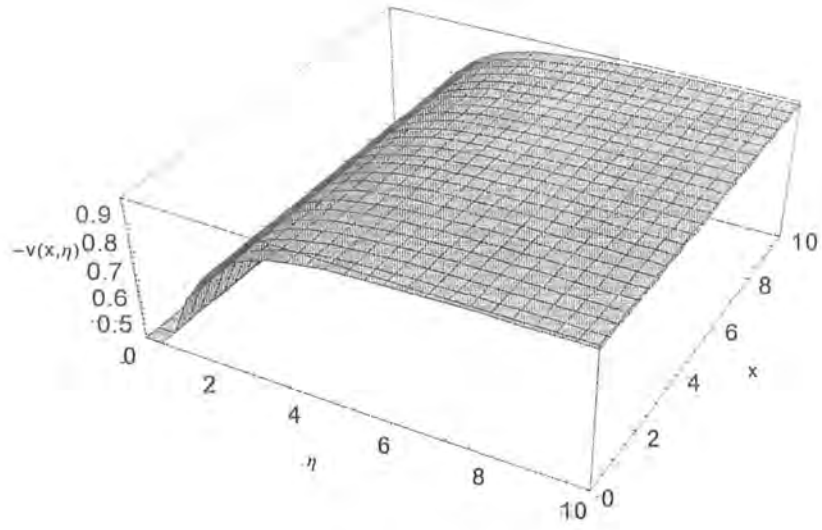
(b)
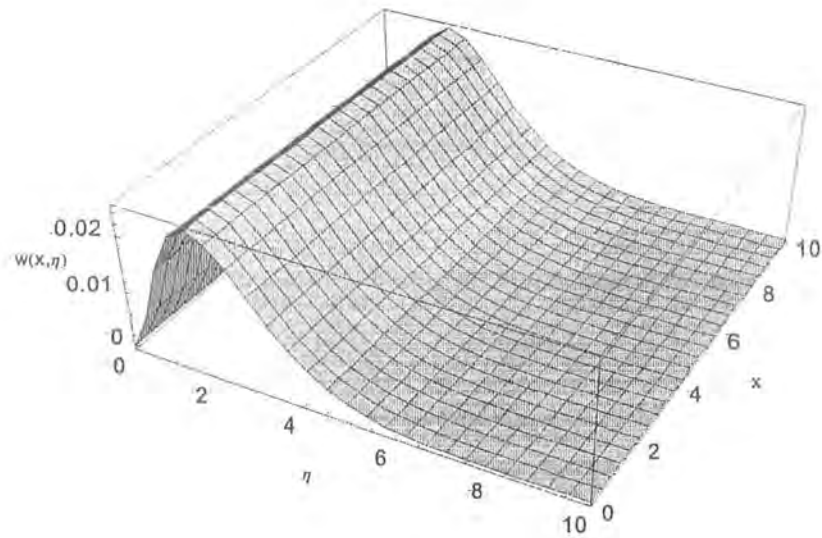
(c)

Fig. 7.22 . $3 - D$ profiles $(a) - (c)$ for x-, y- and z-components of velocity **V** when
$M = 1$, $\beta_i = \beta_e = Gr = Gc = Sc = Sr = Du = \gamma = 0.5$, $Ec = \alpha = 0.2$, $\Pr = 0.72$.

126

Table 7.2. Comparison of the values of $\theta'(0)$ for various values of Pr when $M = \beta_i = \beta_e = Ec = \alpha = Gr = Gc = Sc = Sr = Du = Ec = \gamma = 0$.

Pr	Gupta and Gupta [42]	Grubka and Bobba [43]	Ali [44]	Salem and El-Aziz [67]	Present case
0.7	-		-0.45255	-0.45605	-0.45394
1.0	-0.5820	-0.5820	-0.59988	-0.58223	-0.58197
10.0	-	-2.3080	-2.29589	-2.30789	-2.30841

Table 7.3. Comparison of the values of $\phi'(0)$ for various values of Pr when $M = \beta_i = \beta_e = Ec = \alpha = Gr = Gc = Sc =, Sr = Du = Ec = \text{Pr} = 0$ and $\hbar_{f,g,\theta,\phi} = -1$.

γ	Sc	Salem and El-Aziz [67]		Takhar et al. [92]		Andersson et al. [91]		Present case	
		$n=1$	$n=2$	$n=1$	$n=2$	$n=1$	$n=2$	$n=1$	$n=2$
0.01	1.0	-0.592	-0.588	-0.59216	-0.58844	-0.59157	-0.58777	-0.591354	-0.587525
0.1	1.0	-0.669	-0.636	-0.67044	-0.63724	-0.66902	-0.63567	-0.668980	-0.635464
1.0	1.0	-1.177	-1.000	1.17761	-1.00100	-1.17649	-1.00006	-1.765003	-1.000000
10.0	1.0	3.232	-2.649	-3.23257	-2.64963	-3.23122	-2.65861	-3.231700	-2.658822

Table 7.4. Variation of local skin friction coefficients $-(\mathrm{Re}_x)^{1/2} C_{f_x}$, and $(\mathrm{Re}_x)^{1/2} C_{g_x}$ for different values of physical parameters.

M	β_e	β_i	Sc	Du	Sr	Pr	Ec	γ	Gr	Gc	α	n	$-(\mathrm{Re}_x)^{1/2} C_{f_x}$	$(\mathrm{Re}_x)^{1/2} C_{g_x}$
0.0	0.5	0.5	0.5	0.1	0.1	0.72	0.2	0.1	0.1	0.1	0.2	1	1.1663549	0.00000000
0.5													1.3852115	0.10858296
1.0													1.5822509	0.18545228
1.5													1.7612221	0.24589401
1.0	0.0	0.5	0.5	0.1	0.1	0.72	0.2	0.1	0.1	0.1	0.2	1	1.7321168	0.00000000
	0.5												1.5826413	0.18529386
	1.0												1.4635188	0.22682243
	1.5												1.3872204	0.22203901
1.0	0.5	0.0	0.5	0.1	0.1	0.72	0.2	0.1	0.1	0.1	0.2	1	1.6473675	0.25655622
		0.5											1.5826413	0.18529386
		1.0											1.5311486	0.13961970
		1.5											1.4900176	0.10880590
1.0	0.5	0.5	0.1	0.1	0.1	0.72	0.2	0.1	0.1	0.1	0.2	1	1.5647110	0.19022608
			0.5										1.5824632	0.18539396
			0.9										1.5936065	0.18316706
			1.3										1.6006082	0.18212349
1.0	0.5	0.5	0.5	0.0	0.1	0.72	0.2	0.1	0.1	0.1	0.2	1	1.5837327	0.18511950
				0.5									1.5766798	0.18662729
				1.0									1.5696491	0.18807463
				1.5									1.5626383	0.18946375
1.0	0.5	0.5	0.5	0.1	0.0	0.72	0.2	0.1	0.1	0.1	0.2	1	1.5832224	0.18521013
					0.5								1.5785432	0.18633514
					1.0								1.5738162	0.18743742
					1.5								1.5690418	0.18851717

M	P	β_i	Sc	Du	Sr	Pr	Ec	γ	Gr	Gc	α	n	$-\left(\mathrm{Re}_x\right)^{1/2}C_{f_x}$	$\left(\mathrm{Re}_x\right)^{1/2}C_{g_x}$
1.0	0.5	0.5	0.5	0.1	0.1	0.2	0.0	0.1	0.1	0.1	0.2		1.5648967	0.19030446
							0.5						1.5624298	0.19070290
							1.0						1.5599658	0.19110023
							1.5						1.5575044	0.19149649
1.0	0.5	0.5	0.5	0.1	0.1	0.2	0.2	-0.4	0.1	0.1	0.2	2	1.5493416	0.19277509
								-0.2					1.5559665	0.19189035
								0.0					1.5605606	0.19114576
								0.2					1.5639814	0.19060778
								0.4					1.5666749	0.19019655
1.0	0.5	0.5	0.5	0.1	0.1	0.2	0.2	0.1	-1.0	0.1	0.2	2	2.9757076	0.17105209
									-0.5				2.1828670	0.09269391
									0.0				1.6541914	0.18031099
									0.5				1.2243210	0.22055477
									1.0				0.8413970	0.24495816
1.0	0.5	0.5	0.5	0.1	0.1	0.2	0.2	0.1	0.1	-1.0	0.2	2	2.7344675	0.011718916
										-0.5			2.0605725	0.13666233
										0.0			1.6389280	0.18402560
										0.5			1.2914199	0.20743536
										1.0			0.97738185	0.22270061
1.0	0.5	0.5	0.5	0.1	0.1	0.2	0.2	0.1	0.1	0.5	0.0	2	1.1745120	0.13187594
											0.1		1.3808950	0.16241369
											0.2		1.5655312	0.18980003
											0.3		1.7321162	0.21454441
1.0	0.5	0.5	0.5	0.1	0.1	0.2	0.2	0.1	0.1	0.1	0.	1	1.3787840	0.16327912
												2	1.3763868	0.16392356
												3	1.3768225	0.16359519

Table 7.5. Variation of local Nusselt number $-(\mathrm{Re}_x)^{-1/2}\,Nu_x$ and local Sherwood number $(\mathrm{Re}_x)^{-1/2}\,Sh_x$ for different values of physical parameters.

M	β_e	β_i	Sc	Du	Sr	Pr	Ec	γ	Gr	Gc	α	n	$-(\mathrm{Re}_x)^{-1/2}\,Nu_x$	$-(\mathrm{Re}_x)^{-1/2}\,Sh_x$
0.0	0.5	0.5	0.5	0.1	0.1	0.72	0.2	0.1	0.1	0.1	0.2	3	0.23942634	0.43416163
0.5													0.22187514	0.41404857
1.0													0.20753339	0.39781659
1.5													0.19558465	0.38468334
1.0	0.0	0.5	0.5	0.1	0.1	0.72	0.2	0.1	0.1	0.1	0.2	3	0.22218851	0.39888947
	0.5												0.22919554	0.40331893
	1.0												0.23404018	0.40683697
	1.5												0.23755164	0.40967385
1.0	0.5	0.1	0.5	0.1	0.1	0.72	0.2	0.1	0.1	0.1	0.2	3	0.21722203	0.39518044
		0.5											0.22919554	0.40331893
		1.0											0.23781684	0.41074593
		1.5											0.24321683	0.41606596
1.0	0.5	0.5	0.1	0.1	0.1	0.72	0.2	0.1	0.1	0.1	0.2	3	0.20311895	0.39585639
			0.5										0.17651187	0.39739000
			0.9										0.14967781	0.39893176
			1.3										0.12261449	0.40048178
1.0	0.5	0.5	0.5	0.0	0.1	0.72	0.2	0.1	0.1	0.1	0.2	3	0.17756893	0.39490704
				0.5									0.17756893	0.39490704
				1.0									0.17756893	0.39490704
				1.5									0.17756893	0.39490704
1.0	0.5	0.5	0.5	0.1	0.0	0.72	0.2	0.1	0.1	0.1	0.2	1	0.33356052	0.43225859
					0.5								0.33844636	0.38726267
					1.0								0.34335988	0.34067412
					1.5								0.34830369	0.29245995

M	P	β_i	Sc	Du	Sr	Pr	Ec	γ	Gr	Gc	α	n	$-(\text{Re}_x)^{-1/2} Nu_x$	$-(\text{Re}_x)^{-1/2} S$
1.0	0.5	0.5	0.5	0.1	0.1	0.02	0.2	0.1	0.1	0.1	0.2	1	0.12858532	0.43759775
						0.37							0.26975829	0.42773699
						0.72							0.40585807	0.41928801
						1.07							0.50725160	0.41365387
1.0	0.5	0.5	0.5	0.1	0.1	0.2	0.0	0.1	0.1	0.1	0.2		0.21255936	0.43208164
							0.5						0.13317139	0.43610503
							1.0						0.054001321	0.44011604
							1.5						0.024953293	0.44411478
1.0	0.5	0.5	0.5	0.1	0.1	0.2	0.2	-0.4	0.1	0.1	0.2	2	0.19062668	0.12391180
								-0.2					0.18750769	0.26097151
								0.0					0.18513262	0.36326801
								0.2					0.18320744	0.44590223
								0.4					0.18157469	0.51628702
1.0	0.5	0.5	0.5	0.1	0.1	0.2	0.2	0.1	-1.0	0.1	0.2	2	0.03839030	0.14839565
									-0.5				0.13543195	0.30642781
									0.0				0.17982347	0.39358181
									0.5				0.20969153	0.44905966
									1.0				0.22989409	0.48769112
1.0	0.5	0.5	0.5	0.1	0.1	0.2	0.2	0.1	0.1	-1.0	0.2	2	0.094489580	0.28647815
										-0.5			0.15770562	0.37584591
										0.0			0.18847211	0.42575587
										0.5			0.20717609	0.45790694
										1.0			0.22024252	0.48127050
1.0	0.5	0.5	0.5	0.1	0.1	0.2	0.2	0.1	0.1	0.1	0.0	2	0.18466328	0.41863866
											0.1		0.18719554	0.42647387
											0.2		0.18932115	0.43327002
											0.3		0.19117455	0.43927908

7.5 Final remarks

The combined effects of thermal-diffusion, diffusion-thermo, viscous dissipation, joule heating and chemical reaction on boundary layer mixed convection three-dimensional flow of a second grade fluid over stretching sheet with Hall and ion-slip currents are examined. Computations are performed for the nonlinear analysis. Main findings of the presented analysis are listed below.

- Convection parameters Gr and Gc have similar behavior on $f'(\eta)$ and $g(\eta)$.

- Convection parameters Gr and Gc have similar behavior on $\theta(\eta)$ and $\phi(\eta)$ in a qualitative sense.

- $\phi(\eta)$ is an increasing function of Sr and M whereas it decreases for Sc and α.

- Skin friction coefficient $-(\mathrm{Re}_x)^{1/2} C_{f_x}$ is an increasing function of M, Sc, Pr, γ, $Gr < 0$, $Gc < 0$, α and n whereas it decreases when β_e, β_i, Du, Sr, Ec, $Gc > 0$ and $Gr > 0$ are increased.

- $(\mathrm{Re}_x)^{1/2} C_{g_x}$ increases by increasing M, Du, Sr, Gc, Gr and α while it decreases when Sc, Pr and γ are increased.

- $(\mathrm{Re}_x)^{-1/2} Nu_x$ is an increasing function of Sr, Pr, Gr, Gc, α and n but it decreases when M, Du, Sc, Ec and γ are increased.

- $(\mathrm{Re}_x)^{-1/2} Sh_x$ increases with the increase of β_e, β_i, Sc, Du, Ec, γ, Gr, Gc and α whereas it decreases by increasing M, Sr and Pr.

- Boundary layer thickness corresponding to tangential velocity $f'(\eta)$ can be controlled through Hartman number and convection parameters. Boundary layer thickness corresponding to lateral velocity $g(\eta)$ can be decreased by the ion-slip current.

- Thermal boundary layer thickness and concentration boundary layer thickness can be controlled through convection parameters Gr and Gc.

132

Chapter 8

Axisymmetric flow of magnetohydro-dynamic micropolar fluid between radially stretching sheets

This chapter deals with the magnetohydrodynamic axisymmetric flow of a micropolar fluid between the radially stretching sheets in the presence of constant magnetic field. The governing partial differential equations are transformed into the ordinary differential equations. The magnetohydrodynamic (MHD) nonlinear problem is treated using the homotopy analysis method (HAM). Convergence of solutions is checked. The velocity profiles are predicted for the pertinent parameters. The values of skin friction and wall couple stress coefficients are obtained for the various values of Reynolds number (Re), Hartman number (M) and micropolar fluid parameter (K).

8.1 Mathematical analysis

Let us consider the steady two-dimensional flow of an incompressible micropolar fluid between the radially stretching sheets at $z = \pm L$. The velocity is denoted by $(u, 0, w)$ and microrotation vector by $(0, N_2, 0)$. A constant magnetic field $\mathbf{B}_0$ is applied perpendicular to the plane of sheets. The induced magnetic field is neglected under the assumption of small magnetic Reynolds number. No external electric field is present *i.e.* $\mathbf{E} = 0$. Physical model and coordinate system

are shown in Fig. 8.1. The microstructure associated with microrotations is taken into account. The equations governing the flow under above stated assumptions (see Takhar et al. [46]) are

$$\frac{\partial u}{\partial r} + \frac{u}{r} + \frac{\partial w}{\partial z} = 0, \tag{8.1}$$

$$
\begin{aligned}
u\frac{\partial u}{\partial r} + w\frac{\partial u}{\partial z} &= -\frac{1}{\rho}\frac{\partial p}{\partial r} + \frac{1}{\rho}\left(\mu + k\right)\left[\frac{\partial^2 u}{\partial r^2} + \frac{1}{r}\frac{\partial u}{\partial r} + \frac{\partial^2 u}{\partial z^2} - \frac{u}{r^2}\right] \\
&\quad - \frac{k}{\rho}\frac{\partial N_2}{\partial z} - \frac{\sigma B_0^2}{\rho}u,
\end{aligned}
\tag{8.2}
$$

$$u\frac{\partial w}{\partial r} + w\frac{\partial w}{\partial z} = -\frac{1}{\rho}\frac{\partial p}{\partial z} + \frac{1}{\rho}\left(\mu + k\right)\left[\frac{\partial^2 w}{\partial r^2} + \frac{1}{r}\frac{\partial w}{\partial r} + \frac{\partial^2 w}{\partial z^2}\right] - \frac{k}{\rho}\left[\frac{\partial N_2}{\partial r} + \frac{N_2}{r}\right], \tag{8.3}$$

$$u\frac{\partial N_2}{\partial r} + w\frac{\partial N_2}{\partial z} = \frac{\gamma_\nu}{\rho j}\left[\frac{\partial^2 N_2}{\partial r^2} + \frac{1}{r}\frac{\partial N_2}{\partial r} + \frac{\partial^2 N_2}{\partial z^2} - \frac{N_2}{r^2}\right] - \frac{k}{\rho j}\left[2N_2 + \frac{\partial w}{\partial r} - \frac{\partial u}{\partial z}\right], \tag{8.4}$$

where u and w are the velocity components along the radial (r) and axial (z) directions respectively and N_2 is the azimuthal component of microrotation vector. σ is the electrical conductivity of the fluid, j is the microinertia per unit mass and taken $j = \nu/a$ [53], ρ is the fluid density, μ and k are the viscosity coefficients and γ_ν is the spin viscosity.
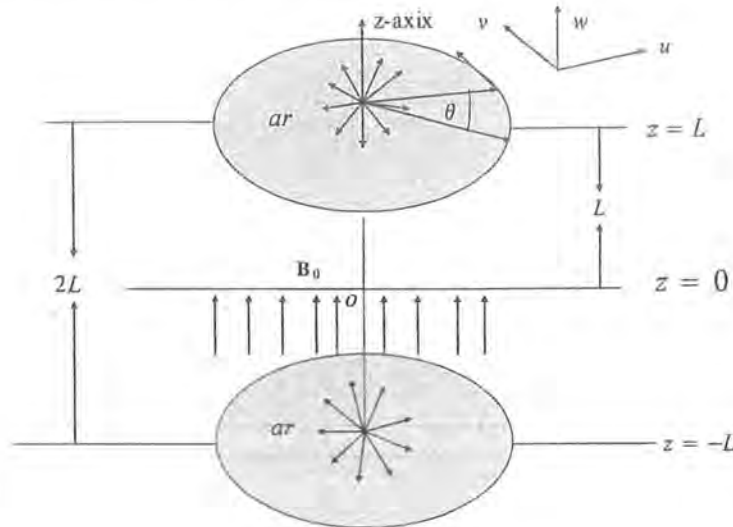

Fig. 8.1. Physical model and coordinate system.

The subjected boundary conditions are

$$u = ar, \ w = 0, \ N_2 = 0 \quad \text{at } z = L, \\ \frac{\partial u}{\partial z} = 0, \ w = 0, \ N_2 = 0 \quad \text{at } z = 0. \biggr\}$$

(8.5)

It is worth mentioning that putting $k = 0$, Eqs. (8.2) and (8.3) reduce to governing equations for classical Newtonian fluid flow in the presence of constant magnetic field. Basically this is the case when global motion is unaffected by the microrotations [45]. Since flow in radial direction is due to stretching of sheets and flow becomes two dimensional due to viscous nature of fluid. Since at free stream fluid behaves like inviscid one and flow becomes unidirectional. Therefore axial component of velocity vanishes i.e. $w = 0$ at $z = 0$. Furthermore, the fluid particles in upper region ($0 < z < L$) rotate in clockwise direction whereas the fluid particles in lower region ($-L < z < 0$) rotate in anti-clockwise direction. Thus these opposite rotations cancels out the effect of each other at $z = 0$. Hence $N_2 = 0$ at $z = 0$. Basically fluid vorticity in the flows induced by boundary walls is maximum near the solid boundaries and zero at central line of the channel i.e. $N_2 = 0$ at $z = 0$ [46]. The arising flow equations and boundary conditions are reduced to dimensionless form by introducing the following variables:

$$u = ar f'(\eta), \ w = -2aL f(\eta), \ N_2 = \frac{ar}{L} g(\eta), \ \eta = \frac{z}{L}.$$

(8.6)

Now dimensionless problems are

$$(1 + K) f'''' - \operatorname{Re} M f'' + 2 \operatorname{Re} f f''' - K g'' = 0,$$

(8.7)

$$f(0) = 0, \ f(1) = 0, \ f'(1) = 1, \ f''(0) = 0,$$

(8.8)

$$\left(1 + \frac{K}{2}\right) g'' - \operatorname{Re} K (2g - f'') + \operatorname{Re} (2fg' - f'g) = 0,$$

(8.9)

$$g(1) = 0, \ g(0) = 0,$$

(8.10)

where Eq. (8.1) is automatically satisfied. Here $\gamma_\nu = (\mu + k/2) j$ [53] and

$$K = \frac{k}{\mu}, \ \operatorname{Re} = \frac{aL^2}{\nu}, \ M = \frac{\sigma B_0^2}{\rho a},$$

135

respectively are called the micropolar parameter (K), the Reynolds number (Re) and the Hartman number (M).

The skin friction coefficient C_f and wall couple stress C_g at $z = L$ are defined by [46]

$$C_f = \frac{\tau_w}{\rho(ar)^2} - \frac{(\mu + k)}{\rho(ar)^2}\left(\frac{\partial u}{\partial z}\right)\Bigg|_{z=L} = \frac{(1+K)}{\mathrm{Re}_r}f''(1),\tag{8.11}$$

$$C_g = -\frac{L\,\gamma_\nu\frac{\partial N_2}{\partial z}\Big|_{z=L}}{\rho(ar)^2} = -\frac{(1+K/2)}{\mathrm{Re}_r}g'(1),\tag{8.12}$$

where $\mathrm{Re}_r\ (= arL/\nu)$ denotes the local Reynolds number.

8.2 Solutions by homotopy analysis method

Here $f(\eta)$ and $g(\eta)$ are expressed by the set of base functions

$$\left\{\eta^{2n+1},\ n \ge 0\right\},\tag{8.13}$$

in the forms following series

$$f(\eta) = \sum_{n=0}^{\infty} a_n\eta^{2n+1},\ g(\eta) = \sum_{n=0}^{\infty} b_n\eta^{2n+1},\tag{8.14}$$

where a_n and b_n are the coefficients. The initial guesses and linear operators $\mathcal{L}_f$ and $\mathcal{L}_g$ are defined by the following expressions:

$$f_0(\eta) = \frac{1}{2}\left(\eta^3 - \eta\right),\ g_0(\eta) = 0,\tag{8.15}$$

$$\mathcal{L}_f(f(\eta)) = \frac{d^4 f}{d\eta^4},\ \mathcal{L}_g(g(\eta)) = \frac{d^2 g}{d\eta^2},\tag{8.16}$$

$$\mathcal{L}_f\left[C_1 + C_2\eta + C_3\eta^2 + C_4\eta^3\right] = 0,\ \mathcal{L}_g\left[C_5 + C_6\eta\right] = 0,\tag{8.17}$$

with $C_i\ (i = 1 - 6)$ show the arbitrary constants. The subjected problems at the zeroth order are given by

$$(1-q)\mathcal{L}_f\left[\hat{f}(\eta;q) - f_0(\eta)\right] = q\mathcal{N}_f\hbar_f\left[\hat{f}(\eta;q),\hat{g}(\eta;q)\right],\tag{8.18}$$

136

$$\hat{f}(0;q) = 0, \quad \hat{f}(1;q) = 0, \quad \left.\frac{\partial \hat{f}(\eta;q)}{\partial \eta}\right|_{\eta=1} = 1, \quad \left.\frac{\partial^2 \hat{f}(\eta;q)}{\partial \eta^2}\right|_{\eta=0} = 0, \tag{8.19}$$

$$(1-q)\mathcal{L}_g\left[\hat{g}(\eta;q) - g_o(\eta)\right] = q\hbar_g \mathcal{N}_g\left[\hat{g}(\eta;q), \hat{f}(\eta;q)\right], \tag{8.20}$$

$$\hat{g}(1;q) = 0, \quad \hat{g}(0;q) = 0, \tag{8.21}$$

in which $q \in [0,1]$ is the embedding parameter and $\hbar_f \neq 0$ and $\hbar_g \neq 0$ are the convergence control parameters such that $\hat{f}(\eta;0) = f_0(\eta)$, $\hat{g}(\eta;0) = g_0(\eta)$, $\hat{f}(\eta;1) = f(\eta)$ and $\hat{g}(\eta;1) = g(\eta)$. When q varies from 0 to 1, $\hat{f}(\eta;q)$ approaches $f_0(\eta)$ to $f(\eta)$ and $\hat{g}(\eta;q)$ from $g_0(\eta)$ to $g(\eta)$. Furthermore, the nonlinear operators $\mathcal{N}_f$ and $\mathcal{N}_g$ are given by

$$\begin{aligned}
\mathcal{N}_f\left[\hat{f}(\eta;q), \hat{g}(\eta;q)\right] &= (1+K)\frac{\partial^4 \hat{f}(\eta;q)}{\partial \eta^4} - \operatorname{Re} M \frac{\partial^2 \hat{f}(\eta;q)}{\partial \eta^2} \\
&\quad + 2\operatorname{Re}\hat{f}(\eta;q)\frac{\partial^3 \hat{f}(\eta;q)}{\partial \eta^3} - K\frac{\partial^2 \hat{g}(\eta;q)}{\partial \eta^2},
\end{aligned} \tag{8.22}$$

$$\begin{aligned}
\mathcal{N}_g\left[\hat{g}(\eta;q), \hat{f}(\eta;q)\right] &= \left(1+\frac{K}{2}\right)\frac{\partial^2 \hat{g}(\eta;q)}{\partial \eta^2} - K\operatorname{Re}\left[2\hat{g}(\eta;q) - \frac{\partial^2 \hat{f}(\eta;q)}{\partial \eta^2}\right] \\
&\quad + \operatorname{Re}\left[2\hat{f}(\eta;q)\frac{\partial \hat{g}(\eta;q)}{\partial \eta} - \hat{g}(\eta;q)\frac{\partial \hat{f}(\eta;q)}{\partial \eta}\right].
\end{aligned} \tag{8.23}$$

By using Taylor series we have

$$\hat{f}(\eta;q) = f_o(\eta) + \sum_{m=1}^{\infty} f_m(\eta) q^m, \quad \hat{g}(\eta;q) = g_o(\eta) + \sum_{m=1}^{\infty} g_m(\eta) q^m, \tag{8.24}$$

$$f_m(\eta) = \frac{1}{m!}\left.\frac{\partial^m \hat{f}(\eta;q)}{\partial \eta^m}\right|_{q=0}, \quad g_m(\eta) = \frac{1}{m!}\left.\frac{\partial^m \hat{g}(\eta;q)}{\partial \eta^m}\right|_{q=0}. \tag{8.25}$$

The deformation problems corresponding to the mth-order are

$$\mathcal{L}_f\left[f_m(\eta) - \chi_m f_{m-1}(\eta)\right] = \hbar_f \mathcal{R}_m^f\left(f_{m-1}(\eta), g_{m-1}(\eta)\right),$$
$$f_m(0) = 0, \quad f_m(1) = 0, \quad f_m'(1) = 0, \quad f_m''(0) = 0, \tag{8.26}$$

$$\mathcal{L}_g \left[g_m(\eta) - \chi_m g_{m-1}(\eta) \right] = \hbar_g \mathcal{R}_m^g \left(g_{m-1}(\eta), f_{m-1}(\eta) \right),$$

$$g_m(1) = 0, \quad g_m(0) = 0, \tag{8.27}$$

$$\chi_m = \begin{cases} 0, m \leq 1 \\ 1, m > 1 \end{cases},$$

$$\mathcal{R}_m^f \left(f_m(\eta), g_m(\eta) \right) = (1+K) f_{m-1}'''' - \operatorname{Re} M f_{m-1}'' + 2 \operatorname{Re} \sum_{n=0}^{m-1} \left(\begin{array}{c} f_n''' f_{m-1-n} \\ -K g_{m-1}'' \end{array} \right)$$

$$\mathcal{R}_m^g \left(g_m(\eta), f_m(\eta) \right) = \left(1 + \frac{K}{2} \right) g_{m-1}''' - \operatorname{Re} K \left[2 g_{m-1} - f_{m-1}'' \right]$$

$$+ \operatorname{Re} \sum_{n=0}^{m-1} \left[2 f_n g_{m-1-n}' - f_n' g_{m-1-n} \right]. \tag{8.28}$$

The general solutions at the mth-order are

$$f_m(\eta) = f_m^*(\eta) + C_1^m + C_2^m \eta + C_3^m \eta^3 \tag{8.29}$$

$$g_m(\eta) = g_m^*(\eta) + C_4^m + C_5^m \eta, \tag{8.30}$$

in which $f_m^*(\eta)$ and $g_m^*(\eta)$ are the particular solutions of the Eqs. (8.26) and (8.27). The coefficients $C_i^m (i = 1 - 5)$ are determined by the boundary conditions given in Eqs. (8.26) and (8.27). The systems (8.26) and (8.27) are solved by employing Mathematica.

8.3 Convergence of homotopy solutions

It is a known fact that the convergence of solutions given by Eqs. (8.29) and (8.30) depend upon the auxiliary parameters $\hbar_f$ and $\hbar_g$. Hence we display the the $\hbar_{f,g}$-curves in Figs. 8.2 and 8.3. In order to show the validity of solutions residual errors both for $f(\eta)$ and $g(\eta)$ are also sketched in Figs. 8.4 and 8.5. It is found from Figs. 8.2 − 8.5 that the convergence region for $f(\eta)$ and $f'(\eta)$ is $-0.9 \leq \hbar_f \leq -0.4$ and that for $g(\eta)$ is $-1.1 \leq \hbar_g \leq -0.6$. However the whole analysis has been performed when for $\hbar_f = \hbar_g = -0.7$. Furthermore, Table 7.1 shows that convergence of series solutions is achieved at 20th order of approximations up to 12 decimal
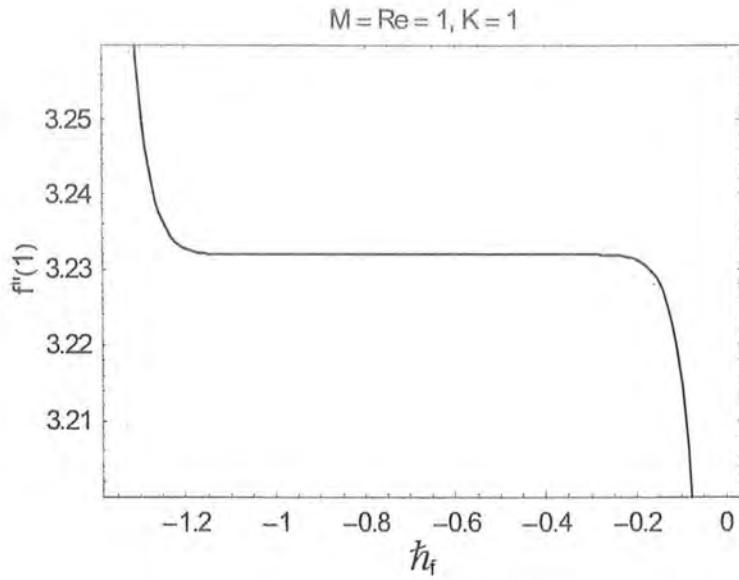
places.

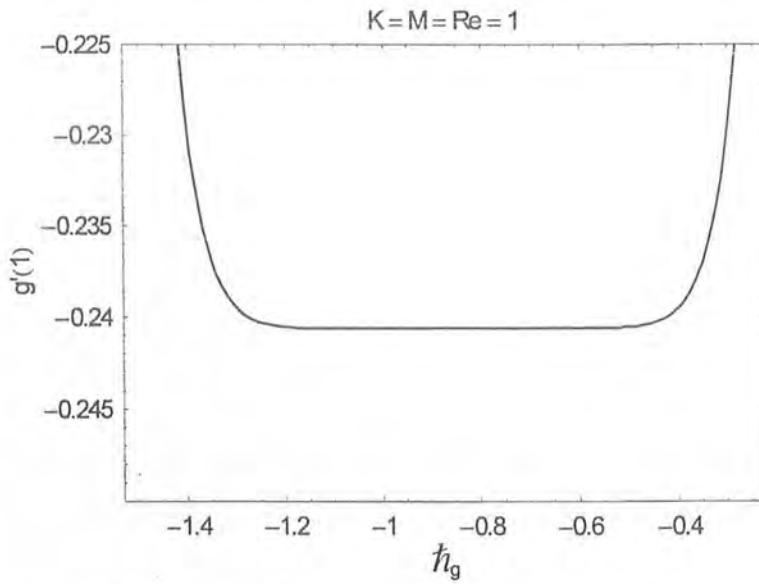Fig. 8.2. $\hbar_f$-curve of $f''(1)$ at 12th order of approximation.

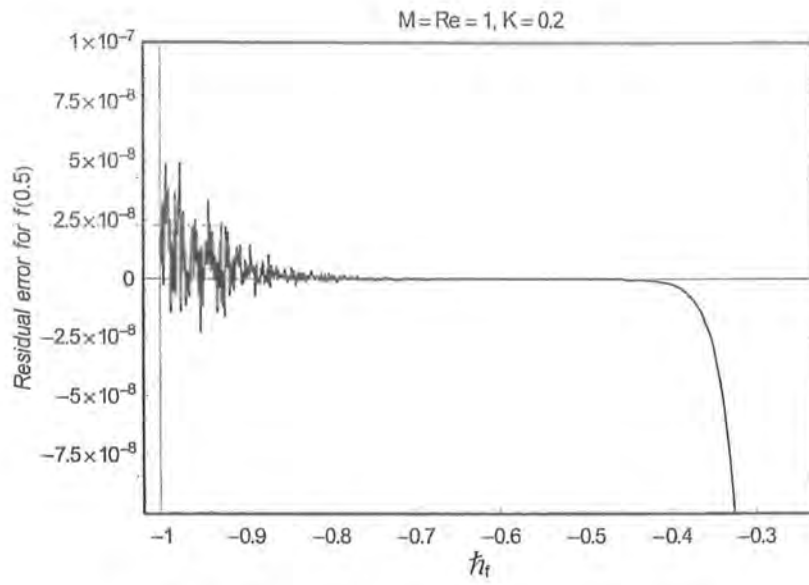Fig. 8.3. $\hbar_g$-curve of $g'(1)$ at 12th order of approximation.

Fig. 8.4. $\hbar_f$-curve for the residual error of $f(0.5)$.
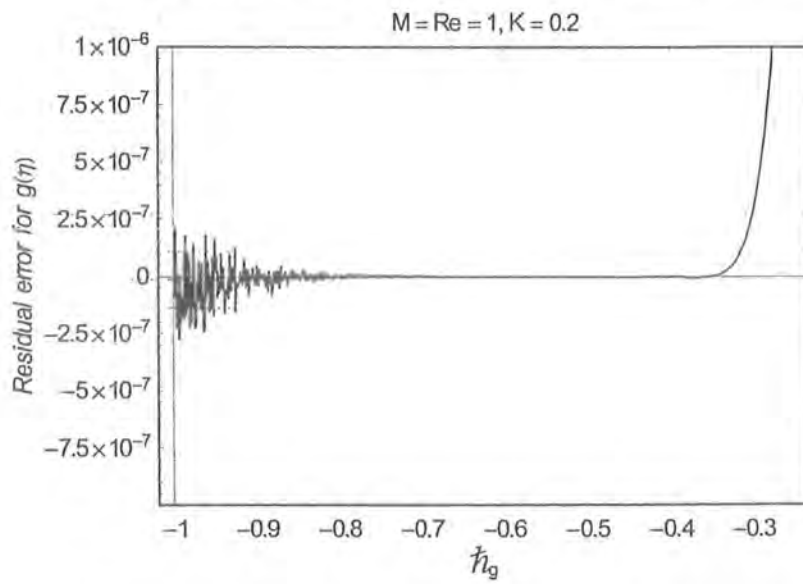

Fig. 8.5. $\hbar_g$-curve for the residual error of $g(0.5)$.

140

Table 8.1. Convergence of HAM solutions when $Re = M = 2.0$, $K = 0.5$ and $\hbar_f = \hbar_g = -0.7$.

Order of approximations	$f''(1)$	$g'(1)$
1	3.72000000000	-0.700000000000
5	3.61057806477	-0.738449167223
10	3.61076391320	-0.738463512754
15	3.61076396332	-0.738463496869
20	3.61076396287	-0.738463496789
25	3.61076396287	-0.738463496789
30	3.61076396287	-0.738463496789
35	3.61076396287	-0.738463496789

8.4 Discussion

In order to illustrate the dimensionless velocity components and microrotation (dimensionless angular velocity) for the emerging parameters of interest, we have plotted the Figs. 8.6 − 8.14. In addition the numerical computations for skin friction coefficient $Re_r C_f$ and couple stress coefficient $Re_r C_g$ have been carried out in Table 8.2. It is seen from Fig. 8.6 that the magnitude of dimensionless radial component $f'(\eta)$ of velocity decreases by increasing the Hartman number M. This shows that Lorentz force retards the fluid motion in radial direction and consequently boundary layer thickness decreases. Hence one can conclude that boundary layer can be controlled through applied magnetic field. It is observed from Fig. 8.7 that the magnitude of dimensionless radial component $f'(\eta)$ of velocity decreases when the Reynolds number Re is increased. Upon increasing the microrotation parameter K, there is an enhancement in the magnitude of dimensionless radial component $f'(\eta)$ of velocity. The boundary layer thickness also increases (Fig. 8.8). Fig. 8.9. depicts that the magnitude of dimensionless axial component $f(\eta)$ of velocity decreases for the various values of Hartman number M. The influence of Reynolds number on the dimensionless axial component $f(\eta)$ of velocity has been shown in Fig. 8.10. It is found from this Fig. that there is reduction in the magnitude of $f(\eta)$ when Re is increased. However, magnitude of $f(\eta)$ increases due to an increase in K (Fig. 8.11). The effects of M, Re and K on the dimensionless angular velocity $g(\eta)$

are shown in the Figs. $8.12-8.14$. Obviously the dimensionless angular velocity $g(\eta)$ decreases by increasing Hartman number M (see Fig. 8.12). It is also noticed that dimensionless angular velocity $g(\eta)$ increases because of an increase in Re and K (Figs. 8.13 and 8.14). The skin friction coefficient $\mathrm{Re}_r\, C_f$ and wall couple stress coefficient $\mathrm{Re}_r\, C_g$ are computed in Table 8.2. This demonstrates that $\mathrm{Re}_r\, C_f$ and $\mathrm{Re}_r\, C_g$ are the increasing functions of M, Re and K.
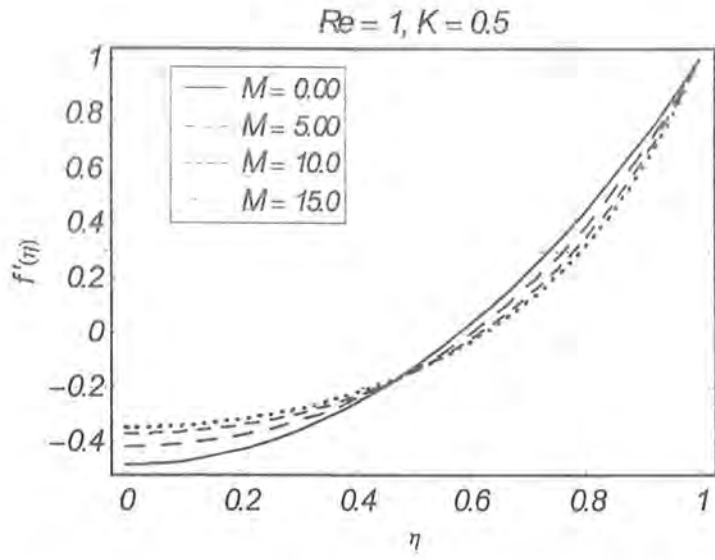
Fig. 8.6. Influence of Hartman number M on dimensionless radial velocity $f'(\eta)$.
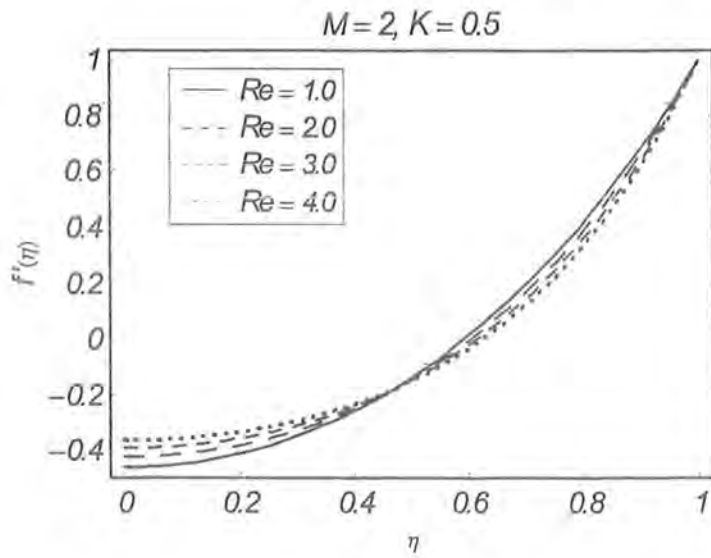

Fig. 8.7. Influence of Reynolds number Re on dimensionless radial velocity $f'(\eta)$.
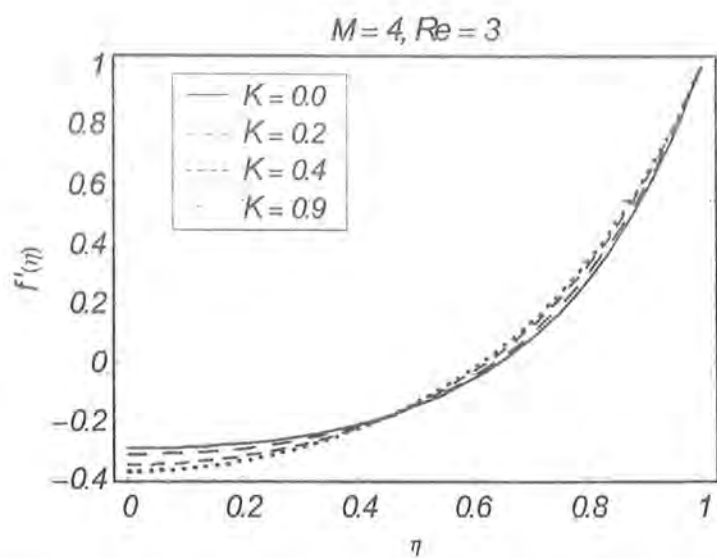
143

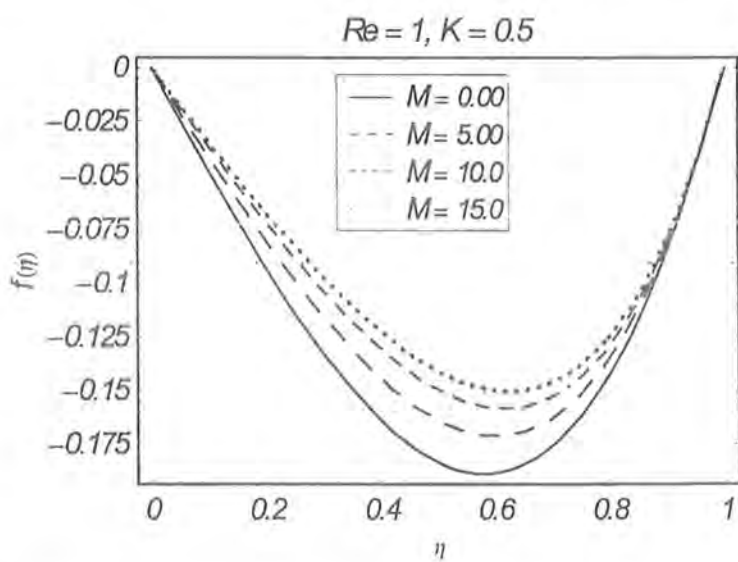Fig. 8.8. Influence of micropolar parameter K on dimensionless radial velocity $f'(\eta)$.

Fig. 8.9. Influence of Hartman number M on dimensionless axial velocity $f(\eta)$.
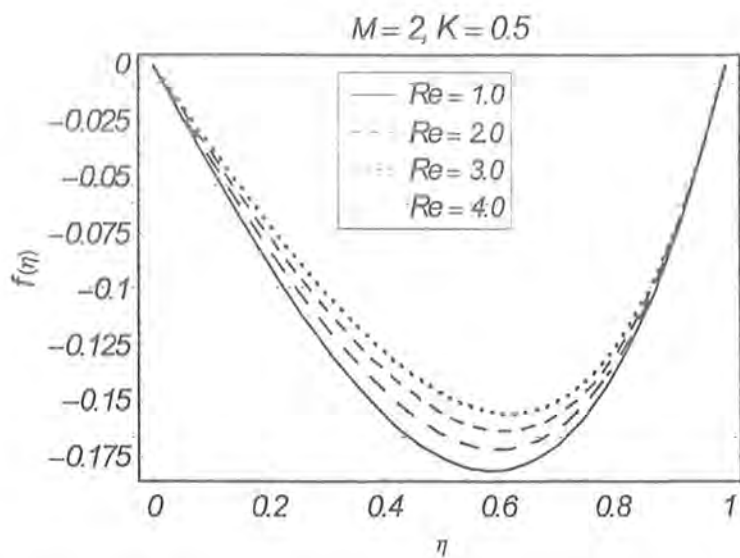
144

Fig. 8.10. Influence of Reynolds number Re on dimensionless axial velocity $f(\eta)$.
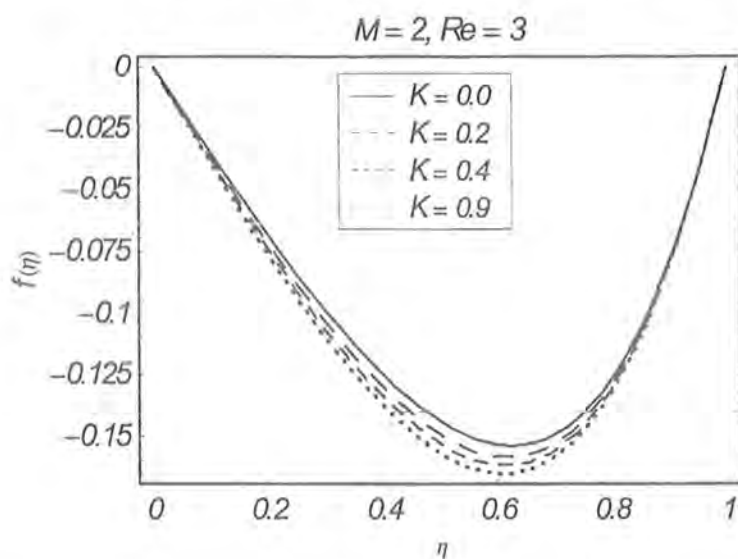

Fig. 8.11. Influence of micropolar parameter K on dimensionless axial velocity $f(\eta)$.
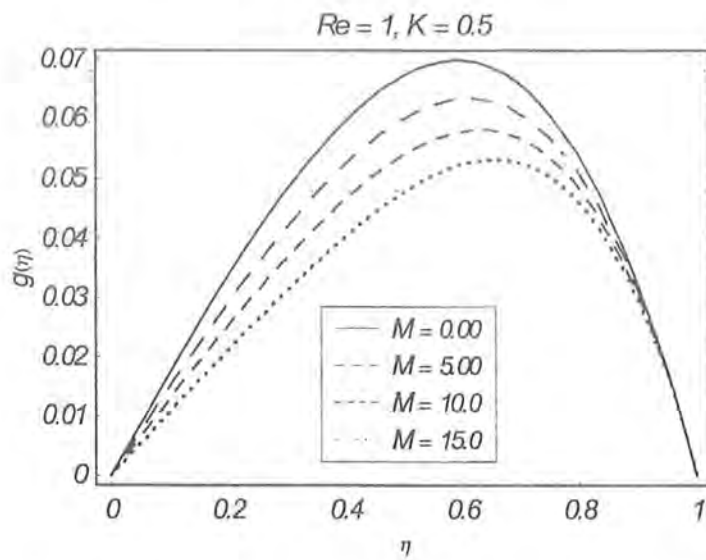
Fig. 8.12. Influence of Hartman number M on dimensionless angular velocity $g(\eta)$.
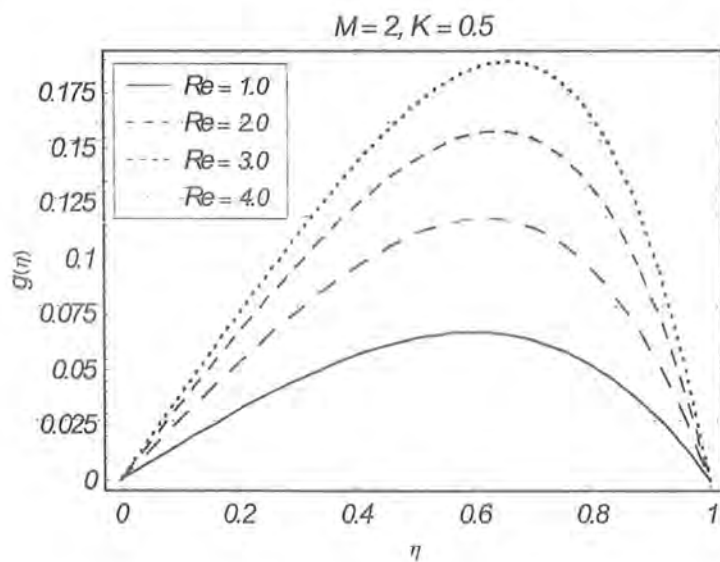

Fig. 8.13. Influence of Reynolds number Re on dimensionless angular velocity $g(\eta)$.
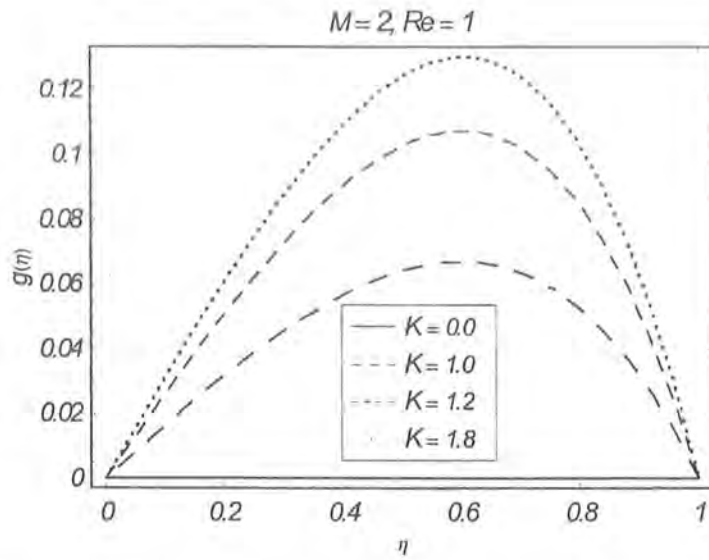
Fig. 8.14. Influence of micropolar parameter K on dimensionless angular velocity $g(\eta)$.

Table 8.2. Numerical values of skin friction coefficient $\mathrm{Re}_r\, C_f$ and wall couple stress coefficient $\mathrm{Re}_r\, C_g$.

M	Re	K	$\mathrm{Re}_r\, C_f$	$-\,\mathrm{Re}_r\, C_g$
0.0	1.0	0.5	4.66731025187	0.918676961138
1.0			5.05533817307	0.920980526582
2.0			5.41614594430	0.923079370986
3.0			5.75398731824	0.925002385109
1.0	1.0	0.5	4.77646547374	0.478773301056
	2.0		5.05533817307	0.920980526582
	3.0		5.33415542042	1.33415055037
	4.0		5.61103357482	1.72430008392
1.0	1.0	0.0	3.31107413404	0.000000000000
		0.2	3.90500594445	0.196869286252
		0.4	4.48804832942	0.386227295205
		0.6	5.06319086907	0.570159417698

147

8.5 Concluding remarks

An analysis for two-dimensional magnetohydrodynamic flow of an incompressible micropolar fluid between the radially stretching sheets has been carried out. Convergent series solution is derived through the homotopy analysis procedure. The interesting observations are presented below.

- The velocity components $f(\eta)$ and $f'(\eta)$ are decreasing functions of Re.

- The effect of Re on $f(\eta)$ and $g(\eta)$ are opposite.

- There is a decrease in magnitudes of $f(\eta)$, $f'(\eta)$ and $g(\eta)$ when M is increased.

- The applied magnetic field provides a mechanism to control the boundary layer.

- The skin friction coefficient $\mathrm{Re}_r\, C_f$ and wall couple stress coefficient $\mathrm{Re}_r\, C_g$ are increasing functions of Re, M and K.

- Qualitative effects of M and K on the skin friction and the wall couple stress coefficients are similar to that of Re.

Chapter 9

Heat transfer analysis on axisymmetric MHD flow of a micropolar fluid between the radially stretching sheets

The research in this chapter extends the contents presented in the previous chapter in the presence of heat transfer. Effect of heat transfer on axisymmetric fow of magnetohydrodynamic micropolar fluid between two radially stretching sheets is considered. Viscous dissipation, micropolar heat conduction and Joule heating are considered. Energy equation is transformed into the ordinary differential equation by using suitable variables. The resulting nonlinear problem is solved by homotopy analysis method (HAM). Dimensionless temperature is plotted against various values of dimensionless parameters. Numerical values of Nusselt number are tabulated with respect to the influence of several physical parameters.

9.1 Mathematical formulation of the problem

Here, we have considered the heat transfer characteristics on axisymmetric MHD flow of a micropolar fluid between two radially stretching sheets at $z = \pm L$. Both sheets are stretching

149

with linear velocity ar ($a > 0$) and are maintained at constant temperature T_w. Sheets are electrically nonconducting whereas fluid is electrically conducting. Micropolar fluid occupies the space between the sheets. Flow is engendered by the stretching of sheets. The viscous dissipation, the micropolar heat conduction and Joule heating are considered. Physical model and coordinate system are shown Fig. 8.1. Due to axial symmetry, the flow fields (see Takhar et al. [46]) are defined as

$$\mathbf{V} = [u(r,z), 0, w(r,z)], \ \mathbf{\Omega} = [0, N_2(r,z), 0], \ T = T(r,z), \tag{9.1}$$

where u and w are the velocity components along the radial (r) and axial (z) directions respectively, N_2 is the azimuthal component of micro-rotation vector $\mathbf{\Omega}$ and T is the temperature.

Using above definitions of flow fields in energy equation (1.8), one obtains

$$u\frac{\partial T}{\partial r} + w\frac{\partial T}{\partial z} = \frac{K_c}{\rho c_p}\left[\frac{\partial^2 T}{\partial r^2} + \frac{1}{r}\frac{\partial T}{\partial r} + \frac{\partial^2 T}{\partial z^2}\right] + \frac{(2\mu+k)}{\rho c_p}\left[\left(\frac{\partial u}{\partial r}\right)^2 + \frac{u^2}{r^2} + \left(\frac{\partial w}{\partial z}\right)^2\right]$$

$$+ \frac{(2\mu+k)}{\rho c_p}\left[\frac{1}{2}\left(\frac{\partial u}{\partial z} + \frac{\partial w}{\partial r}\right)^2\right] + \frac{k}{2\rho c_p}\left(\frac{\partial u}{\partial z} - \frac{\partial w}{\partial r} - 2N_2\right)^2 - 2\beta_\nu\frac{N_2}{r}\frac{\partial N_2}{\partial r}$$

$$+ \frac{\gamma_\nu}{\rho c_p}\left[\left(\frac{\partial N_2}{\partial r}\right)^2 + \frac{N_2^2}{r^2} + \left(\frac{\partial N_2}{\partial z}\right)^2\right] + \frac{\bar{\alpha}}{\rho c_p}\left[\frac{\partial T}{\partial z}\left(\frac{\partial N_2}{\partial r} + \frac{N_2}{r}\right) - \frac{\partial N_2}{\partial z}\frac{\partial T}{\partial r}\right] + \frac{\sigma B_o^2}{\rho c_p}u^2. \tag{9.2}$$

where j is the micro-inertia per unit mass, ρ is the fluid density, μ and k are the viscosity coefficients, c_p is the specific heat of the fluid, K_c is the thermal conductivity, σ is the electrical conductivity, $\bar{\alpha}$ is the micropolar heat conduction coefficient and $\alpha_\nu, \beta_\nu, \gamma_\nu$ are the spin viscosities. Furthermore, μ, k, α_ν, β_ν and γ_ν, satisfy the constraints given in Eq. (1.14). It is worth mentioning that putting $k = \alpha_\nu = \beta_\nu = \gamma_\nu = \bar{\alpha} = 0$, Eq. (9.2) reduces to energy equation for classical Newtonian fluid with Joule heating. Basically this is the case when global motion is unaffected by the microrotations (Eringen [45]).

Appropriate boundary conditions are

$$T = T_w \ \text{at} \ z = L, \ \frac{\partial T}{\partial z} = 0 \qquad \text{at} \qquad z = 0. \tag{9.3}$$

150

Utilizing the following transformations

$$u = arf'(\eta), \ w = -2aLf(\eta), \ N_2 = \frac{ar}{L}g(\eta), \ \theta = \frac{T}{T_w}, \ \eta = \frac{z}{L}, \quad (9.4)$$

in Eqs. (9.2) and (9.3) one obtains

$$\theta'' + 2\Pr\text{Re}\,f\theta' + \Pr Ec\,(2+K)\left[\frac{6}{\delta^2}(f')^2 + \frac{1}{2}(f'')^2\right] + \frac{K}{2}\Pr Ec\left[f''^2 + 4g^2 - 4f''g\right]$$

$$+ \left(1 + \frac{K}{2}\right)\frac{\Pr Ec}{\text{Re}}\left[\frac{2}{\delta^2}g^2 + (g')^2\right] - 2\frac{B\Pr Ec}{\delta^2}g^2 + 2A\Pr\text{Re}\,g\theta' + M\Pr Ec\,\text{Re}\,f'^2 = 0,$$

$$\theta(1) = 1, \ \theta'(0) = 0. \quad (9.5)$$

Here we have taken $\gamma_\nu = (\mu + k/2)j$ and $j = \nu/a$ [53]. It is important to note that $Ec = 0$ corresponds to the case when viscous dissipation and Joule heating are absent whereas $Ec \neq 0$ corresponds to the situation when viscous dissipation and Joule heating are of considerable magnitude.

The dimensionless parameters appearing in Eq. (9.5) are defined by the following expressions

$$K = \frac{k}{\mu}, \text{ ratio of viscosities called the micropolar parameter,}$$

$$\text{Re} = \frac{aL^2}{\nu}, \text{ Reynolds number,}$$

$$M = \frac{\sigma B_0^2}{\rho a}, \text{ Hartman number, } \Pr = \frac{\mu c_p}{k_c}, \text{ Prandtl number,}$$

$$Ec = \frac{(ar)^2}{c_p T_w}, \text{ the local Eckert number,}$$

$$B = \frac{\beta_\nu}{\mu L^2}, \ A = \frac{\bar{\alpha}}{\rho c_p L^2}, \text{ the dimensionless material parameters.}$$

Nusselt number is defined as

$$Nu = \frac{Lq_w}{k_c T_w} = -\frac{L\,k_c\frac{\partial T}{\partial z}\big|_{z=L}}{k_c T_w} = -\theta'(1), \quad (9.6)$$

where $q_w \left(= -K_c\partial T/\partial z, \text{ Fourier law of conduction}\right)$ is the heat flux at the wall and $\text{Re}_r \left(= arL/\nu\right)$ denotes the local Reynolds number.

151

9.2   Solution procedure

Homotopy solution $\theta(\eta)$ in terms of base functions

$$\{\eta^{2n}, \ n \geq 0\} \tag{9.7}$$

can be expressed as

$$\theta(\eta) = \sum_{n=0}^{\infty} c_n \eta^{2n}, \tag{9.8}$$

where c_n are the coefficients. It is important to note that series solution (Eq. 9.8) shows that the dimensionless temperature is an odd function of η and has same value in both the region $0 < \eta < 1$ and $-1 < \eta < 0$. This is due to the symmetric nature of the flow.

The initial guess $\theta_0(\eta)$ and linear operator $\mathcal{L}_\theta$ are given by the following expressions:

$$\theta_0(\eta) = \eta^2, \tag{9.9}$$

$$\mathcal{L}_\theta[\theta(\eta)] = \frac{d^2\theta}{d\eta^2}, \tag{9.10}$$

while the operators satisfy

$$\mathcal{L}_\theta[C_1 + C_2\eta] = 0, \tag{9.11}$$

where C_i $(i = 1, 2)$ are the arbitrary constants.

9.2.1   Zeroth order deformation problems

The problems at the zeroth order are

$$(1 - q)\mathcal{L}_\theta\left[\hat{\theta}(\eta; q) - \theta_o(\eta)\right] = q\hbar_\theta\mathcal{N}_\theta\left[\hat{g}(\eta; q), \hat{f}(\eta; q), \hat{\theta}(\eta; q)\right], \tag{9.12}$$

$$\hat{\theta}(1; q) = 1, \ \frac{\partial\hat{\theta}}{\partial\eta}(0; q) = 0, \tag{9.13}$$

in which $q \in [0, 1]$ is called embedding parameter and $\hbar_\theta$ is known as convergence control parameter (auxiliary parameter) such that

$$\begin{aligned}
\hat{\theta}(\eta; 0) &= \theta_0(\eta), \\
\hat{\theta}(\eta; 1) &= \theta(\eta),
\end{aligned}$$

i.e. when q varies from 0 to 1, $\hat{\theta}(\eta; q)$ varies from $\theta_0(\eta)$ to $\theta(\eta)$. The nonlinear operator $\mathcal{N}_\theta$ is defined as

$$\begin{aligned}
\mathcal{N}_\theta \left[\hat{g}(\eta; q), \hat{f}(\eta; q), \hat{\theta}(\eta) \right] &= \frac{\partial^2 \hat{\theta}(\eta; q)}{\partial \eta^2} + 2 \Pr Ec \hat{f}(\eta; q) \frac{\partial \hat{\theta}(\eta; q)}{\partial \eta} \\
&+ \Pr Ec(2 + K) \left[\frac{6}{\delta^2} \left(\frac{\partial \hat{f}(\eta; q)}{\partial \eta} \right)^2 + \frac{1}{2} \left(\frac{\partial^2 \hat{f}(\eta; q)}{\partial \eta^2} \right)^2 \right] \\
&+ \frac{K}{2} \Pr Ec \left[\left(\frac{\partial^2 \hat{f}(\eta; q)}{\partial \eta^2} \right)^2 + 4 (\hat{g}(\eta; q))^2 - 4 \frac{\partial^2 \hat{f}(\eta; q)}{\partial \eta^2} \hat{g}(\eta; q) \right] \\
&- \frac{2B \Pr Ec}{\delta^2} (\hat{g}(\eta; q))^2 + \Pr Ec \left(1 + \frac{K}{2} \right) \left[\frac{2}{\delta^2} (\hat{g}(\eta; q))^2 + \left(\frac{\partial \hat{g}(\eta; q)}{\partial \eta} \right)^2 \right] \\
&+ 2A \Pr Re \, \hat{g}(\eta; q) \frac{\partial \hat{\theta}(\eta; q)}{\partial \eta} + M \Pr Ec Re \left(\frac{\partial \hat{f}(\eta; q)}{\partial \eta} \right)^2.
\end{aligned} \tag{9.14}$$

By using Taylor series, we can write

$$\hat{\theta}(\eta; q) = \theta_0(\eta) + \sum_{m=1}^{\infty} \theta_m(\eta) q^m,$$

$$\theta_m(\eta) = \frac{1}{m!} \left. \frac{\partial^m \hat{\theta}(\eta; q)}{\partial \eta^m} \right|_{q=0}.$$

The appropriate mth order deformation problems are

$$\begin{aligned}
\mathcal{L}_\theta [\theta_m(\eta) - \chi_m \theta_{m-1}(\eta)] &= \hbar_\theta \mathcal{R}_m^\theta (\theta_{m-1}(\eta), g_{m-1}(\eta), f_{m-1}(\eta)), \\
\theta_m(1) &= 0, \quad \theta_m'(0) = 0,
\end{aligned} \tag{9.15}$$

153

$$\chi_m = \begin{cases} 0, m \leq 1 \\ 1, m > 1 \end{cases}.$$

$$
\begin{aligned}
\mathcal{R}_m^\theta \left(g_m(\eta), f_m(\eta), \theta(\eta) \right) \;=\;& \theta''_{m-1} + 2\Pr \mathrm{Re} \sum_{n=0}^{m-1} \left[f_n \theta'_{m-1-n} \right] \\
&+ \Pr Ec\,(2+K) \sum_{n=0}^{m-1} \left[\frac{6}{\delta^2} f'_n f'_{m-1-n} + \frac{1}{2} f''_n f''_{m-1-n} \right] \\
&+ \frac{K}{2} \Pr Ec \sum_{n=0}^{m-1} \left[f''_n f''_{m-1-n} + 4 g_n g_{m-1-n} - 4 f''_n g_{m-1-n} \right] \\
&- 2 \frac{B \Pr Ec}{\delta^2} \sum_{n=0}^{m-1} g_n g_{m-1-n} + \left(1 + \frac{K}{2} \right) \Pr Ec \times \\
&\sum_{n=0}^{m-1} \left[\frac{2}{\delta^2} g_n g_{m-1-n} + g'_n g'_{m-1-n} \right] \\
&+ 2A \Pr \mathrm{Re} \sum_{n=0}^{m-1} \left[g_n \theta'_{m-1-n} \right] + M \Pr Ec\, \mathrm{Re} \times \\
&\sum_{n=0}^{m-1} f'_n f'_{m-1-n}.
\end{aligned}
\tag{9.16}
$$

The general solutions at the mth-order are

$$\theta_m(\eta) = \theta_m^*(\eta) + C_1^m + C_2^m \eta, \tag{9.17}$$

in which $\theta_m^*(\eta)$ is the particular solution of problem and the coefficients $C_i^m (i = 1, 2)$ are determined by the boundary conditions (9.15).

9.3 Convergence of homotopy solution

We know that the convergence of solution (9.17) strongly depends upon the auxiliary parameter $\hbar_\theta$. Hence we display the $\hbar$-curve in Fig. (9.1). It is noticed that allowed values of $\hbar_\theta$ are $-1.3 \leq \hbar_\theta < -0.6$. The whole analysis has been carried out when $\hbar_\theta = -0.7$. Furthermore, Table 9.1 indicates that convergence is achieved at 20th order of approximations up to 12 decimal places.
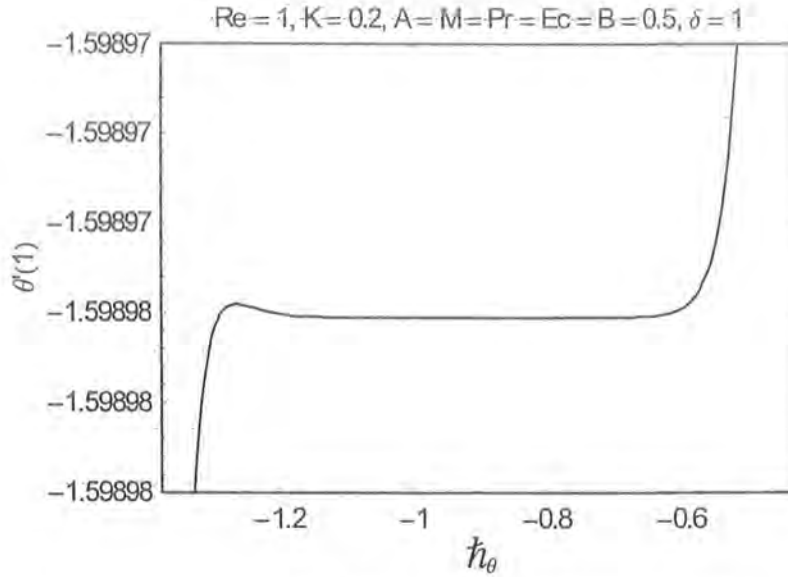
154

Fig. 9.1. $\hbar_\theta$-curve for $\theta'(1)$ at 15th order of approximation.

Table 9.1. Convergence of HAM solution when $Re = M = 2.0$, $K = Ec = 0.5$, $Pr = 0.2$, $A = 1$, $B = 2$, $\delta = 1$ and $\hbar_\theta = -0.7$.

Order of approximations	$\theta'(1)$
1	0.0936666666667
5	0.770075540025
10	0.774245208620
15	0.774249837395
20	0.774249840774
25	0.774249840773
30	0.774249840773

9.4 Results and discussion

This section aims to examine the influence of physical parameters on dimensionless temperature $\theta(\eta)$. Hence Figs. $9.2 - 9.6$ are plotted. Besides this the numerical computations for Nusselt number are presented in Table 9.2. The effects of Prandtl number Pr on dimensionless temper-

155

ature $\theta(\eta)$ is shown in Fig. 9.2. This Fig. shows that dimensionless temperature $\theta(\eta)$ increases with an increase in Prandtl number Pr. The effect of Joule heating and viscous dissipation on dimensionless temperature $\theta(\eta)$ is presented in Fig. 9.3. $Ec = 0$ is the case when viscous dissipation and Joule heating are absent whereas $Ec \neq 0$ corresponds to the situation when viscous dissipation and Joule heating are of considerable magnitude. Since Ec is the ration of kinetic energy to enthalpy. An increase in Ec corresponds to the increase in kinetic energy. Consequently temperature increases. This is obvious from Fig. 9.3. The effect of Reynolds number Re on dimensionless temperature $\theta(\eta)$ is described in Fig. 9.4. It is clear from this Fig. that the dimensionless temperature $\theta(\eta)$ decreases when Reynolds number is increased. We noticed that Re $= 1$ corresponds to the case when inertial and viscous forces are of equal magnitude and Re > 1 leads to the situation when inertial force is dominant. Fig. 9.4 also depicts that when inertial force becomes more and more dominant, there is a decrease in temperature $\theta(\eta)$ of micropolar fluid . Fig. 9.5 illustrates that temperature increases by increasing micropolar parameter K. Here $K = 0$ corresponds to the Newtonian fluid flow and $K \neq 0$ corresponds to the micropolar fluid. Fig. 9.5 also indicates that temperature $\theta(\eta)$ of micropolar fluid $(K \neq 0)$ is higher than that of Newtonian fluid $(K = 0)$ and thermal boundary layer thickness can be reduced by increasing micropolar parameter K. An increase in dimensionless material parameter A results in to decrease the dimensionless temperature $\theta(\eta)$ as shown in Fig. 9.6. It is also noted that the material parameter B has negligible effect on the dimensionless temperature $\theta(\eta)$. Table 9.2 portrayed the influence of physical parameters on Nusselt number Nu which is capable to measure the rate of heat transfer from stretching surface into the fluid. From this Table, it is observed that the rate of heat transfer increases by increasing the Hartman number M, the Reynolds number Re, the micropolar parameter K, the Prandtl number Pr and the Eckert number Ec whereas the rate of heat transfer decreases when B and A are increased. It is also noticed from Table 9.2 that the rate of heat transfer in micropolar fluid $(K \neq 0)$ is higher than of Newtonian fluid $(K = 0)$. From practical point of view, the micropolar fluid can be used instead of Newtonian fluid if some one is interested to increase the rate of heat transfer from surface into the fluid. This is the case when certain temperature is required to improve
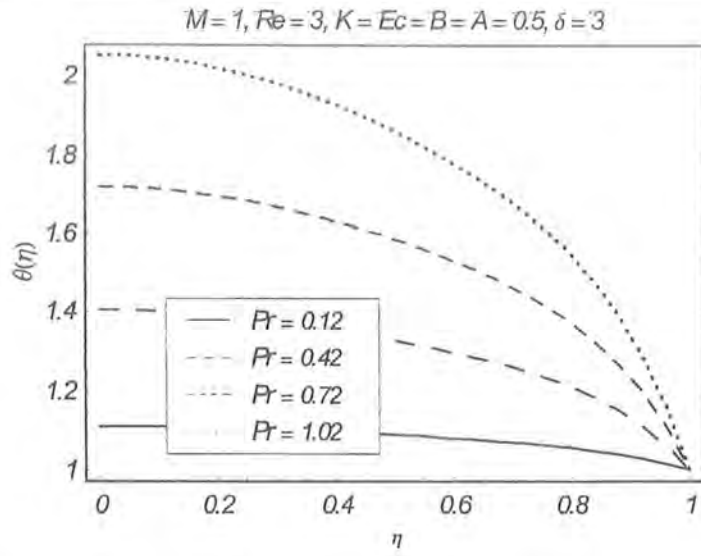
156

the quality of product being manufactured.

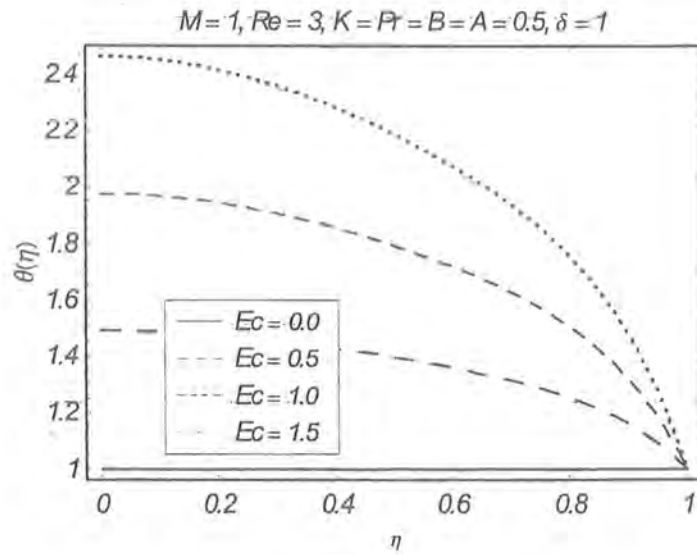Fig. 9.2. Influence of Prandtl number Pr on dimensionless temperature $\theta\left(\eta\right)$.

Fig. 9.3. Influence of Eckert Number Ec on dimensionless temperature $\theta\left(\eta\right)$.
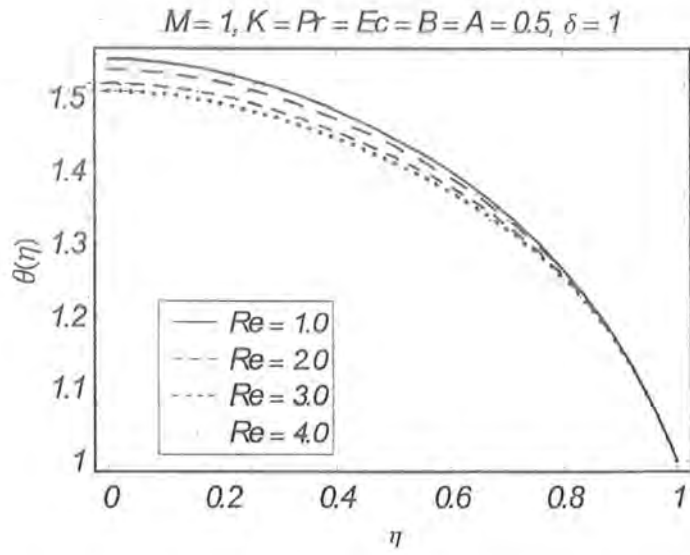
Fig. 9.4. Influence of Reynolds number Re on dimensionless temperature $\theta(\eta)$.
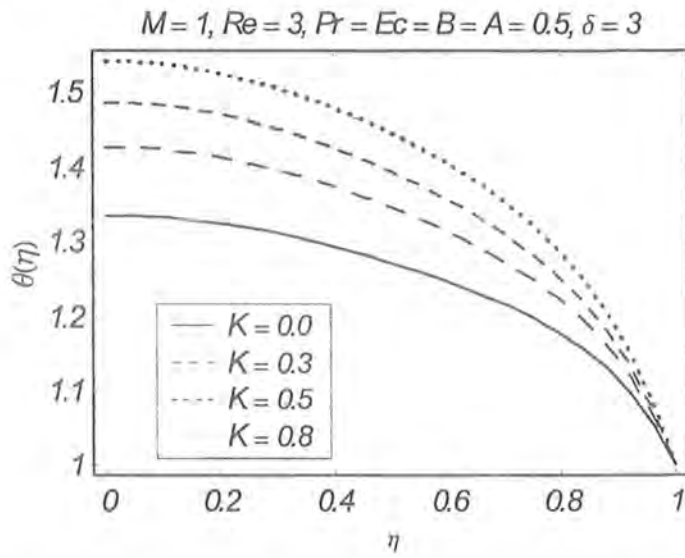

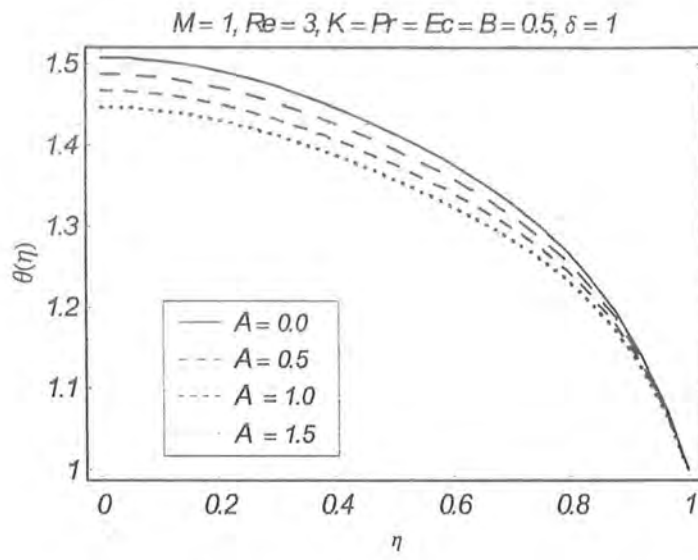Fig. 9.5. Influence of micropolar parameter K on dimensionless temperature $\theta(\eta)$.

Fig. 9.6. Influence of A on dimensionless temperature $\theta(\eta)$.

Table 9.2. Numerical values of Nusselt number Nu for different values of parameters.

M	Re	K	Pr	Ec	B	A	δ	$-Nu$
0.0	1.0	0.2	0.72	0.5	1.0	1.0	1.0	2.31271090137
1.0								2.33756474587
2.0								2.36395766706
3.0								2.39153599402
1.0	0.5	0.5	0.2	0.5	1.0	1.0	1.0	1.58429310808
	1.0							1.60318474778
	1.5							1.61737721445
	2.0							1.62758253929
1.0	1.0	0.0	0.5	0.5	1.0	1.0	1.0	1.39185697948
		0.2						1.60318474754
		0.4						1.81189076519
		0.6						2.01869393983
1.0	1.0	0.2	0.12	0.5	1.0	1.0	1.0	0.37675714532
			0.42					1.34065368956
			0.72					2.33756474587
			1.02					3.36957908505
1.0	1.0	0.2	0.5	0.0	1.0	1.0	1.0	0.00000000000
				0.5				1.60318474780
				1.0				3.20636949560
				1.5				4.80955424340
1.0	1.0	0.2	0.5	0.5	0.0	1.0	1.0	1.60346356189
					0.5			1.60332415485
					1.0			1.60318474780
					1.5			1.60304534076

(continuation of table 9.2)

M	Re	K	Pr	Ec	B	A	δ	$-Nu$
1.0	1.0	0.2	0.5	0.5	1.0	0.0	1.0	1.61286336967
						0.5		1.60800646998
						1.0		1.60318474780
						1.5		1.59839789939

9.5 Conclusions

The heat transfer analysis for in axisymmetric and magnetohydrodynamic flow of an electrically conducting micropolar fluid between the radially stretching sheets is discussed. The following points are worth mentioning:

- Temperature $\theta(\eta)$ is an increasing function of Pr, Ec and K whereas it decreases by increasing A and Re.

- Behavior of B on dimensionless temperature $\theta(\eta)$ is negligible.

- Nusselt number Nu is an increasing function of Pr, Ec, M and Re whereas it decreases when A and B are increased. Hence rate of heat transfer from sheet into the fluid increases when Pr, Ec, M and Re are increased but it decreases by increasing A and B.

161

Chapter 10

Heat and mass transfer in MHD axisymmetric flow of a micropolar fluid with Dufour and Soret effects

This study is concerned with Dufour and Soret effects on steady, two-dimensional axisymmetric flow of an incompressible micropolar fluid between radially stretching sheets subject to constant magnetic field. Joule heating is considered and diffusing species are chemically reacting. In this chapter energy equation and Fick's law are made dimensionless and then solved analytically using HAM. Validity of series solutions is verified through residual errors. Effects of emerging parameters on dimensionless temperature and concentration are seen through graphs. Skin friction coefficient, wall couple stress coefficient, Nusselt and Sherwood numbers are examined.

10.1 Heat and mass transfer analysis

We consider heat and mass transfer characteristics on steady, two-dimensional axisymmetric flow of an incompressible micropolar fluid between electrically non-conducting sheets. The flow is caused by stretching of sheets. Both the sheets have constant temperature T_w. The concentration at the surface of sheets is constant and denoted by C_w. An external magnetic field of constant strength $\mathbf{B_0} = [0, 0, B_0]$ is applied perpendicular to the planes of sheets. Induced magnetic field and electric are not taken. Furthermore, Dufour-Soret effects, Joule

162

heating and first order chemical reaction are considered. If $T(r,z)$ and $C(r,z)$ (see Takhar et al. [46]) denote the temperature and concentration fields for the considered flow then energy equation (1.8) in the absence of viscous dissipation ($\Phi = 0$) and advection diffusion equation (1.9) in the presence of first order chemical reaction ($n = 1$) can be written as

$$u\frac{\partial T}{\partial r} + w\frac{\partial T}{\partial z} = \frac{K_c}{\rho c_p}\left[\frac{\partial^2 T}{\partial r^2} + \frac{1}{r}\frac{\partial T}{\partial r} + \frac{\partial^2 T}{\partial z^2}\right] + \frac{DK_T}{c_p C_s}\left[\frac{\partial^2 C}{\partial r^2} + \frac{1}{r}\frac{\partial C}{\partial r} + \frac{\partial^2 C}{\partial z^2}\right] + \frac{\sigma B_0^2}{\rho c_p}u^2, \quad (10.1)$$

$$u\frac{\partial C}{\partial r} + w\frac{\partial C}{\partial z} = D\left[\frac{\partial^2 C}{\partial r^2} + \frac{1}{r}\frac{\partial C}{\partial r} + \frac{\partial^2 C}{\partial z^2}\right] + \frac{DK_T}{T_m}\left[\frac{\partial^2 T}{\partial r^2} + \frac{1}{r}\frac{\partial T}{\partial r} + \frac{\partial^2 T}{\partial z^2}\right] - K_1 C, \quad (10.2)$$

in which u and w are the velocity components along the radial (r) and axial (z) directions respectively, N_2 is the azimuthal component of micro-rotation vector, T is the temperature, C is the concentration field, ρ is the density, c_p is the specific heat, σ is the electrical conductivity of the fluid, p is the pressure, K_c the thermal conductivity, D is the coefficient of mass diffusivity, C_s is the concentration susceptibility, T_m is the mean fluid temperature, K_T is the thermal-diffusion ratio, K_1 is the first order chemical reaction constant, N_2 is the microrotation field and μ and k are the viscosity coefficients.

The appropriate boundary conditions are

$$\left.\begin{array}{l} T = T_w \quad C = C_w \quad \text{at} \quad z = L, \quad a > 0 \\ \frac{\partial T}{\partial z} = 0, \quad \frac{\partial C}{\partial z} = 0, \quad\quad \text{at} \quad\quad z = 0, \end{array}\right\} \quad (10.3)$$

Using

$$u = arf'(\eta), \quad w = -2aLf(\eta), \quad N_2 = \frac{ar}{L}g(\eta),$$
$$\theta = \frac{T}{T_w}, \quad \phi = \frac{C}{C_w}, \quad \eta = \frac{z}{L} \quad\quad (10.4)$$

the above equations finally yield

$$\theta'' + 2\Pr\mathrm{Re}\,f\theta' + M\Pr Ec\,\mathrm{Re}\,f'^2 + Du\Pr\phi''(\eta) = 0, \quad (10.5)$$

$$\theta(1) = 1, \quad \theta'(0) = 0, \quad (10.6)$$

$$\phi'' + 2Sc\,\mathrm{Re}\,f\phi' + ScSr\theta'' - \mathrm{Re}\,Sc\gamma\phi = 0, \quad (10.7)$$

$$\phi(1) = 1, \quad \phi'(0) = 0. \quad (10.8)$$

163

The dimensionless parameters arising in Eqs. (10.5) − (10.8) are

$$
\begin{aligned}
\mathrm{Re} &= \frac{aL^2}{\nu}, \text{ the Reynolds number, } M = \frac{\sigma B_0^2}{\rho a}, \text{ the Hartman number,} \\
\mathrm{Pr} &= \frac{\mu c_p}{K_c}, \text{ the Prandtl number, } Ec = \frac{(ar)^2}{c_p T_w}, \text{ the local Eckert number,} \\
Du &= \frac{D K_T C_w}{\nu c_p C_s T_w}, \text{ the Dufour Number, } Sc = \frac{\nu}{D}, \text{ the Schmidt number} \\
\gamma &= \frac{K_1}{\rho a}, \text{ the chemical reaction parameter, } Sr = \frac{D K_T T_w}{\nu T_m C_w}, \text{ the Soret number.}
\end{aligned}
$$

It is important to note that for $M = 0$ flow is termed as hydrodynamic flow whereas it is called hydromagnetic if $M \neq 0$. It is evident from the expressions for Dufour and Soret numbers that these are arbitrary constants provided that their product remains constant [70 − 74]. Furthermore $Du = 0$ and $Sr = 0$ correspond to the situation when thermal diffusion and diffusion-thermo effects are smaller order of magnitude than the effects described by Fourier's and Fick's laws [70 − 74]. $\gamma > 0$ shows first order destructive chemical reaction while $\gamma < 0$ corresponds to the generative chemical reaction and $\gamma = 0$ is the case when there is no chemical reaction occurring in the flow regime. $Ec = 0$ is the case when Joule heating is not considered.

Physical quantities of interest are Nusselet number Nu and Sherwood number Sh which are defined as

$$
\begin{aligned}
Nu &= \frac{L q_w}{K_c T_w} = -\frac{L K_c \frac{\partial T}{\partial z}\big|_{z=L}}{K_c T_w} = -\theta'(1), \\
Sh &= \frac{L m_w}{D C_w} = -\frac{L D \frac{\partial C}{\partial z}\big|_{z=L}}{D C_w} = -\phi'(1),
\end{aligned}
\tag{10.9}
$$

where $q_w \, (= -K_c \partial T / \partial z)$ and $m_w \, (= -D \partial C / \partial z)$ are the heat and mass fluxes and $\mathrm{Re}_r \, (= arL/\nu)$ denotes the local Reynold number.

10.2 Homotopy solutions

For homotopy solutions $\theta(\eta)$ and $\phi(\eta)$ in terms of base functions

$$
\{\eta^{2n}, \ n \geq 0\}
\tag{10.10}
$$

164

can be expressed as

$$\theta(\eta) = \sum_{n=0}^{\infty} c_n \eta^{2n}, \quad \phi(\eta) = \sum_{n=0}^{\infty} d_n \eta^{2n}, \tag{10.11}$$

where c_n and d_n are the coefficients. Corresponding initial guesses are chosen as

$$\theta_0(\eta) = \eta^2, \ \phi_0(\eta) = \eta^2. \tag{10.12}$$

Linear operators $\mathcal{L}_\theta$ and $\mathcal{L}_\phi$ are expressed as

$$\mathcal{L}_\theta(\theta(\eta)) = \frac{d^2\theta}{d\eta^2}, \quad \mathcal{L}_\phi(\theta(\eta)) = \frac{d^2\phi}{d\eta^2} \tag{10.13}$$

and these linear operators satisfy the following properties

$$\mathcal{L}_\theta[C_1 + C_2\eta] = 0, \ \mathcal{L}_\phi[C_3 + C_4\eta] = 0, \tag{10.14}$$

where C_i $(i = 1 - 4)$ are the arbitrary constants.

10.2.1 Zeroth order deformation problems

The deformation problems at the zeroth order are as follows

$$(1 - q)\mathcal{L}_\theta\left[\hat{\theta}(\eta; q) - \theta_0(\eta)\right] = q\hbar_\theta \mathcal{N}_\theta\left[\hat{g}(\eta; q), \hat{f}(\eta; q), \hat{\theta}(\eta; q), \hat{\phi}(\eta; q)\right], \tag{10.15}$$

$$\hat{\theta}(1; q) = 1, \ \frac{\partial\hat{\theta}}{\partial\eta}(0; q) = 0, \tag{10.16}$$

$$(1 - q)\mathcal{L}_\phi\left[\hat{\phi}(\eta; q) - \phi_0(\eta)\right] = q\hbar_\phi \mathcal{N}_\phi\left[\hat{g}(\eta; q), \hat{f}(\eta; q), \hat{\theta}(\eta; q), \hat{\phi}(\eta; q)\right], \tag{10.17}$$

$$\hat{\phi}(1; q) = 1, \ \frac{\partial\hat{\phi}}{\partial\eta}(0; q) = 0. \tag{10.18}$$

In above problems embedding parameter $q \in [0, 1]$ and $\hbar_\theta$ $\hbar_\phi$ are convergence control parameters (auxiliary parameters) such that $\hat{\theta}(\eta; 0) = \theta_0(\eta)$, $\hat{\phi}(\eta; 0) = \phi_0(\eta)$ and $\hat{\theta}(\eta; 1) = \theta(\eta)$, $\hat{\phi}(\eta; 1) = \phi_0(\eta)$. When q varies from 0 to 1, $\hat{\theta}(\eta; q)$ varies from $\theta_0(\eta)$ to $\theta(\eta)$ and $\hat{\phi}(\eta; q)$ from

165

$\phi_0(\eta)$ to $\phi(\eta)$. The nonlinear operators $\mathcal{N}_\theta$ and $\mathcal{N}_\phi$ are

$$
\begin{aligned}
\mathcal{N}_\theta \left[\hat{f}(\eta;q), \hat{g}(\eta;q), \hat{\theta}(\eta), \hat{\phi}(\eta;q) \right] &= \frac{\partial^2 \hat{\theta}(\eta;q)}{\partial \eta^2} + 2\Pr \operatorname{Re} \hat{f}(\eta;q) \frac{\partial \hat{\theta}(\eta;q)}{\partial \eta} \\
&\quad + Du \Pr \frac{\partial^2 \hat{\phi}(\eta;q)}{\partial \eta^2} + M \Pr Ec \operatorname{Re} \\
&\quad \times \left(\frac{\partial \hat{f}(\eta;q)}{\partial \eta} \right)^2,
\end{aligned}
\tag{10.19}
$$

$$
\begin{aligned}
\mathcal{N}_\phi \left[\hat{f}(\eta;q), \hat{g}(\eta;q), \hat{\theta}(\eta), \hat{\phi}(\eta;q) \right] &= \frac{\partial^2 \hat{\phi}(\eta;q)}{\partial \eta^2} + 2Sc \operatorname{Re} \hat{f}(\eta;q) \frac{\partial \hat{\phi}(\eta;q)}{\partial \eta} \\
&\quad + SrSc \frac{\partial^2 \hat{\theta}(\eta;q)}{\partial \eta^2} - \operatorname{Re} Sc\gamma \hat{\phi}(\eta;q).
\end{aligned}
\tag{10.20}
$$

According to Taylor series we expand

$$
\begin{aligned}
\hat{\theta}(\eta;q) &= \theta_0(\eta) + \sum_{m=1}^{\infty} \theta_m(\eta) q^m, \ \theta_m(\eta) = \frac{1}{m!} \left. \frac{\partial^m \hat{\theta}(\eta;q)}{\partial \eta^m} \right|_{q=0} \\
\hat{\phi}(\eta;q) &= \phi_0(\eta) + \sum_{m=1}^{\infty} \phi_m(\eta) q^m, \ \phi_m(\eta) = \frac{1}{m!} \left. \frac{\partial^m \hat{\phi}(\eta;q)}{\partial \eta^m} \right|_{q=0}.
\end{aligned}
\tag{10.21}
$$

10.2.2 Higher order deformation problems

The mth order deformation problems are

$$
\mathcal{L}_\theta \left[\theta_m(\eta) - \chi_m \theta_{m-1}(\eta) \right] = \hbar_\theta \mathcal{R}_m^\theta \left(\theta_{m-1}(\eta), g_{m-1}(\eta), f_{m-1}(\eta), \phi_{m-1}(\eta) \right),
$$
$$
\theta_m(1) = 0, \quad \theta_m'(0) = 0,
\tag{10.22}
$$

$$
\mathcal{L}_\phi \left[\phi_m(\eta) - \chi_m \phi_{m-1}(\eta) \right] = \hbar_\phi \mathcal{R}_m^\phi \left(\theta_{m-1}(\eta), g_{m-1}(\eta), f_{m-1}(\eta), \phi_{m-1}(\eta) \right),
$$
$$
\theta_m(1) = 0, \quad \theta_m'(0) = 0,
\tag{10.23}
$$

$$
\chi_m = \begin{cases} 0, m \le 1 \\ 1, m > 1 \end{cases},
$$

166

$$
\begin{aligned}
\mathcal{R}_m^\theta \left(g_m(\eta), f_m(\eta), \theta\left(\eta\right), \phi\left(\eta\right) \right) \;=\;& \theta_{m-1}'' + 2\Pr\operatorname{Re}\sum_{n=0}^{m-1}\left[f_n\theta_{m-1-n}'\right] + Du\Pr\phi_{m-1}'' \\
& + M\Pr Ec\operatorname{Re}\sum_{n=0}^{m-1}f_n'f_{m-1-n}',
\end{aligned}
\tag{10.24}
$$

$$
\mathcal{R}_m^\phi \left(g_m(\eta), f_m(\eta), \theta\left(\eta\right), \phi\left(\eta\right) \right) = \phi_{m-1}'' + 2Sc\operatorname{Re}\sum_{n=0}^{m-1}\left[\begin{array}{c} f_n\phi_{m-1-n}' + SrSc\theta_{m-1}'' \\ -\operatorname{Re}Sc\gamma\phi_{m-1} \end{array}\right].
\tag{10.25}
$$

The general solutions at the mth-order are

$$
\theta_m\left(\eta\right) \;=\; \theta_m^*\left(\eta\right) + C_1^m + C_2^m\eta,
\tag{10.26}
$$

$$
\phi_m\left(\eta\right) \;=\; \phi_m^*\left(\eta\right) + C_3^m + C_4^m\eta,
\tag{10.27}
$$

in which $\theta_m^*\left(\eta\right)$ and $\phi_m^*\left(\eta\right)$ are the particular solutions of problems given in Eqs. (10.22) and (10.23). The the coefficients $C_i^m (i = 1 - 4)$ are determined by the boundary conditions given in Eqs. (10.22) and (10.23). The systems given in Eqs. (10.22) and (10.23) have been solved by using Mathematica.

10.3 Convergence of series solutions

This section deals with the convergence of series solutions (Eqs. (10.26) and (10.27)). These series solutions strongly depend upon the auxiliary parameters $\hbar_\theta$ and $\hbar_\phi$. Hence we display the $\hbar$-curves of the residual errors of $\theta\left(\eta\right)$ and $\phi\left(\eta\right)$ in the Figs. (10.1) and (10.2). It is noticed that permissible values of $\hbar_\theta$ and $\hbar_\phi$ are $-0.9 \leq \hbar_\theta, \hbar_\phi < -0.6$. However the whole forth coming analysis has been carried out for $\hbar_\theta = \hbar_\phi = -0.7$. Furthermore, Table 10.1 indicates that

convergence of $\theta\left(\eta\right)$ and $\phi\left(\eta\right)$ is achieved at 40th order of approximation.
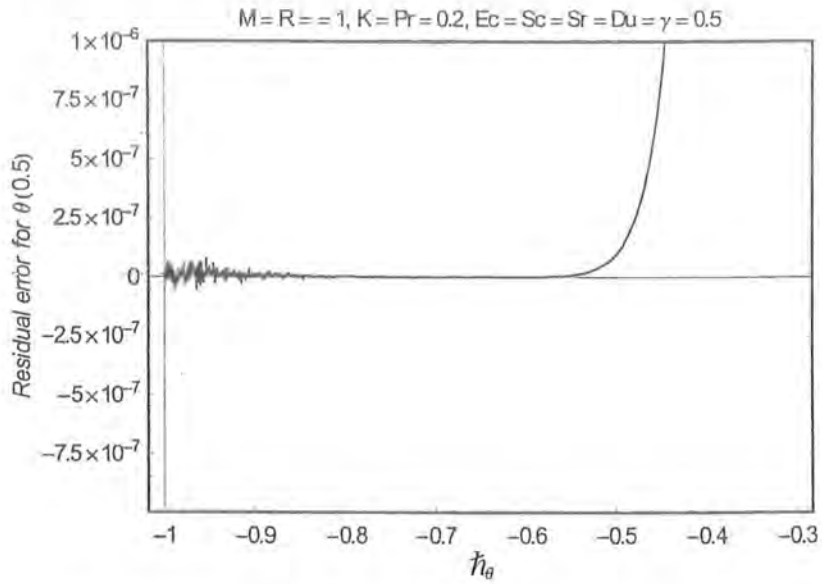
Fig. 10.1. $\hbar_\theta$–curve for residual error of $\theta\left(\eta\right)$ at $\eta = 0.5$.
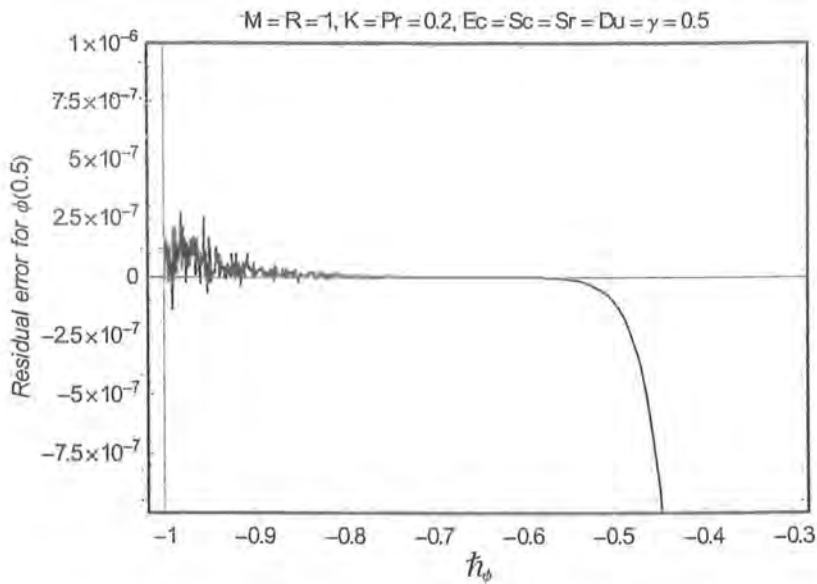

Fig. 10.2. $\hbar_\phi$–curve for residual error of $\phi\left(\eta\right)$ at $\eta = 0.5$.

Table 10.1. Convergence of HAM solutions when $Re = M = 1.0$, $Du = Sr = Sc = K = Ec = 0.5$, $Pr = 0.72$, $\gamma = 1$ and $\hbar_\theta = \hbar_\phi = -0.7$.

Order of approximations	$-\theta'(1)$	$\phi'(1)$
1	0.180000000000	0.460000000000
5	0.254152789818	0.504473160068
10	0.275842111808	0.517997985130
15	0.276571089191	0.518477531958
20	0.276594087908	0.518493503281
25	0.276594768508	0.518494005309
30	0.276594787283	0.518494020207
35	0.276594787759	0.518494020623
40	0.276594787770	0.518494020634
45	0.276594787770	0.518494020634

10.4 Results and discussion

Here in this section we have examined the influence of pertinent parameters on the dimensionless temperature $\theta(\eta)$ and dimensionless concentration $\phi(\eta)$. Furthermore the numerical computations for Nusselt number and Sherwood number for various values of dimensionless parameters are presented in Table 10.2. Figs. 10.3 and 10.4 are sketched to see the influence of Prandtl number Pr on dimensionless temperature $\theta(\eta)$ and dimensionless concentration field $\phi(\eta)$. These Figs. reveal that the effect of Pr on $\theta(\eta)$ is opposite to that of Pr on $\phi(\eta)$. The purpose of Figs. 10.5 and 10.6 is to show the behavior of local Eckert number Ec on $\theta(\eta)$ and $\phi(\eta)$. Here $Ec = 0$ corresponds to the case when Joule heating is negligible small while $Ec \neq 0$ leads to the situation when Joule heating is significant. It is noted from Fig. 10.5 that dimensionless temperature $\theta(\eta)$ increases by increasing Ec. This is due to the fact that an increase in Ec results an increase in kinetic energy. Consequently temperature $\theta(\eta)$ increases. Fig. 10.6 depicts that dimensionless concentration field $\phi(\eta)$ decreases with an increase in local Eckert Ec. Comparison of Figs. 10.5 and 10.6 shows that the effect of Ec on $\theta(\eta)$ is opposite to that of Ec on $\phi(\eta)$. It is observed from Fig. 10.7 that $\theta(\eta)$ has an increasing trend when Dufour Du

169

is increased whereas $\phi(\eta)$ decreases when Du is increased (see Fig. 10.8). Fig 10.7 also reveals that $\theta(\eta)$ decreases when Soret number Sr is increased whereas $\phi(\eta)$ is an increasing function of Soret number Sr. It means Soret number Sr shows opposite behavior on $\theta(\eta)$ and $\phi(\eta)$. Figs. 10.9 and 10.10 are displayed to see the influence of Schmidt number Sc on $\theta(\eta)$ and $\phi(\eta)$. These Figs. clearly show that Sc has opposite effect as that of Pr on $\theta(\eta)$ and $\phi(\eta)$. Temperature $\theta(\eta)$ increases for the case of destructive chemical reaction $(\gamma > 0)$ while it decreases for generative chemical reaction $(\gamma < 0)$ and vice versa for dimensionless concentration $\phi(\eta)$ as shown in Figs. 10.11 and 10.12. It is noted from Fig. 10.13 that by increasing the Hartman number M dimensionless temperature $\theta(\eta)$ increases whereas the dimensionless concentration $\phi(\eta)$ decreases when the Hartmen number M is increased (see Fig. 10.14). The effects of Reynolds number Re on dimensionless temperature $\theta(\eta)$ and the dimensionless concentration $\phi(\eta)$ are also analyzed. It is observed that dimensionless temperature $\theta(\eta)$ increases when Reynolds number is increased but $\phi(\eta)$ is decreasing function of Re. We noticed that Re $= 1$ corresponds to the case when inertial and viscous forces are of equal magnitudes and Re > 1 leads to the situation when inertial force dominates the viscous force. It is noted that when inertial force becomes more and more dominant, there is an increase in temperature of micropolar fluid but vice versa for $\phi(\eta)$. Figs. 10.15 and 10.16 show that temperature of micropolar fluid $(K \neq 0)$ is higher than that of Newtonian fluid $(K = 0)$ but reverse trend is observed for $\phi(\eta)$. Table 10.2 portrayed the influence of physical parameters on Nusselt number Nu and Sherwood number Sh which are respectively capable to measure the rate of heat transfer and rate of diffusion of reacting species from stretching surface into the fluid. From this Table it is found that Nusselt number Nu and Sherwood number Sh are increasing functions of the Hartman number M, the Reynolds number Re, the micropolar parameter K, the Prandtl number Pr, the local Eckert number Ec, the Dufour number Du, the Schmidt number Sc, the Soret number Sr. In fact the rate of heat transfer and rate of diffusion increase by increasing the Hartman number M, the Reynolds number Re, the micropolar parameter K, the Prandtl number Pr, the local Eckert number Ec, the Dufour number Du, the Schmidt number Sc, the Soret number Sr. It is also noticed from Table 10.3 that heat transfer rate and rate of diffusion of impurities are higher in

170

micropolar fluid $(K \neq 0)$ than those of viscous fluid $(K = 0)$.
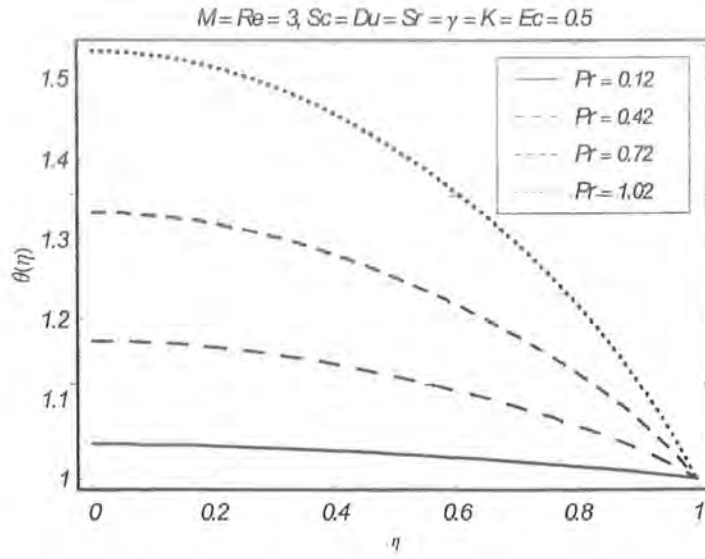

Fig. 10.3. The influence of Prandtl number Pr on dimensionless temperature $\theta(\eta)$.
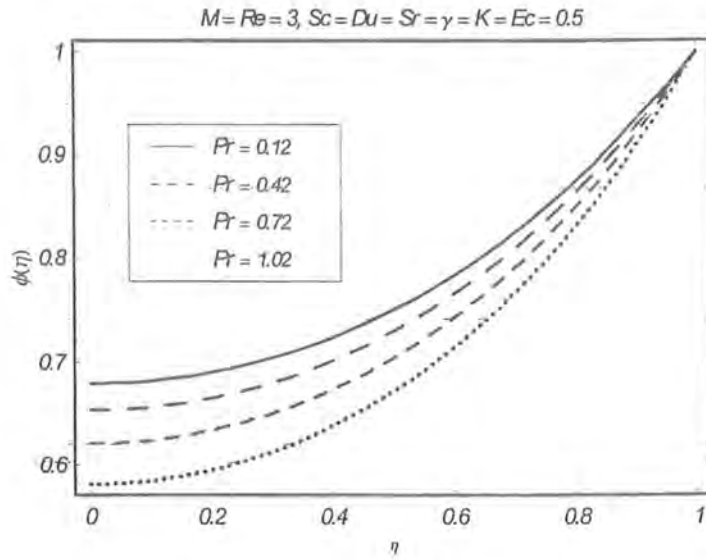

Fig. 10.4. The influence of Prandtl number Pr on dimensionless concentration $\phi(\eta)$.
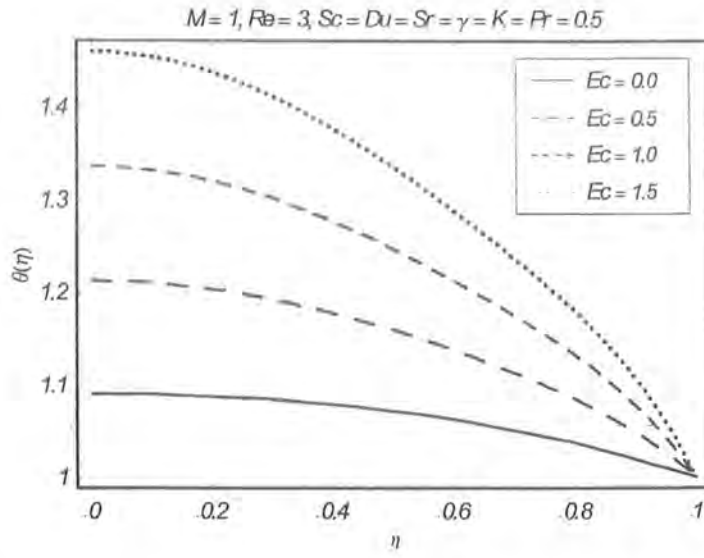
Fig. 10.5 The influence of Eckert number Ec on dimensionless temperature $\theta(\eta)$.
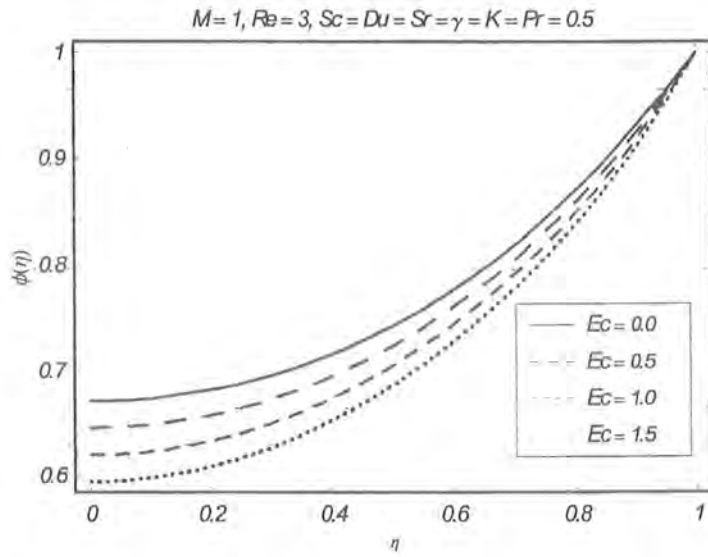

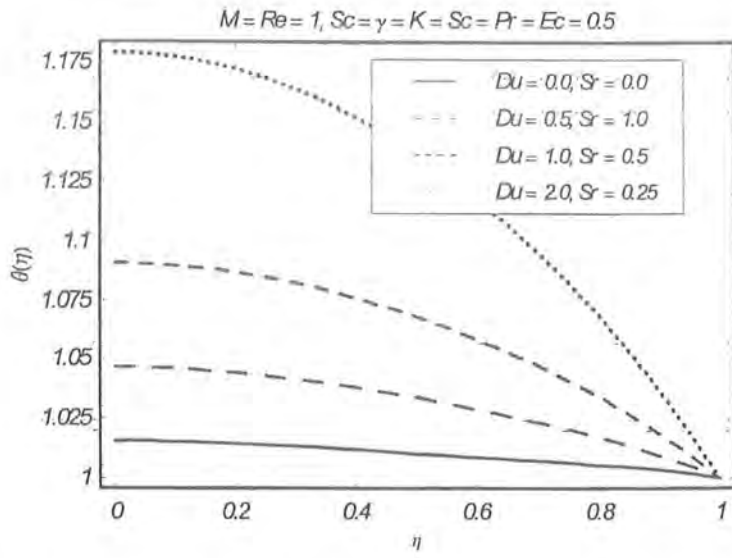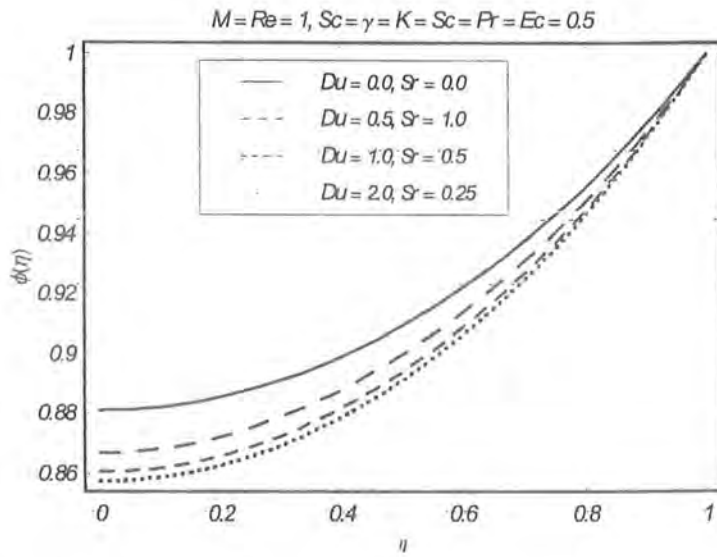Fig. 10.6. The influence of Eckert number Ec on dimensionless concentration $\phi(\eta)$.

172

Fig. 10.7. The influence of Dufour number Du on dimensionless temperature $\theta(\eta)$.

Fig. 10.8. The influence of Dufour number Du on dimensionless concentration $\phi(\eta)$.
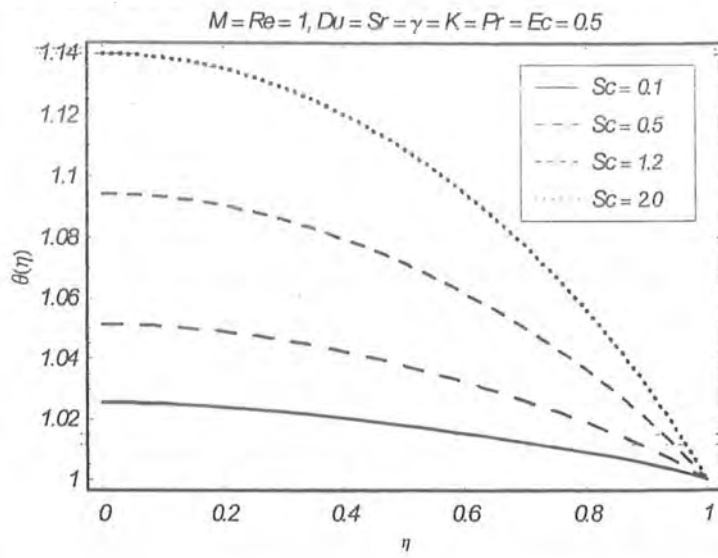
173

Fig. 10.9. The influence of Schmidt number Sc on dimensinless temperature $\theta(\eta)$.
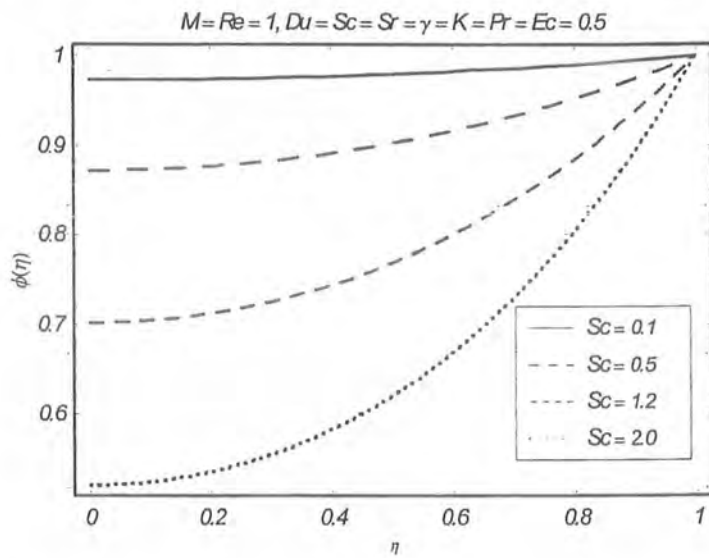

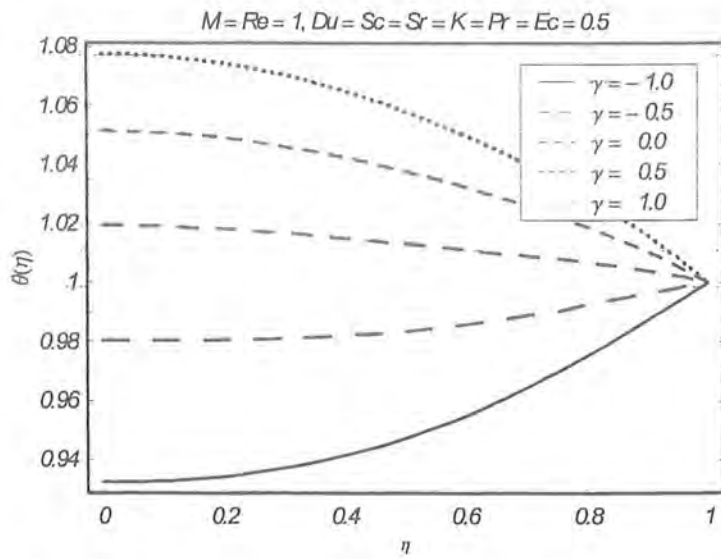Fig. 10.10. The influence of Schmidt number Sc on dimensionless concentration $\phi(\eta)$.

174

Fig. 10.11. The influence of chemical reaction parameter γ on dimensionless temperature $\theta(\eta)$.
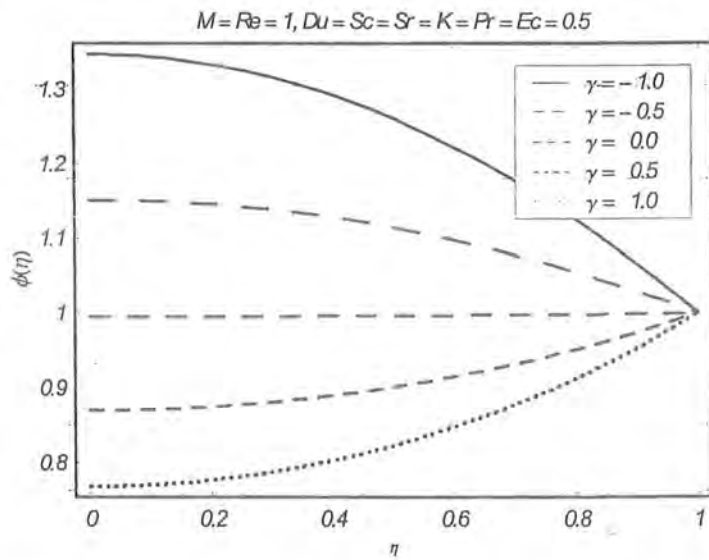

Fig. 10.12. The influence of chemical reaction parameter γ on dimensionless concentration $\phi(\eta)$.
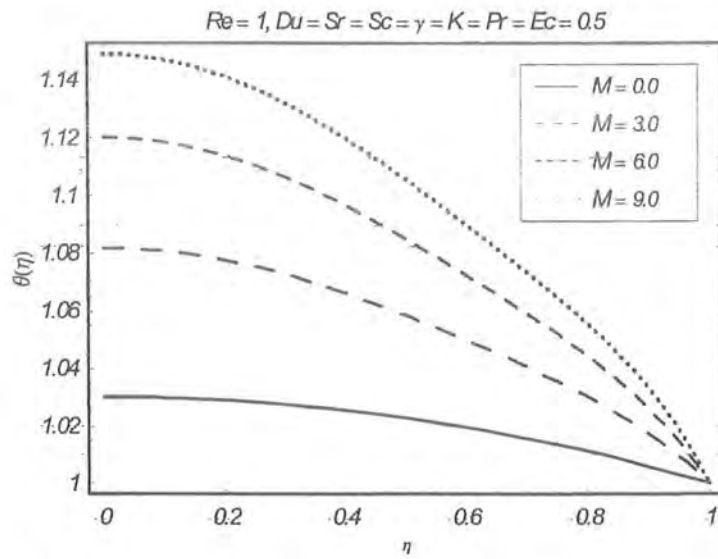
Fig. 10.13. The influence of Hartman number M on dimensionless temperature $\theta(\eta)$.
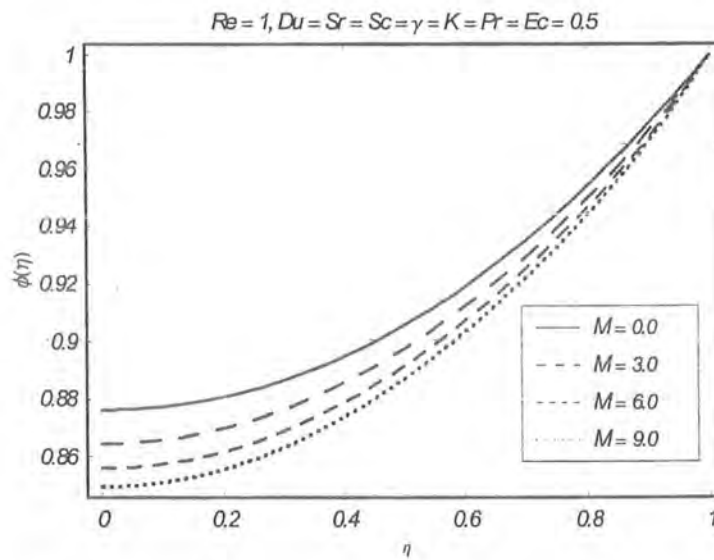

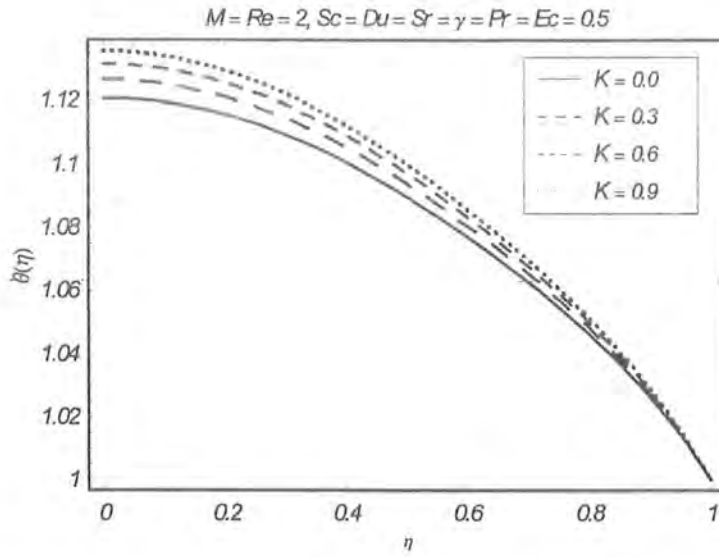Fig. 10.14. The influence of Hartman number M on dimensionless concentration $\phi(\eta)$.

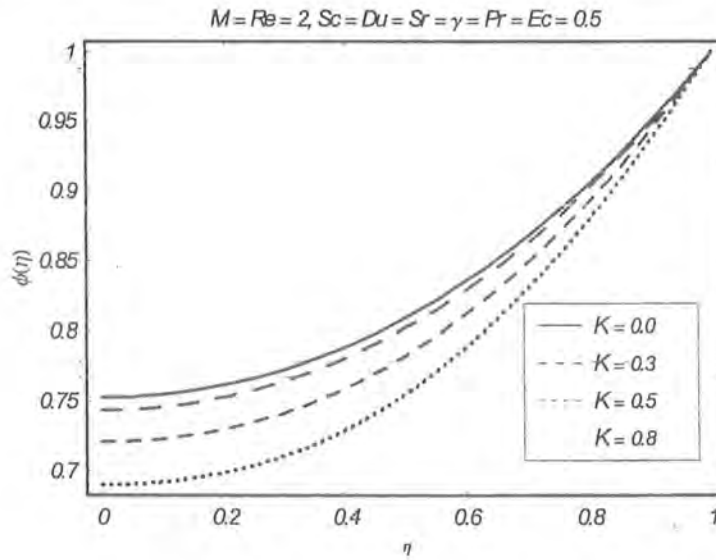Fig.10.15. The influence of micropolar parameter K on dimensionless temperature $\theta(\eta)$.

Fig.10.16. The influence of micropolar parameter K on dimensionless concentration $\phi(\eta)$.

Table 10.2. Numerical values of Nusselt number Nu and Sherwood number Sh for different values of dimensionless parameters.

M	Re	K	Pr	Ec	Du	Sc	Sr	γ	$-Nu$	Sh
0.0	1.0	0.2	0.72	0.5	0.5	0.5	0.5	1.0	0.196967377202	0.500216574212
1.0									0.236713458769	0.509198729447
2.0									0.274572363419	0.517753418874
3.0									0.310697250305	0.525915986054
1.0	0.5	0.5	0.72	0.5	0.5	0.5	0.5	1	0.137959287226	0.271110627134
	1.0								0.274572363419	0.517753418874
	1.5								0.409440501724	0.743321170314
	2.0								0.542289190987	0.950701279402
1.0	1.0	0.0	0.72	0.5	0.5	0.5	0.5	1.0	0.272947830222	0.517155792181
		0.2							0.274572363419	0.517753418874
		0.4							0.275970705362	0.518265878741
		0.6							0.277174457309	0.518705617114
1.0	1.0	0.2	0.12	0.5	0.5	0.5	0.5	1.0	0.0397275063813	0.464053027637
			0.42						0.149427970306	0.489266527247
			0.72						0.276594787769	0.518494020634
			1.02						0.425336957988	0.552682488149
1.0	1.0	0.2	0.5	0.0					0.196572400379	0.499782539157
				0.5					0.276594787770	0.518494020634
				1.0					0.356617175160	0.537205502111
				1.5					0.436639562551	0.555916983588
1.0	1.0	0.5	0.72	0.5	0.0	0.5	0.0	1.0	0.0728582933407	0.454921614577
					1.0		0.5		0.524407937326	0.575138460037
					2.0		0.25		0.960074294654	0.564760875122
					3.0		0.167		1.39574064977	0.561301679868

(continuation of Table 10.2)

M	Re	K	Pr	Ec	Du	Sc	Sr	γ	$-Nu$	Sh
1.0	1.0	0.5	0.72	0.5	0.0	0.1	0.0	1.0	0.113791852253	0.103612556345
						0.6			0.317181328487	0.622656593551
						1.1			0.520794528919	1.14999438899
						1.6			0.728685599389	1.69715747052
1.0	1.0	0.5	0.72	0.5	0.0	0.5	0.0	1.0	0.0728582933407	0.454921614577
					0.5		1.0		0.306574759184	0.595893630212
					0.25		2.0		0.197658170280	0.637403971061
					0.167		3.0		0.161352640511	0.678914311273
1.0	1.0	0.5	0.72	0.5	0.5	0.5	0.5	-1.0	0.216649082245	0.728688930740
								-0.5	0.049861218640	0.309363550576
								0.0	0.0810384681714	0.021226011376
								0.5	0.187514276287	0.291392129234
								1.0	0.276594787770	0.518494020634

10.5 Concluding remarks

Dufour and Soret effects on axisymmetric flow of electrically conducting micropolar fluid between the radially stretching sheets with viscous dissipation and Joule heating are investigated. Variations of Nusselt number and Sherwood number are computed. Main findings are summed up as follows.

- Dimensionless temperature $\theta(\eta)$ increases with an increase in Ec whereas dimensionless concentration $\phi(\eta)$ is decreasing function of Ec. Thus Joule heating has opposite effects on $\theta(\eta)$ and $\phi(\eta)$.

- The effects of Pr, Ec M, Re, Du, Sr, Sc and γ on $\theta(\eta)$ are opposite to that of $\phi(\eta)$.

- Temperature $\theta(\eta)$ increases for the case of destructive chemical reaction ($\gamma > 0$) while it decreases for generative chemical reaction ($\gamma < 0$) and vice versa for dimensionless concentration $\phi(\eta)$.

- With an increase in Re, there is an increase in temperature $\theta(\eta)$ of micropolar fluid but for concentration $\phi(\eta)$ the result is reverse.

- Rate of heat transfer from sheet into the fluid increases when Pr, $Ec\ M$, Re, Du, Sr and Sc are increased.

- Diffusion rate of impurities from surface of sheets into the fluid increases by increasing Pr, $Ec\ M$, Re, Du, Sr and Sc.

- Heat transfer rate and diffusion rate are higher in micropolar fluid ($K \neq 0$) when compared with viscous fluid ($K = 0$).

Chapter 11

Axisymmetric magnetohydrodynamic flow of a micropolar fluid between unsteady stretching surfaces

This chapter explores the time-dependent MHD flow problem of a micropolar fluid between two radially stretching sheets. Both cases of strong and weak concentrations of microelements are taken into account. Suitable transformations are employed for the conversion of partial differential equations into the ordinary differential equations. The solutions of the resulting problems are developed by a homotopy analysis method (HAM). Angular velocity, skin friction coefficient and wall couple stress coefficient are illustrated for various parameters of interest.

11.1 Mathematical modelling

We consider the axisymmetric flow of an incompressible micropolar fluid between two parallel infinite sheets at $z = \pm L$. The sheets are subjected to the stretching velocity $u_w = ar(1 - bt)^{-1}$. The magnetic field of the form $\mathbf{B} = \mathbf{B}_0(1 - bt)^{-1/2}$ is applied perpendicular to the planes of sheets (parallel to z-axis). magnetic Reynolds number is small and induced magnetic field is

neglected. No electric field ($\mathbf{E} = \mathbf{0}$) is applied. Schematic representation and coordinate system are shown in Fig. 11.1. Velocity and microrotation fields for unsteady axisymmetric flow can be defined by $\mathbf{V} = [u(r, z, t), 0, w(r, z, t)]$ and $\Omega = [0, N_2, 0, t]$ (see Takhar et al. [46]). The flow under consideration is governed by the equations

$$\frac{\partial u}{\partial r} + \frac{u}{r} + \frac{\partial w}{\partial z} = 0, \tag{11.1}$$

$$\frac{\partial u}{\partial t} + u\frac{\partial u}{\partial r} + w\frac{\partial u}{\partial z} = -\frac{1}{\rho}\frac{\partial p}{\partial r} + \frac{1}{\rho}(\mu + k)\left[\frac{\partial^2 u}{\partial r^2} + \frac{1}{r}\frac{\partial u}{\partial r} + \frac{\partial^2 u}{\partial z^2} - \frac{u}{r^2}\right] - \frac{k}{\rho}\frac{\partial N_2}{\partial z} - \frac{\sigma B^2}{\rho}u, \tag{11.2}$$

$$\frac{\partial w}{\partial t} + u\frac{\partial w}{\partial r} + w\frac{\partial w}{\partial z} = -\frac{1}{\rho}\frac{\partial p}{\partial z} + \frac{1}{\rho}(\mu + k)\left[\frac{\partial^2 w}{\partial r^2} + \frac{1}{r}\frac{\partial w}{\partial r} + \frac{\partial^2 w}{\partial z^2}\right] - \frac{k}{\rho}\left[\frac{\partial N_2}{\partial r} + \frac{N_2}{r}\right], \tag{11.3}$$

$$\frac{\partial N_2}{\partial t} + u\frac{\partial N_2}{\partial r} + w\frac{\partial N_2}{\partial z} = \frac{\gamma_\nu}{\rho j}\left[\frac{\partial^2 N_2}{\partial r^2} + \frac{1}{r}\frac{\partial N_2}{\partial r} + \frac{\partial^2 N_2}{\partial z^2} - \frac{N_2}{r^2}\right] - \frac{k}{\rho j}\left[2N_2 + \frac{\partial w}{\partial r} - \frac{\partial u}{\partial z}\right], \tag{11.4}$$

in which j is the micro-inertia per unit mass, ρ is the fluid density, μ and k are the viscosity coefficients and α_ν, β_ν, γ_ν are the spin viscosities. Furthermore, μ, k, α_ν, β_ν, and γ_ν satisfy the constraints given in Eq. (1.14)

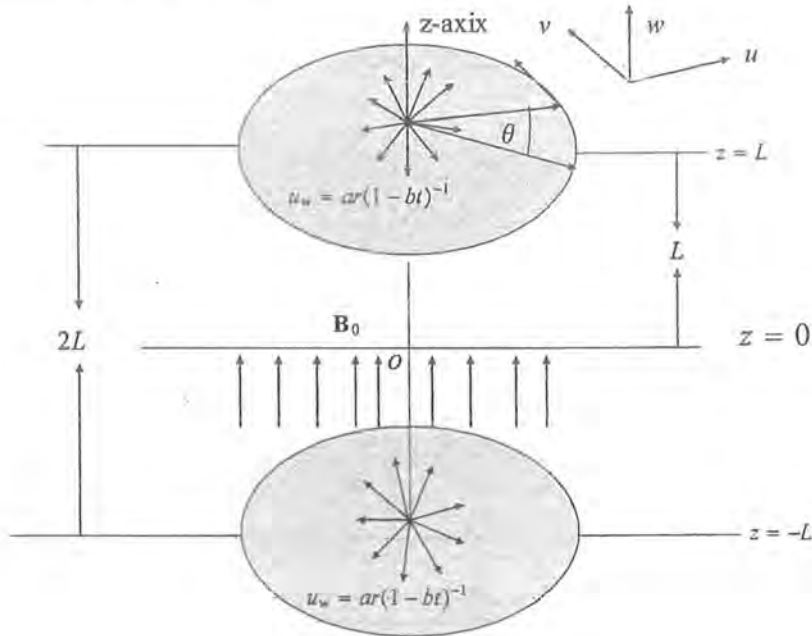

Fig. 11.1. Geometry of the problem and coordinate system.

The boundary conditions are

$$u(r, L, t) = u_w, \quad w(r, L, t) = 0, \quad N_2(r, L, t) = -n \frac{\partial u}{\partial z}\bigg|_{z=L},$$

$$\frac{\partial u(r, z, t)}{\partial z}\bigg|_{z=0} = 0, \quad w(r, 0, t) = 0, \quad N_2(r, 0, t) = 0, \tag{11.5}$$

where n $(0 \leq n \leq 1)$ is a constant. Here $n = 0$ depicts the situation when microelements at the stretching sheets are unable to rotate ($\Omega = 0$ at stretching surfaces). This is also known as the strong concentration of the microelements. When $n = 0.5$ then anti-symmetric part of the stress tensor vanishes and denotes weak concentration of microelements at the sheets. For $n = 1$ one has turbulent boundary layer flow. In the present flow analysis we have considered $n = 0$ and $n = 0.5$ [53].

We nondimensionalize Eqs. (11.1) − (11.5) by utilizing the following transformations

$$u = \frac{ar}{1 - bt} f'(\eta), \quad w = -\frac{2aL}{\sqrt{1 - bt}} f(\eta), \quad N_2 = \frac{ar}{L(1 - bt)^{3/2}} g(\eta), \quad \eta = \frac{z}{L\sqrt{1 - bt}}. \tag{11.6}$$

and eliminating the pressure gradient, we have

$$(1 + K) f'''' - \frac{S \, \text{Re}}{2} [\eta f''' + 3f''] + 2 \, \text{Re} \, ff''' - K g'' - \text{Re} \, M f'' = 0, \tag{11.7}$$

$$f(1) = 0, \quad f'(1) = 1, \quad f(0) = 0, \quad f''(0) = 0, \tag{11.8}$$

$$\left(1 + \frac{K}{2}\right) g'' + \text{Re} \, K \left[f'' - 2g\right] - \frac{S \, \text{Re}}{2} [3g + \eta g'] + \text{Re} \left[2fg' - f'g\right] = 0, \tag{11.9}$$

$$g(1) = -nf''(1), \quad g(0) = 0, \tag{11.10}$$

where Eq. (11.1) is automatically satisfied and $\gamma_\nu = (\mu + k/2) j$ and $j = \nu(1 - bt)/a$ [53]. The dimensionless quantities

$$K = \frac{k}{\mu}, \quad \text{Re} = \frac{aL^2}{\nu}, \quad M = \frac{\sigma B_0^2}{\rho a}, \quad S = \frac{b}{a},$$

respectively indicate the micropolar parameter (K), the Reynolds number (Re), the Hartman number (M) and the unsteadiness parameter (S). Note that for the steady case $S = 0$. Furthermore, Eqs. (11.1) and (11.3) reduce to the classical Navier-Stokes equations when $K = 0$.

183

In fact this is the situation when micro-rotation effects are negligible small and do not affect the flow.

The skin friction coefficient C_f and wall couple stress coefficient C_g at $z = L$ are [46]

$$
\begin{aligned}
C_f &= \frac{\tau_w}{\rho \left(u_w\right)^2} = \frac{(\mu + k)}{\rho \left(ar\right)^2 \left(1 - bt\right)^{-2}} \left(\frac{\partial u}{\partial z} + \frac{\partial w}{\partial r}\right)\bigg|_{z=L} = \frac{(1 + K)}{\mathrm{Re}_r} f''(1), \\
C_g &= -\frac{L \, \gamma_\nu \frac{\partial N_2}{\partial z}\big|_{z=L}}{\rho \left(u_w\right)^2} = -\frac{L \, \gamma_\nu \frac{\partial N_2}{\partial z}\big|_{z=L}}{\rho \left(ar\right)^2 \left(1 - bt\right)^{-2}} = -\frac{(1 + K/2)}{\mathrm{Re}_r} g'(1),
\end{aligned} \tag{11.11}
$$

where $\mathrm{Re}_r \left(= ar/\nu\sqrt{1 - bt}\right)$ denotes the local Reynolds number.

11.2 Solution of the problem

For homotopy solutions we choose the base functions

$$
\left\{\eta^{2n+1}, \; n \geq 0\right\} \tag{11.12}
$$

and write

$$
f(\eta) = \sum_{n=0}^{\infty} a_n \eta^{2n+1}, \quad g(\eta) = \sum_{n=0}^{\infty} b_n \eta^{2n+1}, \tag{11.13}
$$

where a_n and b_n are the coefficients. We take the initial guesses of the form

$$
f_0(\eta) = \frac{1}{2}\left(\eta^3 - \eta\right), \quad g_0(\eta) = -n f''(1)\eta, \tag{11.14}
$$

and suggest the following linear operators

$$
\mathcal{L}_f\left(f(\eta)\right) = \frac{d^4 f}{d\eta^4}, \quad \mathcal{L}_g\left(g(\eta)\right) = \frac{d^2 g}{d\eta^2}, \tag{11.15}
$$

with the properties given below

$$
\mathcal{L}_f\left[C_1 + C_2\eta + C_3\eta^2 + C_4\eta^3\right] = 0, \quad \mathcal{L}_g\left[C_5 + C_6\eta\right] = 0, \tag{11.16}
$$

where C_i $(i = 1 - 6)$ are constants of integration.

184

11.2.1 Zeroth order deformation problems

We construct the zeroth order deformation problems as follows:

$$(1-q)\pounds_f\left[f(\eta;q)-f_0(\eta)\right]=q\hbar_f\mathcal{N}_f\left[\hat{f}(\eta;q),\hat{g}(\eta;q)\right],\tag{11.17}$$

$$\hat{f}(1;q)=0,\quad\left.\frac{\partial\hat{f}(\eta;q)}{\partial\eta}\right|_{\eta=1}=1,\;\hat{f}(0;q)=0,\quad\left.\frac{\partial^2\hat{f}(\eta;q)}{\partial\eta^2}\right|_{\eta=0}=0,\tag{11.18}$$

$$(1-q)\pounds_g\left[\hat{g}(\eta;q)-g_0(\eta)\right]=q\hbar_g\mathcal{N}_g\left[\hat{g}(\eta;q),\hat{f}(\eta;q)\right],\tag{11.19}$$

$$\hat{g}(1;q)=-n\left.\frac{\partial^2\hat{f}(\eta;q)}{\partial\eta^2}\right|_{\eta=1},\;\hat{g}(0;q)=0.\tag{11.20}$$

In above expressions $q\in[0,1]$ and $\hbar_{f,g}\neq0$ are respectively called the embedding and convergence control parameters such that $\hat{f}(\eta;0)=f_0(\eta)$, $g(\eta;0)=g_0(\eta)$, $\hat{f}(\eta;1)=f(\eta)$ and $\hat{g}(\eta;1)=g(\eta)$. When q varies from 0 to 1, $\hat{f}(\eta;q)$ approaches $f_0(\eta)$ to $f(\eta)$ and $\hat{g}(\eta;q)$ from $g_0(\eta)$ to $g(\eta)$. The nonlinear operators $\mathcal{N}_f$ and $\mathcal{N}_g$ are given by

$$\begin{aligned}\mathcal{N}_f\left[\hat{f}(\eta;q),\hat{g}(\eta;q)\right]&=(1+K)\frac{\partial^4\hat{f}(\eta;q)}{\partial\eta^4}-\frac{S\,\mathrm{Re}}{2}\left[\eta\frac{\partial^3\hat{f}(\eta;q)}{\partial\eta^3}+3\frac{\partial^2\hat{f}(\eta;q)}{\partial\eta^2}\right]\\&\quad+2\,\mathrm{Re}\,\hat{f}(\eta;q)\frac{\partial^3\hat{f}(\eta;q)}{\partial\eta^3}-K\frac{\partial^2\hat{g}(\eta;q)}{\partial\eta^2}-\mathrm{Re}\,M\frac{\partial^2\hat{f}(\eta;q)}{\partial\eta^2},\end{aligned}\tag{11.21}$$

$$\begin{aligned}\mathcal{N}_g\left[\hat{g}(\eta;q),\hat{f}(\eta;q)\right]&=\left(1+\frac{K}{2}\right)\frac{\partial^2\hat{g}(\eta;q)}{\partial\eta^2}-K\,\mathrm{Re}\left[2\hat{g}(\eta;q)-\frac{\partial^2\hat{f}(\eta;q)}{\partial\eta^2}\right]\\&\quad-\frac{S\,\mathrm{Re}}{2}\left[3\hat{g}(\eta;q)+\eta\frac{\partial\hat{g}(\eta;q)}{\partial\eta}\right]+\mathrm{Re}\left[2\hat{f}(\eta;q)\frac{\partial\hat{g}(\eta;q)}{\partial\eta}-\hat{g}(\eta;q)\frac{\partial\hat{f}(\eta;q)}{\partial\eta}\right].\end{aligned}\tag{11.22}$$

Expanding $\hat{f}(\eta;q)$ and $\hat{g}(\eta;q)$ in Taylor series we have

$$\hat{f}(\eta;q)=f_0(\eta)+\sum_{m=1}^{\infty}f_m(\eta)q^m,\;\hat{g}(\eta;q)=g_0(\eta)+\sum_{m=1}^{\infty}g_m(\eta)q^m,\tag{11.23}$$

$$f_m(\eta)=\frac{1}{m!}\left.\frac{\partial^m\hat{f}(\eta;q)}{\partial\eta^m}\right|_{q=0},\;g_m(\eta)=\frac{1}{m!}\left.\frac{\partial^m\hat{g}(\eta;q)}{\partial\eta^m}\right|_{q=0}.\tag{11.24}$$

11.2.2 Higher order deformation problems

The mth order deformation problems are

$$\mathcal{L}_f \left[f_m(\eta) - \chi_m f_{m-1}(\eta) \right] = \hbar_f \mathcal{R}_m^f \left(f_{m-1}(\eta), g_{m-1}(\eta) \right),$$
$$f_m(1) = 0, \ f_m'(1) = 0, \ f_m(0) = 0, \ f_m''(0) = 0, \tag{11.25}$$

$$\mathcal{L}_g \left[g_m(\eta) - \chi_m g_{m-1}(\eta) \right] = \hbar_g \mathcal{R}_m^g \left(g_{m-1}(\eta) \right),$$
$$g_m(1) = 0, \ g_m(0) = 0, \tag{11.26}$$

$$\chi_m = \begin{cases} 0, m \leq 1, \\ 1, m > 1, \end{cases} .$$

$$\mathcal{R}_m^f \left(f_m(\eta), g_m(\eta) \right) = (1+K) f_{m-1}'''' - \frac{S \operatorname{Re}}{2} \left[3 f_{m-1}'' + \eta f_{m-1}''' \right] - \operatorname{Re} M f_{m-1}''$$
$$+ 2 \operatorname{Re} \sum_{n=0}^{m-1} f_n''' f_{m-1-n} - K g_{m-1}'', \tag{11.27}$$

$$\mathcal{R}_m^g \left(g_m(\eta), f_m(\eta) \right) = \left(1 + \frac{K}{2} \right) g_{m-1}''' + \operatorname{Re} K \left[f_{m-1}'' - 2 g_{m-1} \right]$$
$$- \frac{S \operatorname{Re}}{2} \left[3 g_{m-1} + \eta g_{m-1}' \right] + \operatorname{Re} \sum_{n=0}^{m-1} \begin{bmatrix} 2 f_n g_{m-1-n}' \\ -f_n' g_{m-1-n} \end{bmatrix} . \tag{11.28}$$

If $f_m^*(\eta)$ and $g_m^*(\eta)$ indicate the particular solutions of problems (11.25) and (11.26) then solution expressions for mth order deformation problems are

$$f_m(\eta) = f_m^*(\eta) + C_1^m + C_2^m \eta + C_3^m \eta^2 + C_4^m \eta^2 \tag{11.29}$$

$$g_m(\eta) = g_m^*(\eta) + C_5^m + C_6^m \eta, \tag{11.30}$$

where $C_i^m (i = 1 - 6)$ are determined by the boundary conditions given in Eqs. (11.25) and (11.26).

11.3 Convergence of homotopy solutions

The series solutions obtained by homotopy analysis method contain convergence control parameters (auxiliary parameters). The auxiliary parameters are employed in the adjustment of convergence regions of the derived series solutions. To examine the effects of auxiliary parameters we plot the $\hbar_{f,g}$ curves in Figs. 11.2 and 11.3. It can be noted from Figs. 11.2 and 11.3 that our series solutions converge when $-1.2 \leq \hbar_f, \hbar_g \leq -0.45$. However, the forthcoming analysis has been presented for fixed value -0.8 of $\hbar_f$ and $\hbar_g$. Table 11.1 shows the convergence of derived series solutions. This Table shows that convergence is achieved at 20th order of approximations up to 12 decimal places.
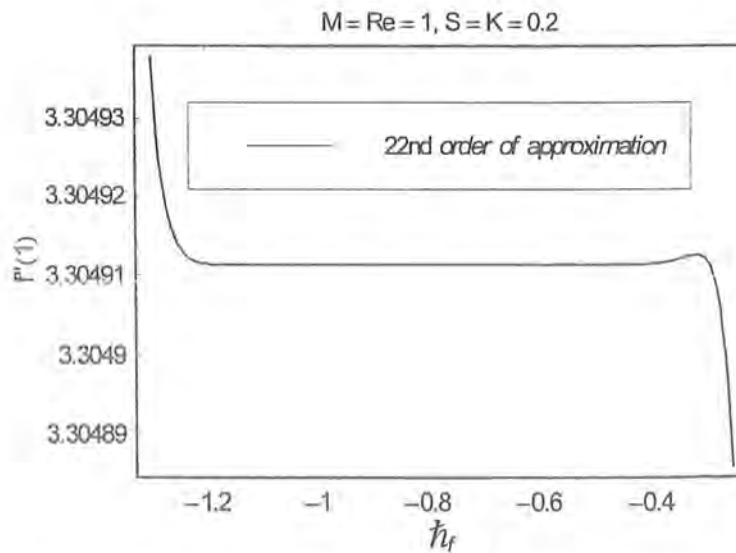

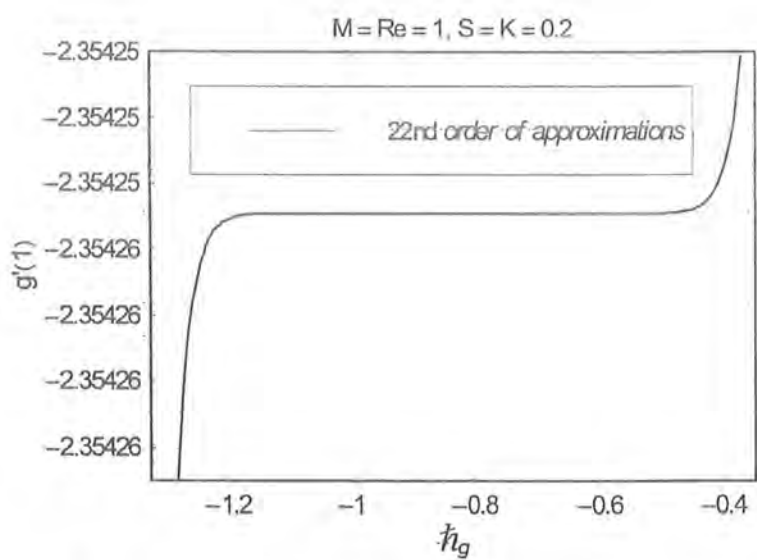Fig. 11.2. $\hbar_f$–curve of $f''(1)$ at 22nd order of approximation.

Fig. 11.3. $\hbar_g$-curve of $g'(1)$ at 22nd order of approximation.

Table 11.1. Convergence of HAM solutions when $Re = M = 2.0, S = K = 0.2$, $n = 0.5$ and $\hbar_f = \hbar_g = -0.8$.

Order of approximations	$f''(1)$	$g'(1)$
1	3.95085714286	-3.57542857143
5	3.88696927534	-3.60590455466
10	3.88710449242	-3.60605273254
15	3.88710458228	-3.60605285000
20	3.88710458233	-3.60605285011
25	3.88710458233	-3.60605285011
30	3.88710458233	-3.60605285011
35	3.88710458233	-3.60605285011

11.4   Results and discussion

Here in this section we have examined the influence of Hartman number M, Reynold number Re, unsteadiness parameter S and micropolar parameter K on $f'(\eta)$, $f(\eta)$ and $g(\eta)$. The effects of Hartman number M on $f(\eta)$ and $f'(\eta)$ are shown in the Figs. 11.4 and 11.5. From these Figs. it can be seen that the magnitude of $f(\eta)$ and $f'(\eta)$ decreases when Hartman number M increases. This is due to the fact that Lorentz force retards the flow both in radial and axial directions. Figs. 11.6 and 11.7 illustrate the effect of magnetic field on the dimensionless angular velocity $g(\eta)$ for both the cases $n = 0$ (strong concentration of microelements) and $n = 0.5$ (weak concentration of microelements). We observe from these Figs. that for the situation when microelements are able to rotate at the stretching sheets ($n = 0.5$) the effect of Hartman number M on $g(\eta)$ is opposite to that of M on $g(\eta)$ when $n = 0$ (when microelements are unable to rotate at the stretching sheet). The magnitude of $f(\eta)$ and $f'(\eta)$ is a decreasing function of Re (Figs. 11.8 and 11.9). It is found from Fig. 11.10 that for $n = 0.5$ Reynolds number Re is more influential on $g(\eta)$ in the vicinity of stretching sheet whereas it has negligible effect on $g(\eta)$ away from the stretching sheet. It is noted from Fig. 11.11 that for $n = 0$ there is an increase in $g(\eta)$ when Reynold number is increased. Upon making an increase in micropolar parameter K, there is an increase in the magnitude of dimensionless axial component $f(\eta)$ and radial component $f'(\eta)$ as shown in Figs. 11.12 and 11.13. Fig. 11.14 depicts that the magnitude

189

of angular velocity $g(\eta)$ decreases by increasing the micropolar parameter K when $n = 0.5$. However it increases when $n = 0$ as shown Fig. 11.15. The effects of unsteadiness parameter S on $f(\eta)$, $f'(\eta)$ and $g(\eta)$ are shown in the Figs. 11.16 − 11.19. Figs. 11.16 and 11.17 reveal that the magnitudes of $f(\eta)$ and $f'(\eta)$ are increasing functions of unsteadiness parameter S whereas $g(\eta)$ decreases with an increase in unsteadiness parameter S for both the cases $n = 0.5$ and $n = 0$ (see Figs. 11.18 and 11.19). Table 11.2 represents the variation of skin friction coefficient for steady flow ($S = 0$) and unsteady flow ($S \neq 0$) for two cases (i) when microelements close to the stretching sheet are unable to rotate ($n = 0$) i.e. strong concentration of microelements and (ii) when microelements close to the stretching sheet are able to rotate ($n = 0.5$ i.e. weak concentration of microelements). This Table indicates that skin friction coefficient $\mathrm{Re}_r C_f$ is an increasing function of Hartman number M, Reynolds number Re and micropolar parameter K. Furthermore, skin friction coefficient $\mathrm{Re}_r C_f$ for unsteady flow ($S \neq 0$) is larger than that for steady flow ($S = 0$). The skin friction coefficient for the case of strong concentration of microelement ($n = 0$) is higher than that when $n = 0.5$ (weak concentration). Skin friction coefficient $\mathrm{Re}_r C_f$ for magnetohydrodynamic flow ($M \neq 0$) is larger than that for hydrodynamic flow ($M = 0$). Skin friction coefficient $\mathrm{Re}_r C_f$ increases when Reynolds number Re is increased. Furthermore, $\mathrm{Re}_r C_f$ for case of dominant inertial force ($Re > 1$) is higher than that when viscous force is dominant ($Re < 1$). Skin friction coefficient $\mathrm{Re}_r C_f$ is an increasing function of micropolar parameter K. Obviously skin friction coefficient $\mathrm{Re}_r C_{f_r}$ for micropolar fluid ($K \neq 0$) is higher than that of viscous fluid ($K = 0$). Table 11.3 is constructed for the influence of various parameters on the wall couple stress coefficient $\mathrm{Re}_r C_g$. This Table indicates that the wall couple stress increases by increasing M, Re and K for both steady flow ($S = 0$) and unsteady ($S \neq 0$) flows. Wall couple stress $\mathrm{Re}_r C_g$ for steady flow ($S = 0$) is larger than that of unsteady ($S \neq 0$) when $n = 0$ whereas wall couple stress coefficient $\mathrm{Re}_r C_g$ for unsteady flow is higher in comparison with $\mathrm{Re}_r C_g$ for steady flow when $n = 0.5$. From Table 11.3 one can see that for $K = 0$ (Newtonian fluid), wall couple stress $\mathrm{Re}_r C_g = 0$ both for steady ($S = 0$) and unsteady ($S \neq 0$) flows when $n = 0$. This is due to the fact that for $K = 0$ Eqs. (11.2) and (11.3) reduce to classical Navier-Stokes equations which are unable to exhibit the property like
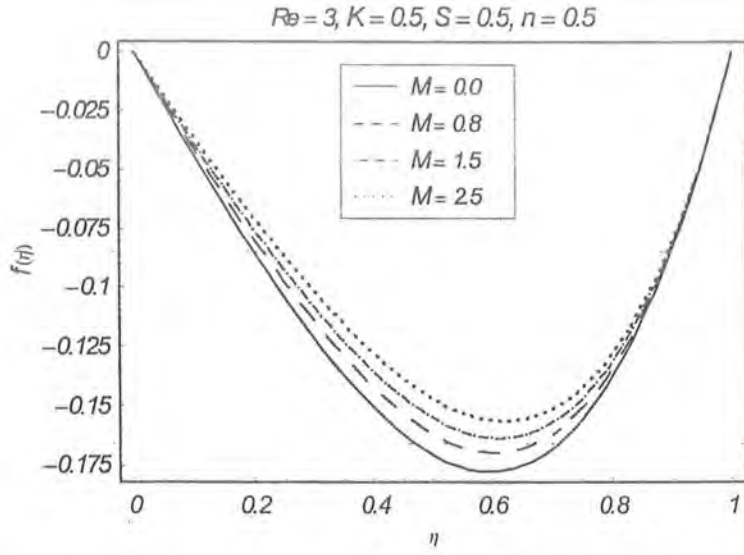
190

couple stress.

Fig. 11.4. Influence of Hartman number M on axial velocity $f(\eta)$ when $n = 0.5$.
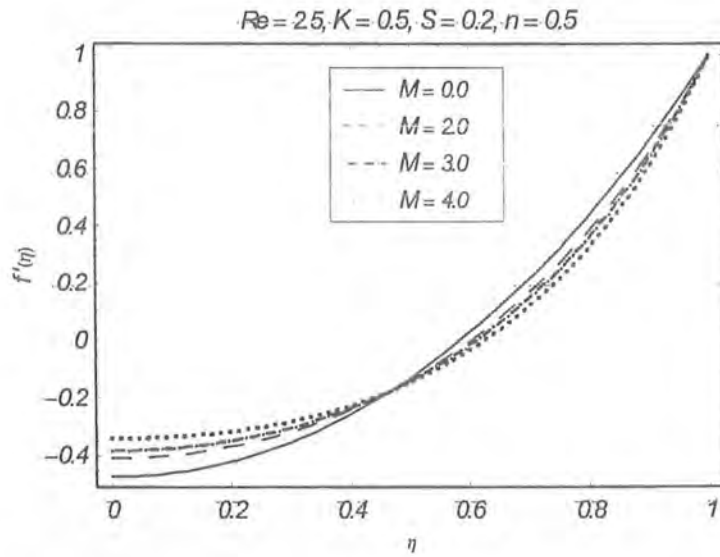

Fig. 11.5. Influence of Hartman number M on radial velocity $f'(\eta)$ when $n = 0.5$.
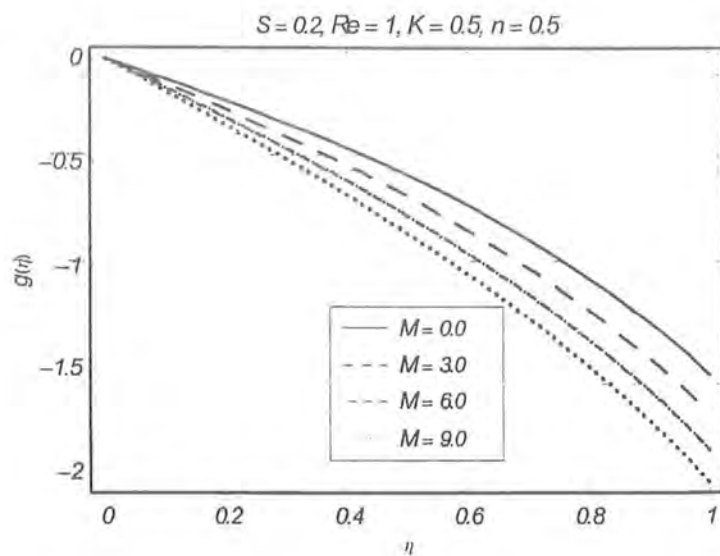
Fig. 11.6. Influence of Hartman number M on angular velocity $g(\eta)$ when $n = 0.5$.
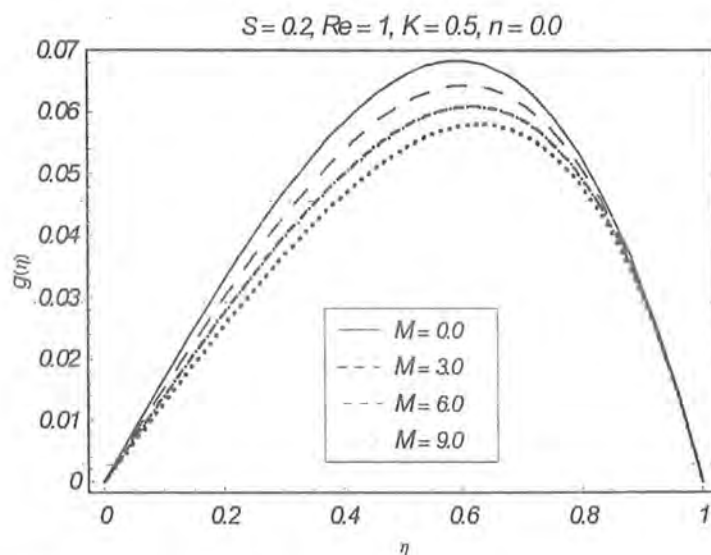

Fig. 11.7. Influence of Hartman number M on angular velocity $g(\eta)$ when $n = 0$.
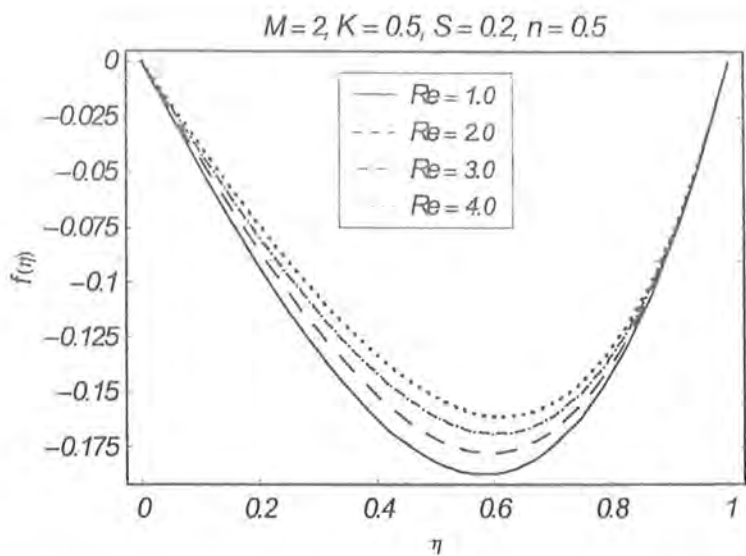
192

Fig. 11.8. Influence of Reynolds number Re on axial velocity $f(\eta)$ when $n = 0.5$.
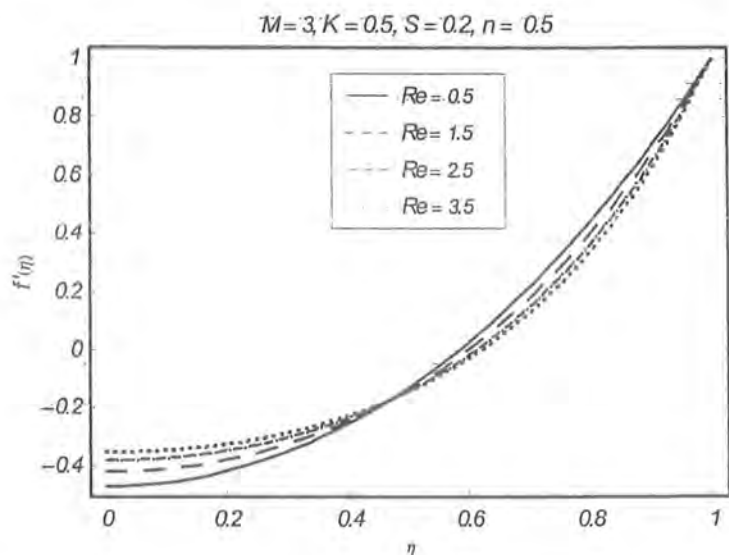

Fig. 11.9. Influence of Reynolds number Re on radial velocity $f'(\eta)$ when $n = 0.5$.
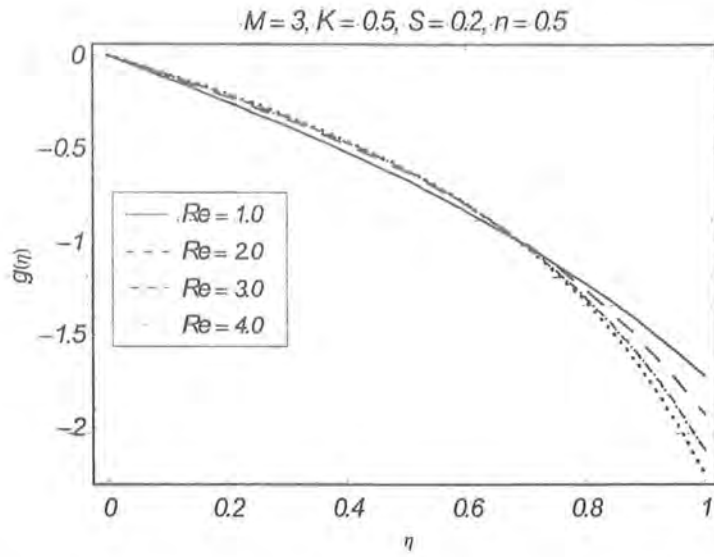
Fig. 11.10. Influence of Reynolds number Re on angular velocity $g(\eta)$ when $n = 0.5$
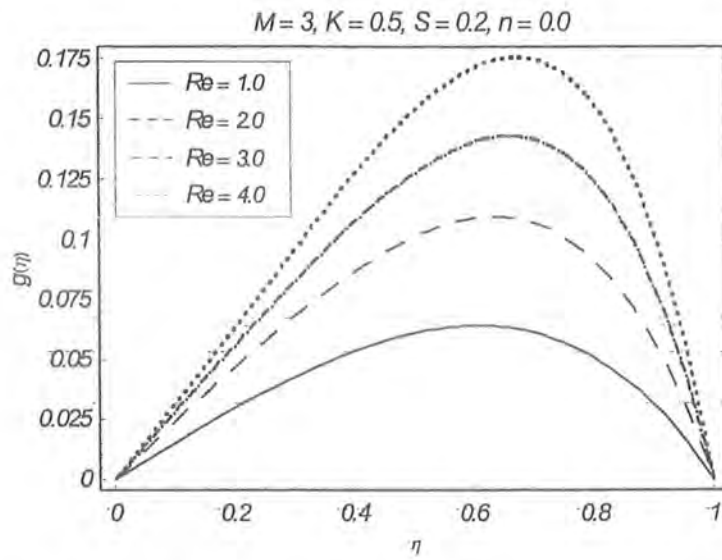

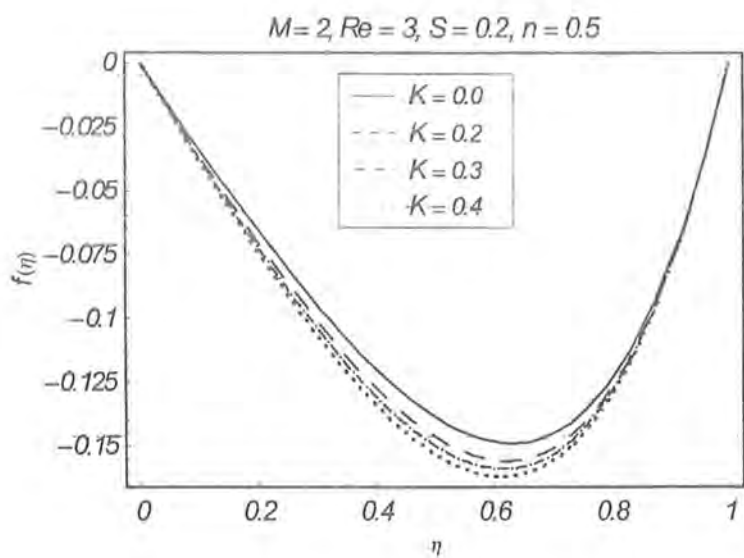Fig. 11.11. Influence of Reynolds number Re on angular velocity $g(\eta)$ when $n = 0$.

194

Fig. 11.12. Influence of micropolar parameter K on axial velocity $f(\eta)$ when $n = 0.5$.
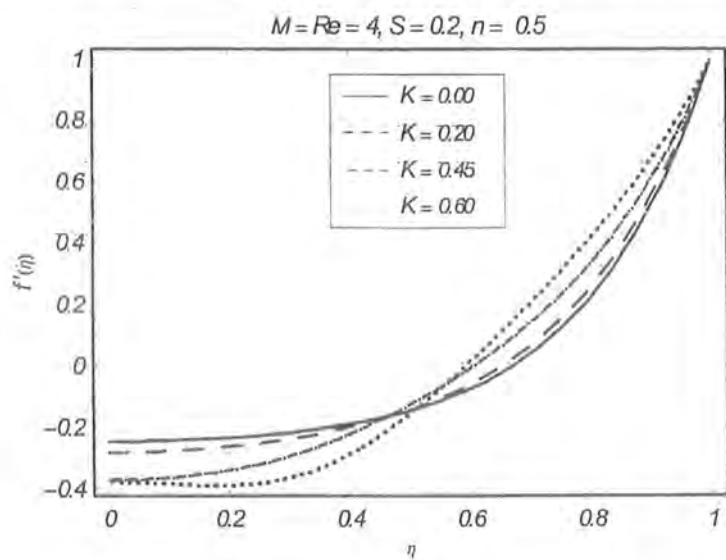

Fig. 11.13. Influence of micropolar parameter K on radial velocity $f'(\eta)$ when $n = 0.5$.

Fig. 11.14. Influence of micropolar parameter K on angular velocity $g(\eta)$ when $n = 0.5$.

Fig. 11.15. Influence of micropolar parameter K on angular velocity $g(\eta)$ when $n = 0$.

196

Fig. 11.16. Influence of unsteadiness parameter S on axial velocity $f(\eta)$ when $n = 0.5$.

Fig. 11.17. Influence of unsteadiness parameter S on radial velocity $f'(\eta)$ when $n = 0.5$.
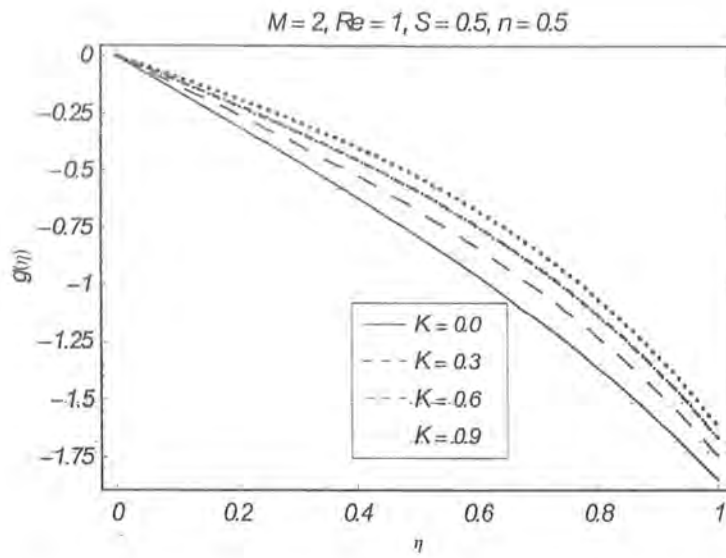
197

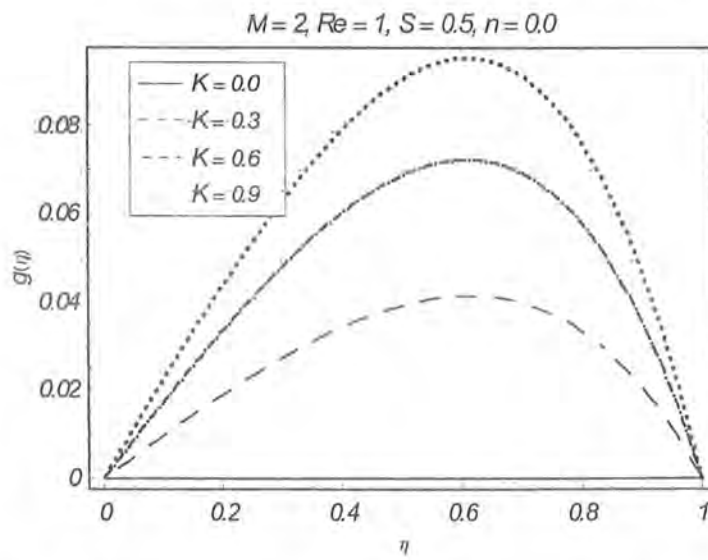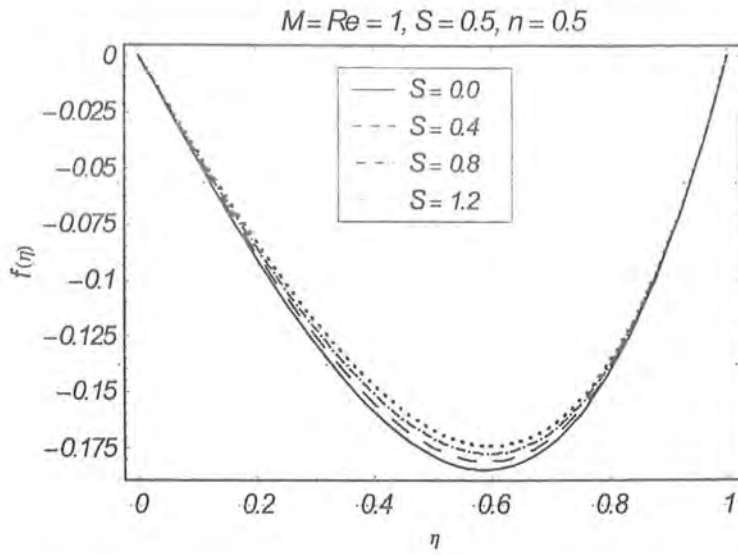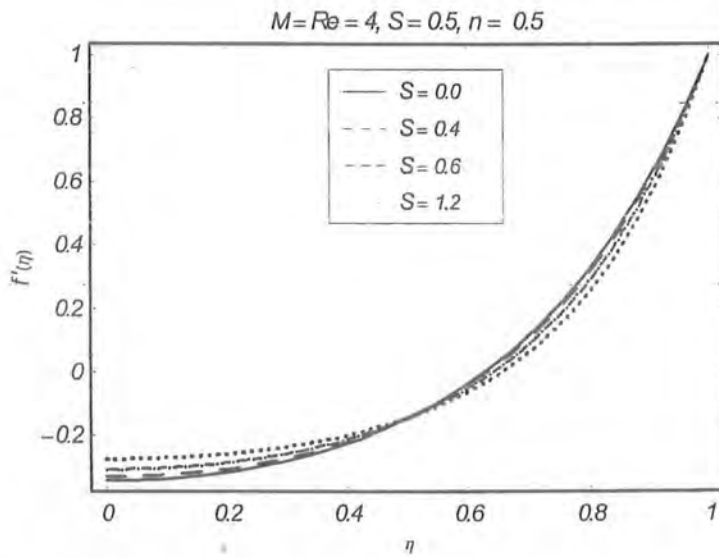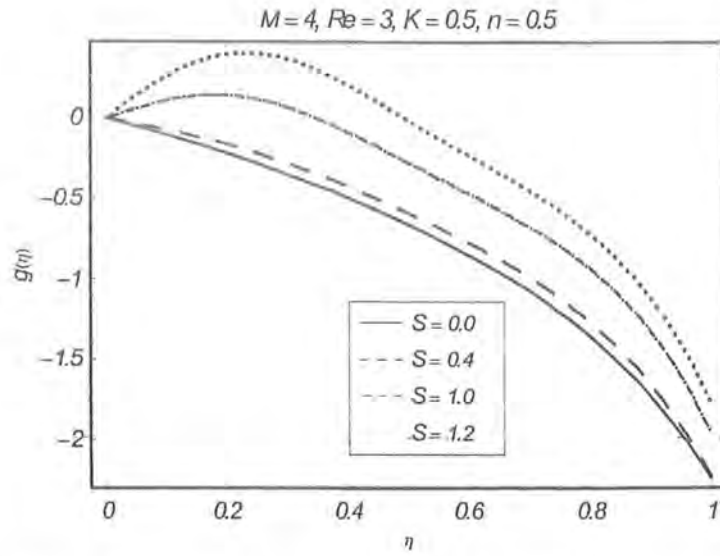Fig. 11.18. Influence of micropolar parameter K on angular velocity $g(\eta)$ when $n = 0.5$
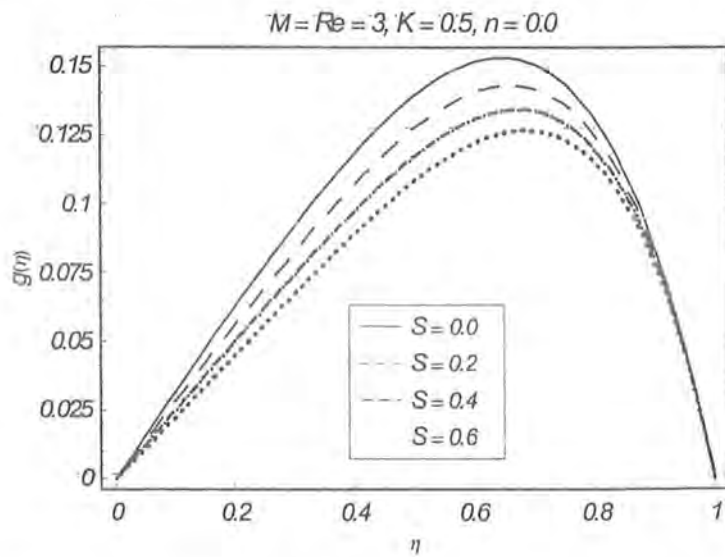

Fig. 11.19. Influence of micropolar parameter K on angular velocity $g(\eta)$ when $n = 0$.

198

Table 11.2. Numerical values of skin friction coefficient $\mathrm{Re}_r\, C_f$ for steady and unsteady flows when $n = 0, 0.5$.

M	Re	K	$\mathrm{Re}_r\, C_f$			
			$S = 0$ (steady flow)		$S = 0.2$ (unsteady flow)	
			$n = 0$	$n = 0.5$	$n = 0$	$n = 0.5$
0.0	2.0	0.2	3.82473020238	3.78726691878	3.99120358926	3.94239935089
1.0	2.0	0.2	4.20445423054	4.16993062067	4.36461630321	4.31907441217
2.0	2.0	0.2	4.55221064458	4.52012817877	4.70732496512	4.66452549879
3.0	2.0	0.2	4.87395229220	4.84393067976	5.02494392674	4.98448554625
2.0	0.5	0.2	3.84961651365	3.84008453269	3.88936488851	3.87647501000
2.0	1.5	0.2	4.32555975365	4.30011894660	4.44291661255	4.40883270045
2.0	2.5	0.2	4.77168425132	4.73368228848	4.96386790599	4.91337165356
2.0	3.5	0.2	5.19046130392	5.14241397560	5.45487945055	5.39148143178
2.0	2.0	0.0	3.95105916698	3.95105916698	4.10439808967	4.10439808967
2.0	2.0	0.1	4.25481522604	4.24120771227	4.40896348844	4.38954617993
2.0	2.0	0.2	4.55221064458	4.52012817877	4.70732496512	4.66452549879
2.0	2.0	0.3	4.84435445313	4.78988331862	5.00051562161	4.93112443178

Table 11.3. Numerical values of wall couple stress coefficient $\mathrm{Re}_r \, C_g$ for steady and unsteady flows when $n = 0, 0.5$.

M	Re	K	$-\mathrm{Re}_r \, C_g$			
			$S = 0$ (steady flow)		$S = 0.2$ (unsteady flow)	
			$n = 0$	$n = 0.5$	$n = 0$	$n = 0.5$
0.0	2.0	0.2	0.387278980109	3.26295324728	0.383145930553	3.68873785110
1.0	2.0	0.2	0.387543251367	3.40770958877	0.383603165498	3.83313488447
2.0	2.0	0.2	0.387797110015	3.54140362983	0.384023949443	3.96665813513
3.0	2.0	0.2	0.388039304423	3.66608133907	0.384412418868	4.09128293110
2.0	0.5	0.2	0.099220968475	2.15103436228	0.0989347234382	2.26476535684
2.0	1.5	0.2	0.293069065641	3.09514318666	0.290798273461	3.42085657147
2.0	2.5	0.2	0.481151680563	3.97237897188	0.475653829432	4.49361404936
2.0	3.5	0.2	0.664043350895	4.79342672977	0.654723551751	5.49774642737
2.0	2.0	0.0	0.000000000000	2.67977836057	0.000000000000	3.13680549337
2.0	2.0	0.2	0.197854021227	3.11911705925	0.195587393503	3.55847831259
2.0	2.0	0.4	0.387797110015	3.54140362983	0.384023949443	3.96665813513
2.0	2.0	0.6	0.571285510760	3.95018724378	0.566534046078	4.36397123775

11.5 Conclusions

This work investigated unsteady flow of an incompressible micropolar fluid between the radially stretching sheets. The following observations have been noted from the performed analysis.

- The effect of unsteadiness parameter S on $f(\eta)$, $f'(\eta)$ and $g(\eta)$ is similar in qualitative sense.

- The variations of M and K on dimensionless angular velocity $g(\eta)$ for case of strong concentration $(n = 0)$ is opposite to that on the dimensionless angular velocity $g(\eta)$ for the case of weak concentration $(n = 0.5)$. However Re and S have similar effects on $g(\eta)$ when $n = 0$ and $n = 0.5$.

- Boundary layer is decreased when Hartman number M increases.

- Skin friction coefficient $\text{Re}_r\, C_f$ and couple stress coefficient $\text{Re}_r\, C_g$ are increasing functions of Re, M, S and K when $n = 0$ and $n = 0.5$.

- Skin friction coefficient $\text{Re}_r\, C_f$ in steady flow ($S = 0$) is less than that of unsteady flow ($S \neq 0$).

- Wall couple stress $\text{Re}_r\, C_g$ for unsteady flow ($S \neq 0$) is less than that for steady flow ($S = 0$) when $n = 0$ while the wall couple stress $\text{Re}_r\, C_g$ for unsteady flow is higher than the wall couple stress $\text{Re}_r\, C_g$ in steady flow when $n = 0.5$.

Bibliography

[1] O. D. Makinde and P. Y. Mhone, Hermite Pade approximations approach to MHD Jeffery-Hamel flows, Appl. Math. Comput. 181 (2006) 966 − 972.

[2] G. Hamel, Spiralförmige Bewgungen Zäher Flüssigkeiten, Jahresbericht der Deutschen Math. Vereinigung 25 (1916) 34 − 60.

[3] G. B. Jeffery, The two-dimensional steady motion of a viscous fluid. Philos. Mag. 6 (1915) 455 − 465.

[4] G. K. Batchelor, An Introduction to Fluid Dynamics, Camberigde University Press, 1967.

[5] I. J. Sobey and I. J. Drazin, Bifurcation of two-dimensional channel flows, J. Fluid Mech. 171 (1986) 263 − 287.

[6] W. H. H. Banks, P.G. Drazin and M. B. Zaturska, On perturbation of Jeffery-Hamel flows, J. Fluid Mech. 186 (1988) 559 − 581.

[7] D. G. Domairry, A. Mohsenzada and M. Famouri, The application of homotopy analysis method to solve nonlinear differential equation governing Jeffery- Hamel flow, Comm. Nonlinear Sci. Numer. Simul. 14 (2009) 85 − 95.

[8] A. A. Joneidi, G. Domairry and M. Babaelahi, Three analytical methods applied to Jeffery–Hamel flow, Comm. Nonlinear Sci. Numer. Simul. 15 (2010) 3423 − 3434.

[9] B. C. Sakiadis, Boundary layer behavior on continuous solid surfaces: I. Boundary layer equations for two dimensional and axisymmetric flow, AIChE J. 7 (1961) 26 − 28.

[10] B. C. Sakiadis, Boundary layer behavior on continuous solid surfaces: II. The boundary layer on a continuous flat surface, AIChE J. 7 (1961) 221-225.

[11] B. C. Sakiadis, Boundary layer behavior on continuous solid surfaces: III. The boundary layer on a continuous cylindrical Surface, AIChE J. 7 (1961) 467-472.

[12] L. E. Erickson, L. T. Fan and V. G. Fox, Heat and mass transfer on a moving continuous flat plate with suction or injection, Ind. Eng. Chem. Fundam. 5 (1966) 19-24.

[13] F. K. Tsou, E. M. Sparrow and R. J. Goldstien, Flow and heat transfer in the boundary layer on a continuous moving surface, Int. J. Heat Mass Transfer 10 (1967) 219-235.

[14] V. M. Soundalgekar and T. V. R. Murthy, Heat transfer past a continuous moving plate with variable temperature, Wa¨rme-rund-Stoffu¨bertragung 14 (1980) 91-93.

[15] M. Ali and F. Al-Yousef, Laminar mixed convection from a continuously moving vertical surface with suction or injection, Heat Mass Transfer 33 (1998) 301-306.

[16] L. J. Crane, Flow past a stretching plate, Z. Angew. Math. Phys. 21 (1970) $645 - 647$.

[17] H. I. Andersson, J. B. Aerseth, B. S. Braud and B. S. Dandapat, Flow of a power-law fluid film on an unsteady stretching sheet, J. Non-Newtonian Fluid Mech. 62 (1996) $1 - 8$.

[18] H. I. Andersson, Slip flow past a stretching surface, Acta Mech. 158 (2002) $121 - 125$.

[19] C. Wang, Analysis of viscous flow due to a stretching sheet with surface slip and suction, Nonlinear Anal.: Real World Applications(RWA) 10 (2009) $375 - 380$.

[20] K. R. Rajagopal, T. Y. Na and A. S. Gupta, Flow of a viscoelastic fluid over a stretching sheet, Rheol. Acta 23 (1984) $213 - 215$.

[21] T. R. Mahapatra and A. S. Gupta, Stagnation-point flow of a viscoelastic fluid towards a stretching surface, Int. J. Nonlinear Mech. 39 (2004) $811 - 820$.

[22] M. Sajid and T. Hayat, Non-similar series solution for boundary layer flow of a third-order fluid over a stretching sheet, Appl. Math. Comput. 189 (2007) $1576 - 1585$.

[23] Z. Abbas, Y. Wang, T. Hayat and M. Oberlack, Hydromagnetic flow in a viscoelastic fluid due to an oscillatory stretching sheet, Int. J. Nonlinear Mech. 43 (2008) 783 − 793.

[24] R. Nazar and N. A. Latip, Numerical investigation of three-dimensional boundary layer flow due to a stretching surface in a viscoelastic fluid, Eur. J. Sci. Res. 29 (2009) 509−517.

[25] P. D. Ariel, Axisymmetric flow of a second grade fluid past a stretching sheet, Int. J. Eng. Sci. 39 (2001) 529 − 553.

[26] H. Mirgolbabaei, D. D. Ganji, M. M. Etghani and A. Sobati, Adapted variational iteration method and axisymmetric flow over a stretching sheet, World J. Model. Simul. 5 (4) (2009) 307 − 314.

[27] P. D. Ariel, Axisymmetric flow due to a stretching sheet with partial slip, Comput. Math. Appl. 54 (2007) 1169 − 1183.

[28] T. Hayat, I. Ahmad and T. Javed, On comparison of the solutions for an axisymmetric flow, Numerical Methods for Partial Differential Equations 25 (2008) 1205-1211.

[29] B. Sahoo, Effects of partial slip on axisymmetric flow of an electrically conducting viscoelastic fluid past a stretching sheet, Cent. Eur. J. Phys. 8(3) (2010) 498 − 508.

[30] M. Sajid, T. Hayat, S. Asghar and K. Vajravelu, Analytic solution for axisymmetric flow over a nonlinearly stretching sheet, Arch. Appl. Mech. 78 (2008) 127 − 134.

[31] P. H. Oosthuizen and D. Naylor, An introduction to Convective Heat Transfer analysis, McGraw-Hill, Singapore, 1999.

[32] T. Hayat and M. Sajid, Analytic solution for axisymmetric flow and heat transfer of a second grade fluid past a stretching sheet, Int. J. Heat Mass Transfer 50 (2007) 75 − 84.

[33] M. Sajid, I. Ahmad, T. Hayat and M. Ayub, Series solution for unsteady axisymmetric flow and heat transfer over a radially stretching sheet, Comm. Nonlinear Sci. Numer. Simul. 13 (2008) 2193 − 2202.

[34] I. Ahmad, M. Sajid and T. Hayat, Heat transfer in unsteady axisymmetric second grade fluid, Appl. Math. Comput. 215 (5) (2009) 1685 − 1695.

204

[35] R. Cortell, A note on flow and heat transfer of a viscoelastic fluid over a stretching sheet, Int. J. Non-Linear Mech. 41 (2006) 78 − 85.

[36] M. Mushtaq, S. Asghar and M. A. Hossain, Mixed convection flow of second grade fluid along a vertical stretching flat surface with variable surface temperature, Heat Mass Transfer 43 (2007) 1049 − 1061.

[37] R. Cortell, Flow and heat transfer of an electrically conducting fluid of second grade over a stretching sheet subject to suction and to a transverse magnetic field, Int. J. Heat Mass Transfer 49 (11 − 12) (2006) 1851 − 1856.

[38] I. Liu, Flow and heat transfer of an electrically conducting fluid of second grade in a porous medium over a stretching sheet subject to a transverse magnetic field, Int. J. Nonlinear Mechanics 40(4) (2005) 465 − 474.

[39] R. C. Bataller, Viscoelastic fluid flow and heat transfer over a stretching sheet under the effects of a non-uniform heat source, viscous dissipation and thermal radiation, Int. J. Heat Mass Transfer 50 (15 − 16) (2007) 3152 − 3162.

[40] T. Hayat, T. Javed and Z. Abbas, Slip flow and heat transfer of a second grade fluid past a stretching sheet through a porous space, Int. J. Heat Mass Transfer 51 (17 − 18) (2008) 4528 − 4534.

[41] M. S. Abel, M. M. Nandeppanavar and S. B. Malipatil, Heat transfer in a second grade fluid through a porous medium from a permeable stretching sheet with non-uniform heat source/sink, Int. J. Heat Mass Transfer 53 (9 − 10) (2010) 1788 − 1795.

[42] P. S. Gupta and T. S. Gupta, Heat and mass transfer on stretching sheet with suction or blowing, Can. J. Chem. Eng. 55 (1977) 744 − 746.

[43] L. J. Grukba and K. M. Bobba, Heat transfer characteristics on a continuous stretching surface with variable temperature, ASME J. Heat Transfer 107 (1985) 248 − 250.

[44] M. E. Ali, On thermal boundary layer on a power-law stretched surface with suction or injection, Int. J. Heat Fluid Flow 16 (1995) 280 − 290.

205

[45] A. C, Eringen, Theory of micropolar fluids, J. Math. Mech. 16 (1) (1966) 1 − 18.

[46] H. S. Takhar, R. Bhargava, R. S. Agrawal and A. V. S. Balaj, Finite element solution of micropolar fluid flow and heat transfer between two porous discs, Int. J. Eng. Sci. 8 (17) (2000) 1907 − 1922.

[47] N. T. Eldabe, E. F. Elshehawey, E. M. E. Elbarbary and N. S. Elgazery, Chebyshev finite difference method for MHD flow of a micropolar fluid past a stretching sheet with heat transfer, Appl. Math. Comput. 160 (2005) 437 − 450.

[48] I. A. Hassanien and R. S. R. Gorla, Heat transfer to a micropolar fluid from a non-isothermal stretching sheet with suction and blowing, Acta Mech. 84 (1990) 191 − 199.

[49] D. Pal and S. Chatterjee, Heat and mass transfer in MHD non-Darcian flow of a micropolar fluid over a stretching sheet embedded in a porous media with non-uniform heat source and thermal radiation, Comm. Nonlinear Sci. Numer. Simul. 15 (7) (2010) 1843 − 1857.

[50] T. Hayat, Z. Abbas and T. Javed, Mixed convection flow of a micropolar fluid over a non-linearly stretching sheet, Phys. Lett. A 372 (5) (2008) 637 − 647.

[51] I. A. Hassanien, A. A. Abdullah and R. S. R. Gorla, Numerical solutions for heat transfer in a micropolar fluid over a stretching sheet, Appl. Mech. Eng. 3 (1998) 377 − 391.

[52] L. Kumar, Finite element analysis of combined heat and mass transfer in hydromagnetic micropolar flow along a stretching sheet, Comput. Mater. Sci. 46 (4) (2009) 841 − 848.

[53] A. Ishak, Thermal boundary layer flow over a stretching sheet in a micropolar fluid with radiation effect, Meccanica 45 (2010) 367 − 373.

[54] I. Pop, The effects of Hall current on hydromagnetic flow near an accelerated plate, J. Math. Phys. Sci. 5 (1971) 375 − 385.

[55] M. Katagiri, The effect of Hall current on the MHD boundary layer flow past a semi-infinite plate, J. Phys. Soc. Jpn. 27 (1969) 1051 − 1059.

[56] A. S. Gupta, Hydromagnetic flow past a porous flat plate with Hall effects, Acta Mech. 22 (1975) 281 − 287.

[57] M. A. Hossain, Effect of Hall current in unsteady hydromagnetic free convection flow near an infinite vertical porous plate, J. Phys. Soc. Jpn. 55 (1986) 2183 − 2190.

[58] M. A. Hossain and K. Mohammad, Effects of Hall current on hydromagnetic free convection flow near an accelerated porous plate, Japn. J. Appl. Phys. 27 (1986) 1531 − 1535.

[59] T. Watanabe and I. Pop, Hall effects on magnetohydrodynamic boundary layer flow over a continuous moving flat plate, Acta Mech. 108 (1995) 35 − 47.

[60] E. M. Abo-Eldahaba, M. A. El-Aziz, A. M. Salem and K. K. Jabera, Hall current effect on MHD mixed convection flow from an inclined continuously stretching surface with blowing/suction and internal heat generation/absorption, Appl. Math. Modelling 3 (19) (2007) 1829 − 1846.

[61] A. A. Megahed, S. R. Komy and A. A. Afify, Similarity analysis in magnetohydrodynamics: effects of Hall and ion-slip currents on free convection flow and mass transfer of a gas past a semi-infinite vertical plate, Acta Mech. 151 (2001) 185 − 194.

[62] E. Osalusi, J. Side and R. Harris, The effects of Ohmic heating and viscous dissipation on unsteady MHD and slip flow over a porous rotating disk with variable properties in the presence of Hall and ion-slip currents, Int. Comm. Heat Mass Transfer 34 (2007) 1017 − 1029.

[63] E. Osalusi, J. Side, R. Harris and B. Johnston, On the effectiveness of viscous dissipation and Joule heating on steady MHD flow and heat transfer of a Bingham fluid over a porous rotating disk in the presence of Hall and ion-slip currents, Int. Comm. Heat Mass Transfer 34 (2007) 1030 − 1040.

[64] O. A. Bég, J. Zueco and H. S. Takhar, Unsteady magnetohydrodynamic Hartmann–Couette flow and heat transfer in a Darcian channel with Hall current, ionslip, viscous and Joule heating effects: Network numerical solutions, Comm. Nonlinear Sci. Numer. Simul.14 (2009) 1082 − 1097.

[65] E. Osalusi, J. Side, R. Harris and P. Clark, The effects of Ohmic heating and viscous dissipation on unsteady MHD and slip flow on a rotating cone in a rotating fluid with

variable properties in the presence of Hall and ion-slip currents, Int. Comm. Heat Mass Transfer 35 (2008) 413 − 429.

[66] M. A. Rana, A. M. Siddiqui and N. Ahmed, Hall effect on Hartmann flow and heat transfer of a Burgers' fluid, Phys. Lett. A 372 (2008) 562 − 568..

[67] A. M. Salem and M. A. El-Aziz, Effects of Hall current and chemical reaction on hydro-magnetic flow of a stretching vertical surface with internal heat generation/absorption, App. Math. Modelling 32 (2008) 1236 − 1254.

[68] N. S. Elgazery, The effects of chemical reaction, Hall and ion-slip currents on MHD flow with temperature dependent viscosity and thermal diffusivity, Comm. Nonlinear Sci. Numer. Simul. 14 (2009) 1267 − 1283.

[69] G. W. Sutton and Sherman, Engineering Magnetohydrodynamics, New York, McGraw-Hill, 1965.

[70] N. G. Kafoussias and E. W. Williams, Thermal-diffusion and diffusion-thermo effects on mixed free-forced convective and mass transfer boundary layer flow with temperature dependent viscosity, Int. J. Eng. Sci. 33(9) (1995) 1369 − 1384.

[71] M. S. Alam and M. M. Rahman, Dufour and Soret Effects on mixed convection flow past a vertical porous flat plate with variable suction, Nonlinear Analysis: Model. Control, 11(1) (2006) 3 − 12.

[72] M. S.Alam and M. M. Rahman, Dufour and Soret effects on MHD free convective heat and mass transfer flow past a vertical porous flat plate embedded in a porous medium, J. Naval Archi. Marine Eng. 1 (2005) 55 − 65.

[73] M. S. Alm, M. Ferdows, M. Ota, and M. A. Maleque, Dufour and Soret effects on steady free convection and mass transfer flow past a semi-infinite vertical porous plate in a porous medium, Int. J. Appl. Mech. Eng. 11(3) (2006) 535 − 545.

[74] M. S. Alam, M. M. Rahman, M. Ferdows, Koji Kaino, Eunice Mureithi and A. Postelnicu, Diffusion-thermo and thermal diffusion effects on free convective heat and mass transfer

flow on a porous medium with time dependent tempeture and concentration, Int. J. Appl. Eng. Rearch, 2(1) (2007) 81 − 96.

[75] A. Postelnicu, Influence of a magnetic field on heat and mass transfer by natural convection from vertical surfaces in porous media considering Soret and Dufour effects, Int. J. Heat Mass Transfer 47 (2004) 1467 − 147.

[76] P. A. L. Narayana, P. V. S. N. Murthy and R. S. R. Gorla, Soret-driven thermosolutal convection induced by inclined thermal and solutal gradients in a shallow horizontal layer of a porous medium, J. Fluid Mech. 612 (2008) 1 − 19.

[77] R. R. Kairi and P. V. S. N Murthy, Effects of melting heat transfer and thermo-diffusion on natural convection heat mass transfer in a non-Newtonian fluid saturated non-Darcy porous medium, The Open Transport Phenomena Journal 1 (2009) 7 − 14.

[78] E. Osalusi, J. Side and R. Harris, Thermal-diffusion and diffusion-thermo effects on combined heat and mass transfer of a steady MHD convective and slip flow due to a rotating disk with viscous dissipation and Ohmic heating, Int. Comm. Heat Mass Transfer 35 (2008) 908 − 915.

[79] M. A. El-Aziz, Thermal-diffusion and diffusion-thermo effects on combined heat and mass transfer by hydromagnetic three-dimensional free convection over a permeable stretching surface with radiation, Phy. Lett. A 372 (2008) 263 − 272.

[80] O. A. Bég, A. Y. Bakier and V. R. Prasad, Numerical study of free convection magnetohydrodynamic heat and mass transfer from a stretching surface to a saturated porous medium with Soret and Dufour effects, Comp. Mater. Sci. 46 (2009) 57 − 65.

[81] R. Tsai and J. S. Huang, Heat and mass transfer for Soret and Dufour's effects on Hiemenz flow through porous medium onto a stretching surface, Int. J. Heat Mass Transfer, 52 (2009) 2399 − 2406.

[82] A. A. Afify, Similarity solution in MHD: Effects of thermal diffusion and diffusion thermo on free convective heat and mass transfer over a stretching surface considering suction or injection, Comm. Nonlinear Sci. Numer. Simu. 14 (2009) 2202 − 2214.

[83] S. Shateyi, S. S. Motsa and P. Sibanda, The effects of thermal radiation, Hall Currents, Soret and Dufour on MHD flow by mixed convection over a vertical surface in porous media, Mathematical Problems in Engineering (2010), ID 627475, 20 pages.

[84] T. Hayat, M. Mustafa, and S. Mesloub, Mixed convection boundary layer flow over a stretching surface filled with a Maxwell fluid in presence of Soret and Dufour effects, Z. Naturforsch. 65a (2010) 401 − 410.

[85] G. D. Menez and O. C. Sandall, Gas absorption accompanied by first order chemical reaction in turbulent liquids, Ind. Eng. Chem. Fundam. 13(1) (1974) 72 − 76.

[86] T. Hayat, Z. Abbas and M. Sajid, Heat and mass transfer analysis on the flow of a second grade fluid in the presence of chemical reaction, Phys. Lett. A 372 (2008) 2400 − 2408.

[87] T. Hayat, Z. Abbas and N. Ali, MHD flow and mass transfer of a upper-convected Maxwell fluid past a porous shrinking sheet with chemical reaction species, Phys. Lett. A 372 (2008) 4698 − 4704.

[88] M. A. El-Aziz and A. M. Salem, MHD-mixed convection and mass transfer from a vertical stretching sheet with diffusion of chemically reactive species and space or temperature-dependent heat source, Canad. J. Phys. 85 (4) (2007) 359 − 373.

[89] R. Cortell, MHD flow and mass transfer of an electrically conducting fluid of second grade in a porous medium over a stretching sheet with chemically reactive species, Chem. Eng. Process 46 (2007) 721 − 728.

[90] R. Cortell, Toward an understanding of the motion and mass transfer with chemically reactive species for two classes of viscoelastic fluid over a porous stretching sheet, Chem. Eng. Process. 46 (2007) 982 − 989.

[91] H. I. Adersson, O. R. Hansen and B. Holmedal, Diffusion of a chemically reactive species from a stretching sheet, Int. J. Heat Mass Transfer 37 (1994) 659 − 664.

[92] H. S. Takhar, A. J. Chamkha and G. Nath, Flow and mass transfer on a stretcing sheet with a magnetic and chemically reactive species, Int. J. Eng. Sci. 38 (2000) 1303 − 1314.

[93] S. J. Liao, Beyond Perturbation: Introduction to homotopy analysis method, Chapman and Hall, CRC Press, Boca Raton (2003).

[94] S. J. Liao, A new branch of solutions of boundary layer flows over an impermeable stretched plate, Int. J. Heat Mass Transfer 48 (2005) 2529 − 2539.

[95] S. Abbasbandy, Approximate solution for the nonlinear model of diffusion and reaction in porous catalysts by means of the homotopy analysis method, Chem. Eng. J. 136 (2008) 144 − 150.

[96] S. Abbasbandy, The application of homotopy analysis method to solve a generalized Hirota-Satsuma coupled Kdv equation, Phys. Lett. A 361 (2007) 478 − 483.

[97] S. Abbasbandy and F. S. Zakaria, Soliton solution for the fifth-order KdV equation with homotopy analysis method, Nonlinear Dyn. 51 (2008) 83 − 37.

[98] S. Abbasbandy, Homotopy analysis method for generalized Benjamin-Bona-Mahony equation, Z. Angew. Math. Phys. 59 (2008) 51 − 62.

[99] S. Abbasbandy and E. Shivanian, Prediction of multiplicity of solutions of nonlinear boundary value problems: Novel application of homotopy analysis method, Comm. Nonlinear Sci. Num. Simul 15 (2010) 3830 − 3846.

[100] S. Abbasbandy, Homotopy analysis method for the Kawahara equation, Nonlinear Anal.: Real World Applications (RWA) 11 (2010) 307 − 312.

[101] M.S.H. Chowdhury, I. Hashim and O. Abdulaziz, Comparison of homotopy analysis method and homotopy-perturbation method for purely nonlinear fin-type problems, Comm. Nonlinear Sci. Num. Simul 14 (2009) 371 − 378.

[102] S. Kechil and I. Hashim, Approximate analytical solution for MHD stagnation-point flow in porous media, Comm. Nonlinear Sci. Num. Simul. 14 (2009) 1346 − 1354.

[103] I. Hashim, O. Abdulaziz and S. Momani, Homotopy analysis method for fractional IVPs, Comm. Nonlinear Sci. Num. Simul. 14 (2009) 674 − 684.

[104] A. S. Bataineh, M. S. M. Noorani and I. Hashim, The homotopy analysis method for Cauchy reaction diffusion problems, Phys. Lett. A 372 (2008) 613 − 618.

[105] A. S. Bataineh, M. S. M. Noorani and I. Hashim, Modified homotopy analysis method for solving systems of second-order BVP's, Comm. Nonlinear Sci. Num. Simul. 14 (2009) 430 − 442.

[106] Z. Abbas and T. Hayat, Radiation effects on MHD flow in porous space, Int. J. Heat Mass Transfer 51 (2008) 1024 − 1033.

[107] T. Hayat and Z. Abbas, Heat transfer analysis on MHD flow of a second grade fluid in a channel with porous medium, Choas, Soliton & Fractals 38 (2008) 556 − 567.

[108] M. M. Rashidi, G. Domairry and S. Dinarvand, Approximate solutions for the Burger and regularized long wave equations by means of the homotopy analysis method, 14(3) (2009) 708 − 717.

[109] T. Hayat, T. Javed and M. Sajid, Analytic solution for MHD rotating flow of a second grade fluid over a shrinking surface, Phys. Lett. A 372 (2008) 3264 − 3273.

[110] T. Hayat, R. Sajjad and S. Asghar, Series solution for MHD channel flow of a Jeffery fluid, Comm. Nonlinear Sci. Numer. Simul. 15 (2010) 2400 − 2406.

[111] T. Hayat, M. Qasim and Z. Abbas, Radiation and mass transfer effects on the magnetohydrodynamic unsteady flow induced by a stretching sheet, Z. Naturforch. 65a(2010)231 − 239.

[112] T. Hayat, Z. Abbas, T. Javed and M. Sajid, Three-dimensional rotating flow induced by a shrinking sheet for suction, Chaos, Solitons & Fractals 39 (2009) 1615 − 1626.

[113] S. Abbasbandy and T. Hayat, Solution of the MHD Falkner–Skan flow by Hankel–Padé method, Phys. Lett. A 373 (2009) 731 − 734.

[114] T. Hayat, S. Iram, T. Javed and S. Asghar, Shrinking flow of second grade fluid in a rotating frame: An analytic solution, Comm. Nonlinear Sci. Numer. Simul. 15 (2010) 2932 − 2941.

[115] T. Hayat, R. Naz and M. Sajid, On the homotopy solution for Poiseuille flow of a fourth grade fluid, Comm. Nonlinear Sci. Numer. Simul. 15 (2010) 581 − 589.